Numerical analysis of finite volume schemes for population balance equations

Dissertation

zur Erlangung des akademischen Grades

doctor rerum naturalium
(Dr. rer. nat.)

von **M.Sc., Rajesh Kumar**

geb. am 08.07.1981 in Jhajha, India

genehmigt durch die Fakultät für Mathematik
der Otto-von-Guericke-Universität Magdeburg

Gutachter:
Prof. Dr. rer. nat. habil. Gerald Warnecke
Prof. Dr. Ansgar Jüngel

Eingereicht am 12.11.2010
Verteidigung am: 18.03.2011

Acknowledgements

As a child, I was always curious about the title 'Dr.' In notebooks, I rewrote my name alongwith the title 'Dr.' It was a childhood fantasy to be called 'Dr. Rajesh Kumar'. However, when I grew up and decided to pursue Mathematics more specifically, this fantasy was shaping into a stronger dream. In my IIT days, I was keen on getting my dream fulfilled. And now I am here, with all the blessings and good wishes of friends and families, with the title I always dreamt of.

Foremost, I express my deep gratitude to my supervisor Prof. Dr. Gerald Warnecke. Besides imparting in me the basic fundamentals of Mathematics, he gave me remarkable suggestions and supervision, which improved my scientific writing. My work grew better with his advices and criticism during our group seminars and discussions. His patience and support helped me to finish my thesis successfully. Under his tutelage, I grew into an able researcher.

I am also grateful to the DFG-Graduiertenkolleg-828, "Micro-Macro-Interactions in Structured Media and Particle Systems", Otto-von-Guericke Universität Magdeburg for the financial support all through this PhD program.

I would like to express my sincere and deep gratitude to Dr. Jitendra Kumar. His advice and encouragement during the course of my research has been great help. The numerical discussions with him helped me to implement the matlab codes efficiently.

At the department of Chemical Process Engineering, I am thankful to Prof. Jürgen Tomas for giving me an opportunity to work in an interdisciplinary project.

I am thankful to the assistance of all members of the Institute of Analysis and Numerics, especially Dr. Walfred Grambow and Stephanie Wernicke. I deeply appreciate the fruitful discussions with my close friends Ankik and Vincent.

To all my friends in Magdeburg and in India who provided support and encouragement to me during my stay here. I am overwhelmingly grateful to all of them: Yashodhan, Ashwini, Ankik, Mini, Vincent, James, Vikrant, Bala, Thiru, Sashi, Sangeeta, Anita, Prabhat, Pankaj and Ravi. I would also like to thank Maxim at TU Eindhoven for the same.

To my very special friend Ankik and Yashodhan, I will always remember the evening walk, the time we spent together after dinner near the library. Our long evenings playing table tennis will always be memorable. I am also obliged to Chetna bhabhi and her delicious food and encouragement. The sheer joy I had while I spent my time with Babu Mahika will always remain with me.

At Indian Institute of Technology Roorkee, I am indebted to Prof. Ramesh Chand Mittal who helped me to get the position in Eramus Mundus program for pursuing my Master studies. I also thank Mr. Rajesh Jha, my school teacher to whom I owe my knowledge of and love for Mathematics.

I am deeply grateful to my wife, Smita for her patience and understanding especially during the last period of my work. I also must thank my in-laws for their warmth and affection. Most importantly, I am eternally obliged to my family Maa-Papaji, brother Rajeev, all sisters, brother-in-laws and their kids in India for their moral support and unconditional love without which this work could not be completed.

Last but not the least, my heartly thanks to my Khatti Meethi for her care, affection and love. Her inspiration and belief in me drove me this far and made me realize who I am. You are so precious and lovable to me and will always be close to my heart.

Abstract

This thesis describes the numerical analysis of finite volume schemes for population balance equations in particulate processes, incorporating aggregation, breakage, growth and source terms. These equations are a type of partial integro-differential equations. Such equations can be solved analytically only for some specific aggregation and breakage kernels. This motivates us to study numerical schemes and the numerical analysis for these equations.

Several mathematical results are available on the existence of weak solutions for the aggregation-breakage equations with different classes of aggregation and breakage kernels. Recently, Bourgade and Filbet [7] have investigated the convergence of finite volume approximated solutions towards weak solutions of the continuous binary aggregation-breakage equations under the assumptions of local boundedness of the kernels. Furthermore, they have shown a first order error estimate only on uniform meshes with more restricted kernels. However, the case of multiple fragmentation and error analysis on general meshes were not discussed. A similar approach is also suitable to show the convergence of the finite volume discretized solutions towards weak solution of the continuous equations when multiple breakage is taken into account. This is the first aim of our work.

The second aim is to study the convergence analysis of a finite volume method for the aggregation and multiple breakage equations on five different types of uniform and non-uniform meshes. We observe that the scheme is second order convergent independently of the grids for the pure breakage problem. Moreover, for pure aggregation as well as for combined equations the technique shows second order convergence only on uniform, non-uniform smooth and locally uniform meshes. In addition, we find only first order convergence on oscillatory and random grids.

A numerical scheme is said to be moment preserving if it correctly reproduces the time behaviour of a given moment. Some authors have proposed different numerical methods which show moment preservation numerically with respect to the total number or total mass for an individual process of aggregation, breakage, growth and source terms. However, coupling of all the processes causes no preservation for any moments. Up to now, there was no mathematical proof which gives the conditions under which a numerical scheme is moment preserving or not. The third aim of this work is to study the criteria for the preservation of different moments. Based on this criteria we determine zeroth and first moments preserving conditions for each process separately. Further, we propose one moment and two moment preserving finite volume schemes for all the coupled processes. We analytically and numerically verify the moment preserving results. The numerical verifications are made for several coupled processes for which analytical solutions are available for the moments.

The fixed pivot (FP) method and the cell average technique (CAT) for solving two-dimensional aggregation equations using a rectangular grid were implemented in J. Kumar et al. [44]. Recently, Chakraborty and Kumar [9] have studied the FP scheme for the same problem on two different types of triangular grids. They found that the method shows better results for number density on triangular grids as compared to rectangular grids. However, the discussion of higher moments was ignored. In our work we compare different moments calculated by the

FP technique on rectangular and triangular meshes with the analytical moments. Numerical simulations show that the method does not improve the results for the higher moments. Further we introduce a new mathematical formulation of the CAT for the two different types of triangular grids as considered by Chakraborty and Kumar [9]. The new formulation is simple to implement and gives better accuracy as compared to the rectangular grids. Three different test problems are considered to analyze the accuracy of both schemes by comparing the analytical and numerical solutions. The new formulation shows good agreement with the analytical results both for number density and higher moments.

Finally we state some applications of aggregation-breakage equations in nano-technology. We solve the equations using the cell average technique and compare the simulation results with the experimental data by using a shear aggregation kernel together with two different breakage kernels.

Zusammenfassung

Diese Doktorarbeit beschreibt die numerische Analysis von Finite-Volumen-Methoden für Populationsbilanzgleichungen in Partikelprozessen, die Aggregation, Bruch, Wachstum und Quellterme einbeziehen. Diese Gleichungen sind eine Art von partiellen Integro-Differentialgleichungen. Solche Gleichungen können nur für einige spezielle Aggregations- und Bruchkerne analytisch gelöst werden. Dies motiviert uns, numerische Verfahren und die numerische Analysis für diese Gleichungen zu studieren.

Es gibt mehrere mathematische Ergebnisse zur Existenz von schwachen Lösungen für die Aggregations-Bruch-Gleichungen mit verschiedenen Klassen von Aggregations- und Bruchkernen. Vor kurzem untersuchten Bourgade und Filbet [7] die Konvergenz von Finite-Volumen-approximierten Lösungen gegen schwache Lösungen der kontinuierlichen binären Aggregations-Bruch-Gleichungen unter der Annahme der lokalen Beschränktheit der Kerne. Weiterhin haben sie nur Fehlerabschätzungen erster Ordnung auf gleichmässigen Gittern mit eingeschränkteren Kernen gezeigt. Allerdings wurden der Fall multipler Fragmentation und die Fehleranalyse auf allgemeinen Gittern nicht diskutiert. Ein ähnlicher Ansatz ist auch geeignet, um die Konvergenz von Finite-Volumen-diskretisierten Lösungen gegen eine schwache Lösung des kontinuierlichen Gleichungen zu zeigen, wenn multipler Bruch in Betracht gezogen wird. Dies ist das erste Ziel dieser Arbeit.

Das zweite Ziel ist es, die Konvergenzanalyse des Finite-Volumen-Methode für die Aggregations- und multiplen Bruchgleichungen auf fünf verschiedenen Arten von gleichmässigen und ungleichmässigen Gittern zu studieren. Wir stellen fest, dass das Schema von zweiter Ordnung konvergent ist, unabhängig vom Gitter für das reine Bruchproblem. Darüber hinaus zeigt sich sowohl für reine Aggregations als auch für kombinierte Gleichungen Konvergenz zweiter Ordnung nur auf gleichmässigen, ungleichmässigen glatten und lokal gleichmässigen Gittern. Zudem haben wir Konvergenz nur erster Ordnung auf oszillierenden und zufälligen Gittern.

Ein numerisches Verfahren wird als Momente-erhaltend bezeichnet, falls es das zeitliche Verhalten eines gegebenen Momentes korrekt wiedergibt. Einige Autoren haben verschiedene numerische Methoden vorgeschlagen, die die Momenteerhaltung numerisch zeigen bezüglich der Gesamtanzahl oder Gesamtmasse für einen einzelnen Prozess der Aggregation, Bruch, Wachstum und Quellterme. Allerdings verursacht die Kopplung aller Prozesse keine Erhaltung irgendwelcher Momente. Bis jetzt gab es keinen mathematischen Beweis, der die Bedingungen angibt, unter denen ein numerisches Schema dann Momente-erhaltend ist oder nicht. Das dritte Ziel dieser Arbeit ist es, die Kriterien für die Erhaltung der verschiedenen Momente zu studieren. Auf der Grundlage dieser Kriterien bestimmen wir für jeden Prozess Bedingungen, unter denen das nullte und erste Moment erhalten bleiben. Ferner schlagen wir Finite-Volumen-Schemen für alle gekoppelten Prozesse vor, die ein Moment oder zwei Momente erhalten. Wir überprüfen die Momente-erhaltenden Resultate analytisch und numerisch. Die numerischen Überprüfungen werden für mehrere gekoppelte Prozesse ausgeführt, für die analytische Lösungen der Momente verfügbar sind.

Die Fixed-Pivot (FP)-Methode und die Cell-Average-Technik (CAT) für des Lösen von zweidimensionalen Aggregationsgleichungen unter Verwendung von einen rechteckigen Gitter wurde

in J. Kumar et al. [44] umgesetzt. Kürzlich untersuchten Chakraborty und Kumar [9] das FP-Schema für das gleiche Problem auf zwei verschiedenen Arten von Dreiecksgittern. Sie fanden heraus, dass die Methode bessere Ergebnisse für die Anzahldichte liefert auf Dreiecksgittern verglichen mit Rechteckgittern. Allerdings wurde die Diskussion von höheren Momenten ignoriert. In unserer Arbeit vergleichen wir verschiedene Momente, die durch die FP-Technik auf Rechtecks- und Dreiecksgittern berechnet wurden, mit analytischen Momenten. Numerische Simulationen zeigen, dass die Methode die Resultate für höhere Momente nicht verbessert. Des Weiteren führen wir eine neue mathematische Formulierung der CAT ein für die beiden verschiedenen Arten von Dreiecksgittern, die von Chakraborty und Kumar [9] betrachtet werden. Die neue Formulierung ist einfach zu implementieren und liefert eine bessere Genauigkeit verglichen mit den Rechteckgittern. Es werden drei verschiedene Testprobleme betrachtet, um die Genauigkeit beider Schemata durch der Vergleich der analytischen und numerischen Lösungen zu analysieren. Die neue Formulierung zeigt eine gute Übereinstimmung mit den analytischen Ergebnissen sowohl für die Anzahldichte als auch für höhere Momente.

Schliesslich stellen wir einige Anwendungen von Aggregations-Bruch-Gleichungen in der Nano-Technologie vor. Wir lösen die Gleichungen unter Verwendung der Cell-Average-Methode und vergleichen die Simulationsergebnisse mit den experimentellen Daten mit Hilfe eines Scher-Aggregationskernes zusammen mit zwei verschiedenen Bruchkernen.

Contents

Nomenclature

Latin Symbol

a_1, a_2, a_3, a_4	Fraction of particles	$-$
b	Breakage function	m^{-3}
B	Birth rate	$m^{-6} \cdot s^{-1}$
C	Constant	$-$
D	Death rate	$m^{-6} \cdot s^{-1}$
E	Error	$-$
F	Mass flux	s^{-1}
g	Volume density function	$-$
H	Heaviside function	$-$
I	Total number of cells	$-$
I_{agg}	Degree of aggregation	$-$
J	Numerical mass flux	$1/s$
f, n	Number density function	m^{-6}
N	Number	m^{-3}
N_0	Initial number of particles	m^{-3}
S	Selection function	s^{-1}
t	Time	s
u, v, x	Volume of particles	m^3
$\bar{v}$	Average volume	m^3
v_0, x_0	Initial mean volume	m^3

Greek Symbols

α	Integer	$-$
β	Aggregation kernel	$m^3 s^{-1}$
$\delta(x)$	Dirac-delta distribution	$-$
δ_{ij}	Kronecker delta	$-$
Δx	Size of a cell	$-$
ϵ	Global truncation error	$-$
λ	Fractions	$-$
Λ	Discretized domain	$-$
μ_r	The rth moment	$m^{3r} \cdot m^{-3}$

ν	Parameter in Gaussian-like distribution	–
σ	Spatial truncation error	–

Subscripts

agg	Aggregation
brk	Breakage
i, j	Index
nuc	Nucleation
src	Source
grt	Growth

Acronyms

CAT	Cell Average Technique
DPBE	Discretized Population Balance Equation
EOC	Experimental Order of Convergence
FP	Fixed Pivot
ODE	Ordinary Differential Equation
PBE	Population Balance Equation
PPD	Particle Property Distribution
PSD	Particle Size Distribution

Chapter 1

Introduction

In this chapter a general introduction about the population balance equations is given. In particular, we study the equations of aggregation or coagulation, breakage or fragmentation, growth and source terms. Then we discuss the existing results and the issues which were not discussed in the previous work. Followed by each such issue we describe the new results provided in this thesis. At the end the outline of the thesis is summarized.

1.1 Population balance equations

This thesis deals with numerical analysis and computations for population balance equations used for particulate processes. These processes are well-known in various branches of engineering and science such as nano-technology, crystallization, precipitation, polymerization, aerosol dynamics and emulsion processes. These processes are characterized by the presence of a continuous phase and a dispersed phase composed of particles with a distribution of properties. The particles might be crystals, grains, drops or bubbles and may have several properties such as size, composition, porosity or enthalpy. However in this work we consider the size (volume) as the only relevant particle property.

The particles may change their properties in a system due to various physical influences. The major part of the current work deals with the aggregation and breakage processes which affect the particle size distributions. However, we also study the case of growth and nucleation or others described by source terms. Aggregation is a process where two or more particles combine together to form a larger particle. When they merge into a single homogeneous particle, as with droplets, this process is also called coagulation. On the other hand, in a fragmentation process particles break into two or more fragments. In a growth process, the particles grow when molecular matter is added to the surface of a particle. The size of a particle increases continuously in this process. The formation of a new particle by condensation or crystallization is called nucleation. The nuclei are usually treated as the smallest possible particles modeled in the system and may be introduced via a source term. Harvesting of a certain particle size could be modeled by a negative source term.

As a result of particle formation mechanisms particles change their properties and therefore a mathematical model named *population balance* is frequently used to describe the changes of

particle properties. Population balances describe the dynamic evolution of the particle number distribution of one or more properties. Population balances are partial integro-differential equations.

By using the basic assumption that two particles combine at a time, Smoluchowski [99] has proposed the following infinite set of nonlinear differential equations for coagulation in 1917

$$\frac{\partial f_i(t)}{\partial t} = \frac{1}{2}\sum_{j=1}^{i-1} \beta_{i-j,j} f_{i-j}(t) f_j(t) - f_i(t) \sum_{j=1}^{\infty} \beta_{i,j} f_j(t). \tag{1.1}$$

Here, the unknown non-negative function $f_i(t)$ with mass i, $i \geq 1$ are the densities of particles of discrete size i at time t. The function $\beta_{i,j}$ is known as coagulation kernel which describes the intensity of interaction between particles of mass i and j. It is non-negative and symmetric, i.e. $\beta_{i,j} \geq 0$ and $\beta_{i,j} = \beta_{j,i}$ for all $i, j \geq 1$. All physical properties of the process are included in the kernel $\beta_{i,j}$. Later in 1928, Müller [79] rewrote the equation (1.1) to the continuous form which is an integro-differential equation for the time evolution of the particle mass density function. If $f(t,x)$ is the particle mass density function with mass $x > 0$ and time $t \geq 0$ then the equation is defined as

$$\frac{\partial f(t,x)}{\partial t} = \frac{1}{2}\int_0^x \beta(x-y,y) f(t,x-y) f(t,y) dy - f(t,x) \int_0^{\infty} \beta(x,y) f(t,y) dy. \tag{1.2}$$

The aggregation kernel $\beta(x,y)$ is introduced by assuming that the average number of coalescence between particles of mass x and those of mass y is $f(t,x)f(t,y)\beta(x,y)$ during at time t. The first term on the right-hand side of the equation (1.2) describes the creation of particles of size x when two particles of masses $x-y$ and y collide. The second integral shows the disappearance of particles of size x after colliding with any particles of size y. Therefore, these two terms are known as the birth and the death terms, respectively. The term $\frac{1}{2}$ is coming into the equation to avoid the double counting. Similar to the discrete case, the aggregation kernel $\beta(x,y)$ is non-negative and symmetric, i.e. $\beta(x,y) \geq 0$ and $\beta(x,y) = \beta(y,x)$.

Further Melzak [76] in 1957 extended this binary aggregation model together with multiple fragmentation equation where a particle splits into more than two small pieces at a time. He introduced the following equation

$$\begin{aligned}\frac{\partial f(t,x)}{\partial t} = \frac{1}{2}\int_0^x \beta(x-y,y) f(t,x-y) f(t,y) dy - f(t,x) \int_0^{\infty} \beta(x,y) f(t,y) dy \\ + \int_x^{\infty} \Gamma(y,x) f(t,y) dy - \frac{f(t,x)}{x} \int_0^x y\Gamma(x,y) dy.\end{aligned} \tag{1.3}$$

The third integral in the above equation describes the formation of particles of size x when particles of size y with $x \leq y < \infty$ breaks. The fourth term reflects disappearance of particles x due to their fragmentation into smaller particles of size y with $0 \leq y \leq x$. The multiple breakage kernel $\Gamma(x,y) \geq 0$ is again introduced with the assumption that $f(t,x)\Gamma(x,y)$ is the average number of particles of mass y created from the breakage of particles of mass x at time t. Hence, we take $\Gamma(x,y) = 0$ if $x < y$. If the breakage kernel Γ satisfies the condition $\Gamma(x,y) = \Gamma(x,x-y)$, the multiple breakage equation turns into the *binary breakage equation*. This implies that the model allows breaking of particles only into two smaller pieces at a time.

This way we have the following form of the breakage equation given by Friedlander [25] in 1960 as

$$\frac{\partial f(t,x)}{\partial t} = \int_0^\infty \widetilde{F}(x,y) f(t,x+y) dy - \frac{f(t,x)}{2} \int_0^x \widetilde{F}(x-y,y) dy. \tag{1.4}$$

The term $\widetilde{F} \geq 0$ is the binary fragmentation kernel and is related to the multiple breakage kernel Γ by $\widetilde{F}(x-y,y) = \Gamma(x,y)$. It should be mentioned that the fragmentation kernel $\widetilde{F}$ is symmetric, i.e.

$$\widetilde{F}(x,y) = \Gamma(x+y,y) = \Gamma(x+y,x) = \widetilde{F}(y,x)$$

unlike the multiple breakage kernel $\Gamma(x,y)$.

As a special case for binary aggregation and binary breakage, Becker and Döring [5] introduced a discrete model in 1935. In this model, they assumed that the particles can combine to form larger particle or break to form smaller ones by an addition or loss of a particle of mass 1, respectively. This equation reads

$$\frac{\partial f_i(t)}{\partial t} = J_{i-1}(f) - J_i(f), \quad 2 \leq i < \infty \tag{1.5}$$

where $J_i(n) = a_i f_1 f_i - b_{i+1} f_{i+1}$ for $i \geq 1$ and a_i, b_i being coagulation and breakage coefficients, respectively. Becker and Döring's model was adjusted in such a way that a stationary state is achieved. In this state the number of monomers, i.e. particles of size 1 becomes measurable and therefore, no evaluation is needed for $f_1(t)$. However, later in 1977, J. Burton [8] reconsidered the Becker and Döring process as

$$\frac{\partial f_i(t)}{\partial t} = J_{i-1}(f) - J_i(f), \quad 2 \leq i < \infty \tag{1.6}$$

together with

$$\frac{\partial f_1(t)}{\partial t} = -J_1(f) - \sum_{i=1}^{\infty} J_i(f). \tag{1.7}$$

Though this new model is also known as Becker and Döring model, the difference between these two models is that the later one satisfies the total mass conservation.

In 1991 Ziff [102] gave another form of the multiple breakage equation by taking

$$\Gamma(y,x) = b(x,y) S(y) \quad \text{and} \quad S(x) = \int_0^x \frac{y}{x} \Gamma(x,y) dy. \tag{1.8}$$

Here, the term $S(x)$ is called the selection function which describes the rate at which particles of size x are selected to break. The breakage function $b(x,y)$ for a given $y > 0$ gives the size distribution of particle sizes $x \in]0,y[$ resulting from the breakage of a particle of size y. The breakage function has the following important properties

$$\int_0^y b(x,y) dx = \overline{N}(y) \quad \text{and} \quad \int_0^y x b(x,y) dx = y, \tag{1.9}$$

for any $y \in]0, \infty[$. The function $\overline{N}(y)$, which may be infinite, represents the number of fragments obtained from the breakage of a particle of size y. The second integral ensures the property that the total mass created from the breakage of a particle of size y is again y.

By extension of the binary aggregation [99] and multiple breakage [102], if we include growth [54, 42] and nucleation [54] or other sources, the general form of the population balance equation is given as

$$\begin{aligned}\frac{\partial f(t,x)}{\partial t} =& \frac{1}{2}\int_0^x \beta(x-y,y)f(t,x-y)f(t,y)dy - \int_0^\infty \beta(x,y)f(t,y)f(t,x)dy \\ &+ \int_x^\infty b(x,y)S(y)f(t,y)dy - S(x)f(t,x) - \frac{\partial[G(x)f(t,x)]}{\partial x} + B_{\text{src}}(t,x). \end{aligned} \tag{1.10}$$

The fifth term on the right-hand side represents particle growth process with a growth rate G. The source term is given by the last term $B_{\text{src}}(t,x)$ where the abbreviation src stands for source. The remaining terms were already explained above. In the case of binary fragmentation $b(x,y) = b(y-x,y)$ and by using the relation (1.9), it is easy to show that the number of fragments produced in the process is 2, i.e.

$$\begin{aligned}\int_0^y b(x,y)dx =& \frac{1}{y}\int_0^y xb(x,y)dx + \frac{1}{y}\int_0^y (y-x)b(x,y)dx \\ =& \frac{1}{y}\int_0^y xb(x,y)dx + \frac{1}{y}\int_0^y (y-x)b(y-x,y)dx = \frac{2}{y}\int_0^y xb(x,y)dx = 2.\end{aligned}$$

Besides the information given by the evolution of the particle number density distribution, some integral properties of the distribution like moments are also of great interest in various applications. The jth moment of the particle size distribution is defined as

$$\mu_j(t) = \int_0^\infty x^j f(t,x)dx. \tag{1.11}$$

The first two moments are of special interest. The zeroth ($j = 0$) and first ($j = 1$) moments are proportional to the total number and total mass of particles respectively. Furthermore, the second moment is proportional to the light scattered by particles in the Rayleigh limit [53, p. 1325], [91, p. 267] in some applications. It is easy to show that the total number of particles $\mu_0(t)$ is an increasing function for the aggregation process and a decreasing function for the breakage events, while the total mass $\mu_1(t)$ should not vary during these two processes. For the total mass conservation

$$\int_0^\infty xf(t,x)\,dx = \int_0^\infty xf(0,x)\,dx, \quad t \geq 0, \tag{1.12}$$

holds. Surprisingly, this depends on the aggregation and breakage kernels and is not always true.

For some special class of kernels when the aggregation kernel β is sufficiently large enough compared to the breakage kernel F or selection function S, a phenomenon called gelation occurs. In this case the total mass of the particles is not conserved but decreasing after a certain point of time. Drake, Leyvraz, Jeon and Escobedo have studied the gelation process in [14, 66, 65, 36,

21, 20]. Several researchers have shown that for the pure aggregation equation the conservation of total mass holds true for $\beta(x,y) = (xy)^{\alpha}$ with $\alpha \in [0, 1/2]$ and breaks down in finite time when $\alpha \in]1/2, 1]$. A detailed description can be found in Leyvraz and Tschudi [66], Leyvraz [65] as well as in further citations. If we include the breakage process, the class of aggregation kernels can be extended for the conservation of total mass, see Escobedo et al. [21, 20].

However, in most cases of the aggregation-breakage process mass conservation holds and the mass density function xf is the conservative variable. Therefore, one can also rewrite the equation in a conservative form of mass density $xf(t,x)$ as

$$\frac{\partial\left[xf(t,x)\right]}{\partial t} + \frac{\partial}{\partial x}\left(F^{\mathrm{agg}}(t,x) + F^{\mathrm{brk}}(t,x)\right) = 0. \tag{1.13}$$

The abbreviations *agg* and *brk* are used for aggregation and breakage terms respectively. The flux functions F^{agg} and F^{brk} are given by

$$F^{\mathrm{agg}}(t,x) = \int_0^x \int_{x-u}^{\infty} u\beta(u,v)f(t,u)f(t,v)dvdu, \tag{1.14}$$

and

$$F^{\mathrm{brk}}(t,x) = -\int_x^{\infty} \int_0^x ub(u,v)S(v)f(t,v)dudv. \tag{1.15}$$

The flux formulation (1.15) is given for the multiple breakage equation. For the case of binary breakage problem, the flux function is defined as

$$F^{\mathrm{brk}}(t,x) = -\int_0^x \int_{x-u}^{\infty} u\widetilde{F}(u,v)f(t,u+v)dvdu. \tag{1.16}$$

It should be mentioned that in our work we only deal with the multiple breakage equation. Details about conservative formulations of aggregation and breakage can be found in Tanaka et al. [95], Makino et al. [72] and J. Kumar [42], respectively. Note that both forms of aggregation-breakage population balance equations (1.10) without growth and source terms and (1.13) are interchangeable by using Leibniz integration rule. Therefore, in this thesis we use both forms depending upon their convenience for calculations. The equivalence between the equations (1.10) and (1.13) is used due to

$$-\frac{1}{x}\frac{\partial}{\partial x}F^{\mathrm{agg}}(t,x) = \frac{1}{2}\int_0^x \beta(x-y,y)f(t,x-y)f(t,y)dy - \int_0^{\infty} \beta(x,y)f(t,y)f(t,x)dy, \tag{1.17}$$

and

$$-\frac{1}{x}\frac{\partial}{\partial x}F^{\mathrm{brk}}(t,x) = \int_x^{\infty} b(x,y)S(y)f(t,y)dy - S(x)f(t,x). \tag{1.18}$$

Here, we emphasize that in the equation (1.10) the growth process has no effect on the number of particles but the total mass of the particles increases. Hence, if we neglect aggregation, breakage and source terms in the equation (1.10) then we are left with a conservative differential equation for the number density function f. In case of pure nucleation, i.e. $\beta, S, G = 0$ in the equation (1.10), neither number density nor the total mass remains conserved.

Mathematical results on existence and uniqueness of solutions of the equation (1.10) and further citations can be found in McLaughlin et al. [75] and W. Lamb [56] for rather general aggregation kernels, breakage and selection functions. The population balance equations (PBEs) (1.10) can only be solved analytically for a limited number of simplified problems, see Ziff [102], Dubovskii et al. [15] and the references therein. This certainly leads to the necessity of using numerical methods for solving general PBEs. Several numerical techniques including the method of successive approximations [87], the method of moments [3, 70, 73], the finite element methods [71, 81, 88], Monte Carlo simulation methods [41, 61, 67, 92] and sectional methods [43, 53, 98] can be found in the literature to solve such PBEs.

Finite volume schemes are frequently used for solving conservation laws, see for example LeVeque [64]. Bennett and Rohani [6] as well as Motz et al. [78] implemented this method to solve the growth and some source terms. However, Filbet and Laurençot [23] were the first to apply this approach for solving aggregation PBEs by discretizing a well-known mass balance formulation (1.13) with $F^{\text{brk}} = 0$. Further, Bourgade and Filbet [7] have extended their scheme to solve the case of aggregation and binary breakage PBEs. Later the scheme has been applied to solve the aggregation and multiple fragmentation equation (1.13) by J. Kumar et al. [48]. The scheme has also been extended to two-dimensional aggregation problems by Qamar and Warnecke [84]. Finally it has been observed that the finite volume scheme is a good alternative to the methods mentioned above for solving the aggregation-breakage equations due to its automatic mass conservation property.

1.2 Existing and new results

In this section we summarize the existing results and briefly highlight our new findings in the theory of numerical solutions of the population balance equations. Our emphasis will be on the numerical analysis of finite volume schemes (FVS) for the aggregation-breakage equations. In particular, we study a finite volume method to solve the multiple fragmentation equations. Furthermore, convergence analysis of the scheme is investigated for such non-linear coagulation-fragmentation equations. In addition, we discuss analytically and numerically the question, "why are certain numerical schemes one moment only or two moments preserving for the coupled aggregation, breakage, growth and source terms?". Thereafter, a small improvement is made in the implementation of the sectional methods for the two-component aggregation problem. Finally, we explain the applications of aggregation-breakage models in nano-technology. Now we give a short description of the new findings mentioned above.

Finite volume scheme for multiple breakage

Several researchers showed the existence of weak solutions for the aggregation-breakage equations with non-increasing mass for a large class of aggregation and fragmentation kernels, see Laurençot [57, 59] and the references therein. Some authors also explained the relationship between discrete and continuous models. For instance, Ziff and McGrady [103] found this relationship for constant and sum breakage kernels while Laurençot and Mischler [59] gave results for the aggregation-breakage models under more general assumptions on the kernels, i.e. for bilinear growth. In the literature, there are various ways to approximate the continuous aggregation-breakage equations. For example, deterministic method [19, 62], Monte Carlo method [30, 18]

and further citations. Recently, Bourgade and Filbet [7] have used a finite volume approximation for the binary aggregation-breakage model (1.13) with the binary breakage flux (1.16). They gave the convergence result of the numerical solutions towards a weak solution of the continuous equation by considering locally bounded kernels, i.e.

$$\beta, \widetilde{F} \in L^{\infty}_{\text{loc}}([0,\infty[\times[0,\infty[).$$

Further, they also provided the first order error estimates between the numerical approximated and weak solutions of the continuous problem by assuming

$$\beta, \widetilde{F} \in W^{1,\infty}_{\text{loc}}(]0,\infty[\times]0,\infty[)$$

on uniform meshes.

Here, our aim in Chapter 2 is to study the finite volume schemes for the multiple fragmentation equations. The analysis of the aggregation process can be taken from the work in Bourgade and Filbet [7] and combined with our work to get the result for the coupled processes. The proof is based on a weak L^1 compactness method and the La Vallée Poussin theorem.

Convergence analysis of the finite volume scheme

As mentioned in the previous subsection, Bourgade and Filbet [7] studied the convergence of a finite volume numerical solution towards a weak solution of the continuous binary aggregation-breakage models on uniform meshes and proved first order accuracy. However, the convergence analysis for aggregation with multiple breakage equation on general meshes was still missing in the literature. In our further work in Chapter 3 we investigate the convergence analysis between the exact and numerical solutions of the truncated coupled problem using the FVS. In particular, we discuss the convergence analysis of the finite volume schemes for the non-linear aggregation problem given by Filbet and Laurençot [23] and multiple breakage equation introduced by J. Kumar [42]. The proof is based on some basic results from the book of Hundsdorfer and Verwer [33] and from the paper of Linz [68]. By using these existing results, we study the consistency first and then proceed further to find the Lipschitz conditions on numerical fluxes to get the convergence of the schemes for a family of meshes. The analysis has been made for two times smooth functions β, S and b.

We determine that the technique is second order consistent and convergent independently of the meshes for the pure breakage problem. Non-linearity of the aggregation process causes difficulties to check the consistency on general meshes. Therefore, in this case we evaluate the consistency order on four different types of meshes separately. Finally, the analysis shows that the scheme is second order consistent and convergent only on uniform and non-uniform smooth meshes. In addition the method is only first order consistent and convergent on oscillatory and non-uniform random meshes. Furthermore, for the coupled problem the scheme is again second order accurate on uniform and non-uniform smooth grids while on the other two types of grids it is of first order. The mathematical results of the convergence analysis are also verified numerically by taking several numerical examples of pure aggregation, pure breakage and combined processes on five different types of uniform and non-uniform grids.

Moment preserving finite volume schemes for coupled processes

As stated before the moments defined in equation (1.11) are very important in many applications, especially the zeroth moment and the first moment. Here, the term moment preservation implies that we are interested to find the numerical schemes which reproduce the correct time behavior of moments that are not conserved. There are several numerical methods which are in good agreement with the analytical moments for an individual process. In particular, the finite volume scheme is a promising method to predict the first moment, i.e. mass, for the coupled aggregation-breakage equation due to its automatic mass conservation property. For details the reader is referred to Filbet and Laurençot [23] for the pure aggregation problem and J. Kumar et al. [42, 48] for the coupled problems. Furthermore, the upwind scheme has been implemented for pure growth problems which automatically satisfies the zeroth moment, i.e. total number, conservation [42]. Kumar and Ramkrishna [54] used a natural discretization for nucleation terms which gives exactly the analytical solution for the zeroth moment.

Coupling of these particulate processes is also of interest in various applications. In coupling corresponding numerical discretizations it is important to understand which moments are preserved by the coupled scheme. Recently, Kumar and Warnecke [47] have proposed two formulations; one is a combination of FVS and method of characteristic and the other is a FVS to solve a coupled aggregation-growth problem. These formulations are shown to be number and mass preserving numerically. However, in the literature, there is no mathematical proof available to explain why certain numerical schemes are better to preserve the number or mass for the coupled problems.

In our work we present some moment preserving finite volume schemes for solving coupled aggregation, breakage, growth and source terms. For this we first introduce the definition of moment preservation as a new concept. Based upon this definition the zeroth and the first moment preserving conditions are obtained for each process separately. Later, we present a finite volume scheme which shows the preservation with respect to one moment depending upon the processes under consideration. In case of aggregation and breakage it satisfies first moment preservation whereas for the growth and source terms we observe zeroth moment preservation. This is due to the well-known property of conservativity of finite volume schemes. However, coupling of all the processes shows no preservation for any moments. To overcome this issue, we reformulate the cell average technique [42, 45, 43] into a conservative formulation which is coupled together with a modified upwind scheme to give moment preservation with respect to the first two moments for all four processes under consideration. This allows for easy coupling of these processes. The moment preservation is proved mathematically and verified numerically. The numerical results for the zeroth and the first moments are verified for various coupled processes where analytical solutions are available.

Two-dimensional aggregation problems

Numerical solution of the two-component aggregation population balance equation is difficult due to the double integral and the non-linearity of the equation. The sectional methods, in particular the cell average technique (CAT) and the fixed pivot (FP) method, are better numerical approaches over the classical schemes due to preservation of important properties of the distribution. In addition, these methods are computationally inexpensive. These schemes have already

been implemented for the bi-component aggregation problem and the results were compared for a rectangular grid, see J. Kumar et al. [44]. Recently, Chakraborty and Kumar [9] have studied the FP scheme for the same problem and determined numerical results for number density on two different triangular grids. Such triangular meshes were obtained by considering rectangular grid as a starting point. They found better accuracy for number density on triangular grids as compared to rectangular meshes. However, they did not compare the results for different higher moments yet we know from Kostoglou and Karabelas [40] that improvement of the numerical results for number density does not imply improvement of the moments of the distributions.

Therefore, we investigate different higher moments by using the FP method on rectangular and triangular meshes and compare the results with the analytical moments. In this case we observe that changing the grid does not improve the results for higher moments. But the main novelty of our work is to discuss the CAT on two different types of triangular grids as considered by Chakraborty and Kumar [9] and then compare the results between rectangular and triangular grids. The triangular formulation is simple to implement and shows good agreement with the analytical results both for number density and higher moments as compared to the rectangular grids. For the numerical verification, three different test problems are considered.

Applications in nano-technology

Finally we discuss some applications of the aggregation-breakage equations in nano-technology. This work has been done in colloboration with the Chemical Engineering Department at OVGU Magdeburg. Titanium dioxide (TiO_2) is one of the most useful oxide materials, because of its widespread applications in photocatalysis, solar energy conversion, sensors and optoelectronics. Controlling particle size of TiO_2 nanoparticles is a challenging task which is of crucial importance from a fundamental and an industrial point of view. We use the breakage equation to predict the particle size distributions of TiO_2. Moreover, in some cases this distribution gets disturbed by the shear rate too. Therefore, we need to model the distributions using the simultaneous aggregation-breakage equations. We solve these equations numerically by using the cell average technique. The simulation results are compared with the experimental data using different aggregation and breakage kernels. It is observed that the experimental data of the particle size distributions at different shear rates of TiO_2 are in good agreement with the numerical results.

1.3 Outline of contents

This thesis is organized as follows. In Chapter 2 we discuss a finite volume scheme for solving multiple breakage equations. Like Bourgade and Filbet [7], we use a weak L^1 compactness method and the La Vallée Poussin theorem to show the convergence of the discretized solutions towards the weak solution of the continuous breakage equations in L^1 space.

Chapter 3 deals with the stability and convergence analysis of the finite volume method for aggregation and multiple breakage equations. We point out that many researchers used this scheme to solve such equations but did not include the error analysis for general grids. The novelty of this work is to find the local and global discretization error on general meshes by using the basic results from Hundsdorfer and Verwer [33] and the paper of Linz [67].

We then proceed to demonstrate the moment preserving numerical techniques for solving coupled aggregation, breakage, growth and source terms in Chapter 4. For instance we investigate one moment and two moment preserving numerical methods for combined problems. The mathematical analysis behind these observations is given and the results are verified numerically for several coupled processes taking various test problems.

Chapter 5 explains the numerical results of two-dimensional aggregation problems by using sectional methods on triangular meshes. These methods have already been implemented on rectangular grids. Here, we compare the numerical simulations between the rectangular and triangular grids by using the cell average and the fixed pivot techniques.

In Chapter 6 we give an overview of applications of aggregation-breakage equations in different engineering problems. In particular we discuss the application in nano-technology and compare the numerical results with experimental data.

Chapter 7 describes general conclusions of this thesis and some open problems are pointed out too.

Finally, we end our work by including some appendices which contain the calculations and some mathematical derivations needed for this thesis. Analytical solutions for the moments for coupled processes are also covered here.

The work in Chapter 3 [50] is submitted while Chapter 4 [51] is under revision in SIAM Journal on Scientific Computing. We have the acceptance of Chapter 5 [52] in Computers and Chemical Engineering Science. Three publications are also submitted from Chapter 6 [28, 29, 49] out of which one is already accepted in Chemical Engineering Science.

Chapter 2

Finite volume scheme for multiple breakage

This chapter deals with the numerical solution using a finite volume scheme for the continuous multiple breakage equation when the breakage and selection functions satisfy some growth conditions. The proof is based on the Dunford-Pettis theorem by using the weak L^1 compactness method. The analysis of the method allows us to prove the convergence of the discretized approximated solution towards a weak solution to the continuous problem in the weighted L^1 space X^+ given by

$$X^+ = \left\{ f \in L^1(\mathbb{R}_{>0}) \cap L^1(\mathbb{R}_{>0}, x\, dx) : f \geq 0, \|f\| < \infty \right\} \quad \text{where} \quad \|f\| = \int_0^\infty (1+x)|f(x)|dx$$

for the non-negative initial condition $f^{in} \in X^+$ and $\mathbb{R}_{>0} =]0, \infty[$. Here the notation $L^1(\mathbb{R}_{>0}, x\, dx)$ stands for the space of the Lebesgue measurable real valued functions on $\mathbb{R}_{>0}$ which are integrable with respect to the measure $x\, dx$. The result we give here is an extension of previous result given by Bourgade and Filbet [7] which deals with aggregation and binary breakage equations. Note that the aggregation part can be added in this work in the same way as discussed by Bourgade and Filbet [7].

The outline of this chapter is as follows. The conservative formulation of the continuous multiple breakage equation, which is needed for further analysis, is discussed in the next section. Section 2.2 gives the numerical approximation of this equation. Finally in Section 2.3 we discuss the convergence of the approximated solution using weak compactness.

2.1 Introduction

We recall from (1.13) that the fragmentation phenomena in the conservative form of mass density are governed by the following equation

$$\frac{x\partial f(t,x)}{\partial t} = \frac{\partial \mathcal{F}(f)}{\partial x}(x), \quad (t,x) \in \mathbb{R}^2_{>0} =]0,\infty[^2 \tag{2.1}$$

where the continuous flux is given as

$$\mathcal{F}(f)(x) := \int_x^\infty \int_0^x ub(u,v)S(v)f(t,v)dudv, \quad x \in \mathbb{R}_{>0}.$$

Given $f^{in} \in X^+$, we consider the initial condition

$$f(0,x) = f^{in}(x), \quad x \in \mathbb{R}_{>0}.$$

The main aim of this work is to present a numerical scheme to solve the equation (2.1) built upon an explicit Euler time discretization with respect to the time variable t and a finite volume discretization with respect to the volume variable x. For the analysis, we have assumed that the multiplicative kernel (product of breakage and selection functions) is locally bounded, i.e. $b\,S \in L^\infty_{\text{loc}}(\mathbb{R}_{>0} \times \mathbb{R}_{>0})$.

2.2 Numerical approximation

The discretization we propose here is to give a mass conservative truncation for the breakage operator: Given a positive real R, it is defined as

$$\mathcal{F}_c^R(f)(x) := \int_x^R \int_0^x ub(u,v)S(v)f(t,v)dudv.$$

Therefore, a conservative formulation for multiple breakage is given by

$$\begin{cases} x\frac{\partial f}{\partial t} = \frac{\partial \mathcal{F}_c^R(f)}{\partial x}(x), & (t,x) \in \mathbb{R}_{>0}\times]0,R]; \\ \\ f(0,x) = f^{in}(x), & x \in]0,R]. \end{cases} \tag{2.2}$$

Mass conservation can easily be seen by integrating equation (2.2) with respect to x from 0 to R.

Now, for the volume discretization of equation (2.2), let $h \in]0,1[$, I^h a positive integer such that $(x_{i-1/2})_{i\in\{0,\dots,\mathrm{I}^h\}}$ is a mesh of $]0,R]$ with the properties

$$x_{-1/2} = 0, \quad x_{\mathrm{I}^h+1/2} = R, \quad x_i = (x_{i-1/2} + x_{i+1/2})/2, \quad \Delta x_i = x_{i+1/2} - x_{i-1/2} \le h$$

and $\Lambda_i^h =]x_{i-1/2}, x_{i+1/2}]$ for $i \ge 0$. For the time discretization, let us assume that Δt denotes the time step such that $N\Delta t = T$ for a large positive integer N and $[0,T]$ is the time domain where we study the equation. We define the time interval

$$\tau_n = [t_n, t_{n+1}[$$

with $t_n = n\Delta t$, $n \ge 0$.

Now we introduce the finite volume method for the equation. We consider the approximation of $f(t,x)$ for $t \in \tau_n$ and $x \in \Lambda_i^h$ as f_i^n for each integer $i \in \{0,\dots,I^h\}$ and each $n \in \{0,\dots,N-1\}$. For the time being we discretize the selection function $S(x)$ and the breakage function $b(u,x)$ in such a way that $S(x) \approx S^h(x) = S_i$ and $b(u,x) \approx b^h(u,x) = b_{j,i}$ for $x \in \Lambda_i^h$ and $u \in \Lambda_j^h$.

Integrating equation (2.2) with respect to x and t over a cell in space Λ_i^h and time τ_n respectively gives

$$\int_{t_n}^{t_{n+1}} \int_{x_{i-1/2}}^{x_{i+1/2}} \frac{\partial(xf(t,x))}{\partial t} dx\,dt = \int_{t_n}^{t_{n+1}} \int_{x_{i-1/2}}^{x_{i+1/2}} \frac{\partial \mathcal{F}_c^R(f)}{\partial x}(x) dx\,dt.$$

This further implies that

$$\int_{x_{i-1/2}}^{x_{i+1/2}} (xf(t_{n+1},x) - xf(t_n,x))dx = \int_{t_n}^{t_{n+1}} \mathcal{F}_c^R(f(t,x_{i+1/2})) - \mathcal{F}_c^R(f(t,x_{i-1/2}))dt.$$

Finally we obtain the following discretization for the multiple breakage equation

$$x_i f_i^{n+1} = x_i f_i^n + \frac{\Delta t}{\Delta x_i}\left(\mathcal{F}_{i+1/2}^n - \mathcal{F}_{i-1/2}^n\right) \tag{2.3}$$

where $\mathcal{F}_{i+1/2}^n$ is the numerical flux which is an approximation of the continuous flux function $\mathcal{F}_c^R(f)(x)$. It is defined as

$$\begin{aligned}
\mathcal{F}_c^R(f)(x_{i+1/2}) &= \int_{x_{i+1/2}}^{R}\int_0^{x_{i+1/2}} ub(u,v)S(v)f^n(v)du\,dv \\
&= \sum_{j=i+1}^{I^h}\int_{\Lambda_j^h} S(v)f^n(v)\sum_{k=0}^{i}\int_{\Lambda_k^h} ub(u,v)du\,dv \\
&\approx \sum_{j=i+1}^{I^h}\sum_{k=0}^{i} x_k S_j b_{k,j} f_j^n \Delta x_j \Delta x_k = \mathcal{F}_{i+1/2}^n.
\end{aligned} \tag{2.4}$$

The initial condition is taken as

$$f_i^{in} = \frac{1}{\triangle x_i}\int_{\Lambda_i^h} f^{in}(x)dx, \quad i \in \{0,\ldots,I^h\}.$$

The breakage fluxes at the boundaries $x_{-1/2}$ and $x_{I^h+1/2}$ are

$$\mathcal{F}_{-1/2}^n = \mathcal{F}_{\mathrm{I}^h+1/2}^n = 0. \tag{2.5}$$

For time we use the explicit Euler discretization while for the volume variable a finite volume approach is considered, see LeVeque [63] and Eymard et al. [22]. Let us denote the characteristic function $\chi_A(x)$ of a set A such that $\chi_A(x) = 1$ if $x \in A$ or 0 elsewhere. Then we define a function f^h on $[0,T]\times]0,R]$ as

$$f^h(t,x) = \sum_{n=0}^{N-1}\sum_{i=0}^{\mathrm{I}^h} f_i^n\,\chi_{\Lambda_i^h}(x)\,\chi_{\tau_n}(t). \tag{2.6}$$

This implies that the function f^h depends on the time and volume steps and note that

$$f^h(0,\cdot) = \sum_{i=0}^{\mathrm{I}^h} f_i^{in}\chi_{\Lambda_i^h}(\cdot)$$

converges strongly to f^{in} in $L^1]0,R]$ as $h \to 0$. We also define the breakage and selection functions in discrete form as

$$b^h(u,v) = \sum_{j=0}^{\mathrm{I}^h}\sum_{i=0}^{\mathrm{I}^h} b_{i,j}\chi_{\Lambda_i^h}(u)\chi_{\Lambda_j^h}(v) \quad \text{where} \quad b_{i,j} = \frac{1}{\Delta x_i \Delta x_j}\int_{\Lambda_j^h}\int_{\Lambda_i^h} b(u,v)dudv \tag{2.7}$$

and

$$S^h(v) = \sum_{i=0}^{\mathrm{I}^h} S_i \chi_{\Lambda_i^h}(v) \quad \text{where} \quad S_i = \frac{1}{\Delta x_i} \int_{\Lambda_i^h} S(v)dv. \tag{2.8}$$

Such discretization ensures that $\|b^h - b\|_{L^1(]0,R]\times]0,R])} \to 0$ and $\|S^h - S\|_{L^1(]0,R])} \to 0$ as $h \to 0$.

2.3 Convergence of solution

In the following we state our main theorem for the convergence of approximated solutions towards a weak solution of the equation (2.2).

Theorem 2.3.1. *Let the breakage function b and the selection function S be such that $bS \in L^\infty_{loc}(\mathbb{R}_{>0} \times \mathbb{R}_{>0})$ and $f^{in} \in X^+$. We also assume that there exists a constant $\theta > 0$ such that the time step Δt satisfies the stability condition*

$$C(T,R)\Delta t \leq \theta < 1, \tag{2.9}$$

where

$$C(T,R) := \|bS\|_{L^\infty} R. \tag{2.10}$$

Then up to the extraction of a subsequence,

$$f^h \to f \quad in \quad L^\infty(0,T;L^1\,]0,R]),$$

where f is the weak solution to (2.2) on $[0,T]$ with initial data f^{in}. Precisely, the function $f \geq 0$ satisfies

$$\int_0^T \int_0^R x f(t,x) \frac{\partial \varphi}{\partial t}(t,x)dx\,dt + \int_0^R x f^{in}(x)\varphi(0,x)dx = \int_0^T \int_0^R \mathcal{F}_c^R(t,x) \frac{\partial \varphi}{\partial x}(t,x)dx\,dt \tag{2.11}$$

for all continuously differential functions φ compactly supported in $[0,T[\times[0,R]$.

It is clear from this theorem that our main aim is to show that the sequence of functions $(f^h)_{h\in\mathbb{N}}$ converges weakly to a function f in $L^1]0,R]$ as h and Δt go to zero. The proof relies on the following Dunford-Pettis theorem [17] which gives a necessary and sufficient condition for compactness with respect to the weak convergence in L^1.

Theorem 2.3.2. *[17, Theorem 3.2] Let $|\Omega| < \infty$ and $f^h : \Omega \mapsto \mathbb{R}$ be a sequence in $L^1(\Omega)$. Suppose that the sequence $\{f^h\}$ satisfies*

- *$\{f^h\}$ is equibounded in $L^1(\Omega)$, i.e.*

$$\sup \|f^h\|_{L^1(\Omega)} < \infty \tag{2.12}$$

- *$\{f^h\}$ is equiintegrable, iff*

$$\int_\Omega \Phi(|f^h|)dx < \infty \tag{2.13}$$

for some increasing function $\Phi : [0,\infty[\mapsto[0,\infty[$ satisfying

$$\lim_{r\to\infty} \frac{\Phi(r)}{r} \to \infty.$$

Then f^h lies in a weakly compact set in $L^1(\Omega)$ which implies that there exists a subsequence of f^h that converges weakly in $L^1(\Omega)$.

Therefore, in order to prove the Theorem 2.3.1, we must show the equiboundedness and the equiintegrability of the family f^h in L^1 as in (2.12) and (2.13), respectively. In the following proposition, we prove the non-negativity and equiboundedness of the function f^h. For this we use a mid-point approximation of a point x by $X^h(x)$, i.e. $X^h(x) = x_i$ for $x \in \Lambda_i^h$.

Proposition 2.3.3. *Let us assume that the time step Δt satisfies (2.9). Then f^h is a non-negative function satisfying the mass conservation*

$$\int_0^R X^h(x) f^h(t,x)dx = \int_0^R X^h(x) f^h(s,x)dx, \quad 0 \le s \le t \le T$$

and for all $t \in [0,T]$,

$$\int_0^R f^h(t,x)dx \le \|f^{in}\|_{L^1} e^{R\|bS\|_{L^\infty} t}. \tag{2.14}$$

Proof. We prove the non-negativity and equiboundedness of f^h by using induction. We know that at $t = 0$, $f^h(0) \ge 0$ and belongs to $L^1]0,R]$. Assume next that the function $f^h(t^n) \ge 0$ and

$$\int_0^R f^h(t^n,x)dx \le \|f^{in}\|_{L^1} e^{R\|bS\|_{L^\infty} t^n}. \tag{2.15}$$

Now we will prove that $f^h(t^{n+1}) \ge 0$. We do this first for the cell at the boundary which has the index $i = 0$. Note that by (2.4) we have $\mathcal{F}^n_{i\pm 1/2} \ge 0$. Therefore, in this case from the equation (2.3) and by using the flux $\mathcal{F}^n_{-1/2} = 0$, we get

$$x_0 f_0^{n+1} = x_0 f_0^n + \frac{\Delta t}{\Delta x_0} \mathcal{F}^n_{1/2} \ge x_0 f_0^n.$$

Hence we obtain $f_0^{n+1} \ge 0$. Now for $i \ge 1$,

$$x_i f_i^{n+1} = x_i f_i^n + \frac{\Delta t}{\Delta x_i} \Big(\mathcal{F}^n_{i+1/2} - \mathcal{F}^n_{i-1/2} \Big).$$

From the equation (2.4) and the nonnegativity of $f^h(t^n)$, we calculate

$$\begin{aligned}
\frac{\mathcal{F}^n_{i+1/2} - \mathcal{F}^n_{i-1/2}}{\Delta x_i} &= \frac{1}{\Delta x_i} \Bigg[\sum_{j=i+1}^{I^h} \sum_{k=0}^{i} x_k S_j b_{k,j} f_j^n \Delta x_j \Delta x_k - \sum_{j=i}^{I^h} \sum_{k=0}^{i-1} x_k S_j b_{k,j} f_j^n \Delta x_j \Delta x_k \Bigg] \\
&= \frac{1}{\Delta x_i} \Bigg[- \sum_{k=0}^{i-1} x_k S_i b_{k,i} f_i^n \Delta x_i \Delta x_k + \sum_{j=i+1}^{I^h} x_i S_j b_{i,j} f_j^n \Delta x_j \Delta x_i \Bigg] \\
&\ge - \sum_{k=0}^{i-1} x_k S_i b_{k,i} f_i^n \Delta x_k.
\end{aligned} \tag{2.16}$$

Since $k < i$ implies that $x_k < x_i$, we further simplify (2.16) into

$$\begin{aligned}\frac{\mathcal{F}^n_{i+1/2} - \mathcal{F}^n_{i-1/2}}{\Delta x_i} &\geq -\sum_{k=0}^{i-1} x_i S_i b_{k,i} f_i^n \Delta x_k \\ &\geq -\sum_{k=0}^{I^h} (S_i b_{k,i} \Delta x_k) x_i f_i^n.\end{aligned}$$

Therefore, we estimate that

$$x_i f_i^{n+1} \geq \left(1 - \Delta t \sum_{k=0}^{\mathrm{I}^h} S_i b_{k,i} \Delta x_k\right) x_i f_i^n.$$

Finally, using the stability condition (2.9) on the time step Δt and the L^1 estimate (2.15) give

$$f^h(t^{n+1}) \geq 0.$$

Next, the total mass conservation follows by summing (2.3) with respect to i and using (2.5)

$$\sum_{i=0}^{\mathrm{I}^h} \Delta x_i x_i f_i^{n+1} = \sum_{i=0}^{\mathrm{I}^h} \Delta x_i x_i f_i^n + \Delta t \sum_{i=0}^{I^h} \left(\mathcal{F}^n_{i+1/2} - \mathcal{F}^n_{i-1/2}\right) = \sum_{i=0}^{\mathrm{I}^h} \Delta x_i x_i f_i^n.$$

Now, we prove that $f^h(t^{n+1})$ enjoys a similar estimate as (2.15). Multiplying equation (2.3) by $\Delta x_i / x_i$ and taking summation over i yield

$$\sum_{i=0}^{\mathrm{I}^h} \Delta x_i f_i^{n+1} = \sum_{i=0}^{\mathrm{I}^h} \Delta x_i f_i^n + \Delta t \sum_{i=0}^{\mathrm{I}^h} \frac{\mathcal{F}^n_{i+1/2} - \mathcal{F}^n_{i-1/2}}{x_i}.$$

Analogously as for (2.16) we may estimate

$$\sum_{i=0}^{\mathrm{I}^h} \frac{\mathcal{F}^n_{i+1/2} - \mathcal{F}^n_{i-1/2}}{x_i} \leq \sum_{i=0}^{\mathrm{I}^h} \Delta x_i \sum_{j=i+1}^{\mathrm{I}^h} \Delta x_j S_j b_{i,j} f_j^n \tag{2.17}$$

and therefore

$$\sum_{i=0}^{\mathrm{I}^h} \Delta x_i f_i^{n+1} \leq (1 + R\|bS\|_{L^\infty} \Delta t) \sum_{i=0}^{\mathrm{I}^h} \Delta x_i f_i^n.$$

Finally, using (2.15) at step n and the inequality $1 + x < \exp(x)$ for all $x > 0$ gives

$$\sum_{i=0}^{\mathrm{I}^h} \Delta x_i f_i^{n+1} \leq \|f^{in}\|_{L^1} e^{R\|bS\|_{L^\infty} t^{n+1}}$$

and therefore the result (2.14) follows. □

Next we will prove the equiintegrability for the function f^h. The following property on convex functions, as stated in the La Vallée Poussin theorem [31, Proposition I.1.1], and Lemma 2.3.4 are used to show this result. Since $f^{in} \in L^1\,]0,R]$, hence by the La Vallée Poussin theorem, there exists a convex function $\Phi \geq 0$, continuously differentiable on $\mathbb{R}_{>0}$ with $\Phi(0) = 0$, $\Phi^{'}(0) = 1$ such that $\Phi^{'}$ is concave,

$$\frac{\Phi(r)}{r} \to \infty, \quad \text{as} \quad r \to \infty$$

and

$$\int_0^R \Phi(f^{in})(x)dx < +\infty. \tag{2.18}$$

Lemma 2.3.4. *[58, Lemma B.1.] Let $\Phi \in C^1(\mathbb{R}_{>0})$ be convex such that $\Phi^{'}$ is concave, $\Phi(0) = 0, \Phi^{'}(0) = 1$ and $\Phi(r)/r \to \infty$ as $r \to \infty$. Then for all $(x,y) \in \mathbb{R}_{>0} \times \mathbb{R}_{>0}$,*

$$x\Phi^{'}(y) \leq \Phi(x) + \Phi(y).$$

Now, we are in a position to prove the equiintegrability in the following.

Proposition 2.3.5. *Let $f^{in} \geq 0 \in L^1]0,R]$ and let f^h be defined for all h and Δt by (2.3) where Δt satisfies (2.9). Then the family $(f^h)_{(h,\Delta t)}$ is weakly relatively sequentially compact in $L^1(]0,T[\times]0,R])$.*

Proof. Our aim is to get a similar estimate as (2.18) for the function f^h. We know that the integral of $\Phi(f^h)$ is related to the sequence f_i^n through

$$\begin{aligned}\int_0^T \int_0^R \Phi(f^h(t,x))dx\,dt &= \sum_{n=0}^{N-1}\sum_{i=0}^{\mathrm{I}^h} \int_{\tau_n}\int_{\Lambda_i^h} \Phi\Big(\sum_{k=0}^{N-1}\sum_{j=0}^{\mathrm{I}^h} f_j^k \chi_{\Lambda_j^h}(x)\chi_{\tau_k}(t)\Big)dx\,dt \\ &= \sum_{n=0}^{N-1}\sum_{i=0}^{\mathrm{I}^h} \Delta t \Delta x_i \Phi(f_i^n).\end{aligned}$$

Since Φ is a convex function, we can estimate

$$\left(f_i^{n+1} - f_i^n\right)\Phi^{'}(f_i^{n+1}) \geq \Phi(f_i^{n+1}) - \Phi(f_i^n).$$

Hence, multiplying this equation by Δx_i and taking summation over i on both sides we get

$$\sum_{i=0}^{I^h} \Delta x_i \left[\Phi(f_i^{n+1}) - \Phi(f_i^n)\right] \leq \sum_{i=0}^{I^h} \Delta x_i \left[(f_i^{n+1} - f_i^n)\Phi^{'}(f_i^{n+1})\right].$$

By using the discrete equation (2.3), it can be rewritten as

$$\sum_{i=0}^{I^h} \Delta x_i \left[\Phi(f_i^{n+1}) - \Phi(f_i^n)\right] \leq \sum_{i=0}^{I^h} \frac{\Delta t}{x_i}\left(\mathcal{F}_{i+1/2}^n - \mathcal{F}_{i-1/2}^n\right)\Phi^{'}(f_i^{n+1}).$$

Since Φ is a convex function, its derivative is non-decreasing. Therefore, $\Phi^{'}(0) = 1$ implies that $\Phi^{'}(x) > 0$ for $x \geq 0$. Further simplification as in (2.17) gives

$$\begin{aligned}\sum_{i=0}^{I^h} \Delta x_i \left[\Phi(f_i^{n+1}) - \Phi(f_i^n)\right] \leq & \sum_{i=0}^{I^h} \frac{\Delta t}{x_i} \sum_{j=i+1}^{I^h} x_i S_j b_{i,j} f_j^n \Delta x_j \Delta x_i \Phi^{'}(f_i^{n+1}) \\ \leq & \|bS\|_{L^\infty} \Delta t \sum_{i=0}^{I^h} \sum_{j=i+1}^{I^h} \Delta x_j \Delta x_i f_j^n \Phi^{'}(f_i^{n+1}).\end{aligned}$$

Using the property $x\Phi^{'}(y) \leq \Phi(x) + \Phi(y)$ from Lemma 2.3.4, it reduces to

$$\begin{aligned}\sum_{i=0}^{I^h} \Delta x_i \left[\Phi(f_i^{n+1}) - \Phi(f_i^n)\right] \leq & \|bS\|_{L^\infty} \Delta t \sum_{i=0}^{I^h} \Delta x_i \sum_{j=i+1}^{I^h} \Delta x_j \left(\Phi(f_j^n) + \Phi(f_i^{n+1})\right) \\ \leq & (\|bS\|_{L^\infty} \Delta t R) \left(\sum_{j=0}^{I^h} \Delta x_j \Phi(f_j^n) + \sum_{i=0}^{I^h} \Delta x_i \Phi(f_i^{n+1}) \right).\end{aligned}$$

Changing the index from j to i for the first term on the right-hand side and taking $\|bS\|_{L^\infty} R = C(T, R)$, we obtain

$$(1 - \Delta t C(T,R)) \sum_{i=0}^{I^h} \Delta x_i \Phi(f_i^{n+1}) \leq (1 + \Delta t C(T,R)) \sum_{i=0}^{I^h} \Delta x_i \Phi(f_i^n).$$

Equivalently, it can be rewritten as

$$(1 - \Delta t C(T,R)) \sum_{i=0}^{I^h} \Delta x_i (\Phi(f_i^{n+1}) - \Phi(f_i^n)) \leq 2\Delta t C(T,R) \sum_{i=0}^{I^h} \Delta x_i \Phi(f_i^n). \tag{2.19}$$

This gives using $\lambda = \frac{2C(T,R)}{1 - \Delta t C(T,R)} > 0$

$$\sum_{i=0}^{I^h} \Delta x_i \Phi(f_i^{n+1}) \leq (1 + \lambda \Delta t) \sum_{i=0}^{I^h} \Delta x_i \Phi(f_i^n)$$

for any n. Hence, we achieve the result that

$$\begin{aligned}\sum_{i=0}^{I^h} \Delta x_i \Phi(f_i^n) \leq & (1 + \lambda \Delta t)^n \sum_{i=0}^{I^h} \Delta x_i \Phi(f_i^0) \\ \leq & \exp(\lambda \Delta t n) \sum_{i=0}^{I^h} \Delta x_i \Phi(f_i^0).\end{aligned}$$

For time $t \in \tau_n = [t_n, t_{n+1}[$ the above expression becomes

$$\begin{aligned}\int_0^R \Phi(f^h(t,x)) dx \leq & \exp(\lambda t) \sum_{i=0}^{I^h} \Delta x_i \Phi(f_i^{in}) \\ \leq & \exp(\lambda t) \sum_{i=0}^{I^h} \Delta x_i \Phi\left(\frac{1}{\Delta x_i} \int_{\Lambda_i^h} f^{in}(x) dx \right).\end{aligned}$$

We apply Jensen's inequality to get

$$\int_0^R \Phi(f^h(t,x))dx \leq \exp(\lambda t) \sum_{i=0}^{I^h} \Delta x_i/\Delta x_i \int_{\Lambda_i^h} \Phi(f^{in}(x))dx.$$

Equivalently, we have

$$\int_0^R \Phi(f^h(t,x))dx \leq \exp\left(\frac{2C(T,R)t}{1-\Delta t C(T,R)}\right) \int_0^R \Phi(f^{in}(x))dx.$$

As we know from (2.9) that $1-\Delta t C(T,R) \geq 1-\theta$. This implies that

$$\int_0^R \Phi(f^h(t,x))dx \leq \exp\left(\frac{2C(T,R)t}{1-\theta}\right) \int_0^R \Phi(f^{in}(x))dx, \quad \text{for all} \quad t \in [0,T[$$

and it concludes the proof. □

Hence, the sequence $(f^h)_{h\in\mathbb{N}}$ is weakly compact in L^1 due to the Dunford-Pettis theorem. Here, the exponent is uniformly bounded with respect to h and Δt as long as the time step restriction (2.9) holds. This implies that there exists a subsequence of $(f^h)_{h\in\mathbb{N}}$ and a function $f \in L^1(]0,T[\times]0,R])$ such that $f^h \rightharpoonup f$ as $h \to 0$.

So far we have seen that the sequence f_i^n is built from the numerical scheme as a sequence of step functions f^h depending on the mesh size h and the time step Δt. We have already seen the weak compactness of this sequence. Now in order to prove Theorem 2.3.1, it remains to show that the discrete breakage flux converges weakly towards the continuous flux when it is written in terms of the function f^h. This is done in Lemma 2.3.7 later.

We use the following point approximations for further analysis. First we define the midpoint approximation as

$$X^h : x \in]0,R[\to X^h(x) = \sum_{i=0}^{\mathrm{I}^h} x_i \chi_{\Lambda_i^h}(x).$$

Then right and left endpoint approximations are taken respectively as

$$\Xi^h : x \in]0,R[\to \Xi^h(x) = \sum_{i=0}^{\mathrm{I}^h} x_{i+1/2} \chi_{\Lambda_i^h}(x),$$

and

$$\xi^h : x \in]0,R[\to \xi^h(x) = \sum_{i=0}^{\mathrm{I}^h} x_{i-1/2} \chi_{\Lambda_i^h}(x).$$

It should be mentioned that the approximations $(X^h)_h$, $(\Xi^h)_h$ and $(\xi^h)_h$ converge pointwise, i.e. for all $x \in]0,R[$,

$$X^h(x) \to x, \quad \Xi^h(x) \to x \quad \text{and} \quad \xi^h(x) \to x$$

as $h \to 0$. We also use the following classical lemma to prove the convergence of the numerical flux towards the continuous flux. The proof of this lemma is based on the Dunford-Pettis and Egorov theorems.

Lemma 2.3.6. *[58, Lemma A.2] Let Ω be an open subset of $\mathbb{R}^m$ and let there exist a constant $k > 0$ and two sequences $(v_n)_{n\in\mathbb{N}}$ and $(w_n)_{n\in\mathbb{N}}$ such that $(v_n) \in L^1(\Omega), v \in L^1(\Omega)$ and*

$$v_n \rightharpoonup v, \quad \text{weakly in } L^1(\Omega), \text{as } n \to \infty,$$

$(w_n) \in L^\infty(\Omega), w \in L^\infty(\Omega)$, and for all $n \in \mathbb{N}, |w_n| \leq k$ with

$$w_n \to w, \quad \text{almost everywhere (a.e.) in } \Omega, \text{ as } n \to \infty.$$

Then

$$\lim_{n\to\infty} \|v_n(w_n - w)\|_{L^1(\Omega)} = 0$$

and

$$v_n\, w_n \rightharpoonup v\, w, \quad \text{weakly in } L^1(\Omega), \text{as } n \to \infty.$$

Consider the definitions of f^h, b^h and S^h given by (2.6), (2.7) and (2.8) respectively. The following lemma state the convergence result of the numerical flux towards the continuous flux.

Lemma 2.3.7. *Let us define the approximation of the fragmentation terms as*

$$\mathcal{F}^h(t,x) = \int_0^R \int_0^R \chi_{[0,\Xi^h(x)]}(u)\chi_{[\Xi^h(x),R]}(v)X^h(u)b^h(u,v)S^h(v)f^h(t,v)dudv.$$

There exists a subsequence of $(f^h)_{h\in\mathbb{N}}$, such that

$$\mathcal{F}^h \rightharpoonup \mathcal{F}_c^R \quad \text{in } L^1(]0,T[\times]0,R]) \text{ as } h \to 0.$$

Before proving this lemma, it is worth to mention that actually the $\mathcal{F}^h(t,x)$ coincide with $\mathcal{F}_i^n$ whenever $t \in \tau_n$ and $x \in \Lambda_i^h$. It can be seen easily that for $x \in \Lambda_i^h$

$$\begin{aligned}
\mathcal{F}^h(t,x) &= \int_{x_{i+1/2}}^R \int_0^{x_{i+1/2}} X^h(u)b^h(u,v)S^h(v)f^h(t,v)dudv \\
&= \sum_{j=i+1}^{\mathrm{I}^h} \int_{\Lambda_j^h} \sum_{k=0}^{i} \int_{\Lambda_k^h} \Bigg[X^h(u) \Bigg(\sum_{\ell=0}^{\mathrm{I}^h} \sum_{m=0}^{\mathrm{I}^h} b_{m,\ell}\chi_{\Lambda_m^h}(u)\chi_{\Lambda_\ell^h}(v) \Bigg) \Bigg(\sum_{\ell=0}^{\mathrm{I}^h} S_\ell \chi_{\Lambda_\ell^h}(v) \Bigg) \\
&\quad \cdot \Bigg(\sum_{\ell=0}^{\mathrm{I}^h} f_\ell^n \chi_{\Lambda_\ell^h}(v) \Bigg) \Bigg] dudv \\
&= \sum_{j=i+1}^{\mathrm{I}^h} \sum_{k=0}^{i} \int_{\Lambda_j^h} \int_{\Lambda_k^h} x_k b_{k,j} S_j f_j^n dudv = \mathcal{F}_{i+1/2}^n.
\end{aligned}$$

Proof. [Lemma 2.3.7]
We know that for all $(t,x) \in]0,T[\times]0,R]$ and for $u \in]0,R]$ almost everywhere that the sequence

$$X^h(\cdot)b^h(\cdot,v)S^h(v) \in L^\infty]0,R] \quad \text{for almost all} \quad v \in]0,R].$$

It is uniformly bounded and

$$\chi_{[0,\Xi^h(x)]}(u)\chi_{[\Xi^h(x),R]}(v)X^h(u)b^h(u,v)S^h(v) \to \chi_{[0,x]}(u)\chi_{[x,R]}(v)ub(u,v)S(v)$$

pointwise almost everywhere as $h \to 0$. We also know that $f^h \rightharpoonup f$ in $L^1]0,R]$. Hence, applying Lemma 2.3.6 yields

$$\chi_{[0,\Xi^h(x)]}(u)\chi_{[\Xi^h(x),R]}(v)X^h(u)b^h(u,v)S^h(v)f^h(t,v) \rightharpoonup \chi_{[0,x]}(u)\chi_{[x,R]}(v)ub(u,v)S(v)f(t,v)$$

in $L^1]0,R]$. Therefore, we have

$$\int_0^R \chi_{[0,\Xi^h(x)]}(u)\chi_{[\Xi^h(x),R]}(v)X^h(u)b^h(u,v)S^h(v)f^h(t,v)dv \to \int_0^R \chi_{[0,x]}(u)\chi_{[x,R]}(v)ub(u,v)S(v)f(t,v)dv. \tag{2.20}$$

This implies that (2.20) holds for each t,x and almost every u. Finally, by applying dominated convergence theorem we get

$$\mathcal{F}^h(t,x) \to \mathcal{F}_c^R(t,x)$$

for every $(t,x) \in]0,T[\times]0,R]$. As $\mathcal{F}^h$ is bounded, this pointwise convergence implies weak convergence for $\mathcal{F}^h$. □

Now we have gathered all the results needed to prove Theorem 2.3.1. The proof is given below. For this, let us consider a test function $\varphi \in C^1([0,T[\times[0,R])$ which is compactly supported. For Δt small enough, the support of φ w.r.to t satisfies $\mathrm{Supp}_t\varphi \subset [0,t_{N-1}]$. Define the finite volume (in time) and left endpoint (in space) approximation of φ on $\tau_n \times \Lambda_i^h$ by

$$\varphi_i^n = \frac{1}{\Delta t}\int_{t_n}^{t_{n+1}} \varphi(t,x_{i-1/2})dt.$$

Multiplying (2.3) by φ_i^n and summing over $n \in \{0,...,N-1\}$ as well as $i \in \{0,...,\mathrm{I}^h\}$ give

$$\sum_{n=0}^{N-1}\sum_{i=0}^{\mathrm{I}^h}\left[\Delta x_i x_i(f_i^{n+1}-f_i^n)\varphi_i^n - \Delta t\left(\mathcal{F}_{i+1/2}^n - \mathcal{F}_{i-1/2}^n\right)\varphi_i^n\right] = 0.$$

If we open the summation for both i and n, discrete integration by parts yields

$$\sum_{n=0}^{N-1}\sum_{i=0}^{\mathrm{I}^h}\Delta x_i x_i f_i^{n+1}(\varphi_i^{n+1}-\varphi_i^n) + \sum_{i=0}^{\mathrm{I}^h}\Delta x_i x_i f_i^{in}\varphi_i^0 - \sum_{n=0}^{N-1}\sum_{i=0}^{\mathrm{I}^h-1}\Delta t\mathcal{F}_{i+1/2}^n(\varphi_{i+1}^n-\varphi_i^n) = 0. \tag{2.21}$$

Now, we evaluate the first two terms on the left-hand side by writing them in terms of the function f^h as

$$\sum_{n=0}^{N-1}\sum_{i=0}^{\mathrm{I}^h}\Delta x_i x_i f_i^{n+1}(\varphi_i^{n+1}-\varphi_i^n) + \sum_{i=0}^{\mathrm{I}^h}\Delta x_i x_i f_i^{in}\varphi_i^0 = \sum_{n=0}^{N-1}\sum_{i=0}^{\mathrm{I}^h}\int_{\tau_{n+1}}\int_{\Lambda_i^h} X^h(x)f^h(t,x)\frac{\varphi(t,\xi^h(x))-\varphi(t-\Delta t,\xi^h(x))}{\Delta t}dxdt + \sum_{i=0}^{\mathrm{I}^h}\int_{\Lambda_i^h} X^h(x)f^h(0,x)\frac{1}{\Delta t}\int_0^{\Delta t}\varphi(t,\xi^h(x))dtdx.$$

Further it can be written as

$$\sum_{n=0}^{N-1}\sum_{i=0}^{\mathrm{I}^h}\Delta x_i x_i f_i^{n+1}(\varphi_i^{n+1}-\varphi_i^n)+\sum_{i=0}^{\mathrm{I}^h}\Delta x_i x_i f_i^{in}\varphi_i^0 =$$
$$\int_{\Delta t}^{T}\int_0^R X^h(x)f^h(t,x)\frac{\varphi(t,\xi^h(x))-\varphi(t-\Delta t,\xi^h(x))}{\Delta t}dxdt$$
$$+\int_0^R X^h(x)f^h(0,x)\frac{1}{\Delta t}\int_0^{\Delta t}\varphi(t,\xi^h(x))dtdx.$$

Since, $\varphi\in C^1([0,T[\times[0,R])$ with compact support and the derivative of φ is bounded, we have

$$\frac{1}{\Delta t}\int_0^{\Delta t}\varphi(t,\xi^h(x))dt\to\varphi(0,x)$$

uniformly with respect to t,x as $\max\{h,\Delta t\}$ goes to 0. Moreover, we know that $X^h(x)$ converges pointwise in $[0,R]$ and $f^h(0,x)\to f^{in}$ in $L^1]0,R]$. Thus we achieve by using Lemma 2.3.6

$$\int_0^R X^h(x)f^h(0,x)\frac{1}{\Delta t}\int_0^{\Delta t}\varphi(t,\xi^h(x))dtdx\to\int_0^R xf^{in}(x)\varphi(0,x)dx$$

as $\max\{h,\Delta t\}$ goes to 0.

Now, using Taylor expansion of the smooth function φ yields

$$\frac{\varphi(t,\xi^h(x))-\varphi(t-\Delta t,\xi^h(x))}{\Delta t}=\frac{\varphi(t,x)+(x-\xi^h(x))\frac{\partial\varphi}{\partial x}-\varphi(t,x)+\Delta t\frac{\partial\varphi}{\partial t}-(x-\xi^h(x))\frac{\partial\varphi}{\partial x}+O(h\,\Delta t)}{\Delta t}.$$

It implies that

$$\frac{\varphi(t,\xi^h(x))-\varphi(t-\Delta t,\xi^h(x))}{\Delta t}\to\frac{\partial\varphi}{\partial t}(t,x)$$

uniformly as $\max\{h,\Delta t\}$ goes to 0. Applying Lemma 2.3.6, together with Proposition 2.3.5, ensures that for $\max\{h,\Delta t\}$ goes to 0

$$\int_0^T\int_0^R X^h(x)f^h(t,x)\frac{\varphi(t,\xi^h(x))-\varphi(t-\Delta t,\xi^h(x))}{\Delta t}dx\,dt\to\int_0^T\int_0^R xf(t,x)\frac{\partial\varphi}{\partial t}(t,x)dx\,dt.$$

Hence, we obtain

$$\int_{\Delta t}^T\int_0^R\underbrace{X^h(x)f^h(t,x)\frac{\varphi(t,\xi^h(x))-\varphi(t-\Delta t,\xi^h(x))}{\Delta t}}_{A}dx\,dt=$$
$$\int_0^T\int_0^R A\,dx\,dt-\int_0^{\Delta t}\int_0^R A\,dx\,dt\to\int_0^T\int_0^R xf(t,x)\frac{\partial\varphi}{\partial t}(t,x)dx\,dt$$

as $\max\{h,\Delta t\}\to 0$. Finally, writing the remaining third term of the equation (2.21) in terms of $\mathcal{F}^h$ gives

$$\sum_{n=0}^{N-1}\sum_{i=0}^{\mathrm{I}^h-1}\Delta t\mathcal{F}^n_{i+1/2}(\varphi^n_{i+1}-\varphi^n_i)=\sum_{n=0}^{N-1}\sum_{i=0}^{\mathrm{I}^h-1}\int_{\tau_n}\int_{\Lambda_i^h}\mathcal{F}^n_{i+1/2}\frac{1}{\Delta x_i}\left[\varphi(t,x_{i+1/2})-\varphi(t,x_{i-1/2})\right]dxdt$$
$$=\int_0^T\int_0^{R-\Delta x_{\mathrm{I}^h}}\mathcal{F}^h(t,x)\frac{\partial\varphi}{\partial x}(t,x)dxdt.$$

By using the weak convergence for the flux from Lemma 2.3.7, i.e. $\mathcal{F}^h \rightharpoonup \mathcal{F}_c^R$ in $L^1(]0,T[\times]0,R])$, we determine

$$\int_0^T \int_0^{R-\Delta x_{\mathrm{I}h}} \mathcal{F}^h(t,x)\frac{\partial\varphi}{\partial x}(t,x)dxdt = \left(\int_0^T\int_0^R - \int_0^T\int_{\Delta x_{\mathrm{I}h}}\right)\mathcal{F}^h(t,x)\frac{\partial\varphi}{\partial x}(t,x)dxdt$$
$$\to \int_0^T\int_0^R \mathcal{F}_c^R\frac{\partial\varphi}{\partial x}(t,x)dxdt, \quad \text{as } h\to 0.$$

Therefore, the corresponding terms in (2.11) are obtained.

Chapter 3

Convergence analysis of the finite volume scheme

In this chapter we discuss the convergence analysis of the finite volume schemes for the aggregation problem introduced by Filbet and Laurençot [23] and the multiple breakage equation studied by J. Kumar [42]. We demonstrate the consistency and the convergence of the schemes. We notice that the method shows second order convergence independently of the meshes for the pure breakage problem. However, due to the non-linearity of the aggregation process we observe that the scheme is second order convergent only on uniform and non-uniform smooth meshes for the pure aggregation and combined aggregation-breakage problems. Furthermore, in these cases the method is only first order accurate on oscillatory and non-uniform random meshes. Finally, numerical simulations are performed by considering various examples of the pure aggregation, pure breakage and the combined processes. These simulations are made on five different types of uniform and non-uniform grids to verify the mathematical results of the convergence analysis.

The contents of this chapter are as follows. In the following section we give a short introduction of the problem. Section 3.2 summarizes the numerical scheme. Then we recall from the book of Hundsdorfer and Verwer [33] and from the paper of Linz [68], some useful definitions and theorems, which are used in the further analysis of this work in Section 3.3. Here, we discuss the consistency and the Lipschitz conditions which are needed to show the convergence of the scheme. At the end in Section 3.4, numerical results are provided.

3.1 Introduction

From (1.13) we know that the non-linear aggregation and multiple breakage equation in a conservative form of mass density $xf(t,x)$ is written as

$$\frac{\partial\left[xf(t,x)\right]}{\partial t}+\frac{\partial}{\partial x}\left(F^{\mathrm{agg}}(t,x)+F^{\mathrm{brk}}(t,x)\right)=0, \tag{3.1}$$

where we have used the abbreviations *agg* and *brk* for aggregation and breakage terms respectively. The flux functions F^{agg} and F^{brk} are given by

$$F^{\mathrm{agg}}(t,x)=\int_0^x\int_{x-u}^{\infty}u\beta(u,v)f(t,u)f(t,v)dvdu, \tag{3.2}$$

and

$$F^{\text{brk}}(t,x) = -\int_x^\infty \int_0^x ub(u,v)S(v)f(t,v)dudv. \tag{3.3}$$

It is worth here to mention that the equation (3.1) reduces into the case of pure aggregation or pure breakage process when $F^{\text{brk}}(t,x)$ or $F^{\text{agg}}(t,x)$ is zero, respectively.

In the population balance equation (3.1) the volume variable x ranges from 0 to ∞. In order to apply a numerical scheme for the solution of the equation a first step is to fix a finite computational domain $\Omega :=]0, x_{\max}]$ for an $0 < x_{\max} < \infty$. Hence, for $x \in \Omega$ and time $t \in (0,T]$ where $T < \infty$, the aggregation and the breakage fluxes for the truncated conservation law for n, i.e. for

$$\frac{\partial\left[xn(t,x)\right]}{\partial t} + \frac{\partial}{\partial x}\left(F^{\text{agg}}(t,x) + F^{\text{brk}}(t,x)\right) = 0 \tag{3.4}$$

are given as

$$F^{\text{agg}}(t,x) = \int_0^x \int_{x-u}^{x_{\max}} u\beta(u,v)n(t,u)n(t,v)dvdu, \tag{3.5}$$

and

$$F^{\text{brk}}(t,x) = -\int_x^{x_{\max}} \int_0^x ub(u,v)S(v)n(t,v)dudv. \tag{3.6}$$

Here the variable $n(t,x)$ denotes the solution to the truncated equation. We are given with initial data

$$n(0,x) = f^{\text{in}}(x), \quad x \in \Omega. \tag{3.7}$$

For further analysis in this work we consider

$$\beta, b \in \mathcal{C}^2(]0,x_{\max}]\times]0,x_{\max}]) \text{ and } \; S \in \mathcal{C}^2]0,x_{\max}]. \tag{3.8}$$

Additionally we assume the boundedness of the kernels, namely

$$\beta(x,y) \le Q \quad \text{and} \quad b(x,y)S(y) \le Q_1 \tag{3.9}$$

for $x, y \in]0, x_{\max}]$ and for some non-negative constants Q and Q_1 depending on $x_{\max}$.

Remark 3.1.1. *The formulation we use here is a non-conservative truncation for the pure aggregation operator as $F^{agg}(t,x_{max}) \ge 0$ while it is mass conserving for the pure breakage equation, i.e. $F^{brk}(t,x_{max}) = 0$. Hence, the combined formulation (3.4) is a non-conservative truncation as used by Bourgade and Filbet [7]. One could make a conservative truncation by replacing x_{max} by $x_{max} - u$ in (3.5). This would give $F^{agg}(t,x_{max}) = 0$. But it describes an artificial interruption of the aggregation process without a real physical justification. With our truncation particles that are too large leave the system.*

3.2 Finite volume scheme

Finite volume methods are a class of discretization schemes used to solve mainly conservation laws, see LeVeque [64]. Conservation laws describe many physical processes. It has been observed that many differential equations which we would like to solve come from conservation laws which are integrals over volumes. For a semi-discrete scheme, the interval $]0, x_{\max}]$ is discretized into small cells

$$\Lambda_i :=]x_{i-1/2}, x_{i+1/2}], \quad i = 1, ..., I,$$

with

$$x_{1/2} = 0, \quad x_{I+1/2} = x_{\max}, \quad \Delta x_i = x_{i+1/2} - x_{i-1/2} \leq \Delta x,$$

where Δx is the maximum mesh size. The representative of each size, usually the center of each cell $x_i = (x_{i-1/2} + x_{i+1/2})/2$, is called pivot or grid point. The finite volume idea has been carried over to the discretization of such equations by instead of interpreting $\hat{n}_i(t)$ as an approximation to a point value at a grid point, i.e. $n(t, x_i)$, rather taking an approximation of the cell average of the solution on cell i at time t

$$\hat{n}_i(t) \approx n_i = \frac{1}{\Delta x_i} \int_{x_{i-1/2}}^{x_{i+1/2}} n(t, x) \mathrm{d}x. \tag{3.10}$$

Note that for $n(t, x) \in \mathcal{C}^2(]0, x_{\max}])$, we have the relation $n_i = n(t, x_i) + \mathcal{O}(\Delta x^2)$ by applying mid-point rule. Integrating the conservation law on a cell in space Λ_i, the finite volume scheme in a semi-discrete form is given as [64]

$$\frac{x_i d\hat{n}_i(t)}{dt} = -\frac{1}{\Delta x_i} \left[J^{\mathrm{agg}}_{i+1/2} - J^{\mathrm{agg}}_{i-1/2} + J^{\mathrm{brk}}_{i+1/2} - J^{\mathrm{brk}}_{i-1/2} \right]. \tag{3.11}$$

The term $J^{-}_{i+1/2}$ is called *the numerical flux* which is an appropriate approximation of the truncated continuous flux function F^{agg} and/or F^{brk} depending upon the processes under consideration.
In case of a breakage process, the numerical flux may be approximated from the mass flux F^{brk} as follows

$$\begin{aligned} F^{\mathrm{brk}}(x_{i+1/2}) &= -\int_{x_{i+1/2}}^{x_{\max}} \int_{0}^{x_{i+1/2}} ub(u, \epsilon) S(\epsilon) n(t, \epsilon)\, du\, d\epsilon \\ &= -\sum_{k=i+1}^{I} \int_{\Lambda_k} S(\epsilon) n(t, \epsilon) \sum_{j=1}^{i} \int_{\Lambda_j} ub(u, \epsilon)\, du\, d\epsilon. \end{aligned} \tag{3.12}$$

Using our assumptions that $S \in \mathcal{C}^2(]0, x_{\max}])$, $b \in \mathcal{C}^2(]0, x_{\max}] \times]0, x_{\max}])$ and applying the mid-point rule we can rewrite (3.12) as

$$F^{\mathrm{brk}}(x_{i+1/2}) = \underbrace{-\sum_{k=i+1}^{I} n_k(t) S(x_k) \Delta x_k \sum_{j=1}^{i} x_j b(x_j, x_k) \Delta x_j}_{=: J^{\mathrm{brk}}_{i+1/2}(n)} + \mathcal{O}(\Delta x^2). \tag{3.13}$$

Similarly for the aggregation problem, we have

$$F^{\text{agg}}(x_{i+1/2}) = \int_0^{x_{i+1/2}} \int_{x_{i+1/2}-u}^{x_{\max}} u\beta(u,v)n(t,u)n(t,v)dvdu. \tag{3.14}$$

From Filbet and Laurençot [23], the above equation can be written as

$$F^{\text{agg}}(x_{i+1/2}) = \sum_{k=1}^{i}(xn)_k\Delta x_k\left(\sum_{j=\alpha_{i,k}}^{I}(xn)_j\int_{\Lambda_j}\frac{\beta(x,x_k)}{x}dx+(xn)_{\alpha_{i,k}-1}\int_{x_{i+1/2}-x_k}^{x_{\alpha_{i,k}-1/2}}\frac{\beta(x,x_k)}{x}dx\right) + \mathcal{O}(\Delta x^2).$$

Here, the parameter I denotes the number of cells. The integer $\alpha_{i,k}$ corresponds to the index of each cell such that

$$x_{i+1/2} - x_k \in \Lambda_{\alpha_{i,k}-1}. \tag{3.15}$$

Applying mid point approximation for the first term and Taylor series expansion of the second term about the point $x_{\alpha_{i,k}-1}$ give

$$F^{\text{agg}}(x_{i+1/2}) = \underbrace{\sum_{k=1}^{i}x_kn_k\Delta x_k\left(\sum_{j=\alpha_{i,k}}^{I}n_j\beta_{j,k}\Delta x_j + n_{\alpha_{i,k}-1}\beta_{\alpha_{i,k}-1,k}(x_{\alpha_{i,k}-1/2}-(x_{i+1/2}-x_k))\right)}_{=:J^{\text{agg}}_{i+1/2}(n)} + \mathcal{O}(\Delta x^2). \tag{3.16}$$

Note that the above conservative formulations for the numerical fluxes $J^{\text{agg}}_{i+1/2}$ and $J^{\text{brk}}_{i+1/2}$ can directly be obtained by discretizing the standard form of the population balance equations as given in Appendix A.1.

Let us denote the average values of the exact solution n by the vector $\mathbf{n} := [n_1, \ldots, n_I]$ obtained using (3.10). We also define the vectors

$$\Delta\mathbf{J}^{\text{agg}}(\mathbf{n}) := [\Delta J^{\text{agg}}_1(\mathbf{n}), \ldots, \Delta J^{\text{agg}}_I(\mathbf{n})] \quad \text{and} \quad \Delta\mathbf{J}^{\text{brk}}(\mathbf{n}) := [\Delta J^{\text{brk}}_1(\mathbf{n}), \ldots, \Delta J^{\text{brk}}_I(\mathbf{n})]$$

where

$$\Delta J^{\text{agg}}_i(\mathbf{n}) = \frac{1}{x_i\Delta x_i}\left[J^{\text{agg}}_{i+1/2}(\mathbf{n}) - J^{\text{agg}}_{i-1/2}(\mathbf{n})\right], \quad \Delta J^{\text{brk}}_i(\mathbf{n}) = \frac{1}{x_i\Delta x_i}\left[J^{\text{brk}}_{i+1/2}(\mathbf{n}) - J^{\text{brk}}_{i-1/2}(\mathbf{n})\right]. \tag{3.17}$$

Substituting the values of $J^{\text{agg}}_{i+1/2}$ and $J^{\text{brk}}_{i+1/2}$ from the equations (3.16) and (3.13), respectively, we get

$$\Delta x_i\Delta J^{\text{agg}}_i(\mathbf{n}) = \sum_{k=1}^{i-1}\frac{x_k}{x_i}n_k\Delta x_k\Bigg(-\sum_{j=\alpha_{i-1,k}}^{\alpha_{i,k}-1}n_j\beta_{j,k}\Delta x_j + \beta_{\alpha_{i,k}-1,k}n_{\alpha_{i,k}-1}(x_{\alpha_{i,k}-1/2}-(x_{i+1/2}-x_k)) - \beta_{\alpha_{i-1,k}-1,k}n_{\alpha_{i-1,k}-1}(x_{\alpha_{i-1,k}-1/2}-(x_{i-1/2}-x_k))\Bigg) + n_i\Delta x_i\Bigg(\sum_{j=\alpha_{i,i}}^{I}n_j\beta_{j,i}\Delta x_j + n_{\alpha_{i,i}-1}\beta_{\alpha_{i,i}-1,i}(x_{\alpha_{i,i}-1/2}-(x_{i+1/2}-x_i))\Bigg) \tag{3.18}$$

and

$$\Delta x_i \Delta J_i^{\mathrm{brk}}(\mathbf{n}) = -\sum_{k=i+1}^{I} S(x_k) n_k \Delta x_k b(x_i, x_k) \Delta x_i + S(x_i) n_i \Delta x_i \sum_{j=1}^{i-1} \frac{x_j}{x_i} b(x_j, x_i) \Delta x_j. \tag{3.19}$$

By denoting the vector $\hat{\mathbf{n}} := [\hat{n}_1, \ldots, \hat{n}_I]$ for the approximations of the average values of $n(t, x)$, the equation (3.11) can be rewritten as

$$\frac{d\hat{\mathbf{n}}(t)}{dt} = -\left[\Delta \mathbf{J}^{\mathrm{agg}}(\hat{\mathbf{n}}) + \Delta \mathbf{J}^{\mathrm{brk}}(\hat{\mathbf{n}})\right] = \mathbf{J}(\hat{\mathbf{n}}). \tag{3.20}$$

In order to retain the overall high accuracy, the semi-discrete scheme (3.20) can be combined with any higher order time integration method. It is worth to mention here that for the pure breakage problem $\Delta \mathbf{J}^{\mathrm{agg}}(\hat{\mathbf{n}}) = 0$ while for the pure aggregation $\Delta \mathbf{J}^{\mathrm{brk}}(\hat{\mathbf{n}}) = 0$. Therefore, dealing with the pure cases of aggregation or breakage is easy by setting one of the two numerical fluxes is zero. Before proceeding further to establish the consistency, stability and convergence of the semi-discrete scheme, we have the following obvious proposition to show some characteristic features of the numerical solution.

Proposition 3.2.1. *The semi-discrete formulation (3.11) is mass dissipating. Thus, we have*

$$\frac{d}{dt} \sum_i \left(x_i \hat{n}_i(t) \Delta x_i\right) \leq 0. \tag{3.21}$$

Furthermore, if $\phi : [0, +\infty[\to [0, +\infty[$ *is a non-increasing function, then*

$$\frac{d}{dt} \sum_i \left(\phi(x_i) x_i \hat{n}_i(t) \Delta x_i\right) \geq 0 \tag{3.22}$$

for the pure breakage problem and for the pure aggregation

$$\frac{d}{dt} \sum_i \left(\phi(x_i) x_i \hat{n}_i(t) \Delta x_i\right) \leq 0. \tag{3.23}$$

Proof. The volume dissipation property (3.21) and properties (3.22) and (3.23) can easily be proved by multiplying the equation (3.11) by Δx_i and by $\phi(x_i)\Delta x_i$, respectively, and summing with respect to i. □

It should also be mentioned that the mass dissipation (3.21) turns into the mass conservation, i.e. $\frac{d}{dt} \sum_i \left(x_i \hat{n}_i(t) \Delta x_i\right) = 0$ by making an assumption that the fluxes at the boundaries $x_{1/2} = 0$ and $x_{I+1/2} = x_{\max}$ are zero.

3.3 Convergence analysis

Before discussing the convergence of the semi-discrete scheme, let us review some useful definitions and theorems that will be used in the subsequent analysis. Details can be found in the

book of Hundsdorfer and Verwer [33] and the paper of Linz [68]. Let $\|\cdot\|$ denote the discrete L^1 norm on $\mathbb{R}^I$ that is defined as

$$\|\hat{\mathbf{n}}(t)\| = \sum_{i=1}^{I} |\hat{n}_i(t)|\Delta x_i. \tag{3.24}$$

In the subsequent analysis, we work with this norm by interpreting the discrete data as step functions.

Definition 3.3.1. *The **spatial truncation error** is defined by the residual left by substituting the exact solution $\mathbf{n}(t) = [n_1(t), \ldots, n_I(t)]$ into equation (3.20) as*

$$\boldsymbol{\sigma}(t) = \frac{d\mathbf{n}(t)}{dt} + (\Delta\mathbf{J}^{agg}(\mathbf{n}) + \Delta\mathbf{J}^{brk}(\mathbf{n})). \tag{3.25}$$

The scheme (3.20) is called consistent of order p if, for $\Delta x \to 0$,

$$\|\boldsymbol{\sigma}(t)\| = \mathcal{O}(\Delta x^p), \quad \text{uniformly for all } t, \quad 0 \le t \le T. \tag{3.26}$$

Definition 3.3.2. *The **global discretization error** is defined by $\boldsymbol{\epsilon}(t) = \mathbf{n}(t) - \hat{\mathbf{n}}(t)$. The scheme (3.20) is called convergent of order p if, for $\Delta x \to 0$,*

$$\|\boldsymbol{\epsilon}(t)\| = \mathcal{O}(\Delta x^p), \quad \text{uniformly for all } t, \quad 0 \le t \le T. \tag{3.27}$$

Remark 3.3.3. *It should be mentioned that the actual error is*

$$\epsilon_1(t, x) = n(t, x) - I_{\Delta x}\hat{\mathbf{n}}(\mathbf{t}) \tag{3.28}$$

where $I_{\Delta x}\hat{\mathbf{n}}(\mathbf{t}) = \sum_{i=1}^{I} \hat{n}_i(t)\chi_{\Lambda_i}(x)$. The term $\chi_{\Lambda_i}(x)$ is the characteristic function, defined by $\chi_{\Lambda_i}(x) = 1$ if $x \in \Lambda_i$ else 0 everywhere. We can rewrite (3.28) as

$$\epsilon_1(t, x) = n(t, x) - I_{\Delta x}\mathbf{n}(\mathbf{t}) + I_{\Delta x}\mathbf{n}(\mathbf{t}) - I_{\Delta x}\hat{\mathbf{n}}(\mathbf{t}).$$

Taking the L^1 norm in space on both sides gives

$$\|\epsilon_1(t)\|_{L^1(]0,x_{max}])} \le \|n(t) - I_{\Delta x}\mathbf{n}(t)\|_{L^1(]0,x_{max}])} + \|I_{\Delta x}\mathbf{n}(\mathbf{t}) - I_{\Delta x}\hat{\mathbf{n}}(\mathbf{t})\|_{L^1(]0,x_{max}])}.$$

It is easy to show that $\|n(t) - I_{\Delta x}\mathbf{n}(t)\|_{L^1(]0,x_{max}])} = \mathcal{O}(\Delta x^2)$ for $n(t) \in \mathcal{C}^2(]0, x_{max}])$ and

$$\|I_{\Delta x}\mathbf{n}(\mathbf{t}) - I_{\Delta x}\hat{\mathbf{n}}(\mathbf{t})\|_{L^1(]0,x_{max}])} = \sum_{i=1}^{I} \Delta x_i |n_i(t) - \hat{n}_i(t)| = \|\epsilon(t)\|.$$

Hence, $\|\epsilon_1(t)\|_{L^1(]0,x_{max}])} \le \mathcal{O}(\Delta x^2) + \|\epsilon(t)\|$. Clearly, the order of convergence of the scheme is at most 2. The actual order of convergence of the scheme may depend on $\|\epsilon(t)\|$.

It is important that our numerical solution remains non-negative for all times. This is guaranteed by the next well known theorem. In the following theorem we write $\hat{\mathbf{M}} \ge 0$ for a vector $\hat{\mathbf{M}} \in \mathbb{R}^I$ iff all its components are non-negative.

Theorem 3.3.4. *(Hundsdorfer and Verwer [33, Chap. 1, Theorem 7.1]). Suppose that* $\Delta\mathbf{J}^{agg}(\hat{\mathbf{n}})$ *and* $\Delta\mathbf{J}^{brk}(\hat{\mathbf{n}})$ *are continuous and satisfy the Lipschitz conditions*

$$\|\Delta\mathbf{J}^{agg}(\hat{\mathbf{n}}) - \Delta\mathbf{J}^{agg}(\hat{\mathbf{m}})\| \leq L_1\|\hat{\mathbf{n}} - \hat{\mathbf{m}}\| \quad \textit{for all} \quad \hat{\mathbf{n}}, \hat{\mathbf{m}} \in \mathbb{R}^I$$

and

$$\|\Delta\mathbf{J}^{brk}(\hat{\mathbf{n}}) - \Delta\mathbf{J}^{brk}(\hat{\mathbf{m}})\| \leq L_2\|\hat{\mathbf{n}} - \hat{\mathbf{m}}\| \quad \textit{for all} \quad \hat{\mathbf{n}}, \hat{\mathbf{m}} \in \mathbb{R}^I.$$

Then the solution of the semi-discrete system (3.11) is non-negative if and only if for any vector $\hat{\mathbf{n}} \in \mathbb{R}^I$ *and all* $i = 1, \ldots, I$ *and* $t \geq 0$,

$$\hat{\mathbf{n}} \geq 0, \quad \hat{n}_i = 0 \qquad \Longrightarrow \qquad J_i(\hat{\mathbf{n}}) \geq 0.$$

Now we state a useful theorem from Linz [68] which we use to show that the FVS is convergent.

Theorem 3.3.5. *Let us assume that a Lipschitz condition on* $\mathbf{J}(\mathbf{n})$ *is satisfied for* $0 \leq t \leq T$ *and for all* $\mathbf{n}, \hat{\mathbf{n}} \in \mathbb{R}^I$ *where* $\mathbf{n}$ *and* $\hat{\mathbf{n}}$ *are the projected exact and numerical solutions defined in (3.4) and (3.20), respectively. More precisely there exists a Lipschitz constant* $L < \infty$ *such that*

$$\|\mathbf{J}(\mathbf{n}) - \mathbf{J}(\hat{\mathbf{n}})\| \leq L\,\|\mathbf{n} - \hat{\mathbf{n}}\|, \tag{3.29}$$

holds. Then a consistent discretization method is also convergent and the convergence is of the same order as the consistency.

We need the following Gronwall Lemma to prove this theorem. A more general result is proven in Linz [68]. However, for completeness we give the short proof.

Lemma 3.3.6. *If* $v(t)$ *satisfies*

$$|v(t)| \leq k\int_0^t |v(\tau)|d\tau + \int_0^t |r(\tau)|d\tau \tag{3.30}$$

with $k > 0$ *and*

$$\max_{0\leq t\leq T} |r(t)| \leq R > 0,$$

then

$$|v(t)| \leq \frac{R}{k}[\exp(kt) - 1]. \tag{3.31}$$

Proof. Let $z(t)$ be the solution of

$$z(t) = k\int_0^t z(\tau)d\tau + tR.$$

Since $z(t)$ is a positive and increasing function of t, we have

$$z(t) \geq k\int_0^t z(\tau)d\tau + \int_0^t |r(\tau)|d\tau.$$

A comparison with (3.30) ensures that

$$z(t) \geq |v(t)|.$$

But $z(t)$ is given as

$$z(t) = \frac{R}{k}[\exp(kt) - 1],$$

and therefore (3.31) follows. □

Proof. [Theorem 3.3.5]
We know from the Definition 3.3.2 that

$$\boldsymbol{\epsilon}(t) = \mathbf{n}(t) - \hat{\mathbf{n}}(t).$$

Differentiating with respect to time yields

$$\frac{d}{dt}\boldsymbol{\epsilon}(t) = \frac{d\mathbf{n}}{dt} - \frac{d\hat{\mathbf{n}}}{dt} = \boldsymbol{\sigma}(t) + \mathbf{J}(\mathbf{n}) - \mathbf{J}(\hat{\mathbf{n}}).$$

Taking norm both sides, we obtain

$$\frac{d}{dt}\|\boldsymbol{\epsilon}(t)\| \leq \|\boldsymbol{\sigma}(t)\| + \|\mathbf{J}(\mathbf{n}) - \mathbf{J}(\hat{\mathbf{n}})\|.$$

Integrating with respect to t, $\boldsymbol{\epsilon}(0) = 0$ and by Lipschitz condition on $\mathbf{J}(\mathbf{n})$, we get

$$\|\boldsymbol{\epsilon}(t)\| \leq \int_0^t \|\boldsymbol{\sigma}(\tau)\| d\tau + L \int_0^t \underbrace{\|\mathbf{n} - \hat{\mathbf{n}}\|}_{\|\boldsymbol{\epsilon}(t)\|} d\tau.$$

Hence, Gronwall's lemma gives

$$\|\boldsymbol{\epsilon}(t)\| \leq \frac{e_h}{L}(e^{Lt} - 1)$$

where $e_h = \max_{0 \leq t \leq T}\|\boldsymbol{\sigma}(t)\|$. If the scheme is consistent then $\lim_{h \longrightarrow 0} e_h = 0$ and then we have convergence. □

Therefore, due to Theorem 3.3.5, for the convergence of our scheme it remains to show that the method is consistent and the Lipschitz condition (3.29) is satisfied by the fluxes.

3.3.1 Consistency

The following lemma gives the consistency order of the finite volume scheme for aggregation-breakage population balance equations.

Lemma 3.3.7. *Consider the function $S \in \mathcal{C}^2]0, x_{max}]$ and $b, \beta \in \mathcal{C}^2(]0, x_{max}] \times]0, x_{max}])$. Then, for any family of meshes, the consistency of the semi-discrete scheme (3.20) is of second order for the pure breakage process, i.e. with $\Delta\mathbf{J}^{agg}(\hat{\mathbf{n}}) = 0$. For the aggregation and coupled processes, the scheme is second order consistent only on uniform and non-uniform smooth meshes while on oscillatory and non-uniform random meshes it is first order consistent.*

Proof. The spatial truncation error (3.25) is given by

$$\sigma_i(t) = \frac{dn_i(t)}{dt} + (\Delta {J_i}^{\text{agg}}(\mathbf{n}) + \Delta {J_i}^{\text{brk}}(\mathbf{n})). \tag{3.32}$$

Integrating (3.4) over Λ_i and applying the mid-point rule in the time derivative term, we have

$$\frac{dn_i(t)}{dt} = \frac{-1}{x_i \Delta x_i}\left[F^{\text{agg}}(x_{i+1/2}) - F^{\text{agg}}(x_{i-1/2}) + F^{\text{brk}}(x_{i+1/2}) - F^{\text{brk}}(x_{i-1/2})\right] + \mathcal{O}(\Delta x^2).$$

Substituting this into the equation (3.32) and using (3.17) give the following form

$$\begin{aligned}\sigma_i(t) = \frac{-1}{x_i \Delta x_i}\Big[&F^{\text{agg}}(x_{i+1/2}) - F^{\text{agg}}(x_{i-1/2}) - J^{\text{agg}}_{i+1/2}(\mathbf{n}) + J^{\text{agg}}_{i-1/2}(\mathbf{n}) \\ &+ F^{\text{brk}}(x_{i+1/2}) - F^{\text{brk}}(x_{i-1/2}) - J^{\text{brk}}_{i+1/2}(\mathbf{n}) + J^{\text{brk}}_{i-1/2}(\mathbf{n})\Big] + \mathcal{O}(\Delta x^2) \\ = \sigma_i^{\text{agg}}(t) + \sigma_i^{\text{brk}}(t) + \mathcal{O}(\Delta x^2).&\end{aligned}$$

Let us now begin with

$$\begin{aligned}F^{\text{brk}}(x_{i+1/2}) - F^{\text{brk}}(x_{i-1/2}) = -\Bigg(&\sum_{k=i+1}^{I}\int_{\Lambda_k} S(\epsilon) n(t,\epsilon) \int_0^{x_{i+1/2}} ub(u,\epsilon)\, du\, d\epsilon \\ &- \sum_{k=i}^{I}\int_{\Lambda_k} S(\epsilon) n(t,\epsilon) \int_0^{x_{i-1/2}} ub(u,\epsilon)\, du\, d\epsilon\Bigg).\end{aligned}$$

We now use Taylor series expansion of the functions $\mathcal{K}_{x_{i\pm1/2}}(\epsilon) := n(t,\epsilon)\int_0^{x_{i\pm1/2}} ub(u,\epsilon)\, du$ about x_k to get

$$\begin{aligned}F^{\text{brk}}(x_{i+1/2}) - F^{\text{brk}}(x_{i-1/2}) = -\Bigg(&\sum_{k=i+1}^{I}\int_{\Lambda_k} S(\epsilon)\left(K_{x_{i+1/2}}(x_k) + (\epsilon - x_k)K'_{x_{i+1/2}}(x_k)\right) d\epsilon \\ &- \sum_{k=i}^{I}\int_{\Lambda_k} S(\epsilon)\left(K_{x_{i-1/2}}(x_k) + (\epsilon - x_k)K'_{x_{i-1/2}}(x_k)\right) d\epsilon\Bigg) + \mathcal{O}(\Delta x^3).\end{aligned}$$

Replacing $\mathcal{K}_{x_{i\pm1/2}}(x_k)$ from the first and third terms on the right-hand side of the equation and using the mid-point rule, we obtain

$$\begin{aligned}F^{\text{brk}}(x_{i+1/2}) - F^{\text{brk}}(x_{i-1/2}) = -\Bigg(&- J^{\text{brk}}_{i+1/2}(\mathbf{n}) + \sum_{k=i+1}^{I}\int_{\Lambda_k} S(\epsilon)(\epsilon - x_k)K'_{x_{i+1/2}}(x_k) d\epsilon \\ &+ J^{\text{brk}}_{i-1/2}(\mathbf{n}) - \sum_{k=i}^{I}\int_{\Lambda_k} S(\epsilon)(\epsilon - x_k)K'_{x_{i-1/2}}(x_k) d\epsilon\Bigg) + \mathcal{O}(\Delta x^3).\end{aligned}$$

Hence, we determine the local truncation error for the breakage process by

$$\sigma_i^{\text{brk}}(t) = \frac{1}{x_i\Delta x_i}\Bigg(\sum_{k=i+1}^{I}\mathcal{K}'_{x_{i+1/2}}(x_k)\int_{\Lambda_k}S(\epsilon)(\epsilon-x_k)\,d\epsilon - \sum_{k=i}^{I}\mathcal{K}'_{x_{i-1/2}}(x_k)\int_{\Lambda_k}S(\epsilon)(\epsilon-x_k)\,d\epsilon + \mathcal{O}(\Delta x^3)\Bigg)$$

$$= \frac{1}{x_i\Delta x_i}\Bigg(\sum_{k=i+1}^{I}\Big[\mathcal{K}'_{x_{i+1/2}}(x_k) - \mathcal{K}'_{x_{i-1/2}}(x_k)\Big]\int_{\Lambda_k}S(\epsilon)(\epsilon-x_k)\,d\epsilon - \mathcal{K}'_{x_{i-1/2}}(x_i)\int_{\Lambda_i}S(\epsilon)(\epsilon-x_i)\,d\epsilon + \mathcal{O}(\Delta x^3)\Bigg).$$

Applying again the mid-point rule, it should be noted that

$$\int_{\Lambda_k}S(\epsilon)(\epsilon-x_k)\,d\epsilon = 0 + \mathcal{O}(\Delta x^3),$$

and $\mathcal{K}'_{x_{i+1/2}}(x_k) - \mathcal{K}'_{x_{i-1/2}}(x_k) = \mathcal{O}(\Delta x)$. Thus we obtain

$$\sigma_i^{\text{brk}}(t) = \mathcal{O}(\Delta x^2). \tag{3.33}$$

Hence, for the pure breakage process, the consistency of the semi-discrete scheme (3.20) is two which is determined by using (3.24) as

$$\|\boldsymbol{\sigma}(t)\| = \sum_{i=1}^{I}|\sigma_i^{\text{brk}}(t)|\Delta x_i = \mathcal{O}(\Delta x^2),$$

independently of the type of meshes.

Due to the non-linearity of the aggregation problem, it is not easy to determine the consistency order on general meshes. Therefore, we evaluate the consistency of the semi-discrete scheme (3.20) in this case on various meshes separately. The results can be combined to the result of breakage process to give the consistency of the coupled processes. We know from the equation (3.14)

$$F^{\text{agg}}(x_{i+1/2}) - F^{\text{agg}}(x_{i-1/2}) = \Bigg(\sum_{j=1}^{i}\int_{\Lambda_j}u\,n(t,u)\int_{x_{i+1/2}-u}^{x_{\max}}\beta(u,v)n(t,v)dvdu - \sum_{j=1}^{i-1}\int_{\Lambda_j}u\,n(t,u)\int_{x_{i-1/2}-u}^{x_{\max}}\beta(u,v)n(t,v)dvdu\Bigg).$$

Define $\mathcal{L}_{x_{i\pm1/2}}(u) := n(t,u)\int_{x_{i\pm1/2}-u}^{x_{\max}}\beta(u,v)n(t,v)dv$. Taylor series expansion of the functions $\mathcal{L}_{x_{i\pm1/2}}(u)$ about x_j gives

$$F^{\text{agg}}(x_{i+1/2}) - F^{\text{agg}}(x_{i-1/2}) = \Bigg(\sum_{j=1}^{i}\int_{\Lambda_j}u\left(\mathcal{L}_{x_{i+1/2}}(x_j) + (u-x_j)\mathcal{L}'_{x_{i+1/2}}(x_j)\right)du - \sum_{j=1}^{i-1}\int_{\Lambda_j}u\left(\mathcal{L}_{x_{i-1/2}}(x_j) + (u-x_j)\mathcal{L}'_{x_{i-1/2}}(x_j)\right)du\Bigg) + \mathcal{O}(\Delta x^3). \tag{3.34}$$

Applying the mid-point rule, it should again be noted that

$$\int_{\Lambda_j} u(u - x_j)\, du = \mathcal{O}(\Delta x^3),$$

and $\mathcal{L}'_{x_{i+1/2}}(x_j) - \mathcal{L}'_{x_{i-1/2}}(x_j) = \mathcal{O}(\Delta x)$. Therefore, by defining $LHS := F^{\text{agg}}(x_{i+1/2}) - F^{\text{agg}}(x_{i-1/2})$, the equation (3.34) reduces to

$$LHS = \left(\sum_{j=1}^{i} \int_{\Lambda_j} u\mathcal{L}_{x_{i+1/2}}(x_j) du - \sum_{j=1}^{i-1} \int_{\Lambda_j} u\mathcal{L}_{x_{i-1/2}}(x_j) du \right) + \mathcal{O}(\Delta x^3).$$

Substituting the values of $\mathcal{L}_{x_{i\pm 1/2}}(x_j)$ and using the relation $n_i = n(t, x_i) + \mathcal{O}(\Delta x^2)$ yield (leaving the third order terms)

$$LHS = \Bigg(\underbrace{\sum_{j=1}^{i} \int_{\Lambda_j} u n_j \int_{x_{i+1/2}-x_j}^{x_{\max}} \beta(x_j, v) n(t, v) dv du}_{I_1} - \underbrace{\sum_{j=1}^{i-1} \int_{\Lambda_j} u n_j \int_{x_{i-1/2}-x_j}^{x_{\max}} \beta(x_j, v) n(t, v) dv du}_{I_2} \Bigg).$$

Now, I_1 is equivalent to

$$I_1 = \sum_{j=1}^{i} \int_{\Lambda_j} u n_j \left[\int_{x_{i+1/2}-x_j}^{x_{\alpha_{i,j}-1/2}} + \sum_{k=\alpha_{i,j}}^{I} \int_{\Lambda_k} \right] \beta(x_j, v) n(t, v) dv du.$$

Applying the mid-point approximation for the second term, we obtain

$$\begin{aligned} I_1 = &\sum_{j=1}^{i} x_j n_j \Delta x_j \Bigg[\int_{x_{i+1/2}-x_j}^{x_{\alpha_{i,j}-1/2}} \beta(x_j, v) n(t, v) dv \\ &+ \sum_{k=\alpha_{i,j}}^{I} \beta_{j,k} n_k \Delta x_k + \sum_{k=\alpha_{i,j}}^{I} \int_{\Lambda_k} (v - x_k)^2 / 2 (\beta(x_j, v) n(t, v))'' \Bigg] dv + \mathcal{O}(\Delta x^3). \end{aligned}$$

Similarly, we estimate

$$\begin{aligned} I_2 = &\sum_{j=1}^{i-1} x_j n_j \Delta x_j \Bigg[\int_{x_{i-1/2}-x_j}^{x_{\alpha_{i-1,j}-1/2}} \beta(x_j, v) n(t, v) dv \\ &+ \sum_{k=\alpha_{i-1,j}}^{I} \beta_{j,k} n_k \Delta x_k + \sum_{k=\alpha_{i-1,j}}^{I} \int_{\Lambda_k} (v - x_k)^2 / 2 (\beta(x_j, v) n(t, v))'' \Bigg] dv + \mathcal{O}(\Delta x^3). \end{aligned}$$

Subtracting the third term from I_2 to I_1 gives

$$\begin{aligned} &\left[\sum_{j=1}^{i} \sum_{k=\alpha_{i,j}}^{I} - \sum_{j=1}^{i-1} \sum_{k=\alpha_{i-1,j}}^{I} \right] x_j n_j \Delta x_j \int_{\Lambda_k} (v - x_k)^2 / 2 (\beta(x_j, v) n(t, v))'' dv = \\ &\left[- \sum_{j=1}^{i-1} \sum_{k=\alpha_{i-1,j}}^{k=\alpha_{i,j}-1} \right] x_j n_j \Delta x_j \int_{\Lambda_k} (v - x_k)^2 / 2 (\beta(x_j, v) n(t, v))'' dv + \mathcal{O}(\Delta x^3). \end{aligned}$$

By using Lemma 3.3.8 which is stated in the next section, the summation over k is finite in this term. Hence, the right-hand side of this equation becomes of order $\mathcal{O}(\Delta x^3)$ and can be omitted. Therefore, we calculate now

$$LHS = \sum_{j=1}^{i} x_j n_j \Delta x_j \Bigg[\underbrace{\int_{x_{i+1/2}-x_j}^{x_{\alpha_{i,j}-1/2}} \beta(x_j, v) n(t, v) dv}_{I_3} + \sum_{k=\alpha_{i,j}}^{I} \beta_{j,k} n_k \Delta x_k \Bigg]$$
$$- \sum_{j=1}^{i-1} x_j n_j \Delta x_j \Bigg[\underbrace{\int_{x_{i-1/2}-x_j}^{x_{\alpha_{i-1,j}-1/2}} \beta(x_j, v) n(t, v) dv}_{I_4} + \sum_{k=\alpha_{i-1,j}}^{I} \beta_{j,k} n_k \Delta x_k \Bigg] \Bigg) + \mathcal{O}(\Delta x^3).$$

Open the Taylor series about the points $x_{\alpha_{i,j}-1}$ in I_3 and $x_{\alpha_{i-1,j}-1}$ in I_4 as well as by using the relation (3.16), we finally obtain

$$LHS = J^{\text{agg}}_{i+1/2} + \sum_{j=1}^{i} x_j n_j \Delta x_j \int_{x_{i+1/2}-x_j}^{x_{\alpha_{i,j}-1/2}} (v - x_{\alpha_{i,j}-1}) (\beta(x_j, v) n(t, v))' |_{v=x_{\alpha_{i,j}-1}} dv$$
$$- J^{\text{agg}}_{i-1/2} - \sum_{j=1}^{i-1} x_j n_j \Delta x_j \int_{x_{i-1/2}-x_j}^{x_{\alpha_{i-1,j}-1/2}} (v - x_{\alpha_{i-1,j}-1}) (\beta(x_j, v) n(t, v))' |_{v=x_{\alpha_{i-1,j}-1}} dv + \mathcal{O}(\Delta x^3).$$

Let $f(x_j, v) = \beta(x_j, v) n(t, v)$ and $\frac{\partial f}{\partial v}|_{v=x_{\alpha_{i,j}}} = f'(x_j, x_{\alpha_{i,j}})$. This implies that

$$\sigma^{\text{agg}}_i(t) = \frac{-1}{x_i \Delta x_i} \Bigg[\sum_{j=1}^{i} x_j n_j \Delta x_j \int_{x_{i+1/2}-x_j}^{x_{\alpha_{i,j}-1/2}} (v - x_{\alpha_{i,j}-1}) f'(x_j, x_{\alpha_{i,j}-1}) dv$$
$$- \sum_{j=1}^{i-1} x_j n_j \Delta x_j \int_{x_{i-1/2}-x_j}^{x_{\alpha_{i-1,j}-1/2}} (v - x_{\alpha_{i-1,j}-1}) f'(x_j, x_{\alpha_{i-1,j}-1}) dv \Bigg] + \mathcal{O}(\Delta x^2). \tag{3.35}$$

Now we will evaluate the consistency order on four different types of meshes:

Uniform mesh

Let us assume that the first mesh is uniform, i.e. $\Delta x_i = \Delta x$ for all i. In this case $x_{i+1/2} - x_j$ and $x_{\alpha_{i,j}-1}$ become the same and are equal to the pivot point x_{i-j+1}. Similarly,

$$x_{i-1/2} - x_j = x_{\alpha_{i-1,j}-1} = x_{i-j}. \tag{3.36}$$

Applying the Taylor series expansion of the function $f'(x_j, x_{\alpha_{i-1,j}-1} + (x_{\alpha_{i,j}-1} - x_{\alpha_{i-1,j}-1}))$ about

the point $x_{\alpha_{i-1,j}-1}$ in the equation (3.35) to get

$$\begin{aligned}\sigma_i^{\text{agg}}(t) = \frac{-1}{x_i\Delta x_i}\Bigg[&\sum_{j=1}^{i} x_j n_j \Delta x_j \int_{x_{i+1/2}-x_j}^{x_{\alpha_{i,j}-1/2}} (v - x_{\alpha_{i,j}-1}) f'(x_j, x_{\alpha_{i-1,j}-1}) dv + \mathcal{O}(\Delta x^3)\\ &- \sum_{j=1}^{i-1} x_j n_j \Delta x_j \int_{x_{i-1/2}-x_j}^{x_{\alpha_{i-1,j}-1/2}} (v - x_{\alpha_{i-1,j}-1}) f'(x_j, x_{\alpha_{i-1,j}-1}) dv\Bigg] + \mathcal{O}(\Delta x^2)\\ = \frac{-1}{x_i\Delta x_i}\Bigg[&\sum_{j=1}^{i-1} x_j n_j \Delta x_j f'(x_j, x_{\alpha_{i-1,j}-1})\Bigg(\int_{x_{i+1/2}-x_j}^{x_{\alpha_{i,j}-1/2}} (v - x_{\alpha_{i,j}-1}) dv\\ &- \int_{x_{i-1/2}-x_j}^{x_{\alpha_{i-1,j}-1/2}} (v - x_{\alpha_{i-1,j}-1}) dv\Bigg)\Bigg] + \mathcal{O}(\Delta x^2).\end{aligned}$$

Further by simplifying the integrals and using the relation (3.36), we estimate

$$\sigma_i^{\text{agg}}(t) = \frac{-1}{x_i\Delta x_i}\Bigg[\sum_{j=1}^{i-1} x_j n_j \Delta x_j f'(x_j, x_{\alpha_{i-1,j}-1})\Bigg(\frac{\Delta x^2_{\alpha_{i,j}-1}}{8} - \frac{\Delta x^2_{\alpha_{i-1,j}-1}}{8}\Bigg)\Bigg] + \mathcal{O}(\Delta x^2).$$

Hence, for a uniform mesh $\sigma_i^{\text{agg}}(t) = \mathcal{O}(\Delta x^2)$ and so the order of consistency is given by using (3.24) as

$$\|\boldsymbol{\sigma}(t)\| = \sum_{i=1}^{I} |\sigma_i^{\text{agg}}(t)|\Delta x_i = \mathcal{O}(\Delta x^2).$$

Therefore, the scheme is second order consistent on uniform grids.

Non-uniform smooth mesh

A smooth transformation from uniform grids leads to such meshes. In this case grids are assumed to be smooth in the sense that $\Delta x_i - \Delta x_{i-1} = \mathcal{O}(\Delta x^2)$ and $2\Delta x_i - (\Delta x_{i-1} + \Delta x_{i+1}) = \mathcal{O}(\Delta x^3)$, where Δx is the maximum mesh width. For example, let us consider a variable ξ with uniform mesh and a smooth transformation $x = g(\xi)$ to get non-uniform smooth mesh, see Figure 3.1. For the analysis here, we have considered the exponential transformation as $x = \exp(\xi)$. Such a mesh is also known as a geometric mesh, i.e. $x_{i+1/2} = r x_{i-1/2}$ with $r = \exp(\bar{h})$. The term $\bar{h}$ is the width of the uniform grid. Similar to the uniform mesh case we again have second order consistency on such grids.

Equation (3.35) can be rewritten by setting $j = j - 1$ in second term as

$$\begin{aligned}\sigma_i^{\text{agg}}(t) = \frac{-1}{x_i\Delta x_i}\Bigg[&\underbrace{\sum_{j=1}^{i} x_j n_j \Delta x_j \int_{x_{i+1/2}-x_j}^{x_{\alpha_{i,j}-1/2}} (v - x_{\alpha_{i,j}-1}) f'(x_j, x_{\alpha_{i,j}-1}) dv}_{A}\\ &\underbrace{- \sum_{j=2}^{i} x_{j-1} n_{j-1} \Delta x_{j-1} \int_{x_{i-1/2}-x_{j-1}}^{x_{\alpha_{i-1,j-1}-1/2}} (v - x_{\alpha_{i-1,j-1}-1}) f'(x_{j-1}, x_{\alpha_{i-1,j-1}-1}) dv}_{B}\Bigg] + \mathcal{O}(\Delta x^2).\end{aligned}$$

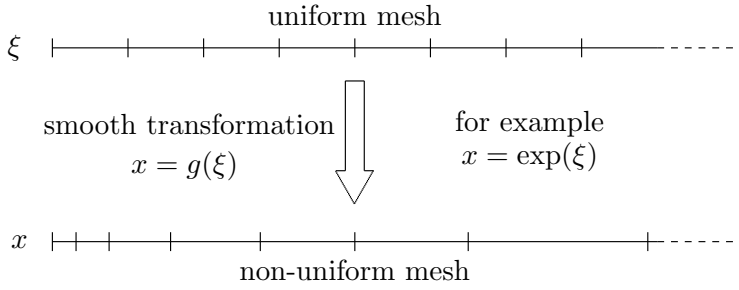

Figure 3.1: Non-uniform smooth mesh.

Now we simplify $A - B$ as

$$\begin{aligned}
A - B =& \sum_{j=2}^{i} x_{j-1} n_{j-1} \Delta x_j \int_{x_{i+1/2}-x_j}^{x_{\alpha_{i,j}-1/2}} (v - x_{\alpha_{i,j}-1}) f'(x_{j-1}, x_{\alpha_{i-1,j-1}-1}) dv \\
& - \sum_{j=2}^{i} x_{j-1} n_{j-1} \Delta x_{j-1} \int_{x_{i-1/2}-x_{j-1}}^{x_{\alpha_{i-1,j-1}-1/2}} (v - x_{\alpha_{i-1,j-1}-1}) f'(x_{j-1}, x_{\alpha_{i-1,j-1}-1}) dv + \mathcal{O}(\Delta x^3) \\
=& \sum_{j=2}^{i} x_{j-1} n_{j-1} (\Delta x_j - \Delta x_{j-1}) \int_{x_{i+1/2}-x_j}^{x_{\alpha_{i,j}-1/2}} (v - x_{\alpha_{i,j}-1}) f'(x_{j-1}, x_{\alpha_{i-1,j-1}-1}) dv \\
& + \sum_{j=2}^{i} x_{j-1} n_{j-1} \Delta x_{j-1} \int_{x_{i+1/2}-x_j}^{x_{\alpha_{i,j}-1/2}} (v - x_{\alpha_{i,j}-1}) f'(x_{j-1}, x_{\alpha_{i-1,j-1}-1}) dv \\
& - \sum_{j=2}^{i} x_{j-1} n_{j-1} \Delta x_{j-1} \int_{x_{i-1/2}-x_{j-1}}^{x_{\alpha_{i-1,j-1}-1/2}} (v - x_{\alpha_{i-1,j-1}-1}) f'(x_{j-1}, x_{\alpha_{i-1,j-1}-1}) dv + \mathcal{O}(\Delta x^3).
\end{aligned}$$

It is worth to mention that we will prove the term $A - B$ is of $\mathcal{O}(\Delta x^3)$ to have a second order consistency of the method. For such smooth meshes, we know that $(\Delta x_j - \Delta x_{j-1}) = \mathcal{O}(\Delta x^2)$. Setting

$$g_{i,j} = x_{j-1} n_{j-1} \Delta x_{j-1} f'(x_{j-1}, x_{\alpha_{i-1,j-1}-1})$$

and $\alpha_{i,j} - 1 = \alpha_1$ as well as $\alpha_{i-1,j-1} - 1 = \alpha_2$ we obtain

$$A - B = \sum_{j=2}^{i} g_{i,j} \left(\int_{x_{i+1/2}-x_j}^{x_{\alpha_1+1/2}} (v - x_{\alpha_1}) dv - \int_{x_{i-1/2}-x_{j-1}}^{x_{\alpha_2+1/2}} (v - x_{\alpha_2}) dv \right) + \mathcal{O}(\Delta x^3).$$

It can further be facilitated as

$$A - B = \sum_{j=2}^{i} \frac{g_{i,j}}{2} \left(\frac{\Delta x_{\alpha_1}^2}{4} - \frac{\Delta x_{\alpha_2}^2}{4} + \left[(x_{i-1/2} - x_{j-1}) - x_{\alpha_2} \right]^2 - \left[(x_{i+1/2} - x_j) - x_{\alpha_1} \right]^2 \right) + \mathcal{O}(\Delta x^3).$$

By our assumption, $x_{i+1/2} - x_j \in \Lambda_{\alpha_{i,j}-1}$ and so $x_{i-1/2} - x_{j-1} \in \Lambda_{\alpha_{i-1,j-1}-1}$. Further notice that $x_{i+1/2} - x_j = r(x_{i-1/2} - x_{j-1})$ and therefore $\alpha_1 = \alpha_2 + 1$. Again by using the condition $(\Delta x_j - \Delta x_{j-1}) = \mathcal{O}(\Delta x^2)$ for such smooth meshes, we determine $\Delta x_{\alpha_1}^2 - \Delta x_{\alpha_2}^2 = \mathcal{O}(\Delta x^3)$.

Now, to get a second order consistency of the scheme, we are remained to show that

$$\left[(x_{i-1/2} - x_{j-1}) - x_{\alpha_2}\right]^2 - \left[(x_{i+1/2} - x_j) - x_{\alpha_1}\right]^2 = \mathcal{O}(\Delta x^3)$$

or equivalently,

$$\left[(x_{i-1/2} - x_{j-1}) - x_{\alpha_2}\right] - \left[(x_{i+1/2} - x_j) - x_{\alpha_1}\right] = \mathcal{O}(\Delta x^2). \tag{3.37}$$

Let us consider ξ_1, ξ_2 are corresponding points in the uniform mesh for x_{α_2} and $x_{i-1/2} - x_{j-1}$, respectively. Consider $h_1 = \xi_2 - \xi_1$ which is given as

$$h_1 = \xi_2 - \xi_1 = \log\left(x_{i-1/2} - x_{j-1}\right) - \log\left(x_{\alpha_2}\right) = \log\left(\frac{x_{i-1/2} - x_{j-1}}{x_{\alpha_2}}\right).$$

Similarly, taking $h_2 = \xi_4 - \xi_3$ where ξ_3 and ξ_4 are the points in the uniform mesh corresponding to the points x_{α_1} and $x_{i+1/2} - x_j$, respectively, we evaluate

$$h_2 = \xi_4 - \xi_3 = \log\left(x_{i+1/2} - x_j\right) - \log\left(x_{\alpha_1}\right) = \log\left(\frac{x_{i+1/2} - x_j}{x_{\alpha_1}}\right) = \log\left(\frac{x_{i-1/2} - x_{j-1}}{x_{\alpha_2}}\right) = h_1.$$

Hence, we obtain $h = h_1 = h_2$. Further we calculate

$$\xi_3 - \xi_1 = \log\left(x_{\alpha_1}\right) - \log\left(x_{\alpha_2}\right) = \log\left(\frac{x_{\alpha_1}}{x_{\alpha_2}}\right) = \log\left(r\right) = \bar{h}.$$

Finally, we estimate (3.37) by using Taylor series expansion as

$$\begin{aligned}\left[(x_{i-1/2} - x_{j-1}) - x_{\alpha_2}\right] - \left[(x_{i+1/2} - x_j) - x_{\alpha_1}\right] &= [g(\xi_2) - g(\xi_1)] - [g(\xi_4) - g(\xi_3)] \\ &= hg^{'}(\xi_1) - hg^{'}(\xi_3) + \mathcal{O}(h^2) \\ &= h(g^{'}(\xi_1) - g^{'}(\xi_1 + \bar{h})) + \mathcal{O}(h^2) \\ &= -h\bar{h}g^{''}(\xi_1) + \mathcal{O}(h^2) = \mathcal{O}(h^2).\end{aligned}$$

Hence, $\sigma_i^{\text{agg}}(t) = \mathcal{O}(\Delta x^2)$. Thus by using the definition of norm (3.24) the order of consistency for the pure aggregation process is two for the smooth meshes $x_{i+1/2} = r x_{i-1/2}$.

Oscillatory and non-uniform random meshes

A mesh is known to be oscillatory mesh, if for $r > 0\,(r \neq 1)$ it is given as

$$\Delta x_{i+1} := \begin{cases} r\Delta x_i & \text{if} \quad i \ \text{ is odd}, \\ \frac{1}{r}\Delta x_i & \text{if} \quad i \ \text{ is even}. \end{cases} \tag{3.38}$$

From the equation (3.35), it is clear that the first two terms on the right-hand side can not be cancel out for oscillatory or random mesh. Therefore, $\sigma_i^{\text{agg}}(t) = \mathcal{O}(\Delta x)$ and so the accuracy of the semi-discrete scheme (3.20) is one by using the relation (3.24) on such meshes.

Now for the coupled aggregation and breakage problems, the local truncation error of each process can be combined and give second order consistency on uniform and non-uniform smooth meshes whereas it is only of first order on the other two types of grids. □

3.3.2 Lipschitz continuity of the fluxes

To prove the Lipschitz continuity of the numerical flux $\mathbf{J}(\hat{\mathbf{n}})$ in (3.20), we use the following three lemmas.

Lemma 3.3.8. *Let us assume that the points $x_{i+j-\frac{1}{2}} - x_k$ for given i, k and $j = 1, 2, \ldots, p$ where $p \geq 2$ lie in the same cell Λ_α for some index α. We also assume that our grid satisfies the quasi-uniformity condition*

$$\frac{\Delta x_{max}}{\Delta x_{min}} \leq C \tag{3.39}$$

for some constant C. Then p is bounded by $C + 1$.

Proof. Our assumption on the points implies that by (3.15), we have

$$\alpha_{i,k} - 1 = \alpha_{i+1,k} - 1 = \ldots = \alpha_{i+p-1,k} - 1 = \alpha.$$

Clearly, $\Delta x_\alpha \geq \Delta x_{i+1} + \Delta x_{i+2} + \ldots + \Delta x_{i+p-1}$. This implies that

$$\frac{\Delta x_\alpha}{\Delta x_l} \leq \frac{\Delta x_{\max}}{\Delta x_{\min}} \leq C \quad \Rightarrow \quad \frac{\Delta x_\alpha}{C} \leq \Delta x_l \quad \text{for} \quad l = i+1, \cdots, i+p-1.$$

Therefore, we obtain

$$\begin{aligned} \Delta x_\alpha \geq & \frac{\Delta x_\alpha}{C} + \frac{\Delta x_\alpha}{C} + \ldots + \frac{\Delta x_\alpha}{C} \\ = & (p-1)\frac{\Delta x_\alpha}{C}, \end{aligned}$$

giving $p \leq (C + 1)$. □

In the next two lemmas we discuss the boundedness of the total number of particles for the aggregation and multiple breakage equations.

Lemma 3.3.9. *Let us assume that the kernels β, S and b satisfy the boundedness conditions as stated in (3.9). Then the total number of particles for the continuous aggregation-breakage equation (3.4) is bounded by a constant $C_{T,x_{max}} > 0$ depending on T and x_{max}, namely*

$$\int_0^{x_{max}} n(t,x)dx = N(t) = \sum_{i=1}^{I} N_i(t) \leq N(0)\exp(x_{max}Q_1T) = C_{T,x_{max}}.$$

Proof. The proof can be found in Appendix A.2.1. □

Lemma 3.3.10. *Under the same assumptions on β, S and b considered in the previous lemma, we have boundedness of the total number of particles for the discrete aggregation-breakage equation (3.11) by using the finite volume schemes. The bound in this case is again $C_{T,x_{max}}$ as before, i.e.*

$$\sum_{i=1}^{I} \hat{n}_i \Delta x_i = \hat{N}(t) = \sum_{i=1}^{I} \hat{N}_i(t) \leq \hat{N}(0)\exp(x_{max}Q_1T) = C_{T,x_{max}} \tag{3.40}$$

provided that the initial data $\hat{N}(0)$ and $N(0)$ are the same.

Proof. The proof has been given in Appendix A.2.2. □

Now, we prove the Lipschitz continuity of the numerical flux $\mathbf{J}(\hat{\mathbf{n}})$ defined as in (3.20).

Lemma 3.3.11. *Let us assume that our grid satisfies the quasi-uniformity condition (3.39). We also assume that the kernels β, S and b satisfy the bounds (3.9) which are $\beta \leq Q$ and $bS \leq Q_1$. Then there exists a Lipschitz constant $L := (4C+6)QC_{T,x_{max}} + 2Q_1 x_{max} < \infty$ for some constants $C, C_{T,x_{max}} > 0$ such that*

$$\|\mathbf{J}(\mathbf{n}) - \mathbf{J}(\hat{\mathbf{n}})\| \leq L \|\mathbf{n} - \hat{\mathbf{n}}\|, \tag{3.41}$$

holds.

Proof. From (3.20), we have the following discretized form of the equation

$$\frac{d\hat{\mathbf{n}}(t)}{dt} = -\Big[\Delta\mathbf{J}^{\mathrm{agg}}(\hat{\mathbf{n}}) + \Delta\mathbf{J}^{\mathrm{brk}}(\hat{\mathbf{n}})\Big] = \mathbf{J}(\hat{\mathbf{n}}). \tag{3.42}$$

To prove the Lipschitz conditions on $\mathbf{J}(\hat{\mathbf{n}})$, it is sufficient to find the Lipschitz conditions on $\Delta\mathbf{J}^{\mathrm{agg}}(\hat{\mathbf{n}})$ and $\Delta\mathbf{J}^{\mathrm{brk}}(\hat{\mathbf{n}})$ for the aggregation and breakage problems separately. For the aggregation we have

$$\|\Delta\mathbf{J}^{\mathrm{agg}}(\mathbf{n}) - \Delta\mathbf{J}^{\mathrm{agg}}(\hat{\mathbf{n}})\| = \sum_{i=1}^{I} \Delta x_i |\Delta J_i^{\mathrm{agg}}(\mathbf{n}) - \Delta J_i^{\mathrm{agg}}(\hat{\mathbf{n}})|.$$

Substituting the value of $\Delta J_i^{\mathrm{agg}}(\mathbf{n})$ from equation (3.18), we obtain

$$\begin{aligned}
\|\Delta\mathbf{J}^{\mathrm{agg}}(\mathbf{n}) - \Delta\mathbf{J}^{\mathrm{agg}}(\hat{\mathbf{n}})\| \leq{}& \sum_{i=1}^{I} \left| \sum_{k=1}^{i-1} \frac{x_k}{x_i} \Delta x_k \sum_{j=\alpha_{i-1,k}}^{\alpha_{i,k}-1} \beta_{j,k} \Delta x_j (-n_j n_k + \hat{n}_j \hat{n}_k) \right| \\
&+ \sum_{i=1}^{I} \left| \sum_{k=1}^{i-1} \frac{x_k}{x_i} \beta_{\alpha_{i,k}-1,k} \Delta x_k (x_{\alpha_{i,k}-1/2} - (x_{i+1/2} - x_k))(n_k n_{\alpha_{i,k}-1} - \hat{n}_k \hat{n}_{\alpha_{i,k}-1}) \right| \\
&+ \sum_{i=1}^{I} \left| \sum_{k=1}^{i-1} \frac{x_k}{x_i} \beta_{\alpha_{i-1,k}-1,k} \Delta x_k (x_{\alpha_{i-1,k}-1/2} - (x_{i-1/2} - x_k))(n_k n_{\alpha_{i-1,k}-1} - \hat{n}_k \hat{n}_{\alpha_{i-1,k}-1}) \right| \\
&+ \sum_{i=1}^{I} \Bigg(\Bigg| \sum_{j=\alpha_{i,i}}^{I} \beta_{j,i} \Delta x_i \Delta x_j (n_i n_j - \hat{n}_i \hat{n}_j) \\
&\qquad + \beta_{\alpha_{i,i}-1,i} \Delta x_i (x_{\alpha_{i,i}-1/2} - (x_{i+1/2} - x_i))(n_i n_{\alpha_{i,i}-1} - \hat{n}_i \hat{n}_{\alpha_{i,i}-1}) \Bigg| \Bigg) \\
&\leq S_1 + S_2 + S_3 + S_4.
\end{aligned} \tag{3.43}$$

Now we evaluate the terms S_i, $i = 1, \cdots, 4$ in (3.43) one by one. First we simplify term S_1 which may be estimated as

$$S_1 \leq \sum_{i=1}^{I} \sum_{k=1}^{i-1} \frac{x_k}{x_i} \Delta x_k \sum_{j=\alpha_{i-1,k}}^{\alpha_{i,k}-1} \beta_{j,k} \Delta x_j |n_j n_k - \hat{n}_j \hat{n}_k|.$$

Since $k < i$ implies that $x_k < x_i$ and by using the relation

$$xy - \hat{x}\hat{y} = 1/2[(x - \hat{x})(y + \hat{y}) + (x + \hat{x})(y - \hat{y})],$$

we get

$$S_1 \leq \sum_{i=1}^{I} \sum_{k=1}^{i-1} \frac{\Delta x_k}{2} \sum_{j=\alpha_{i-1,k}}^{\alpha_{i,k}-1} \beta_{j,k} \Delta x_j |(n_j + \hat{n}_j)(n_k - \hat{n}_k) + (n_j - \hat{n}_j)(n_k + \hat{n}_k)|.$$

We have the estimate $0 \leq \beta(x, y) \leq Q$ for some constant $Q \geq 0$ and $x, y \in]0, x_{\max}]$. Setting $N_i = n_i \Delta x_i$ gives

$$S_1 \leq \frac{Q}{2} \sum_{i=1}^{I} \left(\sum_{k=1}^{I} \Delta x_k |n_k - \hat{n}_k| \sum_{j=\alpha_{i-1,k}}^{\alpha_{i,k}-1} (N_j + \hat{N}_j) + \sum_{k=1}^{I} (N_k + \hat{N}_k) \sum_{j=\alpha_{i-1,k}}^{\alpha_{i,k}-1} \Delta x_j |n_j - \hat{n}_j| \right).$$

Now we open the summation for each i to have

$$S_1 \leq \frac{Q}{2} \sum_{k=1}^{I} \Delta x_k |n_k - \hat{n}_k| \sum_{j=\alpha_{0,k}}^{\alpha_{I,k}-1} (N_j + \hat{N}_j) + \frac{Q}{2} \sum_{k=1}^{I} (N_k + \hat{N}_k) \sum_{j=\alpha_{0,k}}^{\alpha_{I,k}-1} \Delta x_j |n_j - \hat{n}_j|.$$

By using Lemmas 3.3.9 and 3.3.10, which say that the total number of particles is bounded by a constant $C_{T,x_{\max}}$, we figure out

$$S_1 \leq 2QC_{T,x_{\max}} \|\mathbf{n} - \hat{\mathbf{n}}\|.$$

Now we evaluate the term S_2 from (3.43) which is taken as

$$S_2 \leq \sum_{i=1}^{I} \sum_{k=1}^{i-1} \frac{x_k}{x_i} \beta_{\alpha_{i,k}-1,k} \Delta x_k (x_{\alpha_{i,k}-1/2} - (x_{i+1/2} - x_k)) \, |n_k n_{\alpha_{i,k}-1} - \hat{n}_k \hat{n}_{\alpha_{i,k}-1}|.$$

Further simplifications as in the previous case yield

$$\begin{aligned} S_2 &\leq \sum_{i=1}^{I} \sum_{k=1}^{i-1} \frac{Q}{2} \Delta x_k \Delta x_{\alpha_{i,k}-1} \left(|(n_k - \hat{n}_k)(n_{\alpha_{i,k}-1} + \hat{n}_{\alpha_{i,k}-1}) + (n_k + \hat{n}_k)(n_{\alpha_{i,k}-1} - \hat{n}_{\alpha_{i,k}-1})| \right) \\ &\leq \frac{Q}{2} \sum_{i=1}^{I} \sum_{k=1}^{i-1} \Delta x_k |n_k - \hat{n}_k| \, (N_{\alpha_{i,k}-1} + \hat{N}_{\alpha_{i,k}-1}) + \frac{Q}{2} \sum_{i=1}^{I} \sum_{k=1}^{i-1} \Delta x_{\alpha_{i,k}-1} |n_{\alpha_{i,k}-1} - \hat{n}_{\alpha_{i,k}-1}| (N_k + \hat{N}_k). \end{aligned}$$

Changing the order of summation gives

$$\begin{aligned} S_2 \leq \frac{Q}{2} \sum_{k=1}^{I} \Delta x_k |n_k - \hat{n}_k| \sum_{i=k+1}^{I} (N_{\alpha_{i,k}-1} + \hat{N}_{\alpha_{i,k}-1}) \\ + \frac{Q}{2} \sum_{k=1}^{I} (N_k + \hat{N}_k) \sum_{i=k+1}^{I} \Delta x_{\alpha_{i,k}-1} |n_{\alpha_{i,k}-1} - \hat{n}_{\alpha_{i,k}-1}|. \end{aligned}$$

Note that for different values of i, we may have same indices of $\alpha_{i,k}-1$. Therefore, by using the Lemma 3.3.8 which shows that the number of repetition of index in a cell is finite and bounded by some constant C, we obtain

$$S_2 \leq 2CQC_{T,x_{\max}}\|\mathbf{n}-\hat{\mathbf{n}}\|.$$

The case of term S_3 is similar and the difference is only that the index $i-1$ is used instead of i. Hence, we get the same bound on S_2 as

$$S_3 \leq 2CQC_{T,x_{\max}}\|\mathbf{n}-\hat{\mathbf{n}}\|.$$

Finally we simplify the term S_4 from (3.43) as

$$\begin{aligned}
S_4 \leq & \sum_{i=1}^{I}\Bigg(\sum_{j=\alpha_{i,i}}^{I}\beta_{j,i}\Delta x_i\Delta x_j|n_in_j-\hat{n}_i\hat{n}_j| \\
& \quad +\beta_{\alpha_{i,i}-1,i}\Delta x_i(x_{\alpha_{i,i}-1/2}-(x_{i+1/2}-x_i))\,|n_in_{\alpha_{i,i}-1}-\hat{n}_i\hat{n}_{\alpha_{i,i}-1}|\Bigg) \\
\leq & \frac{Q}{2}\sum_{i=1}^{I}\sum_{j=\alpha_{i,i}}^{I}\Delta x_i\Delta x_j|(n_i+\hat{n}_i)(n_j-\hat{n}_j)+(n_i-\hat{n}_i)(n_j+\hat{n}_j)| \\
& \quad +\frac{Q}{2}\sum_{i=1}^{I}\Delta x_i\Delta x_{\alpha_{i,i}-1}|(n_i-\hat{n}_i)(n_{\alpha_{i,i}-1}+\hat{n}_{\alpha_{i,i}-1})+(n_i+\hat{n}_i)(n_{\alpha_{i,i}-1}-\hat{n}_{\alpha_{i,i}-1})| \\
\leq & \frac{Q}{2}\sum_{i=1}^{I}\sum_{j=1}^{I}(N_i+\hat{N}_i)\Delta x_j|n_j-\hat{n}_j|+\frac{Q}{2}\sum_{i=1}^{I}\sum_{j=1}^{I}(N_j+\hat{N}_j)\Delta x_i|n_i-\hat{n}_i| \\
& \quad +\frac{Q}{2}\sum_{i=1}^{I}\Delta x_i|n_i-\hat{n}_i|(N_{\alpha_{i,i}-1}+\hat{N}_{\alpha_{i,i}-1})+\frac{Q}{2}\sum_{i=1}^{I}(N_i+\hat{N}_i)\Delta x_{\alpha_{i,i}-1}|n_{\alpha_{i,i}-1}-\hat{n}_{\alpha_{i,i}-1}|.
\end{aligned}$$

Further simplification gives

$$S_4 \leq 4QC_{T,x_{\max}}\|\mathbf{n}-\hat{\mathbf{n}}\|.$$

Adding all the results from S_1, S_2, S_3 and S_4, we get finally

$$\|\Delta\mathbf{J}^{\mathrm{agg}}(\mathbf{n})-\Delta\mathbf{J}^{\mathrm{agg}}(\hat{\mathbf{n}})\| \leq (4C+6)QC_{T,x_{\max}}\|\mathbf{n}-\hat{\mathbf{n}}\|, \tag{3.44}$$

with a Lipschitz constant $L_1=(4C+6)QC_{T,x_{\max}}$.

Similarly, for the breakage problem, we have

$$\|\Delta\mathbf{J}^{\mathrm{brk}}(\mathbf{n})-\Delta\mathbf{J}^{\mathrm{brk}}(\hat{\mathbf{n}})\| = \sum_{i=1}^{I}\Delta x_i\left|\Delta J_i^{\mathrm{brk}}(\mathbf{n})-\Delta J_i^{\mathrm{brk}}(\hat{\mathbf{n}})\right|.$$

By using the equation (3.19), the above equation reduces to

$$\|\Delta\mathbf{J}^{\mathrm{brk}}(\mathbf{n})-\Delta\mathbf{J}^{\mathrm{brk}}(\hat{\mathbf{n}})\| \leq \sum_{i=1}^{I}\left|\sum_{k=i+1}^{I}S_k(n_k-\hat{n}_k)\Delta x_k\Delta x_ib_{i,k}-S_i(n_i-\hat{n}_i)\sum_{j=1}^{i-1}\frac{x_j}{x_i}b_{j,i}\Delta x_j\Delta x_i\right|.$$

Since $x_j < x_i$ for $j < i$, it can be simplified as

$$\|\Delta\mathbf{J}^{\text{brk}}(\mathbf{n}) - \Delta\mathbf{J}^{\text{brk}}(\hat{\mathbf{n}})\| \leq \sum_{i=1}^{I}\sum_{k=i+1}^{I} S_k b_{i,k}\Delta x_i \Delta x_k \left|n_k - \hat{n}_k\right| + \sum_{i=1}^{I} S_i \left|n_i - \hat{n}_i\right| \sum_{j=1}^{i-1} b_{j,i}\Delta x_i \Delta x_j.$$

Using $bS \leq Q_1$ yields

$$\begin{aligned}\|\Delta\mathbf{J}^{\text{brk}}(\mathbf{n}) - \Delta\mathbf{J}^{\text{brk}}(\hat{\mathbf{n}})\| &\leq Q_1 \sum_{i=1}^{I}\sum_{k=i+1}^{I} \Delta x_i \Delta x_k \left|n_k - \hat{n}_k\right| + Q_1 \sum_{i=1}^{I} \left|n_i - \hat{n}_i\right| \sum_{j=1}^{i-1} \Delta x_i \Delta x_j \\ &\leq Q_1 \sum_{i=1}^{I} \Delta x_i \sum_{k=1}^{I} \Delta x_k \left|n_k - \hat{n}_k\right| + Q_1 \sum_{i=1}^{I} \left|n_i - \hat{n}_i\right| \Delta x_i \sum_{j=1}^{I} \Delta x_j. \quad (3.45)\end{aligned}$$

Hence, we obtain

$$\|\Delta\mathbf{J}^{\text{brk}}(\mathbf{n}) - \Delta\mathbf{J}^{\text{brk}}(\hat{\mathbf{n}})\| \leq 2Q_1 x_{\max}\|\mathbf{n} - \hat{\mathbf{n}}\|,$$

with a Lipschitz constant $L_2 = 2Q_1 x_{\max}$. Hence, we have proved the Lipschitz conditions for $\mathbf{J}(\hat{\mathbf{n}})$ with a Lipschitz constant $L = (4C + 6)QC_{T,x_{\max}} + 2Q_1 x_{\max}$. □

Therefore, by applying Theorem 3.3.5 the order of convergence of the FVS for the pure aggregation or pure breakage or coupled processes is same as the order of consistency which we have stated before in Lemma 3.3.7.

3.4 Numerical results

The mathematical results on convergence analysis are verified numerically for aggregation and breakage problems separately and also for the combined processes considering several test problems. All numerical simulations below were carried out to investigate the experimental order of convergence (EOC) on the five different types of meshes discussed later. The detailed comparisons between the numerical results and the analytical solutions for number density and moments can be found in [48].

We observed analytically that the finite volume scheme gives second order of convergence independently of the meshes for the pure breakage problem while for the aggregation and simultaneous processes it is second order only on uniform and non-uniform smooth meshes. Moreover, the scheme is only first order accurate on oscillatory and random grids for the aggregation and coupled problems. It is important here to mention that we have done the numerical computations on a locally uniform mesh, which is defined little further down, and found that the method is experimentally second order convergent for all the processes. Due to non-linearity of the aggregation and combined aggregation-breakage problems, it is not easy to see mathematically the consistency order of the method on such grids. Therefore, this case is still an open problem.

If the analytical solution is available for the problem, the following formula is used to calculate the EOC

$$\text{EOC} = \ln(E_I/E_{2I})/\ln(2). \quad (3.46)$$

Here E_I and E_{2I} are the discrete relative error norms calculated by dividing the error $\|N - \hat{N}\|$ by $\|N\|$ where $N, \hat{N}$ are the number of particles obtained mathematically and numerically, respectively. The symbols I and $2I$ correspond to the number of degrees of freedom.

Now, in case of unavailability of the analytical solutions for the problem, the EOC can be computed as

$$\text{EOC} = \ln\left(\frac{\|\hat{N}_I - \hat{N}_{2I}\|}{\|\hat{N}_{2I} - \hat{N}_{4I}\|}\right) / \ln(2). \tag{3.47}$$

Here $\hat{N}_I$ denotes the total number of particles obtained by the numerical scheme by using a mesh with I degrees of freedom.

Before going into the details of the test cases, in the following we discuss briefly five different types of uniform and non-uniform meshes where global truncation errors are obtained numerically. Four of these mesh types have also been used in Kumar and Warnecke [46].

Meshes

Uniform mesh

A uniform mesh is obtained when we have $\Delta x_i = \Delta x$ for all i.

Non-uniform smooth mesh

We are familiar with such meshes from the previous section and Figure 3.1. For the numerical computations we have considered a geometric mesh.

Locally uniform mesh

An example of a locally uniform mesh is considered in Figure 3.2. Let us consider that the computational domain is divided into finitely many sub-domains and each sub-domain is divided into an equal size mesh. In this way we get a locally uniform mesh. In our numerical simulation a geometric mesh is taken initially with 30 mesh points and for further level of computations each cell is divided into two equal parts.

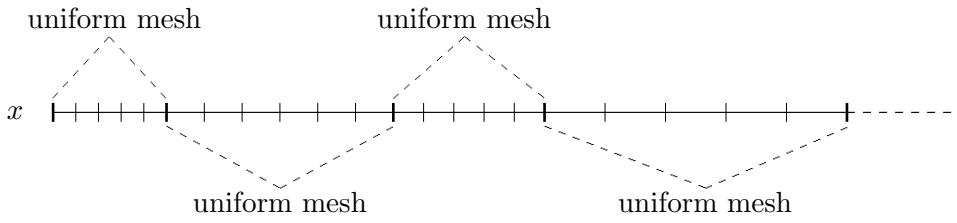

Figure 3.2: Locally uniform mesh.

Oscillatory mesh

The numerical verification has been done on an oscillatory mesh by taking $r = 2$ in the equation (3.38). We have evaluated the EOC in this case numerically by dividing the computation domain into 30 uniform mesh points initially. Then we divide each cell by a 1:2 ratio on further levels of computation.

Non-uniform random mesh

We also analyze the scheme for random grids. Similar to the previous case, we started again with a geometric mesh with 30 grid points but then each cell is divided into two parts of random width in the further refined levels of computation. Here, we performed ten runs on different random grids and the relative errors are measured. The average of these errors over ten runs is used to calculate the EOC.

Numerical examples
Now we consider various test problems of aggregation or breakage or simultaneous processes to verify the convergence results.

Pure aggregation

Test case 1:

First we discuss the numerical verification of the experimental order of convergence of the FVS for aggregation by taking two problems, namely the case of sum and product aggregation kernels. The analytical solutions for both problems taking the negative exponential $n(0, x) = \exp(-\alpha x)$ as initial condition has been given in Scott [90]. Hence, the EOC is computed by using the relation (3.46). Table 3.1 shows that the EOC is 2 on uniform, non-uniform smooth and locally uniform meshes and is 1 on oscillatory and random grids in both cases. The computational domain in this case is taken as $[1E{-}6, 1000]$ which corresponds to the ξ domain $[\ln(1E{-}6), \ln(1000)]$ for the exponential transformation $x = \exp(\xi)$ for the geometric mesh. The parameter $\alpha = 10$ was taken in the initial condition. The simulation result is presented at time $t = 0.5$ and $t = 0.3$ respectively for the sum and the product aggregation kernels corresponding to the aggregation extent $\hat{N}(t)/\hat{N}(0) \approx 0.80$.

Pure breakage

Test case 2:

Here, we calculate the EOC for the binary breakage problem for which an analytical solution is available. We consider the problem with the linear and quadratic selection functions, i.e. $S(x) = x$ and $S(x) = x^2$ with uniform binary breakage $b(x, y) = 2/y$. A mono-disperse initial condition of size unity $n(0, x) = \delta(x - 1)$ is used for the simulation. The analytical solution for the problem has been given in Ziff and McGrady [103]. Hence, we use the relation (3.46) to compute the EOC. Table 3.2 shows the order of convergence and we observe that the FVS is second order convergent on all the grids. The computational domain in this case is taken

as $[1E-3, 1]$. Since the rate of breaking particles taking quadratic selection function is less than that of linear selection function, we take $t = 100$, 200 for linear and quadratic selection functions, respectively. The time has been chosen differently for both the selection functions to have the same extent of breakage $\hat{N}(t)/\hat{N}(0) \approx 22$.

Test case 3:

Now we consider the case of multiple breakage problem where an analytical solution is not known. Therefore, the EOC has been calculated using the numerical results by (3.47). For this problem we have used the normal distribution as an initial condition, i.e.

$$n(0,x) = \frac{1}{\sigma\sqrt{2\pi}} \exp\left(-\frac{(x-\mu)^2}{2\sigma^2}\right). \tag{3.48}$$

The computation has been done for two breakage functions considered by Diemer [13] and Ziff [102], respectively

- case(i): $b(x,y) = \dfrac{px^c(y-x)^{c+(c+1)(p-2)}[c+(c+1)(p-1)]!}{y^{pc+p-1}c![c+(c+1)(p-2)]!}, \quad p \in \mathbb{N}, p \geq 2$
- case(ii): $b(x,y) = \dfrac{12x}{y^2}\left(1-\dfrac{x}{y}\right)$.

We took the quadratic selection function $S(x) = x^2$. In case(i) the relation

$$\int_0^y b(x,y)dx = p$$

holds. So p gives the total number of fragments per breakage event. The parameter $c \geq 0$ is responsible for the shape of the daughter particle distributions. For details concerning this breakage function, the reader is also referred to Sommer et al. [93]. The numerical solutions have been obtained using $p = 4, c = 2$. The second breakage function gives ternary breakage. For the numerical simulations we have taken the minimum and maximum values of x as $1E-3$ and 1 respectively. The time $t = 100$ is set to get the breakage extent $\hat{N}(t)/\hat{N}(0) \approx 22$ in case(i) while $t = 150$ is used for case(ii). The experimental order of convergence (EOC) has been summarized in Table 3.3. As expected from the mathematical analysis, we again observe from the table that the finite volume scheme shows convergence of second order on all the meshes. We also made computations for higher values of p up to 19 and observed that there is no marked difference in the EOC.

Coupled aggregation-breakage

Test case 4:

Now we discuss the EOC for the simultaneous aggregation-breakage problems. We consider a constant aggregation kernel $\beta(x,y) = \beta_0$, uniform binary breakage $b(x,y) = 2/y$ together with a linear selection function $S(x) = x$. The analytical solutions for this problem are given by Lage [55] for the following two different initial conditions

- case(i): $n(0,x) = N_0 \left[\frac{2N_0}{x_0}\right]^2 x \exp\left(-2x\frac{N_0}{x_0}\right)$
- case(ii): $n(0,x) = N_0 \left[\frac{N_0}{x_0}\right] \exp\left(-x\frac{N_0}{x_0}\right).$

This is a special case where the number of particles stays constant. The later initial condition is a steady state solution. For the simulation the computational domain $[1E-2, 10]$ with $N_0 = x_0 = 1$ and time $t = 0.3$ is taken. From Table 3.4, we find that the FVS is second order convergent on uniform, non-uniform smooth as well as on locally uniform meshes and it gives first order on oscillatory and random meshes using (3.46).

Test case 5:

Now we consider the case of product aggregation kernel $\beta(x,y) = xy$ and the linear selection function $S(x) = x$ taken together with two different general breakage functions as stated in **Test case 3**. Analytical solutions are not available for such problems and so the EOC is calculated from numerical solutions by formula (3.47). The computational domain and the time parameters are taken same as in the previous case with the normal distributed initial condition (3.48). We observe here again from Table 3.5 that the FVS shows similar results of convergence as obtained in the previous case for all the meshes.

Table 3.1: EOC (3.46) of the numerical schemes for **Test case 1**.

(a) Uniform mesh

Grid points	$\beta(x,y) = x + y$ Error	EOC	$\beta(x,y) = xy$ Error	EOC
60	0.24E-3	-	0.0177	-
120	0.11E-3	1.95	0.0045	1.96
240	0.04E-3	1.93	0.0012	1.94
480	0.01E-3	1.94	0.0003	1.92

(b) Non-uniform smooth mesh

Grid points	$\beta(x,y) = x + y$ Error	EOC	$\beta(x,y) = xy$ Error	EOC
60	0.0047	-	0.0086	-
120	0.0012	1.99	0.0023	1.90
240	0.0003	1.98	0.0006	1.96
480	0.0001	2.00	0.0001	1.99

(c) Locally uniform mesh

Grid points	$\beta(x,y) = x + y$ Error	EOC	$\beta(x,y) = xy$ Error	EOC
60	0.0055	-	0.0092	-
120	0.0014	1.99	0.0026	1.85
240	0.0003	1.98	0.0007	1.94
480	0.0001	2.00	0.0002	1.96

(d) Oscillatory mesh

Grid points	$\beta(x,y) = x + y$ Error	EOC	$\beta(x,y) = xy$ Error	EOC
60	0.0029	-	0.0048	-
120	0.0014	1.01	0.0019	1.29
240	6.05E-4	1.24	7.66E-4	1.31
480	2.20E-4	1.31	3.52E-4	1.12

(e) Non-uniform random mesh

Grid points	$\beta(x,y) = x + y$ Error	EOC	$\beta(x,y) = xy$ Error	EOC
60	0.79E-3	-	0.0017	-
120	0.42E-3	0.98	8.22E-4	1.06
240	0.22E-3	1.02	2.82E-4	1.21
480	0.82E-4	1.21	1.46E-4	1.02

Table 3.2: EOC (3.46) of the numerical schemes for **Test case 2**.

(a) Uniform smooth mesh

Grid	$S(x) = x$		$S(x) = x^2$	
points	Error	EOC	Error	EOC
60	0.3312	-	0.1870	-
120	0.0829	1.99	0.0482	1.95
240	0.0207	2.00	0.0126	1.94
480	0.0052	2.00	0.0034	1.90

(b) Non-uniform smooth mesh

Grid	$S(x) = x$		$S(x) = x^2$	
points	Error	EOC	Error	EOC
60	0.0526	-	0.1638	-
120	0.0136	1.95	0.0423	1.95
240	0.0034	1.99	0.0112	1.92
480	0.0009	2.00	0.0031	1.85

(c) Locally uniform mesh

Grid	$S(x) = x$		$S(x) = x^2$	
points	Error	EOC	Error	EOC
60	0.0530	-	0.1685	-
120	0.0136	1.96	0.0437	1.95
240	0.0034	1.99	0.0115	1.93
480	0.0009	2.00	0.0031	1.88

(d) Oscillatory mesh

Grid	$S(x) = x$		$S(x) = x^2$	
points	Error	EOC	Error	EOC
60	0.0577	-	0.1310	-
120	0.0157	1.88	0.0376	1.80
240	0.0042	1.91	0.0105	1.84
480	0.0011	1.91	0.0030	1.82

(e) Non-uniform random mesh

Grid	$S(x) = x$		$S(x) = x^2$	
points	Error	EOC	Error	EOC
60	0.3516	-	1.1106	-
120	0.1001	1.81	0.3301	1.75
240	0.0282	1.83	0.0944	1.81
480	0.0078	1.85	0.0268	1.82

Table 3.3: EOC (3.47) of the numerical schemes for **Test case 3**.

(a) Uniform smooth mesh

Grid	case(i)		case(ii)	
points	Error	EOC	Error	EOC
60	-	-	-	-
120	2.0655	-	4.7916	-
240	0.6548	1.70	2.5829	2.16
480	0.1789	1.93	0.4364	1.91
960	0.0441	2.10	0.1792	1.67

(b) Non-uniform smooth mesh

Grid	case(i)		case(ii)	
points	Error	EOC	Error	EOC
60	-	-	-	-
120	0.0244	-	0.0113	-
240	0.0060	2.02	0.0028	2.01
480	0.0015	1.98	0.0007	2.00
960	0.0004	2.02	0.0002	2.00

(c) Locally uniform mesh

Grid	case(i)		case(ii)	
points	Error	EOC	Error	EOC
60	-	-	-	-
120	0.0244	-	0.0114	-
240	0.0060	2.02	0.0029	1.99
480	0.0015	1.98	0.0007	2.00
960	0.0004	2.02	0.0002	2.00

(d) Oscillatory mesh

Grid	case(i)		case(ii)	
points	Error	EOC	Error	EOC
60	-	-	-	-
120	0.0244	-	0.0114	-
240	0.0060	2.02	0.0029	1.99
480	0.0015	1.98	0.0007	2.00
960	0.0004	2.02	0.0002	2.00

(e) Non-uniform random mesh

Grid	case(i)		case(ii)	
points	Error	EOC	Error	EOC
60	-	-	-	-
120	0.0244	-	0.0114	-
240	0.0060	2.02	0.0029	1.99
480	0.0015	1.98	0.0007	2.00
960	0.0004	2.02	0.0002	2.00

Table 3.4: EOC (3.46) of the numerical schemes for **Test case 4**.

(a) Uniform mesh

Grid	case(i)		case(ii)	
points	Error	EOC	Error	EOC
60	0.3E-2	-	0.0032	-
120	0.1E-2	1.75	0.0009	1.83
240	0.3E-3	1.86	2.4E-3	1.90
480	0.7E-4	2.01	0.7E-4	1.89

(b) Non-Uniform smooth mesh

Grid	case(i)		case(ii)	
points	Error	EOC	Error	EOC
60	0.0066	-	0.0018	-
120	0.0018	1.90	0.0005	1.95
240	0.0004	1.97	0.0001	1.98
480	0.0001	2.00	2.9E-5	2.00

(c) Locally uniform mesh

Grid	case(i)		case(ii)	
points	Error	EOC	Error	EOC
60	0.0082	-	0.0021	-
120	0.0022	1.92	0.0006	1.91
240	0.0006	1.94	0.0001	1.99
480	0.0001	2.01	3.4E-5	2.02

(d) Oscillatory mesh

Grid	case(i)		case(ii)	
points	Error	EOC	Error	EOC
60	0.0019	-	0.0053	-
120	0.62E-3	1.28	0.31E-2	0.98
240	0.29E-3	1.13	1.34E-3	1.07
480	0.15E-3	1.02	0.71E-3	1.06

(e) Non-uniform random mesh

Grid	case(i)		case(ii)	
points	Error	EOC	Error	EOC
60	0.0082	-	0.0042	-
120	0.0037	1.07	0.0023	0.91
240	1.45E-3	1.22	0.0011	1.10
480	0.86E-3	1.01	0.04E-2	1.23

Table 3.5: EOC (3.47) of the numerical schemes for **Test case 5**.

(a) Uniform mesh

Grid	case(i)		case(ii)	
points	Error,	EOC	Error,	EOC
60	-	-	-	-
120	0.13E-4	-	0.17E-4	-
240	0.03E-4	1.98	0.41E-5	2.04
480	0.01E-4	1.91	0.11E-5	1.94
960	0.03E-5	1.88	0.31E-6	1.86

(b) Non-Uniform smooth mesh

Grid	case(i)		case(ii)	
points	Error,	EOC	Error,	EOC
60	-	-	-	-
120	0.90E-3	-	0.97E-3	-
240	0.27E-3	1.71	0.28E-3	1.81
480	0.07E-3	1.89	0.07E-3	1.92
960	0.02E-3	1.96	0.02E-3	1.97

(c) Locally uniform mesh

Grid	case(i)		case(ii)	
points	Error,	EOC	Error,	EOC
60	-	-	-	-
120	0.83E-3	-	0.89E-3	-
240	0.23E-3	1.83	0.24E-3	1.89
480	0.06E-3	1.95	0.06E-3	1.97
960	0.01E-3	1.99	0.02E-3	1.99

(d) Oscillatory mesh

Grid	case(i)		case(ii)	
points	Error,	EOC	Error,	EOC
60	-	-	-	-
120	0.5552	-	0.3255	-
240	0.2878	0.95	0.1648	0.98
480	0.1434	1.08	0.0823	1.00
960	0.0711	1.12	0.0401	1.04

(e) Non-uniform random mesh

Grid	case(i)		case(ii)	
points	Error,	EOC	Error,	EOC
60	-	-	-	-
120	0.1489	-	0.1097	-
240	0.0837	0.84	0.0490	1.16
480	0.0426	0.98	0.0232	1.08
960	0.0232	0.92	0.0120	0.96

Chapter 4

Moment preserving methods

This chapter deals with the moment preserving numerical schemes for solving general population balance equations. We consider unified numerical approaches to simultaneous aggregation, breakage, growth and source terms such as nucleation. We discuss the criteria for the preservation of different moments. Further we present a finite volume scheme which is one moment preserving depending upon the processes under consideration. For instance, in case of aggregation or breakage or both problems it shows the first moment preservation whereas for the growth and source terms we find the zeroth moment preservation. These preservation are due to the well-known property of conservativity of finite volume methods. However, we observe that coupling of all the processes causes non preservation for any moments.

Therefore, the question arises how to couple the zeroth and first moment preservation in an efficient manner. For this we rewrite the cell average technique into a conservative formulation for the aggregation, breakage and source terms. These formulations are coupled together with a modified upwind scheme for the growth process to give moment preservation with respect to the zeroth and first moments for all the coupled processes. We verify the moment preservation mathematically and numerically. The numerical verifications are performed by taking several coupled processes for which analytical solutions are available.

Let us now briefly outline the contents of this chapter. First we recall a brief description of equations from Chapter 1 and then discuss the finite volume schemes in Section 4.2. Further, in Section 4.3 issues of preservation with respect to the moments are given. Here, we also present one moment and two moment preserving numerical methods. Finally we proceed in Section 4.4 to show the numerical results for many test problems under various coupled processes.

4.1 Introduction

We know from (1.10) the general form of continuous population balance equation for simultaneous aggregation [99], breakage [102], growth [42] and nucleation [54] or other sources is given as

$$\frac{\partial f(t,x)}{\partial t} + \frac{\partial [G(x)f(t,x)]}{\partial x} = \frac{1}{2}\int_0^x \beta(x-u,u)f(t,x-u)f(t,u)du - \int_0^\infty \beta(x,u)f(t,u)f(t,x)du + \int_x^\infty b(x,u)S(u)f(t,u)du - S(x)f(t,x) + B_{\text{src}}(t,x). \tag{4.1}$$

Here f denotes the number density distribution function. Note that the coagulation kernel β is non-negative and satisfies the symmetry condition $\beta(x,y) = \beta(y,x)$ and the breakage function b has the following important properties

$$\int_0^x b(u,x)du = \overline{N}(x), \quad \int_0^x ub(u,x)du = x, \tag{4.2}$$

for any $x \in]0,\infty[$. In order to close the system, the equation (4.1) must be supplemented with appropriate initial and possibly boundary conditions at $x = 0$. We also recall from (1.11) the jth moment of the particle size distribution which is given as

$$\mu_j(t) = \int_0^\infty x^j f(t,x)dx. \tag{4.3}$$

It should be mentioned that the total number of particles changes in an aggregation or breakage process while the total mass (volume) remains conserved. Therefore, the mass density function xf is the conservative variable for any aggregation-breakage processes. On the other hand the growth process has no effect on the number of particles but the total mass of the particles increases. If we neglect aggregation, breakage and source terms in the equation (4.1) then we are left with a conservative differential equation for the number density function f. In case of pure nucleation neither number density nor the total mass remains conserved. Since the aggregation and breakage terms are mass conservative, we have the following conservative form of the equations from (1.13) with mass density $xf(t,x)$ as conserved quantity

$$\frac{\partial\left[xf(t,x)\right]}{\partial t} + \frac{\partial}{\partial x}\left(F^{\text{agg}}(t,x) + F^{\text{brk}}(t,x)\right) = 0. \tag{4.4}$$

The flux functions F^{agg} and F^{brk} are given by

$$F^{\text{agg}}(t,x) = \int_0^x \int_{x-u}^\infty u\beta(u,v)f(t,u)f(t,v)dvdu, \tag{4.5}$$

and

$$F^{\text{brk}}(t,x) = -\int_x^\infty \int_0^x ub(u,v)S(v)f(t,v)dudv. \tag{4.6}$$

As stated before in Chapter 1 that both forms of aggregation-breakage population balance equations (PBEs) (4.1), without growth and source terms and (4.4) are interchangeable. Hence, we will be using both forms depending upon their convenience for calculations.

Analytical solutions are available only for a limited number of simplified problems and therefore numerical solutions are frequently needed to solve the PBEs (4.1). In all PBEs mentioned above, the volume variable may vary from 0 to ∞. In order to apply a numerical scheme we consider truncated equations replacing ∞ by a sufficiently large number $R \in \mathbb{R}$. This could involve an extra boundary condition at $x = R$. To distinguish between the solutions of this truncated system from the original one we use the number density n instead of f.

4.2 Finite volume schemes

A typical conservation law with source term (nucleation) is given by the following equation

$$\frac{\partial(x^p n(t,x))}{\partial t} + \frac{\partial F(t,x)}{\partial x} = x^p B_{\text{src}}(t,x) \quad \text{for} \quad p=0 \quad \text{or} \quad p=1. \tag{4.7}$$

Here n is the unknown variable and the function F is called flux function. The variable n typically represents a number density for sizes x and the quantity xn a size density in the case $p=1$. The equation (4.7) represents different processes discussed above depending upon the values of p or the nature of F and B_{src}. For example, it models the combined aggregation-breakage processes for $p=1, F=F^{\text{agg}}+F^{\text{brk}}$ and $B_{\text{src}}=0$. The case of pure growth is obtained by setting $p=0, F=G(x)n(t,x), B_{\text{src}}=0$. Taking $p=0$ or $p=1$ and $F=0$ leads to a parameter dependent ordinary differential equation for the pure source term, e.g. for a nucleation process.

We discretize the domain $]0,R]$ into small *cells* $\Lambda_i =]x_{i-1/2}, x_{i+1/2}]$ for $i=1,\ldots,I$. We define the mid points $x_i=(x_{i-1/2}+x_{i+1/2})/2$, taking $x_{1/2}=0$, $x_{I+1/2}=R$ and the width of cell i to be $\Delta x_i = x_{i+1/2}-x_{i-1/2}$. We denote by $\Delta x = \max_{i=1,\ldots,I}\Delta x_i$ the *mesh size*. If $\Delta x_i = \Delta x$ for $i=1,\ldots,I$ we call this a *uniform* mesh. For later use we also introduce a ghost cell at each boundary by setting $x_0=-x_1, \Delta x_0=\Delta x_1, x_{I+1}=x_I+\Delta x_I$ and $\Delta x_{I+1}=\Delta x_I$. The finite volume scheme in an almost semi-discrete form is given as [64]

$$x_i^p \frac{dn_i(t)}{dt} = -\frac{1}{\Delta x_i}\left(J_{i+1/2}-J_{i-1/2}\right) + \frac{x_i^p}{\Delta x_i}\int_{x_{i-1/2}}^{x_{i+1/2}} B_{\text{src}}(t,x)dx, \quad i=1,\ldots,I, \tag{4.8}$$

where $n_i(t)$ numerically approximates the average number density $\frac{1}{\Delta x_i}\int_{x_{i-1/2}}^{x_{i+1/2}} n(t,x)dx$. The term $J_{i+1/2}$ is called *the numerical flux* which is an appropriate approximation of the continuous flux function F. Various numerical methods can be obtained from different choices of the numerical flux $J_{i+1/2}$. For the source integral one would take exact integration when possible or some numerical quadrature otherwise. When the values of the integral for each i have been made precise, we have a fully semi-discrete form of the equation (4.8). For simplicity, we are assuming the following compact supports

$$\beta(x,y)=0, \qquad \text{for} \quad x+y\geq R,$$
$$S(x)=0, \qquad \text{for} \quad x>R \tag{4.9}$$
$$B_{\text{src}}(t,x)=0, \qquad \text{for} \quad x>R \quad \text{or} \quad x<x_{1/2}. \tag{4.10}$$

We will be discussing mass or number preservation under the above mentioned conditions on the kernels. The preservation with respect to the number and mass for the growth problem is discussed for any growth rate without having compact support. For notational convenience, in what follows we use n_i for $n_i(t)$.

4.3 Issues of moment preservation

Besides the numerical prediction of the number density distribution, an accurate prediction of moments is important in some applications. Also this turns out to be a desirable property for

numerical schemes to preserve one or more moments. Therefore, before we go into a further discussion of the numerical methods let us discuss some issues of moment preservation.

Definition of moment preservation

Assume that we are given an exact solution n of (4.7) and a numerical solution $n_i(t)$ of (4.8). Let us define the *jth numerical moment* with respect to the number density n as

$$\mu_j^{\Delta x} = \sum_{i=1}^{I} x_i^j \Delta x_i n_i. \tag{4.11}$$

Multiplying the discretized equation (4.8) by $x_i^{j-p}\Delta x_i$ for $p = 0$ or $p = 1$ and summation over i gives the following moment equation

$$\frac{d\mu_j^{\Delta x}}{dt} = -\sum_{i=1}^{I} x_i^{j-p}\Big(J_{i+1/2} - J_{i-1/2}\Big) + \sum_{i=1}^{I} x_i^j \int_{x_{i-1/2}}^{x_{i+1/2}} B_{\text{src}}(t,x)dx. \tag{4.12}$$

Let us now transform the continuous equation (4.7) into a moment equation for the number density n by multiplication with x^{j-p} and integration from 0 to $x_{I+1/2}$ to give

$$\frac{d\mu_j}{dt} = \frac{d}{dt}\left(\int_0^{x_{I+1/2}} x^j n(t,x)dx\right) = -\int_0^{x_{I+1/2}} x^{j-p}\frac{\partial F(t,x)}{\partial x}dx + \int_0^{x_{I+1/2}} x^j B_{\text{src}}(t,x)dx. \tag{4.13}$$

From the preceding equation, we now wish to derive a differential equation similar to (4.12) for the calculation of moments. This we do by inserting the numerical solution n_i into (4.13) in the following manner. We interpret the numerical solution as a singular measure. Clearly this is possible if we interpret the L^1-function $n(t,x)$, which is an exact solution of equation (4.7) truncated to $]0,R]$, in equation (4.13) as a density of a measure that is absolutely continuous with respect to Lebesgue measure [16]. This we approximate by a discrete measure using the average value given by the numerical solution n_i on each grid cell. Using the Dirac measure δ_x, we take as number density the time dependent discrete measure

$$n(t,\cdot) \approx \sum_{i=1}^{I} n_i(t)\Delta x_i \delta_{x_i}(\cdot) \tag{4.14}$$

obtained from the numerical solution. First note in passing that if we put this measure into the right hand side of (4.3) and integrate with respect to the $d\delta_{x_i}$, we obtain the right hand side of (4.11). We now replace in the first integral on the right hand side of (4.13) the integration with respect to the measure dx by integration with respect to the singular measures $d\delta_{x_i}$. Note that we are basically using the idea of Kumar and Ramkrishna [53] to interpret the numerical data n_i concentrated at what they termed the *pivot point* x_i. After substitution of n as given in (4.14) into the equation (4.13), we obtain

$$\frac{d\hat{\mu}_j}{dt} := -\int_0^{x_{I+1/2}} x^{j-p}\frac{\partial F(t,x)}{\partial x}\bigg|_{n(t,\cdot)\approx\left(\sum_{i=1}^{I} n_i\Delta x_i\delta_{x_i}(\cdot)\right)} dx + \int_0^{x_{I+1/2}} x^j B_{\text{src}}(t,x)dx. \tag{4.15}$$

Note that $\hat{\mu}_j(t)$ is obtained from the right-hand side by simple integration from 0 to t. For clarification we have to explain how the first term on the right-hand side of the equation (4.15)

is actually computed. For aggregation or breakage, i.e. $p = 1$, we use the relations (1.17) respectively (1.18) to replace the differential term for $j = 0$ and $j = 1$. Details can be found in Appendix B.4. For growth we know $p = 0$. In this case we eliminate $\frac{\partial F(t,x)}{\partial x}$ by an integration by parts as follows:

$$\frac{d\hat{\mu}_j}{dt} = -x^j F(t,x)\Big|_0^{x_{I+1/2}} + \int_0^{x_{I+1/2}} jx^{j-1} F(t,x)\Big|_{n(t,\cdot)\approx\left(\sum_{i=1}^{I} n_i \Delta x_i \delta_{x_i}(\cdot)\right)} dx.$$

More precise formulation for each cases of pure growth, source, aggregation and breakage processes is given in this section later.

Definition 4.3.1. *A finite volume scheme (4.8) is said to be* ***moment preserving with respect to the jth moment*** *if*

$$\frac{d\hat{\mu}_j}{dt} = \frac{d\mu_j^{\Delta x}}{dt}, \tag{4.16}$$

i.e., the right hand sides of equations (4.12) and (4.15) become the same, with the exception of boundary terms in the case of growth. This will be more clear when we discuss the numerical schemes, see Subsections 4.3.1 and 4.3.2. As a special case, ***moment conservation*** *is given if the right hand side of the moment ordinary differential equation is zero.* □

This definition generalizes the concept of conservative scheme to other moments. A *conserved* moment is one which remains constant in time. This is a property that is very easy to verify numerically, because the time derivative of a conserved moment is zero. Our definition allows us to compare schemes with respect to how well they reproduce the correct behavior in time of moments that are not conserved but change in time. The discrete solution is treated like a measure solution of the equations [24, 77]. Interestingly, we show that we can find schemes that exactly give the right moment behavior for more than one moment. It should be emphasized here that the finite volume scheme is automatically moment preserving with respect to the zeroth moment ($j = 0$) for the pure growth using number as conserved dependent variable. It is moment preserving with respect to the first moment ($j = 1$) for aggregation as well as for breakage with mass as conserved dependent variable. In both cases this is due to its conservativity. Therefore, our main concern is to see the moment preserving behavior of the numerical scheme for the first moment ($j = 1$) in case of pure growth while for aggregation and breakage it is zeroth moment ($j = 0$). Moreover, neither of these two moments are conserved by source terms. Hence, we investigate both zeroth and first moment preservation in this case.

We can look at our definition of moment preservation also in the following manner. Rewrite (4.13) in residual form as

$$\frac{d}{dt}\left(\int_0^{x_{I+1/2}} x^j n(t,x)dx\right) + \int_0^{x_{I+1/2}} x^{j-p}\frac{\partial F(t,x)}{\partial x}dx - \int_0^{x_{I+1/2}} x^j B_{\text{src}}(t,x)dx = R_j(t). \tag{4.17}$$

For any exact solution n of (4.7) we have the *residual* $R_j(t) = 0$. Now we insert our numerical solution $n_i(t)$ in the form (4.14) as a discrete measure solution into the equation (4.17). Then we will generally have a non-zero residual $R_j(t)$. Moment preservation is now the special case in which a scheme satisfies $R_j(t) = 0$ for certain j.

Semi-discretization of moments

Let us now formulate the equation (4.15) for the first two moments in the case of the pure growth or source terms and for the zeroth moment for breakage as well as aggregation processes separately. For the pure growth processes we have $p = 0$ and $F = G(x)n(t, x)$. In this case, the zeroth moment is obtained from the equation (4.15) and is given as

$$\begin{aligned}\frac{d\hat{\mu}_0}{dt}|_{\text{grt}} &= -\int_{x_{1/2}=0}^{x_{I+1/2}} \frac{\partial}{\partial x}(G(x)n(t,x))dx \\ &= -G(x_{I+1/2})n(t,x_{I+1/2}) + G(x_{1/2})n(t,x_{1/2}).\end{aligned} \tag{4.18}$$

This reflects the conservativity of particle number, i.e. the total number changes only due to fluxes at the boundaries of the domain.
The first moment is evaluated from the equation (4.15) after integration by parts as

$$\begin{aligned}\frac{d\hat{\mu}_1}{dt}|_{\text{grt}} =& -\int_{x_{1/2}}^{x_{I+1/2}} x\frac{\partial}{\partial x}(G(x)n(t,x))\Big|_{n(t,\cdot)\approx\left(\sum_{i=1}^{I} n_i\Delta x_i\delta_{x_i}(\cdot)\right)} dx \\ =& - x_{I+1/2}G(x_{I+1/2})n(t,x_{I+1/2}) + x_{1/2}G(x_{1/2})n(t,x_{1/2}) \\ &+ \int_{x_{1/2}}^{x_{I+1/2}} G(x)n(t,x)\Big|_{n(t,\cdot)\approx\left(\sum_{i=1}^{I} n_i\Delta x_i\delta_{x_i}(\cdot)\right)} dx \\ =& - x_{I+1/2}G(x_{I+1/2})n(t,x_{I+1/2}) + x_{1/2}G(x_{1/2})n(t,x_{1/2}) + \sum_{i=1}^{I} G(x_i)n_i\Delta x_i.\end{aligned} \tag{4.19}$$

The case of source terms, for which the nucleation process or harvesting are an examples is trivial. The formulations of the equation (4.15) for the zeroth and the first moments in this case are given as

$$\frac{d\hat{\mu}_0}{dt}|_{\text{src}} = \int_0^{x_{I+1/2}} B_{\text{src}}(t,x)dx \tag{4.20}$$

and

$$\frac{d\hat{\mu}_1}{dt}|_{\text{src}} = \int_0^{x_{I+1/2}} xB_{\text{src}}(t,x)dx, \tag{4.21}$$

respectively. Here, we assumed that the source functions B_{src} and xB_{src} can be integrated analytically. Otherwise the right-hand side has to be replaced by a quadrature formula.

To obtain the semi-discrete moment equation for the pure aggregation, we use the relationship (1.17). In this case the equation (4.15) for $j = 0$ reduces to

$$\frac{d\hat{\mu}_0}{dt}|_{\text{agg}} = -\sum_{\substack{j,k \\ (x_j+x_k)\le x_{I+1/2}}}^{j\ge k} \left(1 - \frac{1}{2}\delta_{j,k}\right)\Delta x_j\Delta x_k\beta(x_j,x_k)n_jn_k \tag{4.22}$$

and for $j = 1$ it becomes

$$\frac{d\hat{\mu}_1}{dt}|_{\text{agg}} = 0.$$

The calculation is summarized in Appendix B.4.

Finally we derive a similar semi-discrete equation of the zeroth and the first moment for breakage. Again, we use the equation (4.15) and the relationship (1.18) to get

$$\frac{d\hat{\mu}_0}{dt}|_{\text{brk}} = \sum_{i=1}^{I} S(x_i)\Delta x_i n_i \left(\int_0^{x_i} b(x, x_i)dx - 1 \right) \tag{4.23}$$

and

$$\frac{d\hat{\mu}_1}{dt}|_{\text{brk}} = 0. \tag{4.24}$$

We provide the details in Appendix B.4.

4.3.1 One moment preserving methods

There are two straight forward applications of the finite volume method in this context. One is to the growth term, when number density n is the computed variable that is conserved. The second is for aggregation-breakage in the form (4.4) for the mass density xn as conserved quantity. Therefore, the total mass or number preservation is obvious for the aggregation-breakage or the growth problems, respectively. Since finite volume schemes automatically define conservative difference schemes, these variables are respectively conserved on the discrete level as well. In certain combined systems where e.g., growth and aggregation are combined, the two applications of the finite volume method do not fit together. This causes a complete loss of moment preservation in the formulation. Therefore, the question arises how to couple them efficiently. The aim here is to present moment preserving formulations of the combined aggregation, breakage and growth processes including source terms.

Following the idea of Kumar and Warnecke [47], we use the basic approaches of FVS for aggregation-breakage and source terms as well as the simple upwind scheme (SUS) for growth process to solve the general one-dimensional PBEs (4.1). In this and the following section, we will present numerical methods which are moment preserving with respect to only one moment or to two moments, respectively. However, in this section we also show that the straight forward FVS for the aggregation-breakage is not the zeroth moment preserving. Analogously, this is true for the first moment in the case of the growth process. The moment preservation and non-preservation are shown analytically and are also verified numerically later on.

FVS for aggregation and breakage

We use the following discretization of the aggregation-breakage population balance equations

$$\frac{x_i dn_i}{dt} = -\frac{1}{\Delta x_i}\left[J^{\text{agg}}_{i+1/2} - J^{\text{agg}}_{i-1/2} + J^{\text{brk}}_{i+1/2} - J^{\text{brk}}_{i-1/2} \right]. \tag{4.25}$$

Here the numerical flux $J^{\text{agg}}_{i+1/2}$, given by Filbet and Laurençot [23] is defined as

$$J^{\text{agg}}_{i+1/2} = \sum_{k=1}^{i} \Delta x_k (xn)_k \left(\sum_{j=\alpha_{i,k}}^{I} \int_{\Lambda_j} \frac{\beta(u, x_k)}{u}\, du\, (xn)_j + \int_{x_{i+1/2-x_k}}^{x_{\alpha_{i,k}-1/2}} \frac{\beta(u, x_k)}{u}\, du\, (xn)_{\alpha_{i,k}-1} \right). \tag{4.26}$$

The parameter I denotes the number of cells. The integer $\alpha_{i,k}$ corresponds to the index of each cell such that $x_{i+1/2} - x_k \in \Lambda_{\alpha_{i,k}-1}$. For breakage processes, we have the numerical flux $J^{\text{brk}}_{i+1/2}$ from J. Kumar [42] as

$$J^{\text{brk}}_{i+1/2} = -\sum_{k=i+1}^{I} (xn)_k \int_{\Lambda_k} \frac{S(\epsilon)}{\epsilon}\, d\epsilon \int_0^{x_{i+1/2}} ub(u, x_k)\, du. \tag{4.27}$$

Note that for the truncated fluxes F^{agg}_R and F^{brk}_R, which are obtained from (4.5) and (4.6) by replacing ∞ by R, we have using our assumption (4.9)

$$F^{\text{agg}}_R(t, 0) = F^{\text{agg}}_R(t, R) = F^{\text{brk}}_R(t, 0) = F^{\text{brk}}_R(t, R) = 0,$$

implies

$$J^{\text{agg}}_{1/2} = J^{\text{agg}}_{I+1/2} = J^{\text{brk}}_{1/2} = J^{\text{brk}}_{I+1/2} = 0.$$

It is well known that the total mass conservation in this case can easily be obtained by multiplying (4.25) by Δx_i, summing with respect to i and by using that the fluxes at the boundaries $x_{1/2} = 0$ and $x_{I+1/2} = R$ are zero. This gives

$$\sum_{i=1}^{I} x_i \Delta x_i \frac{dn_i}{dt} = \frac{d\mu_1^{\Delta x}}{dt} = 0.$$

Using counter examples, below we prove that the formulation (4.25) is not the zeroth moment preserving in either the pure aggregation or the pure breakage problem.

Non preservation of the zeroth moment for aggregation and breakage

First we discuss the case of pure aggregation for the case of a uniform mesh, i.e., $\Delta x_i = \Delta x$ for all i together with $\beta(x, y) = \beta_0$ where β_0 is a positive constant. Considering a uniform grid leads to the following simplified form of the flux (4.26) as

$$J^{\text{agg}}_{i+1/2} = \sum_{k=1}^{i} (xn)_k \Delta x \left(\sum_{j=i-k+2}^{I} \int_{\Lambda_j} \frac{\beta(u, x_k)}{u}\, du\, (xn)_j + \int_{x_{i-k+1}}^{x_{i-k+3/2}} \frac{\beta(u, x_k)}{u}\, du\, (xn)_{i-k+1} \right).$$

Further simplification by taking the special case of the constant kernel $\beta(x, y) = \beta_0$ gives,

$$J^{\text{agg}}_{i+1/2} = \sum_{k=1}^{i} \beta_0 (xn)_k \Delta x \left(\sum_{j=i-k+2}^{I} (xn)_j \log\left(\frac{x_{j+1/2}}{x_{j-1/2}}\right) + (xn)_{i-k+1} \log\left(\frac{x_{i-k+3/2}}{x_{i-k+1}}\right) \right). \tag{4.28}$$

Multiplying (4.25) by $\Delta x_i/x_i$ and taking summation over i with $J^{\text{brk}}_{i\pm1/2} = 0$, we obtain

$$\frac{d\mu_0^{\Delta x}}{dt} = \sum_{i=1}^{I} -\frac{1}{x_i}\left[J^{\text{agg}}_{i+1/2} - J^{\text{agg}}_{i-1/2}\right].$$

Substituting the value of $J^{\text{agg}}_{i+1/2}$ from (4.28) yields

$$\begin{aligned}
\frac{d\mu_0^{\Delta x}}{dt} =& \sum_{i=1}^{I} \frac{-1}{x_i}\Bigg[\sum_{k=1}^{i-1}(xn)_k\Delta x\beta_0\Bigg(-(xn)_{i-k+1}\log\left(\frac{x_{i-k+3/2}}{x_{i-k+1/2}}\right) + (xn)_{i-k+1}\log\left(\frac{x_{i-k+3/2}}{x_{i-k+1}}\right) \\
& - (xn)_{i-k}\log\left(\frac{x_{i-k+1/2}}{x_{i-k}}\right)\Bigg) + (xn)_i\Delta x\beta_0\left(\sum_{j=2}^{I}(xn)_j\log\left(\frac{x_{j+1/2}}{x_{j-1/2}}\right) + (xn)_1\log\left(\frac{x_{3/2}}{x_1}\right)\right)\Bigg] \\
=& \beta_0\Delta x\sum_{i=1}^{I}\sum_{k=1}^{i-1}\frac{(xn)_k}{x_i}\left((xn)_{i-k}\log\left(\frac{x_{i-k+1/2}}{x_{i-k}}\right) - (xn)_{i-k+1}\log\left(\frac{x_{i-k+1/2}}{x_{i-k+1}}\right)\right) \\
& - \beta_0\Delta x\sum_{i=1}^{I} n_i\left(\sum_{k=2}^{I}(xn)_k\log\left(\frac{x_{k+1/2}}{x_{k-1/2}}\right) + (xn)_1\log\left(\frac{x_{3/2}}{x_1}\right)\right). \qquad (4.29)
\end{aligned}$$

Taking the same uniform mesh with the constant aggregation kernel, we get the following form of the zeroth moment from (4.22) as

$$\frac{d\hat{\mu}_0}{dt} = -\frac{1}{2}\beta_0\Delta x^2\sum_{i=1}^{I}\sum_{k=1}^{I-i+1} n_i n_k. \qquad (4.30)$$

It is easy to see that the difference between the right hand side of the equations (4.29) and (4.30) is not equal to zero for the particular value of $I = 2$. We did not find a way to show where exactly the difference would be zero on a uniform mesh. But it looks very obvious that the method is in general not the zeroth moment preserving in this case.

Now we consider the pure breakage case for $b(x, y) = 2/y$ and $S(x) = x$ on a uniform mesh of size Δx. We know from (4.25),

$$\begin{aligned}
\frac{d\mu_0^{\Delta x}}{dt} &= \sum_{i=1}^{I} -\frac{1}{x_i}\left[J^{\text{brk}}_{i+1/2} - J^{\text{brk}}_{i-1/2}\right] \\
&= \sum_{i=1}^{I}\frac{1}{x_i}\left[\sum_{k=i}^{I} 2\Delta x^2 n_k x_i - \Delta x n_i x^2_{i+1/2}\right].
\end{aligned}$$

Changing the order of summation for the first term and $x_{i+1/2} = i\Delta x$ yields

$$\begin{aligned}
\frac{d\mu_0^{\Delta x}}{dt} = \sum_{i=1}^{I} n_i\Delta x\left[\sum_{k=1}^{i} 2\Delta x - \frac{x^2_{i+1/2}}{x_i}\right] &= \Delta x\sum_{i=1}^{I} n_i\left[2\,i\Delta x - \frac{x^2_{i+1/2}}{x_i}\right] \\
&= \Delta x^2\sum_{i=1}^{I} n_i\frac{2i(i-1)}{2i-1}. \qquad (4.31)
\end{aligned}$$

For the above assumptions on breakage and selection functions, the equation (4.23) reduces to

$$\frac{d\hat{\mu}_0}{dt} = \sum_{i=1}^{I} S(x_i)\Delta x_i n_i \left(\int_0^{x_i} b(x, x_i)dx - 1 \right) = \sum_{i=1}^{I} x_i n_i \Delta x = \Delta x^2 \sum_{i=1}^{I} (i - 1/2) n_i. \tag{4.32}$$

Hence, the difference between the right-hand side of the equations (4.31) and (4.32) becomes $\Delta x^2 \sum_{i=1}^{I} n_i \frac{-1}{2(2i-1)}$ which is not equal to zero for any values of I. Thus the scheme is not the zeroth moment preserving for the breakage processes.

FVS for sources

For nucleation frequently two types of source terms are used. These are a singular measure for monodisperse nucleation, i.e. $B_{\text{src}}(t, x) = B_0 \delta_{x_s}$ for $x_s \in]0, x_{\max}]$ or a continuous source which can be an exponential distribution of the nucleii, see [54, 85] for both possibilities. Another possibility is a Gaussian distribution, which would also be used in a process of seeding with small particles. Following the idea of Kumar and Ramakrishna [54], the source term $B_{\text{src}}(t, x)$ in the equation (4.7) can be handled by the following discretization

$$\frac{dn_i}{dt} = \frac{1}{\Delta x_i} \int_{x_{i-1/2}}^{x_{i+1/2}} B_{\text{src}}(t, x)dx. \tag{4.33}$$

For the particular case of monodisperse nucleation, the above equation reduces to

$$\frac{dn_i}{dt} = \begin{cases} \dfrac{B_0}{\Delta x_i}, & x_s \in \Lambda_i \\ 0, & \text{elsewhere.} \end{cases} \tag{4.34}$$

Note that the zeroth moment preservation in both cases is trivial by multiplying the equation (4.33) and (4.34) respectively by Δx_i and taking summation over i.

Now we prove that the scheme is not the first moment preserving for any source terms except for the constant source functions $B_{\text{src}}(t, x) = B_0$.

Non preservation of the first moment for source terms

Multiplying the equation (4.33) by $x_i \Delta x_i$ and summing with respect to i gives

$$\frac{d\mu_1^{\Delta x}}{dt} = \sum_{i=1}^{I} x_i \int_{x_{i-1/2}}^{x_{i+1/2}} B_{\text{src}}(t, x)dx. \tag{4.35}$$

Similarly, for the monodisperse nucleation we obtain

$$\frac{d\mu_1^{\Delta x}}{dt} = \sum_{i=1}^{I} x_i B_0 \quad \text{for} \quad x_s \in \Lambda_i.$$

From (4.21), we have the following form of the first moment

$$\frac{d\hat{\mu}_1}{dt} = \sum_{i=1}^{I} \int_{x_{i-1/2}}^{x_{i+1/2}} x B_{\text{src}}(t, x)dx. \tag{4.36}$$

We conclude that the method is first moment preserving, i.e. the right-hand side of the equations (4.35) and (4.36) are equal, only for the case of the constant source term. Any other source functions will be non preserving with respect to the first moment, when exact integration is used. It should be mentioned that the first moment preservation is obvious for the monodisperse source only if the nucleation occurs exactly at the pivot points. This can be seen by substituting the value of $B_{\text{src}}(t,x) = B_0\delta_{x_s}$ in the equation (4.36).

Remark 4.3.2. *Another way to discretize the pure source terms using a finite volume scheme is given as*

$$x_i^p \frac{dn_i}{dt} = \frac{1}{\Delta x_i}\int_{x_{i-1/2}}^{x_{i+1/2}} x^p B_{src}(t,x)dx. \tag{4.37}$$

The moment preserving conditions for the zeroth and first moments in this case are the same as mentioned in (4.20) and (4.21), respectively both for $p=0$ or $p=1$. However, this formulation shows mass preservation but not the number preservation for $p=1$. For the case of $p=0$, both the formulations (4.33) and (4.37) are the same. To see this, let us consider for $p=1$

$$\frac{x_i dn_i}{dt} = \frac{1}{\Delta x_i}\int_{x_{i-1/2}}^{x_{i+1/2}} x B_{src}(t,x)dx. \tag{4.38}$$

Multiplying it by Δx_i and summing over i to get the formulation for the first moment as

$$\frac{d\mu_1^{\Delta x}}{dt} = \sum_{i=1}^{I}\int_{x_{i-1/2}}^{x_{i+1/2}} x B_{src}(t,x)dx = \int_0^{x_{I+1/2}} x B_{src}(t,x)dx,$$

which is exactly the same as (4.21) for the preservation of the mass. Now, multiplying (4.38) again by $\frac{\Delta x_i}{x_i}$ and taking summation with respect to i, we get the following formula for the zeroth moment

$$\frac{d\mu_0^{\Delta x}}{dt} = \sum_{i=1}^{I}\frac{1}{x_i}\int_{x_{i-1/2}}^{x_{i+1/2}} x B_{src}(t,x)dx.$$

A comparison with the equation (4.20) shows that the scheme is not zeroth moment preserving, except for constant source functions.

Upwind scheme for growth

For solving growth problem we have considered two different choices of numerical schemes. First choice is the following upwind scheme (US)

$$\frac{dn_i}{dt} = -\frac{1}{\Delta x_i}\left[G(x_{i+1/2})n_i - G(x_{i-1/2})n_{i-1}\right], \tag{4.39}$$

which for advection with a variable coefficient can be found in LeVeque [64, Section 9.5.2]. Another form of simple upwind scheme (SUS) is, e.g. see again LeVeque [64, Section 9.2], given as

$$\frac{dn_i}{dt} = -\frac{1}{\Delta x_i}\left[G(x_i)n_i - G(x_{i-1})n_{i-1}\right], \tag{4.40}$$

The above two formulations give preservation with respect to the zeroth moment but not for the first moment.

Multiplying the equations (4.39) and (4.40) by Δx_i and summing with respect to i yields the following expression, respectively for the zeroth moment, compare with (4.18),

$$\frac{d\mu_0^{\Delta x}}{dt} = -G(x_{I+1/2})n_I + G(x_{1/2})n_0 \tag{4.41}$$

and

$$\frac{d\mu_0^{\Delta x}}{dt} = -G(x_I)n_I + G(x_0)n_0. \tag{4.42}$$

As mentioned before, the moment preservation in this case is discussed with the exception of boundary terms. Here and further on in this paper it implies that to avoid the zero boundary conditions on the growth rate, i.e. requiring that

$$G(x) = 0 \qquad \text{for} \quad x < x_1 \quad \text{or} \quad x \geq x_I, \tag{4.43}$$

we treat the growth rate and the number density at boundary cells differently. It can be seen from the equations (4.41) and (4.42) that if we shift the pivot points for the number density using US and both number density and the growth rate using SUS from the cell midpoint to the right boundary point of the cell, then we get for both the schemes

$$\frac{d\mu_0^{\Delta x}}{dt} = -G(x_{I+1/2})n(t, x_{I+1/2}) + G(x_{1/2})n(t, x_{1/2})$$

which is the required condition (4.18) for the zeroth moment preservation. Naturally, zeroth moment preservation should hold, since both are conservative schemes. This problem of the interpretation of the boundary cell values, which are average values on those cells, occurs for any conservative schemes, when the boundary fluxes are not zero.

In the following, we show that these two schemes are not the first moment preserving even for a constant growth rate.

Non preservation of the first moment for growth

Multiplying the equations (4.39) and (4.40) by $x_i\Delta x_i$ and summing with respect to i give the formulation for the first moment as

$$\begin{aligned}\frac{d\mu_1^{\Delta x}}{dt} =& x_1 G(x_{1/2})n_0 + \sum_{i=1}^{I-1}(x_{i+1} - x_i)G(x_{i+1/2})n_i - x_I G(x_{I+1/2})n_I \\ =& x_1 G(x_{1/2})n_0 + \sum_{i=1}^{I}\frac{1}{2}(\Delta x_{i+1} + \Delta x_i)G(x_{i+1/2})n_i - x_{I+1}G(x_{I+1/2})n_I.\end{aligned} \tag{4.44}$$

using the US while for SUS we obtain

$$\begin{aligned}\frac{d\mu_1^{\Delta x}}{dt} =& x_1 G(x_0)n_0 + \sum_{i=1}^{I-1}(x_{i+1} - x_i)G(x_i)n_i - x_I G(x_I)n_I \\ =& x_1 G(x_0)n_0 + \sum_{i=1}^{I}\frac{1}{2}(\Delta x_{i+1} + \Delta x_i)G(x_i)n_i - x_{I+1}G(x_I)n_I.\end{aligned} \tag{4.45}$$

A comparison of the equation (4.19) with the equations (4.44) and (4.45) shows that these two schemes in general are not first moment preserving by applying the zero boundary condition (4.43) to the growth rate too, for example taking a geometric grid $x_{i+1/2} = rx_{i-1/2}$ for $r \neq 1$. However, it is worth to mention that for the case of a uniform mesh and a constant growth rate the upwind scheme is first moment preserving while the same follows for the simple upwind scheme as well just by taking a uniform grid, again with the exception of the boundary cell terms.

Coupling of the processes

Now the three discretizations (4.25), (4.33) and (4.39) can be coupled for combined aggregation, breakage, nucleation and growth problems to give

$$\frac{x_i dn_i}{dt} = -\frac{1}{\Delta x_i}\left[J^{\text{agg}}_{i+1/2} - J^{\text{agg}}_{i-1/2} + J^{\text{brk}}_{i+1/2} - J^{\text{brk}}_{i-1/2}\right] - \frac{x_i}{\Delta x_i}\left[G(x_{i+1/2})n_i - G(x_{i-1/2})n_{i-1}\right] + \frac{x_i}{\Delta x_i}\int_{x_{i-1/2}}^{x_{i+1/2}} B_{\text{src}}(t,x)dx.$$

The formulation given above is mass preserving, resp. number preserving, if $G, B_{\text{src}} = 0$, resp. $\beta, S, B_{\text{src}} = 0$. Moreover, the formulation is also satisfying the zeroth moment preservation in case of the pure nucleation process. However, coupling of all the processes together yields no preservation for any of the moments. To overcome this, we introduce a new formulation in the next section which is proven to be moment preserving with respect to two moments for coupled processes.

4.3.2 Two moment preserving methods

In the previous subsection, we discussed the preservation with respect to one moment. In particular, they are number and mass conserving in case of pure growth/nucleation and aggregation/breakage, respectively. The foregoing discussion motivates us to derive numerical schemes which are preserving with respect to two moments. In this subsection we present two-moments preserving methods for solving source terms, aggregation, breakage and growth equation by considering the cell average technique (CAT) as basis.

The CAT was obtained by discretizing a non-conservative form of the population balance equation (4.1). Following Kumar et al. [43, 45], the final formulation for the aggregation-breakage problem together with an additional source term (nucleation) [42] in the equation (4.1) with $G = 0$ by the CAT is given as

$$\frac{dn_i \Delta x_i}{dt} = B_i^{\text{CA}} - D_i^{\text{CA}}, \qquad i = 1, 2, ..., I. \tag{4.46}$$

The abbreviation CA is used for cell average. The birth B_i^{CA}, by using the CAT, is defined as

$$\begin{aligned} B_i^{\text{CA}} =& B_{i-1}\lambda_i^-(\bar{v}_{i-1})H(\bar{v}_{i-1} - x_{i-1}) + B_i\lambda_i^+(\bar{v}_i)H(\bar{v}_i - x_i) \\ &+ B_i\lambda_i^-(\bar{v}_i)H(x_i - \bar{v}_i) + B_{i+1}\lambda_i^+(\bar{v}_{i+1})H(x_{i+1} - \bar{v}_{i+1}), \end{aligned} \tag{4.47}$$

where B_i is the total birth of the particles due to aggregation, breakage or source in the ith cell and $\bar{v}_i$ is the average volume of all newborn particles coming into the same cell. Moreover, the

particle birth B_i is sitting at the position $\bar{v}_i \in]x_{i-1/2}, x_{i+1/2}]$. The two terms B_i and $\bar{v}_i$ are to be defined a little further below. The term $\lambda_i^{\pm}$ and the Heaviside step function H are defined as

$$\lambda_i^{\pm}(x) = \frac{x - x_{i\pm1}}{x_i - x_{i\pm1}}, \qquad H(x) = \begin{cases} 1, & x > 0 \\ \frac{1}{2}, & x = 0 \\ 0, & x < 0. \end{cases}$$

We get the following relations for λ_i

$$x_i\lambda_i^+(\bar{v}_i) + x_{i+1}\lambda_{i+1}^-(\bar{v}_i) = \bar{v}_i, \qquad x_i\lambda_i^-(\bar{v}_i) + x_{i-1}\lambda_{i-1}^+(\bar{v}_i) = \bar{v}_i. \tag{4.48}$$

Now, the discrete particle birth rate B_i, the volume average $\bar{v}_i$ and the discrete death D_i^{CA} are defined accordingly for the individual processes of aggregation, breakage and nucleation. Note that it can easily be proven that

$$\sum_{i=1}^{I} B_i^{\mathrm{CA}} = \sum_{i=1}^{I} B_i \tag{4.49}$$

with the help of relations $\lambda_i^+(\bar{v}_i) + \lambda_{i+1}^-(\bar{v}_i) = 1$ and $H(\bar{v}_i - x_i) + H(x_i - \bar{v}_i) = 1$. For the proof, we have also used the condition

$$\bar{v}_1 > x_1 \quad \text{and} \quad \bar{v}_I < x_I. \tag{4.50}$$

For the case of pure aggregation problem, the birth rate B_i and the volume average $\bar{v}_i$ are given as

$$B_i^{\mathrm{agg}} = \sum_{\substack{j,k \\ x_{i-1/2} \le (x_j + x_k) < x_{i+1/2}}}^{j \ge k} \left(1 - \frac{1}{2}\delta_{j,k}\right) \beta(x_j, x_k) n_j n_k \Delta x_j \Delta x_k, \tag{4.51}$$

and

$$\bar{v}_i^{\mathrm{agg}} = \frac{1}{B_i^{\mathrm{agg}}} \sum_{\substack{j,k \\ x_{i-1/2} \le (x_j + x_k) < x_{i+1/2}}}^{j \ge k} \left(1 - \frac{1}{2}\delta_{j,k}\right) \beta(x_j, x_k) n_j n_k \Delta x_j \Delta x_k (x_j + x_k). \tag{4.52}$$

The discrete death D_i^{CA} has the following form

$$D_i^{\mathrm{CA,agg}} = n_i \Delta x_i \sum_{k=1}^{I} \beta(x_i, x_k) n_k \Delta x_k. \tag{4.53}$$

Similarly, B_i and $\bar{v}_i$ for pure breakage are defined as

$$B_i^{\mathrm{brk}} = \sum_{k \ge i} S_k n_k \Delta x_k \int_{x_{i-1/2}}^{p_k^i} b(x, x_k)\, dx, \qquad \bar{v}_i^{\mathrm{brk}} = \frac{1}{B_i^{\mathrm{brk}}} \sum_{k \ge i} S_k n_k \Delta x_k \int_{x_{i-1/2}}^{p_k^i} x b(x, x_k)\, dx, \tag{4.54}$$

and the death term D_i^{CA} as

$$D_i^{\mathrm{CA,brk}} = S_i n_i \Delta x_i \tag{4.55}$$

where $p_k^i = x_i$ for $k = i$ and $p_k^i = x_{i+1/2}$ elsewhere. Note that the death terms for aggregation and breakage using the CAT are the same as for fixed pivot method [53].

Since nucleation is a form of birth of particles, there is no nucleation term to be considered for the death term D_i^{CA}. We get the following form for the discrete birth rate B_i and for the volume average $\bar{v}_i$

$$B_i^{\mathrm{src}} = \int_{x_{i-1/2}}^{x_{i+1/2}} B_{\mathrm{src}}(t,x)dx, \tag{4.56}$$

while

$$\bar{v}_i^{\mathrm{src}} = \frac{1}{B_i^{\mathrm{src}}} \int_{x_{i-1/2}}^{x_{i+1/2}} x B_{\mathrm{src}}(t,x)dx. \tag{4.57}$$

CAT as a FVS for breakage

The numerical scheme we discuss here is a finite volume reformulation of the cell average technique (CAT) [43]. Therefore, here we present a conservative form of the cell average technique. The reformulation steps are summarized in Appendix B.2.1. For the discrete equation (4.25) with $J_{i+1/2}^{\mathrm{agg}} = J_{i-1/2}^{\mathrm{agg}} = 0$, the numerical flux $J_{i+1/2}^{\mathrm{brk}}$ function takes the following form

$$\begin{aligned} J_{i+1/2}^{\mathrm{brk,CA}} = -\Bigg(& \sum_{k=i+1}^{I} S_k n_k \Delta x_k \int_0^{x_{i+1/2}} x b(x,x_k)dx \\ & + B_{i+1}^{\mathrm{brk}} x_i \lambda_i^+(\bar{v}_{i+1}^{\mathrm{brk}}) H(x_{i+1} - \bar{v}_{i+1}^{\mathrm{brk}}) - B_i^{\mathrm{brk}} x_{i+1} \lambda_{i+1}^-(\bar{v}_i^{\mathrm{brk}}) H(\bar{v}_i^{\mathrm{brk}} - x_i) \Bigg). \end{aligned} \tag{4.58}$$

Note that a similar conservative formulation is also obtained in this case for the fixed pivot (FP) technique, introduced by Kumar and Ramkrishna [53]. Here we get the numerical flux

$$J_{i+1/2}^{\mathrm{brk,FP}} = -\sum_{k=i+1}^{I} S_k n_k \Delta x_k \Bigg(\int_0^{x_i} x b(x,x_k)dx + \int_{x_i}^{x_{i+1}} x_i \lambda_i^+(x) b(x,x_k)dx \Bigg). \tag{4.59}$$

Details of the calculation steps are provided in Appendix B.3.1. These numerical fluxes can be treated as modified versions of the first moment preserving numerical flux (4.27). In addition, we show that they preserve the zeroth moment as well. We begin with the formulation (4.58) of the CAT.

Verification of the zeroth moment preservation

For pure breakage, we know from (4.25)

$$\frac{x_i dn_i}{dt} = -\frac{1}{\Delta x_i}(J_{i+1/2}^{\mathrm{brk}} - J_{i-1/2}^{\mathrm{brk}}),$$

where $J^{\text{brk}}_{i+1/2}$ is given by the equation (4.58). Define $N_i = n_i \Delta x_i$. Multiplying the above equation by $\Delta x_i / x_i$ and summing with respect to i yields

$$\begin{aligned}\frac{d\mu_0^{\Delta x}}{dt} =& \sum_{i=1}^{I} \frac{1}{x_i}\Bigg[\sum_{k=i+1}^{I} S_k N_k \int_0^{x_{i+1/2}} x b(x, x_k) dx + B^{\text{brk}}_{i+1} x_i \lambda_i^+(\bar{v}^{\text{brk}}_{i+1}) H(x_{i+1} - \bar{v}^{\text{brk}}_{i+1}) \\ & - B^{\text{brk}}_i x_{i+1} \lambda^-_{i+1}(\bar{v}^{\text{brk}}_i) H(\bar{v}^{\text{brk}}_i - x_i) - \sum_{k=i}^{I} S_k N_k \int_0^{x_{i-1/2}} x b(x, x_k) dx \\ & - B^{\text{brk}}_i x_{i-1} \lambda^+_{i-1}(\bar{v}^{\text{brk}}_i) H(x_i - \bar{v}^{\text{brk}}_i) + B^{\text{brk}}_{i-1} x_i \lambda_i^-(\bar{v}^{\text{brk}}_{i-1}) H(\bar{v}^{\text{brk}}_{i-1} - x_{i-1}) \Bigg].\end{aligned}$$

By using the relations (4.54) and (4.2), we get

$$\begin{aligned}\frac{d\mu_0^{\Delta x}}{dt} = \sum_{i=1}^{I} \frac{1}{x_i}\Bigg[& \bar{v}^{\text{brk}}_i B^{\text{brk}}_i - N_i S_i x_i + B^{\text{brk}}_{i+1} x_i \lambda_i^+(\bar{v}^{\text{brk}}_{i+1}) H(x_{i+1} - \bar{v}^{\text{brk}}_{i+1}) - B^{\text{brk}}_i x_{i+1} \lambda^-_{i+1}(\bar{v}^{\text{brk}}_i) H(\bar{v}^{\text{brk}}_i - x_i) \\ & - B^{\text{brk}}_i x_{i-1} \lambda^+_{i-1}(\bar{v}^{\text{brk}}_i) H(x_i - \bar{v}^{\text{brk}}_i) + B^{\text{brk}}_{i-1} x_i \lambda_i^-(\bar{v}^{\text{brk}}_{i-1}) H(\bar{v}^{\text{brk}}_{i-1} - x_{i-1}) \Bigg].\end{aligned}$$

Using the equation (4.47), it follows that

$$\begin{aligned}\frac{d\mu_0^{\Delta x}}{dt} = \sum_{i=1}^{I} \frac{1}{x_i}\Bigg[& \bar{v}^{\text{brk}}_i B^{\text{brk}}_i - N_i S_i x_i + B^{\text{CA}}_i x_i - B^{\text{brk}}_i x_i \lambda_i^-(\bar{v}^{\text{brk}}_i) H(x_i - \bar{v}^{\text{brk}}_i) - B^{\text{brk}}_i x_i \lambda_i^+(\bar{v}^{\text{brk}}_i) H(\bar{v}^{\text{brk}}_i - x_i) \\ & - B^{\text{brk}}_i x_{i+1} \lambda^-_{i+1}(\bar{v}^{\text{brk}}_i) H(\bar{v}^{\text{brk}}_i - x_i) - B^{\text{brk}}_i x_{i-1} \lambda^+_{i-1}(\bar{v}^{\text{brk}}_i) H(x_i - \bar{v}^{\text{brk}}_i) \Bigg].\end{aligned}$$

Replacing $x_i \lambda_i^{\pm}$ from the equation (4.48) and by the definition of Heaviside function, i.e.

$$H(\bar{v}_i - x_i) + H(x_i - \bar{v}_i) = 1,$$

we obtain

$$\frac{d\mu_0^{\Delta x}}{dt} = \sum_{i=1}^{I} \frac{1}{x_i}\Big[B^{\text{CA}}_i x_i - N_i S_i x_i \Big] = \sum_{i=1}^{I} (B^{\text{CA}}_i - N_i S_i).$$

From the relation (4.49) and substituting the value of B_i from the equation (4.54) leads to

$$\frac{d\mu_0^{\Delta x}}{dt} = \sum_{i=1}^{I} \Bigg[N_i S_i \int_{x_{i-1/2}}^{x_i} b(x, x_i) dx + \sum_{k=i+1}^{I} N_k S_k \int_{x_{i-1/2}}^{x_{i+1/2}} b(x, x_k) dx - N_i S_i \Bigg].$$

Further simplifications by interchanging the order of summation for the second term gives

$$\frac{d\mu_0^{\Delta x}}{dt} = \sum_{i=1}^{I} N_i S_i \Big[\int_0^{x_i} b(x, x_i) dx - 1 \Big],$$

which is same as the required equation (4.23) for the zeroth moment preservation.

In a similar way one can prove the zeroth moment preservation for the formulation (4.59) of the FP scheme.

CAT as a FVS for aggregation

Let the index $\ell_{i,j}$ is defined to be the index such that

$$x_{i+1/2} - x_j \in \Lambda_{\ell_{i,j}} \tag{4.60}$$

holds. We set the term $r_{i,j} = \chi(x_{i+1/2} - x_j - x_{\ell_{i,j}})$ for the function χ, which is given as

$$\chi(x) = \begin{cases} 1, & x > 0 \\ -1, & x \leq 0. \end{cases} \tag{4.61}$$

A similar approach to the breakage process, the cell average technique for aggregation can be rewritten in conservative form with the following numerical flux function

$$J^{\text{agg,CA}}_{i+1/2} = \sum_{j=1}^{i} \sum_{k=\ell_{i,j}+\frac{1}{2}(1+r_{i,j})}^{I} \Bigg(\beta(x_k, x_j) x_j n_j n_k \Delta x_j \Delta x_k + B_i^{\text{agg}} x_{i+1} \lambda_{i+1}^{-}(\bar{v}_i^{\text{agg}}) H(\bar{v}_i^{\text{agg}} - x_i) \\ - B_{i+1}^{\text{agg}} x_i \lambda_i^{+}(\bar{v}_{i+1}^{\text{agg}}) H(x_{i+1} - \bar{v}_{i+1}^{\text{agg}}) \Bigg), \tag{4.62}$$

used in the equation (4.25) with $J^{\text{brk}}_{i+1/2} = J^{\text{brk}}_{i-1/2} = 0$.

FP method as a FVS for aggregation

Let us assume that $\gamma_{i,j}$ is the index such that

$$x_{i+1} - x_j \in \Lambda_{\gamma_{i,j}}, \tag{4.63}$$

and we introduce the term

$$\mathrm{r}_{i,j} = \chi(x_{i+1} - x_j - x_{\gamma_{i,j}}) \tag{4.64}$$

for the function χ defined as in (4.61). Then the FP formulation for the aggregation can also be rewritten in the conservative formulation as the CAT with the numerical flux given as

$$\begin{aligned} J^{\text{agg,FP}}_{i+1/2} =& \sum_{j=1}^{i} \sum_{k=\gamma_{i,j}+\frac{1}{2}(1+\mathrm{r}_{i,j})}^{I} \beta(x_j, x_k) x_j n_j n_k \Delta x_j \Delta x_k \\ &+ \sum_{\substack{j,k \\ x_i \leq (x_j+x_k) < x_{i+1}}}^{j \geq k} \left(1 - \frac{1}{2}\delta_{j,k}\right) x_{i+1} \lambda_{i+1}^{-}(x_j + x_k) \beta(x_j, x_k) n_j n_k \Delta x_j \Delta x_k. \end{aligned} \tag{4.65}$$

The reformulation of the CAT and the FP method into the above conservative forms can be found in the Appendices B.2.2 and B.3.2, respectively. It should be mentioned that these formulations show preservation with respect to the first two moments. The preservation with respect to the total mass is certain due to the conservative flux formulation while below we discuss the zeroth moment preservation for the CAT. A similar approach gives the desired result of number preservation for the FP method as well. Note that the coupling of the aggregation and breakage processes is done by adding the corresponding fluxes.

Verification of the zeroth moment preservation

Proceeding same as in case of breakage problem, we find

$$\begin{aligned}\frac{d\mu_0^{\Delta x}}{dt} = &-\sum_{i=1}^{I}\frac{1}{x_i}\Bigg[\Bigg(\sum_{j=1}^{i}\sum_{k=\ell_{i,j}+\frac{1}{2}(1+r_{i,j})}^{I} - \sum_{j=1}^{i-1}\sum_{k=\ell_{i-1,j}+\frac{1}{2}(1+r_{i-1,j})}^{I}\Bigg)\beta(x_k,x_j)x_jN_jN_k\\ &+ B_i^{\text{agg}}x_{i+1}\lambda_{i+1}^{-}(\bar{v}_i^{\text{agg}})H(\bar{v}_i^{\text{agg}}-x_i) - B_{i+1}^{\text{agg}}x_i\lambda_i^{+}(\bar{v}_{i+1}^{\text{agg}})H(x_{i+1}-\bar{v}_{i+1}^{\text{agg}})\\ &- B_{i-1}^{\text{agg}}x_i\lambda_i^{-}(\bar{v}_{i-1}^{\text{agg}})H(\bar{v}_{i-1}^{\text{agg}}-x_{i-1}) + B_i^{\text{agg}}x_{i-1}\lambda_{i-1}^{+}(\bar{v}_i^{\text{agg}})H(x_i-\bar{v}_i^{\text{agg}})\Bigg].\end{aligned}$$

Following the same approach to the previous case, by using the relation (4.47), replacing $x_i\lambda_i^{\pm}$ and by the definition of the Heaviside function we have

$$\begin{aligned}\frac{d\mu_0^{\Delta x}}{dt} = &-\sum_{i=1}^{I}\frac{1}{x_i}\Bigg[\sum_{k=\ell_{i,i}+\frac{1}{2}(1+r_{i,i})}^{I}\beta(x_k,x_i)x_iN_iN_k\\ &+\sum_{j=1}^{i-1}\Bigg(\sum_{k=\ell_{i,j}+\frac{1}{2}(1+r_{i,j})}^{I} - \sum_{k=\ell_{i-1,j}+\frac{1}{2}(1+r_{i-1,j})}^{I}\Bigg)\beta(x_k,x_j)x_jN_jN_k + B_i^{\text{agg}}\bar{v}_i^{\text{agg}} - B_i^{\text{CA}}x_i\Bigg]\\ = &-\sum_{i=1}^{I}\frac{1}{x_i}\Bigg[\sum_{k=\ell_{i,i}+\frac{1}{2}(1+r_{i,i})}^{I}\beta(x_k,x_i)x_iN_iN_k - \sum_{j=1}^{i-1}\sum_{k=\ell_{i-1,j}+\frac{1}{2}(1+r_{i-1,j})}^{\ell_{i,j}+\frac{1}{2}(-1+r_{i,j})}\beta(x_k,x_j)x_jN_jN_k\\ &+ B_i^{\text{agg}}\bar{v}_i^{\text{agg}} - B_i^{\text{CA}}x_i\Bigg].\end{aligned} \tag{4.66}$$

We know from the equation (4.52)

$$\bar{v}_i^{\text{agg}}B_i^{\text{agg}} = \sum_{\substack{j,k\\ x_{i-1/2}\le(x_j+x_k)<x_{i+1/2}}}^{j\ge k}\left(1-\frac{1}{2}\delta_{j,k}\right)\beta(x_j,x_k)N_jN_k(x_j+x_k).$$

This can be rewritten as

$$\bar{v}_i^{\text{agg}}B_i^{\text{agg}} = \frac{1}{2}\sum_{\substack{j,k\\ x_{i-1/2}\le(x_j+x_k)<x_{i+1/2}}}\beta(x_j,x_k)N_jN_k(x_j+x_k) = \sum_{\substack{j,k\\ x_{i-1/2}\le(x_j+x_k)<x_{i+1/2}}}\beta(x_j,x_k)N_jN_kx_j.$$

We can further rewrite the equation in the following form

$$\bar{v}_i^{\text{agg}}B_i^{\text{agg}} = \sum_{j=1}^{i-1}N_jx_j\sum_{x_{i-1/2}\le(x_j+x_k)<x_{i+1/2}}\beta(x_k,x_j)N_k + N_ix_i\sum_{(x_i+x_k)<x_{i+1/2}}\beta(x_k,x_i)N_k.$$

The summations appearing in the above equation can be replaced using indices $\ell_{i,j}$ as follows

$$\bar{v}_i^{\text{agg}}B_i^{\text{agg}} = \sum_{j=1}^{i-1}N_jx_j\sum_{k=\ell_{i-1,j}+\frac{1}{2}(1+r_{i-1,j})}^{\ell_{i,j}+\frac{1}{2}(-1+r_{i,j})}\beta(x_k,x_j)N_k + N_ix_i\sum_{k=1}^{\ell_{i,i}+\frac{1}{2}(-1+r_{i,i})}\beta(x_k,x_i)N_k. \tag{4.67}$$

From the relation (4.67), the equation (4.66) can be simplified as

$$\begin{aligned}\frac{d\mu_0^{\Delta x}}{dt} &= -\sum_{i=1}^{I}\frac{1}{x_i}\Bigg[\sum_{k=\ell_{i,i}+\frac{1}{2}(1+r_{i,i})}^{I}\beta(x_k,x_i)x_iN_iN_k + N_ix_i\sum_{k=1}^{\ell_{i,i}+\frac{1}{2}(-1+r_{i,i})}\beta(x_k,x_i)N_k - B_i^{\mathrm{CA}}x_i\Bigg]\\ &= \sum_{i=1}^{I}\Bigg[B_i^{\mathrm{CA}} - N_i\sum_{k=1}^{I}\beta(x_k,x_i)N_k\Bigg].\end{aligned}$$

By using the relation (4.49) and thereafter substituting the value of B_i from the equation (4.51) yields

$$\begin{aligned}\frac{d\mu_0^{\Delta x}}{dt} =& \sum_{i=1}^{I}\sum_{\substack{j,k\\ x_{i-1/2}\le(x_j+x_k)<x_{i+1/2}}}^{j\ge k}\left(1-\frac{1}{2}\delta_{j,k}\right)\beta(x_j,x_k)N_jN_k - \sum_{j=1}^{I}N_j\sum_{k=1}^{I}\beta(x_k,x_j)N_k\\ =& \sum_{\substack{j,k\\ (x_j+x_k)<x_{I+1/2}}}^{j\ge k}\left(1-\frac{1}{2}\delta_{j,k}\right)\beta(x_j,x_k)N_jN_k - \sum_{\substack{j,k\\ (x_j+x_k)<x_{I+1/2}}}^{j\ge k}(2-\delta_{j,k})\,\beta(x_j,x_k)N_jN_k\\ &- \sum_{\substack{j,k\\ (x_j+x_k)\ge x_{I+1/2}}}^{j\ge k}(2-\delta_{j,k})\,\beta(x_j,x_k)N_jN_k.\end{aligned}$$

Finally, using the condition (4.9), the compact support on β leads to

$$\frac{d\mu_0^{\Delta x}}{dt} = -\frac{1}{2}\sum_{\substack{j,k\\ (x_j+x_k)<x_{I+1/2}}}^{j\ge k}(2-\delta_{j,k})\,\beta(x_j,x_k)N_jN_k,$$

which is the required formulation (4.22) for the preservation of the zeroth moment.

Modified upwind scheme for growth

As we have seen in the previous section that the upwind schemes are preserving only with respect to the zeroth moment. Therefore, the aim here is to derive a scheme which is preserving at least with the first two moments. We use the idea of the CAT to solve the growth problem. From Kumar et al. [43], we have the following formulation

$$\frac{dn_i\Delta x_i}{dt} = G(x_{i-1})\frac{n_{i-1}\Delta x_{i-1}}{x_i - x_{i-1}} - G(x_i)\frac{n_i\Delta x_i}{x_{i+1}-x_i}. \tag{4.68}$$

Equivalently, the equation (4.68) can be rewritten as

$$\frac{x_i dn_i}{dt} = \frac{x_i}{\Delta x_i}\left[G(x_{i-1})\frac{n_{i-1}\Delta x_{i-1}}{x_i - x_{i-1}} - G(x_i)\frac{n_i\Delta x_i}{x_{i+1}-x_i}\right]. \tag{4.69}$$

Note that the formula (4.69) looks similar to the upwind schemes (4.39) and (4.40). It is exactly the same as US (4.39) for the case of equidistant grids with a constant growth rate and SUS (4.40)

for equidistant meshes. Summing the equation (4.68) with respect to i give the formulation for the zeroth moment as

$$\begin{aligned}\frac{d\mu_0^{\Delta x}}{dt} &= \sum_{i=1}^{I}\left[G(x_{i-1})\frac{n_{i-1}\Delta x_{i-1}}{x_i - x_{i-1}} - G(x_i)\frac{n_i\Delta x_i}{x_{i+1}-x_i}\right] \\ &= \left[G(x_0)\frac{n_0\Delta x_0}{x_1 - x_0} - G(x_I)\frac{n_I\Delta x_I}{x_{I+1}-x_I}\right]. \end{aligned} \tag{4.70}$$

By using the assumption on ghost cells, i.e. $\Delta x_0 = \Delta x_1$ and $\Delta x_I = \Delta x_{I+1}$ we have $\Delta x_0 = x_1 - x_0$ and $\Delta x_I = x_{I+1} - x_I$. Applying this and the same assumptions on the growth rate and the number density at boundaries cells as we discussed before in Subsection 4.3.1, equation (4.70) reduces to

$$\frac{d\mu_0^{\Delta x}}{dt} = G(x_{1/2})n(t, x_{1/2}) - G(x_{I+1/2})n(t, x_{I+1/2}).$$

Hence, a comparison from (4.18) shows that the scheme is zeroth moment preserving. The preservation with respect to the first moment is shown in the following.

Verification of the first moment preservation

Multiplying the equation (4.69) by Δx_i and taking summation over i give the following form

$$\begin{aligned}\frac{d\mu_1^{\Delta x}}{dt} =& \sum_{i=1}^{I} x_i\left[G(x_{i-1})\frac{n_{i-1}\Delta x_{i-1}}{x_i - x_{i-1}} - G(x_i)\frac{n_i\Delta x_i}{x_{i+1}-x_i}\right] \\ =& \frac{x_1 G(x_0)n_0\Delta x_0}{x_1 - x_0} + \sum_{i=1}^{I-1} G(x_i)n_i\Delta x_i - \frac{x_I G(x_I)n_I\Delta x_I}{x_{I+1}-x_I} \\ =& x_1 G(x_0)n_0 + \sum_{i=1}^{I} G(x_i)n_i\Delta x_i - (\Delta x_I + x_I)G(x_I)n_I. \end{aligned} \tag{4.71}$$

Now we recall the assumption of a right ghost cell mid-point $x_{I+1} = \Delta x_I + x_I$ which was made in Section 4.2. Equation (4.71) becomes

$$\frac{d\mu_1^{\Delta x}}{dt} = x_1 G(x_0)n_0 + \sum_{i=1}^{I} G(x_i)n_i\Delta x_i - x_{I+1}G(x_I)n_I. \tag{4.72}$$

This form of the right-hand side is almost identical to (4.19) except for the two boundary terms on the cells Λ_1 and Λ_I. Since these terms needed a special interpretation even in the clear case of zeroth moment preservation by the conservative upwind schemes, we are justified to consider them as exceptional in this case too. Again we shift here the pivot points from the cell midpoint to the right boundary point of the cells for both the growth rate and the number density. In addition, the pivot points x_1 and x_{I+1} are shifted to the left boundary point of the cells. In this way the formulation (4.72) is exactly the same as (4.19) and therefore, the method is first moment preserving. Note that if we apply the boundary condition (4.43) to the growth rate, the formulations (4.72) and (4.19) are the same. It should also be mentioned that the non-preservation result of Subsection 4.3.1 is not due to boundary cells.

Moment preserving treatment of the source terms

Proceeding as before in the case of aggregation and breakage, the cell average scheme for an additional source term can be reformulated in the following conservative form

$$\frac{x_i dn_i}{dt} = -\frac{1}{\Delta x_i}(J^{\mathrm{src,CA}}_{i+1/2} - J^{\mathrm{src,CA}}_{i-1/2}). \tag{4.73}$$

The numerical flux function $J^{\mathrm{src,CA}}_{i+1/2}$ is derived in Appendix B.2.3 as

$$J^{\mathrm{src,CA}}_{i+1/2} = B^{\mathrm{src}}_i x_{i+1}\lambda^-_{i+1}(\bar{v}^{\mathrm{src}}_i)H(\bar{v}^{\mathrm{src}}_i - x_i) - B^{\mathrm{src}}_{i+1}x_i\lambda^+_i(\bar{v}^{\mathrm{src}}_{i+1})H(x_{i+1} - \bar{v}^{\mathrm{src}}_{i+1}) - \int_0^{x_{i+1/2}} xB_{\mathrm{src}}(t,x)dx. \tag{4.74}$$

The above formulation shows preservation for the first two moments. For the preservation of the zeroth moment, a similar approach to the breakage process leads to

$$\frac{d\mu^{\Delta x}_0}{dt} = \sum_{i=1}^{I} B^{\mathrm{src}}_i = \int_0^{x_{I+1/2}} B_{\mathrm{src}}(t,x)dx$$

by substituting the value of B^{src}_i from the equation (4.56). Hence, the scheme is moment preserving with respect to the zeroth moment for any source functions.

Verification of the first moment preservation

Multiplying the equation (4.73) by Δx_i and summing with respect to i gives

$$\frac{d\mu^{\Delta x}_1}{dt} = J^{\mathrm{src,CA}}_{1/2} - J^{\mathrm{src,CA}}_{I+1/2},$$

where

$$J^{\mathrm{src,CA}}_{1/2} = B^{\mathrm{src}}_0 x_1\lambda^-_1(\bar{v}^{\mathrm{src}}_0)H(\bar{v}^{\mathrm{src}}_0 - x_0) - B^{\mathrm{src}}_1 x_0\lambda^+_0(\bar{v}^{\mathrm{src}}_1)H(x_1 - \bar{v}^{\mathrm{src}}_1)$$

and

$$J^{\mathrm{src,CA}}_{I+1/2} = B^{\mathrm{src}}_I x_{I+1}\lambda^-_{I+1}(\bar{v}^{\mathrm{src}}_I)H(\bar{v}^{\mathrm{src}}_I - x_I) - B^{\mathrm{src}}_{I+1}x_I\lambda^+_I(\bar{v}^{\mathrm{src}}_{I+1})H(x_{I+1} - \bar{v}^{\mathrm{src}}_{I+1}) - \int_0^{x_{I+1/2}} xB_{\mathrm{src}}(t,x)dx.$$

Applying the compact support (4.9) on source terms and using (4.56) we have $B^{\mathrm{src}}_0 = B^{\mathrm{src}}_{I+1} = 0$. Using the condition (4.70), i.e. $\bar{v}_1 > x_1$ and $\bar{v}_I < x_I$ implies that $H(x_1 - \bar{v}^{\mathrm{src}}_1) = H(\bar{v}^{\mathrm{src}}_I - x_I) = 0$. Therefore, $J^{\mathrm{src,CA}}_{1/2} = 0$ and $J^{\mathrm{src,CA}}_{I+1/2} = -\int_0^{x_{I+1/2}} xB_{\mathrm{src}}(t,x)dx$. Hence, we obtain

$$\frac{d\mu^{\Delta x}_1}{dt} = \int_0^{x_{I+1/2}} xB_{\mathrm{src}}(t,x)dx.$$

A comparison with the equation (4.21) shows that the technique is first moment preserving independent of the type of sources.

Coupling of the processes

The coupling of various processes, i.e., aggregation, breakage, growth and nucleation, can be done in a similar fashion as explained in the previous subsection. It should also be mentioned that the coupled formulation in this case gives preservation for the first two moments in all combined particulate processes. The preservation with respect to these two moments has been verified numerically in the next section.

4.4 Numerical results

In this section, we give numerical comparisons for the particle size distribution and its different moments by using both the one moment preserving (OMP) and two moment preserving (TMP) formulations. The performance of these formulations is evaluated for various simultaneous processes such as combined aggregation-breakage, aggregation-growth, aggregation-breakage-growth etc. In each case we consider different test problems. The exponential initial condition is used in all comparisons. In each case, we have discretized the continuous domain into non-uniform cells of a geometric mesh with the rule $x_{i+1/2} = rx_{i-1/2}$. The computational domain is taken to be $x_{\min} = 1e-6$, to avoid the singularity at $x = 0$ of the breakage function (4.75), and $x_{\max} = 300$ for the numerical simulations, unless otherwise specified. First we consider the case of combined aggregation and breakage.

Simultaneous aggregation and breakage

We apply the numerical schemes to the aggregation-breakage problem with the following breakage function using the gamma function Γ from Diemer [12]

$$b(x,y) = \frac{px^c(y-x)^{c+(c+1)(p-2)}\Gamma[c+(c+1)(p-1)+1]}{y^{pc+p-1}\Gamma(c+1)\Gamma[c+(c+1)(p-2)+1]}. \tag{4.75}$$

Here, the parameter $p \in \mathbb{N}, p \geq 2$ governs the number of fragments per breakage event and the parameter $c \geq 0$ is responsible for the shape of the daughter particle distributions [93]. The analytical solutions for various selection functions and aggregation kernels have been given in Appendix B.1. Four test problems of constant and sum aggregation kernels together with constant and linear selection functions have been considered. These problems can be solved analytically for the zeroth and the first moments but not for the complete number density distributions. For the simulation $p = 2$, $c = 2$ and 40 grid points have been used. Other simulation parameters have been provided in corresponding figures.

Figure 4.1 presents the number density distribution and temporal evolution of the zeroth moment for $\beta = 1$ and $S(x) = 1$. We observe from the Figure 4.1(a) that the number density distributions are quite similar to each other for both the schemes. As expected from the mathematical analysis, the simulation for zeroth moment in Figure 4.1(b) using TMP method is exactly matching with the analytical solution. On the other hand, OMP scheme shows a very poor prediction of the zeroth moment. Similar results are observed from the Figures 4.2, 4.3 and 4.4 for other three cases. Note that due to the finite volume formulations, numerical results of the first moment using both the OMP and TMP methods are giving exactly the analytical solutions and are constant. Therefore, we omit the plots here.

Blow-up of moments, gelation

For the case of the pure aggregation problem considering the multiplicative kernel $\beta(x,y) = (xy)^\lambda$ with $\lambda \in]1/2, 1]$, the total mass is not conserved anymore but mass is decreasing after a certain point of time. This process is called gelation. In this case mass conservation breaks down in finite time. Moreover, still from Figure 4.5, we observe that the TMP scheme gives better results as compared to the OMP method. Further, if we include the breakage process the

gelation time increases as can be seen from Figure 4.6. Again we find that the TMP method is closer to the analytical solution in comparison to the OMP scheme. It is worth to mention that for a large class of breakage kernels we can also avoid the mass conservation break down. Mathematical details about such classes can be found in Escobedo et al. [20]. Another way to avoid mass loss in finite time or to increase the gelation time is to increase the computational domain by increasing $x_{\max}$. Here we have taken $x_{\max} = 300$. For various numerical results on gelation using finite volume schemes, i.e. OMP method, with different values of $x_{\max}$ readers are referred to Filbet and Laurençot [23].

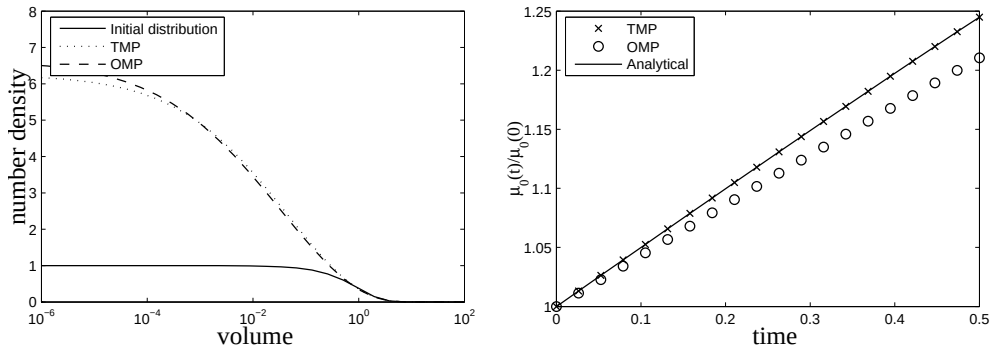

(a) Number density (b) Zeroth moment

Figure 4.1: (a) Number density and (b) zeroth moment using one-moment preserving (OMP) and two-moment preserving (TMP) methods, $S(x) = 1, \beta(x, y) = 1$, 40 grid points.

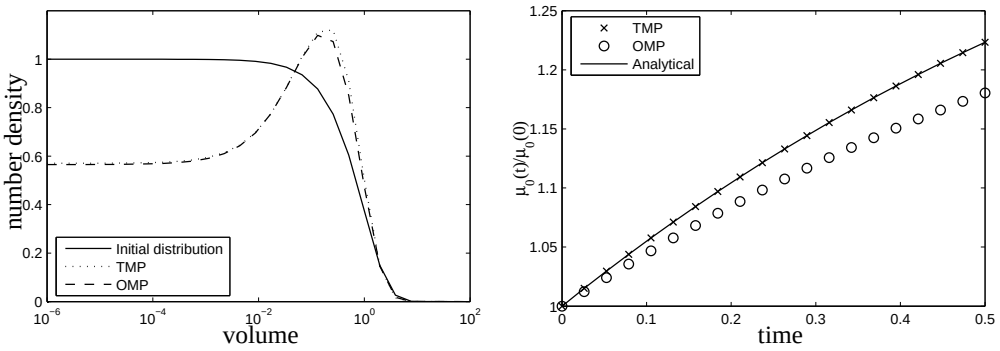

(a) Number density (b) Zeroth moment

Figure 4.2: (a) Number density and (b) zeroth moment using one-moment preserving (OMP) and two-moment preserving (TMP) methods, $S(x) = x, \beta(x, y) = 1$, 40 grid points.

Simultaneous aggregation and growth

The accuracy of both the schemes is evaluated for the case of constant and sum aggregation kernel together with linear growth rate. The analytical solutions for the number density and the

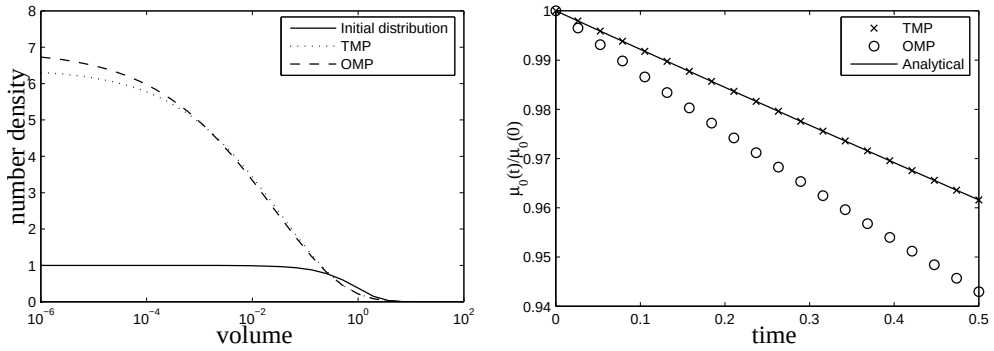

(a) Number density (b) Zeroth moment

Figure 4.3: (a) Number density and (b) zeroth moment using one-moment preserving (OMP) and two-moment preserving (TMP) methods, $S(x) = 1, \beta(x, y) = x + y$, 40 grid points.

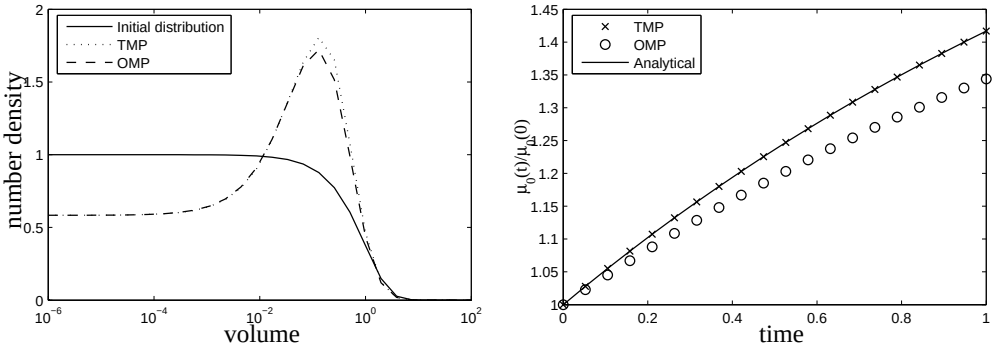

(a) Number density (b) Zeroth moment

Figure 4.4: (a) Number density and (b) zeroth moment using one-moment preserving (OMP) and two-moment preserving (TMP) methods, $S(x) = x, \beta(x, y) = x + y$, 40 grid points.

first two moments can be found in Ramabhadran et al. [86]. We have plotted the number density and the first two moments in Figures 4.7 and 4.8 for the case of constant and sum aggregation kernel, respectively. For the constant kernel, it can be seen from the Figure 4.7(a) that the number densities, using OMP and TMP methods, do not differ from each other and are in good agreement with the analytical number density. In Figures 4.7(b) and 4.7(c), TMP is in excellent agreement with the analytical first two moments whereas OMP over-predicts the results for the total mass. For the case of sum aggregation kernel, Figure 4.8 shows that the TMP method is not only providing the exact prediction with the analytical first two moments but also shows good results for the number density as compared to the OMP scheme for large particle sizes.

Simultaneous breakage and growth

In this section the breakage problem coupled with linear growth has been considered. The numerical results are shown for the zeroth and the first moments using a constant and a linear

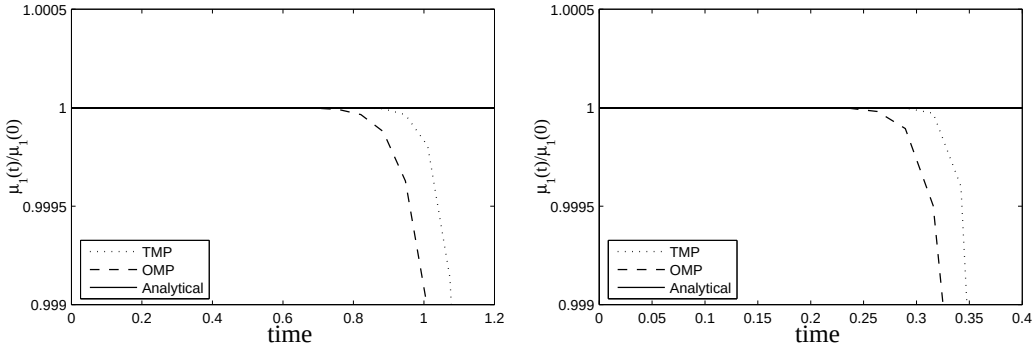

(a) First moment (b) First moment

Figure 4.5: First moment using one-moment preserving (OMP) and two-moment preserving (TMP) methods for (a) $\beta(x,y) = (xy)^{3/4}$ and (b) $\beta(x,y) = (xy)^1$ with 40 grid points.

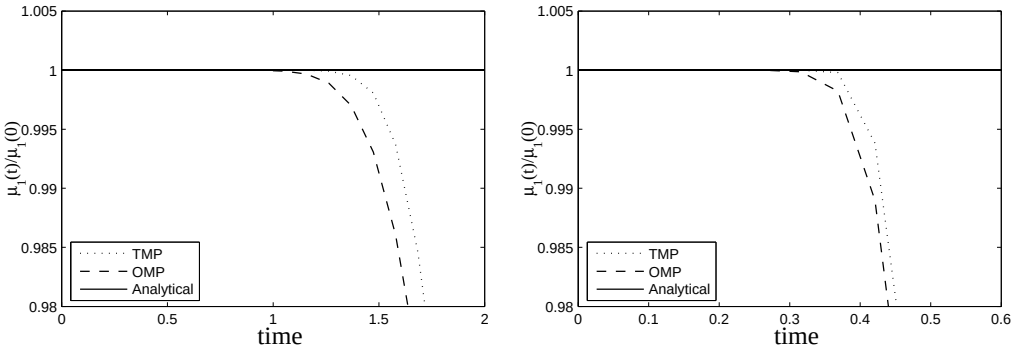

(a) First moment (b) First moment

Figure 4.6: First moment using OMP and TMP methods for (a) $\beta(x,y) = (xy)^{3/4}$, $S(x) = 1$ and (b) $\beta(x,y) = (xy)^1$, $S(x) = 1$ with 40 grid points.

selection rate. We use the same breakage kernel (4.75) as taken in the previous section. We have summarized the analytical solutions for the first two moments in Appendix B.1. The numerical results are shown for $p = 3$, $c = 2$ and for 60 grid points. The simulation with a constant selection rate has been plotted in Figure 4.9 whereas Figure 4.10 shows the comparison for a linear selection rate. We observe from these figures that the TMP scheme gives exact prediction with the analytical first two moments whereas the OMP shows poor prediction in each cases.

Combined aggregation, breakage and growth

In this section, numerical results are shown for the sum aggregation kernel together with the breakage function (4.75) and for a linear growth rate. We do the computations for the constant and linear selection rate. The analytical solutions are given in Appendix B.1. The simulations are made for $p = 2, c = 2$ and for 60 grid points. As can be seen from Figures 4.11 and 4.12 that the numerical results using TMP technique are exactly matching with the analytical first two

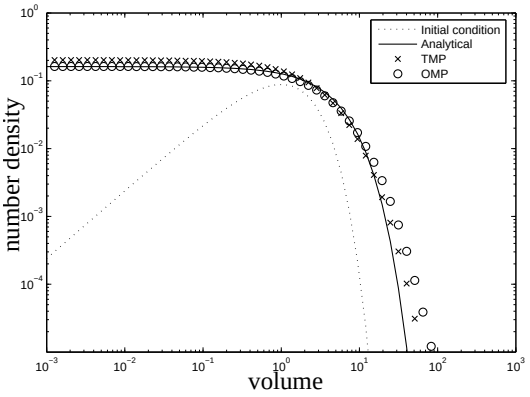

(a) Number density

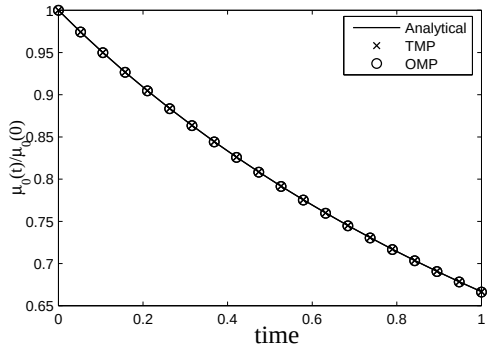

(b) Zeroth moment

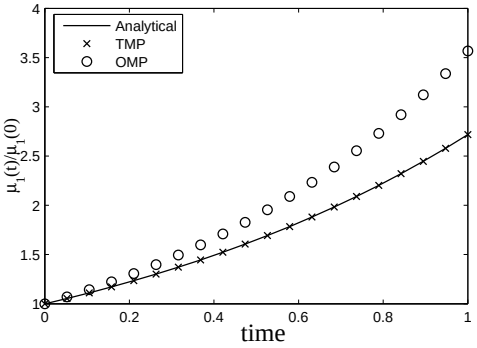

(c) First moment

Figure 4.7: (a) Number density (b) zeroth moment and (c) first moment using OMP and TMP methods, $\beta(x, y) = 1, G(x) = x$, 60 grid points.

moments whereas the OMP method significantly gives poor predictions for both the moments.

Pure source

The numerical results for the first two moments and the number density are compared to the analytical solutions using OMP and TMP methods. Negative exponential source term is taken for the simulation. The analytical solutions are given in Appendix B.1. Again we observe from Figure 4.13 that there is no significant change in number density for both the techniques. It is visible that the OMP method gives exact prediction for the zeroth moment but shows diverging behavior for the total mass. Moreover, the TMP scheme shows preservation with respect to the first two moments. Finally, in the next section we will see that the coupling of source terms with other processes causes no preservation for the zeroth moment by using OMP schemes.

Simultaneous breakage, growth and source

The simulation results are illustrated in this section for combined breakage, growth and source processes. The breakage function (4.75) has been taken with linear selection, linear growth rate

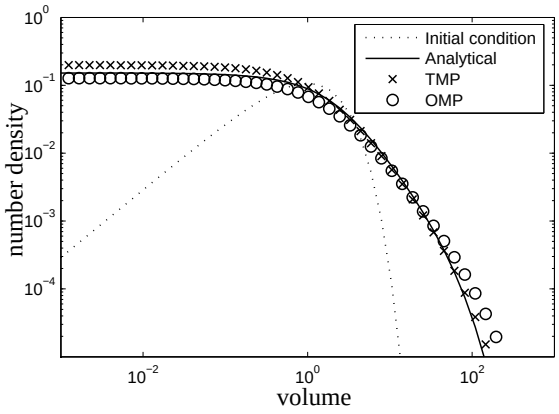

(a) Number density

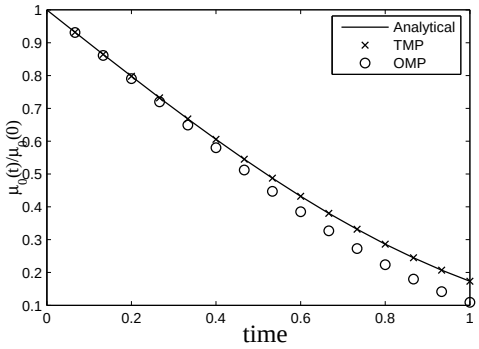

(b) Zeroth moment

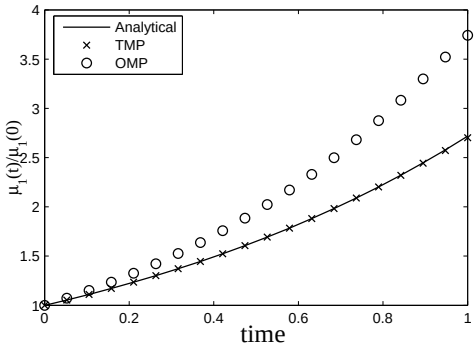

(c) First moment

Figure 4.8: (a) Number density (b) zeroth moment and (c) first moment using OMP and TMP schemes, $\beta(x, y) = x + y, G(x) = x$, 60 grid points.

and with exponential source term. We have given the analytical solutions in Appendix B.1. The numerics has been shown for $p = 2, c = 2$ and for 60 grid points. From Figure 4.14, we observe that the TMP method shows exact prediction with the analytical first two moments whereas the OMP scheme over-predicts the results for both the moments.

Coupled aggregation, breakage, growth and source

The numerical simulations are presented here for all the four coupled processes. In addition to the requirements in the previous case, a product aggregation kernel $\beta(x, y) = xy$ is used for the computations to account for the added aggregation term. The analytical solutions for the first two moments are provided in Appendix B.1. It can easily be seen from Figure 4.15 that the TMP scheme gives exactly the analytical first two moments while the prediction using OMP method is very poor.

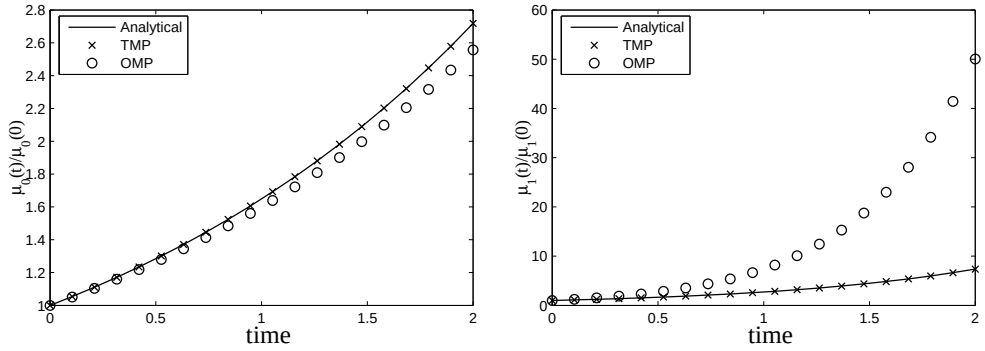

(a) Zeroth moment (b) First moment

Figure 4.9: (a) Zeroth moment and (b) first moment using OMP and TMP methods, $S(x) = 1, G(x) = x$, 60 grid points.

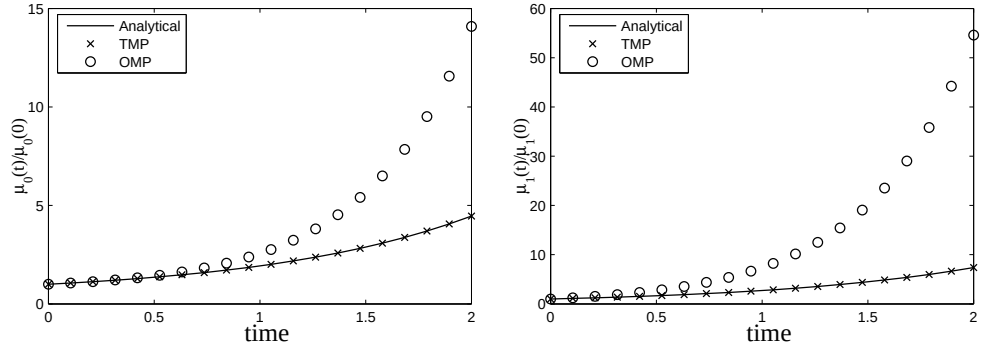

(a) Zeroth moment (b) First moment

Figure 4.10: (a) Zeroth moment and (b) first moment using OMP and TMP methods, $S(x) = x, G(x) = x$, 60 grid points.

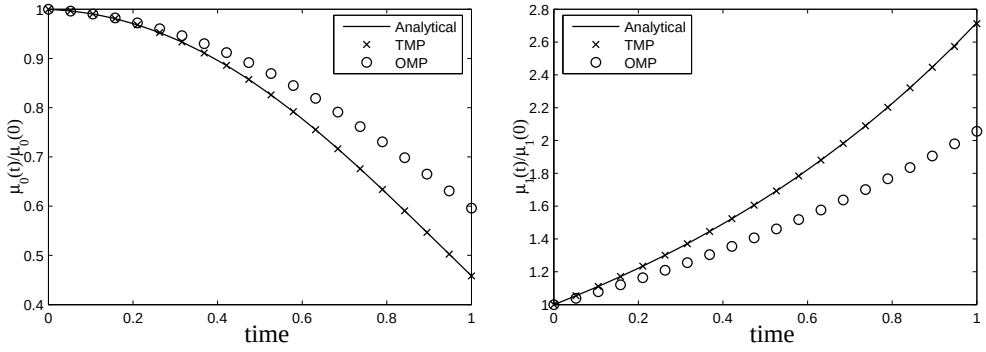

(a) Zeroth moment (b) First moment

Figure 4.11: (a) Zeroth moment and (b) first moment using OMP and TMP methods, $\beta(x, y) = x + y, S(x) = 1, G(x) = x$, 60 grid points.

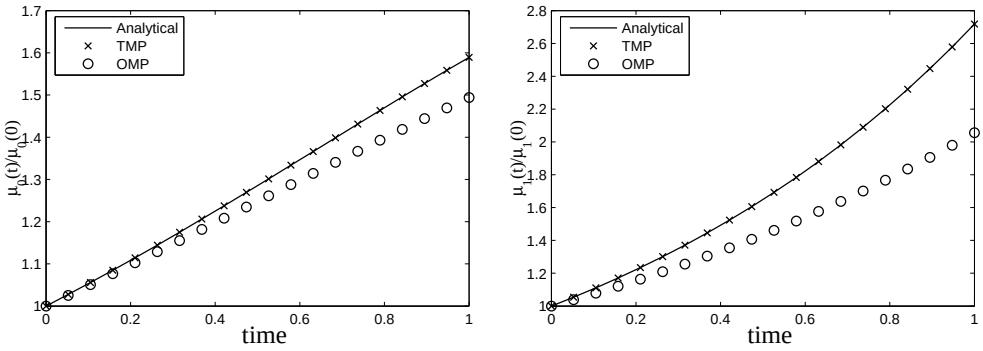

(a) Zeroth moment (b) First moment

Figure 4.12: (a) Zeroth moment and (b) first moment using OMP and TMP methods, $\beta(x, y) = x + y, S(x) = x, G(x) = x$, 60 grid points.

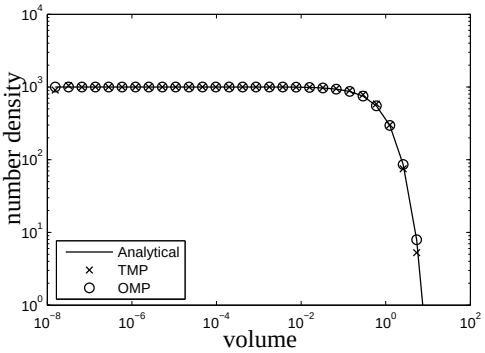

(a) Number density

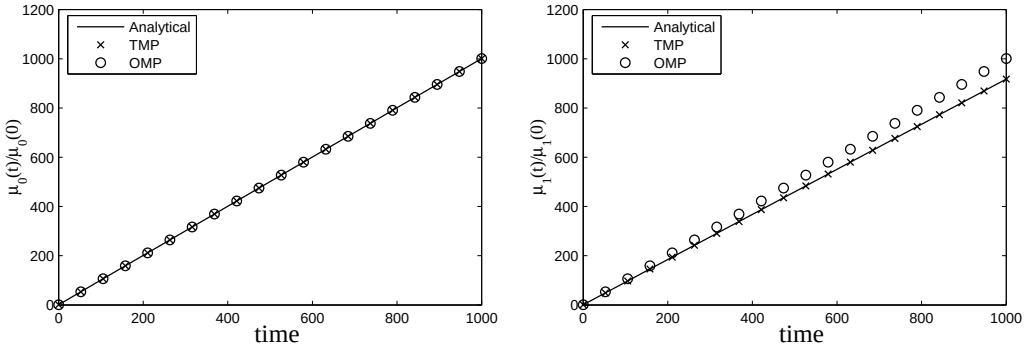

(b) Zeroth moment (c) First moment

Figure 4.13: (a) Number density (b) zeroth moment and (c) first moment using OMP and TMP methods, $B_{\text{src}}(t, x) = \exp(-x)$, 40 grid points.

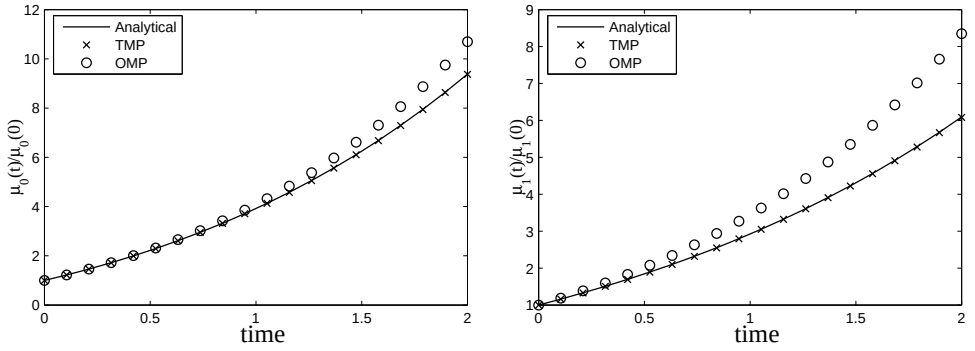

(a) Zeroth moment (b) First moment

Figure 4.14: (a) Zeroth moment and (b) first moment using one-moment preserving (OMP) and two-moment preserving (TMP) methods, $B_{\text{src}}(t,x) = \exp(-x), S(x) = x, G(x) = x$, 60 grid points.

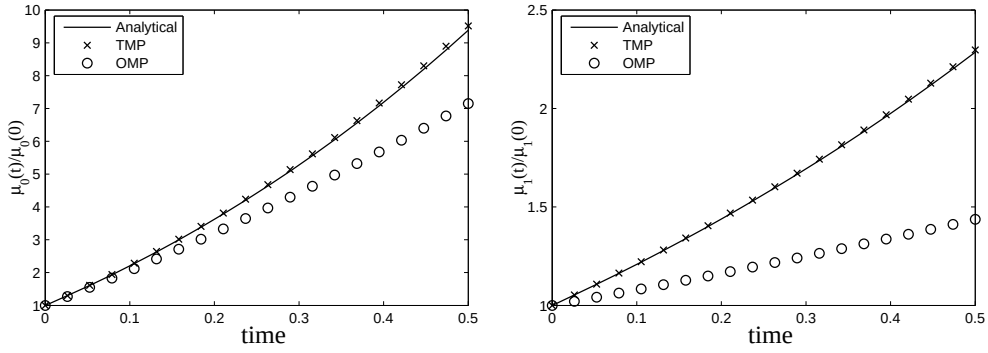

(a) Zeroth moment (b) First moment

Figure 4.15: (a) Zeroth moment and (b) first moment using one-moment preserving (OMP) and two-moment preserving (TMP) schemes, $\beta(x,y) = xy, B_{\text{src}}(t,x) = \exp(-x), S(x) = x, G(x) = x$, 60 grid points.

Chapter 5

Two-dimensional population balance

In this chapter we discuss the numerical schemes for solving two-dimensional aggregation population balance equations. In particular, the cell average technique (CAT) and the fixed pivot (FP) method are studied. Vale and McKeena [97] extended the FP method of Kumar and Ramkrishna [53] to the bi-component aggregation processes on rectangular meshes. Further Chakraborty and Kumar [9] as well as Nandanwar and Kumar [80] have implemented the FP method for multi-component aggregation processes on various meshes. Very recently, Chauhan et al. [10] have used the FP method to solve combined bivariate aggregation-breakage problems on rectangular and radial meshes. Chakraborty and Kumar in [9] also considered two-dimensional problems and determined numerical results for the number density on two different triangular grids. They found out that the method shows better results on triangular meshes as compared to rectangular grids. Moreover, the discussion on moments was ignored. The CAT was also developed to solve bivariate aggregation processes on rectangular meshes and the results were compared to the FP method by J. Kumar et al. [44].

Here in this chapter we compare different moments calculated by the FP technique on rectangular and triangular meshes with the analytical moments. Further, the mathematical formulation of the CAT for two different triangular grids as taken in Chakraborty and Kumar [9] is provided. We observe that the CAT gives better accuracy for number density and higher moments on the new formulation as compared to rectangular grids. It should also be mentioned that changing the grid from rectangular to triangular does not improve the results for the higher moments using the FP method. The numerical verifications are performed by taking three different test problems.

The chapter is organized as follows. In the next section we give the mathematical equations and then the numerical methods in Section 5.2. In the following two subsections we discuss the cell average technique formulation for rectangular and triangular grids. Finally, in Section 5.3 numerical results are provided to see the efficiency of the new work.

5.1 Introduction

The population balance equation describes changes in a particulate system in which each particle has one or more characteristic properties. Aggregation is a size enlargement process in

which two small particles are gathered together to form a larger particle. There are several particle properties which influence the particle density distribution in many aggregation processes. Therefore, a one-dimensional population balance equation (PBE) where the most appropriate particle property, namely particle size, is assumed to be the only particle property is not adequate to simulate such processes. The two-dimensional or two component PBE for binary aggregation is an extension of the one dimensional aggregation process and is given as in [69, 101]

$$\begin{aligned}\frac{\partial f(t,x,y)}{\partial t} =& \frac{1}{2}\int_0^x \int_0^y \beta(x-\epsilon,\epsilon,y-\gamma,\gamma) f(t,x-\epsilon,y-\gamma) f(t,\epsilon,\gamma) d\gamma d\epsilon \\ & - \int_0^\infty \int_0^\infty \beta(x,\epsilon,y,\gamma) f(t,x,y) f(t,\epsilon,\gamma) d\gamma d\epsilon, \end{aligned} \tag{5.1}$$

where β is the aggregation kernel and $f(t,x,y)$ is the particle property distribution with two independent granule characteristics $x, y > 0$ at time $t \geq 0$. The first term on the right-hand side is corresponding to the birth of particles of property (x,y) due to aggregation of smaller particles of properties $(x-\epsilon, y-\gamma)$ and (ϵ,γ), respectively. The last term describes the death of particles of property (x,y) due to the collision of particles having property (ϵ,γ). The aggregation kernel $\beta = \beta(x,\epsilon,y,\gamma)$ describes the rate at which two particles of properties (x,ϵ) and (y,γ) combine together to form a particle of property $(x+y, \epsilon+\gamma)$. It is a non-negative and symmetric function, i.e.

$$0 \leq \beta(x,\epsilon,y,\gamma) = \beta(y,\gamma,x,\epsilon).$$

Besides the particle property distribution f, we are also interested in some integral properties like moments. The ijth moment of the particle size distribution is defined as

$$\mu_{ij}(t) = \int_0^\infty \int_0^\infty x^i y^j f(t,x,y) dx dy. \tag{5.2}$$

The first two orders of moments are of special interest. The zeroth order $(i = j = 0)$ moment denotes the total number where as the first order $(i = 1, j = 0)$ and $(i = 0, j = 1)$ moments give the total amount of the particle properties x and y, respectively. If one of the properties is particle mass then the corresponding first moment is the total mass. Simultaneous agglomeration and drying in fluidized beds, wet granulation of a binary mixture of two solids, coagulation of a two component mixture and tracer studies of high shear granulation are some examples of two or multi-dimensional PBEs. For the details readers are referred to [32, 35, 69, 83].

Numerical solution of the PBE (5.1) is difficult due to the double integral and the non-linearity of the equation. Several numerical techniques can be found in the literature for solving multi-component aggregation problems such as the finite element scheme by Kim and Seinfeld [38] and a Monte carlo method by Laurenzi et al. [60]. Some other numerical schemes were implemented and can be found in Immanuel and Doyle [34], Xiong and Pratsinis [101], Strumendo and Arastoopour [94], Zucca et al. [104], Wright et al. [100] and the references therein. Following the idea of Filbet and Laurençot [23], Qamar and Warnecke [84] have rewritten the bivariate aggregation PBEs into the form of conservation laws and applied the well-known finite volume scheme to solve the problem. However, these numerical methods are having problems either regarding preservation of some important properties of the distributions or they are computationally very expensive.

The sectional methods, in particular the FP method and the CAT have proven to be better approaches to avoid the above difficulties. The basic difference between the CAT and the FP method is as follows: In the fixed pivot technique, all new born particles are assigned to neighboring nodes separately. In case of a one-dimensional problem, the assignment is done between two neighbouring nodes while for a two-component aggregation problem, the new born particles are distributed among four or three neighbouring nodes depending on the rectangular or triangular meshes, respectively. Now, in the CAT the solution strategy follows in two steps: First, we calculate averages of the properties of all the newborn particles in a cell and then we assign them to the neighbouring nodes. The number of nodes taken here is same as in the case of the FP scheme. For both schemes, the assignment of newborn particles is done in such a way that some properties, i.e. the zeroth and the first moments of the distribution are exactly preserved. Recently, a new sectional approach known as the extended cell average technique was introduced by Kostoglou [39] for solving one-dimensional aggregation problems. In this scheme, the assignment of averages of newborn particles is done between three neighbouring nodes in such a way that three moments namely the zeroth, first and second are exactly preserved.

5.2 Numerical methods for two-dimensional PBEs

In order to apply a numerical technique to solve the aggregation PBEs (5.1) we consider truncated equations replacing ∞ by $x_{\max}$ and $y_{\max}$ in x and y directions, respectively with $x_{\max}, y_{\max} < \infty$. With this assumption, we fix the two-dimensional computational domain in the x and y directions as $]0, x_{\max}]$ and $]0, y_{\max}]$ respectively. For the rectangular grid the entire two-dimensional property domain is divided into small cells $C_{i,j}$. The lower and upper boundaries of the ijth cell are denoted by $x_{i-1/2}, x_{i+1/2}$ and $y_{j-1/2}, y_{j+1/2}$ in x and y directions, respectively for $i = 1, \ldots, I_x$ and $j = 1, \ldots, I_y$. Here, the terms I_x and I_y are two large integers such that $x_{I_x+1/2} = x_{\max}$ and $y_{I_y+1/2} = y_{\max}$. We set $x_{1/2} = y_{1/2} = 0$. We choose

$$x_i = (x_{i-1/2} + x_{i+1/2})/2, \quad y_j = (y_{j-1/2} + y_{j+1/2})/2$$

and

$$\Delta x_i = x_{i+1/2} - x_{i-1/2}, \quad \Delta y_j = y_{j+1/2} - y_{j-1/2}.$$

The particles within a cell are assumed to be concentrated at a representative node $p_{i,j}$ of the cell $C_{i,j}$. It should be noted that each node $p_{i,j}$ is associated with two properties x_i and y_j in case of a two-dimensional problem. Now, we formulate the cell average idea mathematically. Let us define the discrete number density $N_{i,j}$, i.e. the total number of particles in a cell by integrating the number density over both properties as

$$N_{i,j} = \int_{x_{i-1/2}}^{x_{i+1/2}} \int_{y_{j-1/2}}^{y_{j+1/2}} f(t, x, y) dy dx.$$

Since particles within a cell $C_{i,j}$ are assumed to be concentrated at the representative node $p_{i,j} = (x_i, y_j)$, the number density can be expressed using Dirac point masses as

$$f(x, y, t) = \sum_{i=1}^{I_x} \sum_{j=1}^{I_y} N_{i,j} \delta(x - x_i) \delta(y - y_j), \tag{5.3}$$

where I_x and I_y are the total number of cells in the x and y directions, respectively. Integrating the equation (5.1) over x and y and substituting the density f from (5.3), we obtain the following equation

$$\frac{dN_{i,j}}{dt} = B_{i,j} - D_{i,j}. \tag{5.4}$$

For the details readers are referred to J. Kumar et al. [44]. Here $B_{i,j}$ is the discrete birth in the cell $C_{i,j}$ and is given as

$$B_{ij} = \sum_{\substack{k,l \\ x_{i-1/2} \le (x_k + x_l) < x_{i+1/2}}}^{k \ge l} \sum_{\substack{m,n \\ y_{j-1/2} \le (y_m + y_n) < y_{j+1/2}}}^{m \ge n} \left(1 - \frac{1}{2}\delta_{k,l}\delta_{m,n}\right) \beta_{klmn} N_{km} N_{ln},$$

and $D_{i,j}$ is the discrete death term defined by

$$D_{ij} = \sum_{p=1}^{I_x} \sum_{q=1}^{I_y} \beta_{ipjq} N_{ij} N_{pq}$$

where $\beta_{klmn} = \beta(x_k, x_l, y_m, y_n)$ and $\delta_{m,n}$ is Kronecker delta.

Numerical computations on uniform linear grids are quite expensive. To avoid this, we do the computation on non-uniform grids such as geometric grids. Non-uniformity in the grids causes inconsistency of the particle properties in the formulation. The birth term has to be modified to resolve this problem, i.e. the reassignment of newborn particles to the neighbouring nodes has to be done. In the CAT, we do the reassignment in such a way that some pre-chosen moments are preserved. A detailed discussion on these issues can be found in J. Kumar et al. [45].

Let us assume that $V_{x,i}$ and $V_{y,j}$ are the net fluxes in the cell $C_{i,j}$ of the property x and y respectively due to the aggregation process and $(\bar{x}_i, \bar{y}_j)$ is the position of average of all newborn particles. Then we have

$$\bar{x}_i = \frac{V_{x,i}}{B_{ij}}, \qquad \bar{y}_j = \frac{V_{y,j}}{B_{ij}}.$$

If the average positions $\bar{x}_i$ and $\bar{y}_j$ of newborn particles are different from the grid points x_i and y_j, we reassign the particles to the neighbouring nodes. It should be mentioned that in case of linear grids in both directions, the averages $\bar{x}_i$ and $\bar{y}_j$ are always equal to x_i and y_j. Hence, all particles will be assigned to the same cell they belong to without any reassignment. Now the question arises: Which and how many neighbouring nodes should be taken for the assignment of particles? The number of nodes for assignment depends on the choice of number of moments we want to preserve during the assignment of particles. We are interested in preserving the zeroth moment μ_{00} and first order of moments μ_{10} and μ_{01}. To preserve these three moments, four surrounding nodes have been used for the reassignment of particles in case of the rectangular grid. In the following subsection, we discuss briefly the mathematical formulation of the CAT for the rectangular grid. A detailed description can be found in J. Kumar et al. [44].

5.2.1 Cell average technique for rectangular grids

As expected from the cell average idea, if the two-dimensional average value lies exactly at the node of the cell, which is again rarely possible, we assign all newborn particles to the node, otherwise these newborn particles must be reassigned to the neighbouring nodes depending upon the position of average properties in the cell. A typical domain discretization with the reassignment of newborn particles is shown in Figure 5.1. The reassignment process is done in such a way that some pre-chosen moments namely the zeroth moment μ_{00} and first order of moments μ_{10} and μ_{01} are exactly preserved. From Figure 5.1, we observe that there are

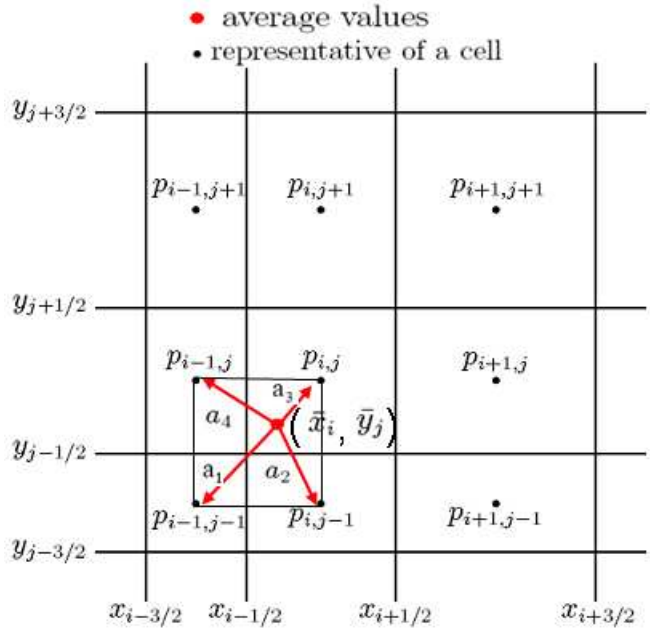

Figure 5.1: Domain discretization with distribution of particles.

9 surrounding nodes which may get a birth contribution from newborn particles in cell C_{ij}. The choice of four neighbouring nodes depends on the position of $(\bar{x}_i, \bar{y}_j)$ in the cell C_{ij}. For $(\bar{x}_i, \bar{y}_j)$ in the Figure 5.1, the particles will be assigned to the nodes $p_{i-1,j-1} = (x_{i-1}, y_{j-1})$, $p_{i,j-1} = (x_i, y_{j-1})$, $p_{i,j} = (x_i, y_j)$ and $p_{i-1,j} = (x_{i-1}, y_j)$.

Let us suppose that a_1, a_2, a_3 and a_4 are the particle fractions assigned to the nodes $p_{i-1,j-1}$, $p_{i,j-1}$, $p_{i,j}$ and $p_{i-1,j}$, respectively. For the consistency of zeroth μ_{00} and first order moments μ_{01} and μ_{10}, we obtain the following relations

$$\begin{aligned} a_1 + a_2 + a_3 + a_4 &= B_{ij}, \\ a_1 x_{i-1} + a_2 x_i &= (a_1 + a_2)\bar{x}_i, \\ a_3 x_i + a_4 x_{i-1} &= (a_3 + a_4)\bar{x}_i, \\ a_1 y_{j-1} + a_4 y_j &= (a_1 + a_4)\bar{y}_j, \\ a_2 y_{j-1} + a_3 y_j &= (a_2 + a_3)\bar{y}_j. \end{aligned}$$

Since the last four equations are dependent, we get a unique solution given as

$$\begin{aligned} a_1 &= \lambda^{+,+}_{i-1,j-1}(\bar{x}_i,\bar{y}_j)B_{ij}; \quad a_2 = \lambda^{-,+}_{i,j-1}(\bar{x}_i,\bar{y}_j)B_{ij}, \\ a_3 &= \lambda^{-,-}_{i,j}(\bar{x}_i,\bar{y}_j)B_{ij}; \quad a_4 = \lambda^{+,-}_{i-1,j}(\bar{x}_i,\bar{y}_j)B_{ij}, \end{aligned}$$

where

$$\lambda^{\pm,\pm}_{i,j}(x,y) = \frac{(x - x_{i\pm1})(y - y_{j\pm1})}{(x_i - x_{i\pm1})(y_j - y_{j\pm1})}.$$

The final formulation considering all the birth contributions to the node $p_{i,j}$ is given in J. Kumar [42] and J. Kumar et al. [44].

As mentioned earlier the number of nodes chosen for assignment depends on the number of moments we want to preserve. For the rectangular grid case, we only preserve three moments, namely the zeroth μ_{00} and the first order moments μ_{01} and μ_{10}. In other words, for the preservation of three moments in the case of rectangular grids we distribute the particles to four neighbouring nodes. Therefore, one can expect that the assignment of the particles among three nodes would give better numerical results as compared to the rectangular grids. This motivates us to apply the scheme on the triangular grids. In 2007, Chakraborty and Kumar [9] introduce two different triangular grids by taking the rectangular grid as basis and implemented the FP method on such triangular meshes. The following subsection gives the mathematical formulations of the bi-component aggregation problems by the CAT for both the triangular grids as discussed in Chakraborty and Kumar [9].

5.2.2 Cell average technique for triangular grids

For a triangular grid, the assignment of the newborn particles is made to three neighbouring nodes instead of four nodes as in the rectangular grid. Following the idea of Chakraborty and Kumar [9], we discuss two different triangular grids which are known as along diagonal and across diagonal triangulation. These grids are obtained by taking a rectangular grid and dividing the rectangles into two triangles each other along the direction of the diagonal $x = y$ or across it, respectively. Figure 5.2 represents the domain discretization for a triangular grid in along and across arrangements of the triangles, respectively. Here, it is worth to state the differences between the implementation of the CAT and the FP method on such triangular meshes. In the FP scheme, the reassignment of the newborn particles is done among three nodes of the lower or upper triangles where the newborn particle lies. However, for the CAT, first we determine the average position of all newborn particles in a rectangular cell. Next, we reassign them among three nodes of the triangle formed by pivot points in which this average position lies.

Here, we explain the mathematical formulation of the CAT for an along diagonal triangular grid. In a similar way one can obtain the formulation for the other grid. Figure 5.3(a) shows the reassignment of the newborn particles for an along triangular grid. We observe from Figure 5.3(b) that there are 7 nodes which may get birth contributions from newborn particles in the cell C_{ij}. The choice of three neighbouring nodes depends on the position of $(\bar{x}_i, \bar{y}_j)$ in the cell C_{ij}. For $(\bar{x}_i, \bar{y}_j)$ in the Figure 5.3(a), if a_1, a_2 and a_3 are the fractions of the newborn particles, these are assigned to the nodes $p_{i-1,j-1}, p_{i,j-1}$ and $p_{i,j}$, respectively. We obtain the following

relations due to the preservation of zeroth μ_{00} as well as first order of moments μ_{01} and μ_{10}

$$\begin{aligned} a_1 + a_2 + a_3 &= B_{ij}, \\ a_1 x_{i-1} + a_2 x_i + a_3 x_i &= (a_1 + a_2 + a_3)\bar{x}_i, \\ a_1 y_{j-1} + a_2 y_{j-1} + a_3 y_j &= (a_1 + a_2 + a_3)\bar{y}_j. \end{aligned}$$

Solving the above system of three equations with three unknowns yields a unique solution for a_1, a_2 and a_3 as

$$a_1 = B_{ij}\left(\frac{x_i - \bar{x}_i}{x_i - x_{i-1}}\right), \quad a_2 = B_{ij}\left(\frac{\bar{x}_i - x_{i-1}}{x_i - x_{i-1}} - \frac{\bar{y}_j - y_{j-1}}{y_j - y_{j-1}}\right), \quad a_3 = B_{ij}\left(\frac{\bar{y}_j - y_{j-1}}{y_j - y_{j-1}}\right).$$

Similarly, we can obtain a_1, a_2 and a_3 for different average positions of $(\bar{x}_i, \bar{y}_j)$ in the Figure 5.3(a).

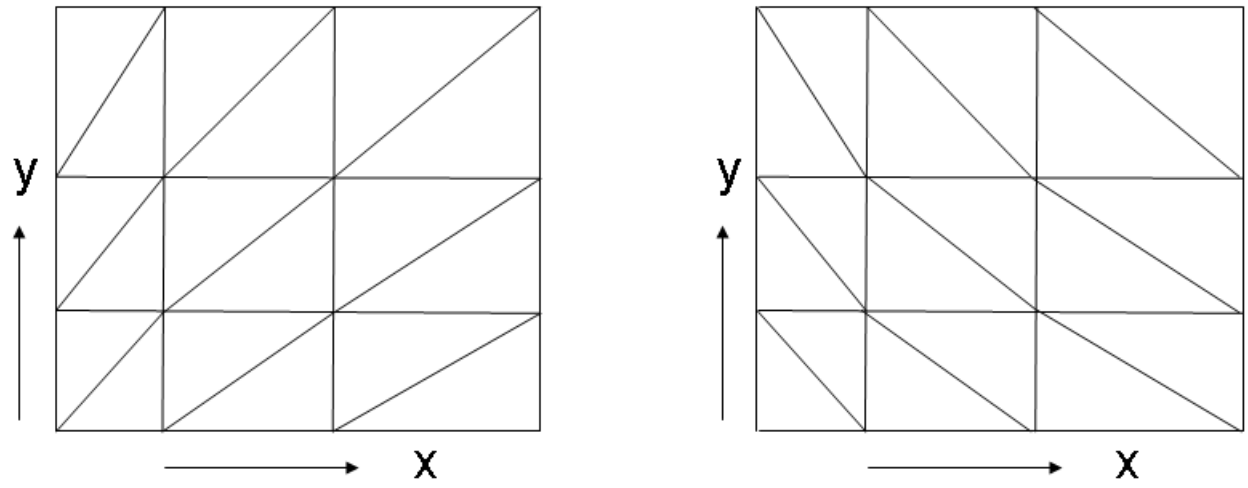

Figure 5.2: (a) Along diagonal and (b) across diagonal arrangements of triangles.

Now we collect all birth contributions to the node $p_{i,j}$ in the cell C_{ij} coming from the six surrounding cells and the cell C_{ij} itself. Introducing a characteristic function H as

$$H(x) = \begin{cases} 1 & \text{if } x \geq 0, \\ 0 & \text{if } x < 0, \end{cases}$$

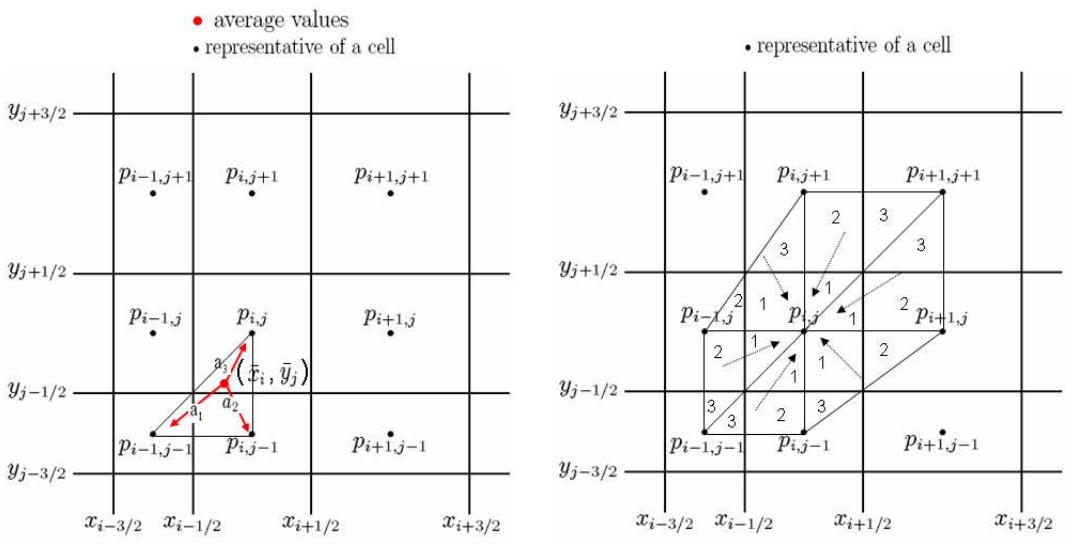

(a) (b)

Figure 5.3: (a) Distribution of particles to neighbouring nodes and (b) collection of particles from neighbouring nodes.

we obtain finally the following formulation

$$
\begin{aligned}
\frac{dN_{ij}}{dt} =& \sum_{p=0}^{1}\sum_{q=0}^{1} B_{i-p,j-q}\frac{y_{j-1}-\bar{y}_{j-q}}{y_{j-1}-y_j}H(x_i-\bar{x}_{i-p})H\left(\frac{(\bar{x}_{i-p}-x_i)(y_j-y_{j-1})}{x_i-x_{i-1}}+y_j-\bar{y}_{j-q}\right)\\
&+\sum_{p=0}^{1}\sum_{q=0}^{1} B_{i-p,j-q}\frac{\bar{x}_{i-p}-x_{i-1}}{x_i-x_{i-1}}H(y_j-\bar{y}_{j-q})H\left(\frac{(\bar{y}_{j-q}-y_j)(x_i-x_{i-1})}{y_j-y_{j-1}}+x_i-\bar{x}_{i-p}\right)\\
&+\sum_{p=0}^{1}\sum_{q=0}^{1}{}_{p+q\le 1} B_{i-p,j+q}\left(1-\frac{\bar{y}_{j+q}-y_j}{y_{j+1}-y_j}-\frac{\bar{x}_{i-p}-x_i}{x_{i-1}-x_i}\right)H(x_i-\bar{x}_{i-p})H(\bar{y}_{j+q}-y_j)\\
&+\sum_{p=0}^{1}\sum_{q=0}^{1} B_{i+p,j+q}\frac{y_{j+1}-\bar{y}_{j+q}}{y_{j+1}-y_j}H(\bar{x}_{i+p}-x_i)H\left(\bar{y}_{j+q}-\frac{(\bar{x}_{i+p}-x_i)(y_{j+1}-y_j)}{x_{i+1}-x_i}+y_j\right)\\
&+\sum_{p=0}^{1}\sum_{q=0}^{1} B_{i+p,j+q}\frac{x_{i+1}-\bar{x}_{i+p}}{x_{i+1}-x_i}H(\bar{y}_{j+q}-y_j)H\left(\bar{x}_{i+p}-\frac{(\bar{y}_{j+q}-y_j)(x_{i+1}-x_i)}{y_{j+1}-y_j}+x_i\right)\\
&+\sum_{p=0}^{1}\sum_{q=0}^{1}{}_{p+q\le 1} B_{i+p,j-q}\left(1-\frac{\bar{y}_{j-q}-y_j}{y_{j-1}-y_j}-\frac{\bar{x}_{i+p}-x_i}{x_{i+1}-x_i}\right)H(\bar{x}_{i+p}-x_i)H(y_j-\bar{y}_{j-q})\\
&-\sum_{p=1}^{I_x}\sum_{q=1}^{I_y}\beta_{ipjq}N_{ij}N_{pq}.
\end{aligned}
$$

Figure 5.3(b) explains the birth terms in the above formulation. Note that the birth contributions to the node $p_{i,j}$ from the nodes $p_{i+1,j-1}$ and $p_{i-1,j+1}$ are zero. We observe the same in the above mathematical formulation. Six major terms (double sum in each) in the birth are corresponding

to the six different domains, shown by the Figure 5.3(b). We find that each major term has a contribution from three cells, numbered 1, 2, 3 in this figure. Therefore, each major term has three terms again. There are a total of 18 terms and many of them may be zero at a particular time depending upon the position of average properties in the cell.

Similarly, we obtain the final formulation for across diagonal triangulation grid as

$$\begin{aligned}
\frac{dN_{ij}}{dt} =& \sum_{p=0}^{1}\sum_{q=0}^{1}{}_{p+q\leq 1} B_{i-p,j-q}\left(1-\frac{\bar{y}_{j-q}-y_j}{y_{j-1}-y_j}-\frac{\bar{x}_{i-p}-x_i}{x_{i-1}-x_i}\right)H(x_i-\bar{x}_{i-p})H(y_j-\bar{y}_{j-q}) \\
&+\sum_{p=0}^{1}\sum_{q=0}^{1} B_{i-p,j+q}\frac{\bar{x}_{i-p}-x_{i-1}}{x_i-x_{i-1}}H(\bar{y}_{j+q}-y_j)H\left(\frac{(\bar{y}_{j+q}-y_j)(x_i-x_{i-1})}{y_j-y_{j+1}}+x_i-\bar{x}_{i-p}\right) \\
&+\sum_{p=0}^{1}\sum_{q=0}^{1} B_{i-p,j+q}\frac{y_{j+1}-\bar{y}_{j+q}}{y_{j+1}-y_j}H(x_i-\bar{x}_{i-p})H\left(\bar{y}_{j+q}-\frac{(\bar{x}_{i-p}-x_i)(y_j-y_{j+1})}{x_i-x_{i-1}}+y_j\right) \\
&+\sum_{p=0}^{1}\sum_{q=0}^{1}{}_{p+q\leq 1} B_{i+p,j+q}\left(1-\frac{\bar{y}_{j+q}-y_j}{y_{j+1}-y_j}-\frac{\bar{x}_{i+p}-x_i}{x_{i+1}-x_i}\right)H(\bar{x}_{i+p}-x_i)H(\bar{y}_{j+q}-y_j) \\
&+\sum_{p=0}^{1}\sum_{q=0}^{1} B_{i+p,j-q}\frac{\bar{x}_{i+p}-x_{i+1}}{x_i-x_{i+1}}H(y_j-\bar{y}_{j-q})H\left(\bar{x}_{i+p}-\frac{(\bar{y}_{j-q}-y_j)(x_{i+1}-x_i)}{y_{j-1}-y_j}+x_i\right) \\
&+\sum_{p=0}^{1}\sum_{q=0}^{1} B_{i+p,j-q}\frac{\bar{y}_{j-q}-y_{j-1}}{y_j-y_{j-1}}H(\bar{x}_{i+p}-x_i)H\left(\frac{(\bar{x}_{i+p}-x_i)(y_{j-1}-y_j)}{x_{i+1}-x_i}+y_j-\bar{y}_{j-q}\right) \\
&-\sum_{p=1}^{I_x}\sum_{q=1}^{I_y}\beta_{ipjq}N_{ij}N_{pq}.
\end{aligned}$$

It should be mentioned here that the birth contributions to the node $p_{i,j}$ from the nodes $p_{i-1,j-1}$ and $p_{i+1,j+1}$ are zero. In the following section we discuss numerical results of both the CAT and the FP scheme by using the rectangular and the triangular grids.

5.3 Numerical results

Very few analytical results are available for two-dimensional PBEs, in particular for the number density. Here, we consider three test problems to analyze the accuracy of the two schemes. The numerical results are compared with the analytical solutions for higher moments. However, we compare also the number density for two problems. In the first test case, we show the computation on a complete two-dimensional problem and compare the results for number density and its moments.

Test case 1

Consider the particular case of the constant aggregation kernel with the following initial condition

$$f(0,x,y)=\frac{16N_0}{c_{10}c_{20}}\left(\frac{x}{c_{10}}\right)\left(\frac{y}{c_{20}}\right)\exp\left(-2\frac{x}{c_{10}}-2\frac{y}{c_{20}}\right).$$

We have the analytical solutions for the number density and moments given by Gelbard and Seinfeld [26]. In numerical simulations, the parameters c_{10} and c_{20} are taken to be 0.08. We set $N_0 = 1$ and the extent of evolution corresponds to the time for which the degree of aggregation is $I_{\text{agg}} = 1 - \mu_{00}(t)/\mu_{00}(0) = 0.953$. We show the numerical comparisons between the rectangular and the triangular grids with along and across arrangements of triangles. The number of grid points in each direction has been taken to be 26 on a geometric grid $x_{i+1/2} = 2x_{i-1/2}$.

First we discuss the results for the fixed pivot scheme. Figure (5.4) shows the complete size distribution for three types of grids. In this figure, we have shown the number of particles corresponding to each pivot point. Here the pivot points are ordered in such a way that the number of particles are monotonically decreasing. We observe that along triangulation grid predicts better results among all the three grids. Figure 5.5(a) represents the first two moments μ_{00} and μ_{10} or μ_{01}. We find that the numerical results accurately reproduce the analytical solutions. It should be mentioned that the mathematical formulations of the CAT and the FP are in such a way that the first two moments are preserved. Therefore, from what follows on we do not plot the results of moments μ_{00}, μ_{10} and μ_{01} for any test problems. For the first cross moment μ_{11} in Figure 5.5(b), the rectangular grid gives an exact prediction of the analytical results where as the along and across diagonal triangulation grids over-predict and under-predict the results, respectively. Figure 5.5(c) shows that the result for the moment μ_{21}, using across diagonal is in good agreement with the analytical where as the rectangular and along diagonal over-predict the results.

The number of particles at each grid point is shown in Figure 5.6 by using the cell average method. This figure shows that changing the grid does not influence the result for number density and the results are in very good agreement with the analytical number density. Figure 5.7 indicates that the along diagonal triangulation grid gives an accurate prediction of the analytical results for higher moments μ_{11} and μ_{21}. We also observe that rectangular and across triangulation grids under-predict the results.

So far we observed that the FP improves the results for number density using an along triangultion grid whereas a diverging behavior with time has been found for the higher moments. Furthermore, we find that the CAT shows significant improvements for the higher moments using the along triangulation grid and also give similar results for the number density. However, we cannot conclude the choice of a better method just from this one test problem. In the next section we will see that the CAT predicts not only the higher moments accurately but also does not suffer from the numerical diffusion, smearing effect, using an along triangulation mesh.

Test case 2

We compute a quasi one-dimensional problem with both the methods. Aggregation of monodisperse 2-mer granules, i.e. each granule is composed of two primary particles of different properties has been considered. Whenever two granules aggregate they form a new granule with an equal number of primary particles of each type. In this way it is a one-dimensional problem. The new granules should be formed along the diagonal only. However, due to the non-linearity of the grids, granules do not appear at the grid points exactly. Therefore, a granule reassignment is done which causes diffusion. In the paper of J. Kumar et al. [44], we already have seen that the CAT shows some diffusion using the rectangular grid. The computation here is done for

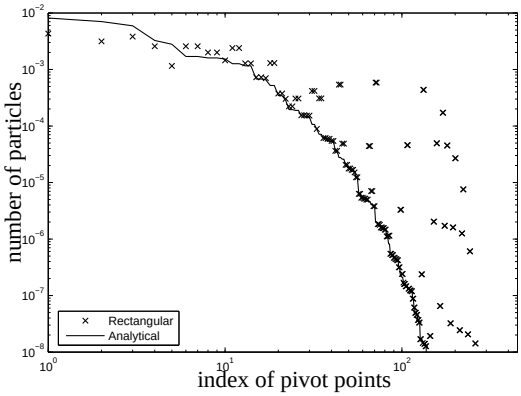

(a) Rectangular grid

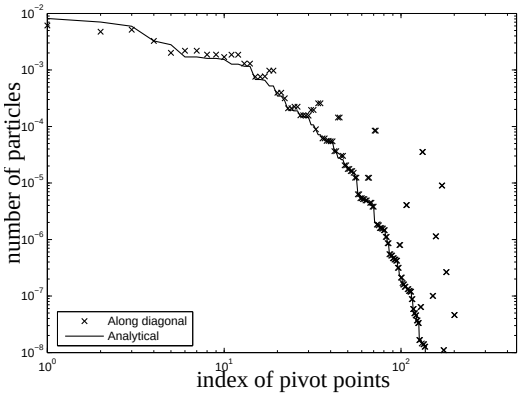

(b) Along diagonal

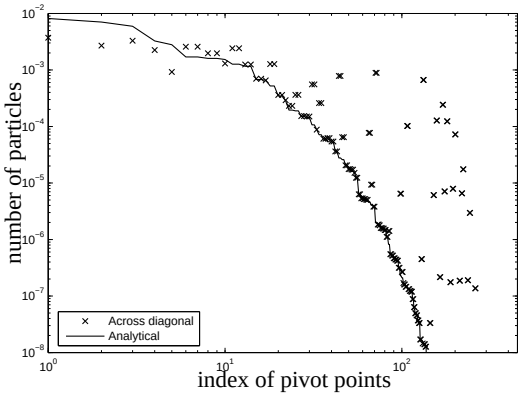

(c) Across diagonal

Figure 5.4: Test case 1: Number density for (a) rectangular grid (b) along diagonal and (c) across diagonal by using the FP method.

the constant aggregation kernel and the grid points in each direction is taken to be 13 with $x_{i+1/2} = 2x_{i-1/2}$. The number of grid points have been shown on the x and y axes.

Figure 5.8 and Figure 5.10 show the numerical diffusion between the rectangular and the triangular grids using the FP scheme and the CAT, respectively. We observe from Figure 5.8(b) and Figure 5.10(b) that the FP method and the CAT clearly indicate no diffusion for the along arrangement of triangulation grids. The smearing effects using the other two grids are quite similar to each other for both the methods. The moments μ_{11} and μ_{20} have been plotted in Figures 5.9 and 5.11 by using the FP technique and the CAT, respectively. Once again the same observations as in the previous case have been obtained for the FP method, i.e. the technique only improves the results for particle size distributions but not for the moments by changing the grids. However, we see clearly that the CAT shows no diffusion for the along triangulation grids and also gives exact prediction of the analytical higher moments.

Test case 3

Now we consider a discrete aggregation problem of two different types of particles with the

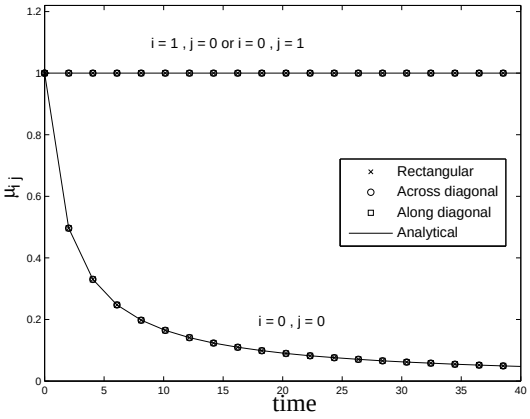

(a) i-j moment

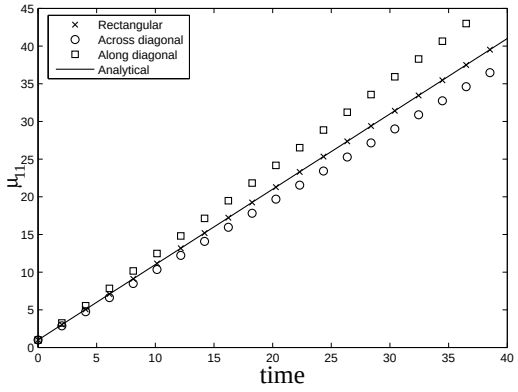

(b) 1-1 moment

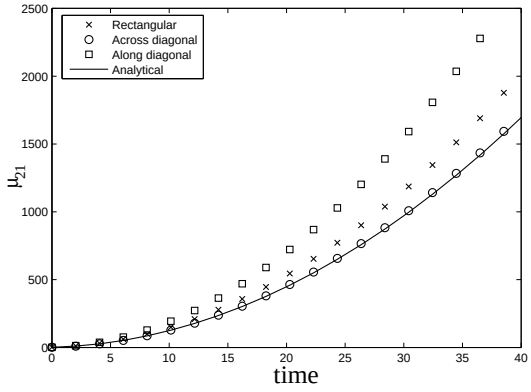

(c) 2-1 moment

Figure 5.5: Test case 1: Moment (a) i-j moment (b) 1-1 moment and (c) 2-1 moment by the FP scheme.

following initial condition from Lushnikov [69]

$$f(0, x, y) = c_1\delta_{x-1} + c_2\delta_{1-y}. \tag{5.5}$$

For the simulation, two different types of mono-disperse particles with the concentration parameters $c_1 = 0.5$ and $c_2 = 0.5$ have been considered as an initial condition (5.5). The number of pivot points in each direction has been taken to be 20 with the rule $x_{i+1/2} = 2x_{i-1/2}$. The numerics has been done at high degree of aggregation, $I_{\text{agg}} = 1 - \mu_{00}(t)/\mu_{00}(0) = 0.98$. The initial condition is plotted in Figure 5.12. Figures 5.13 and 5.14 show the comparison between the numerical and the analytical higher moments μ_{11} and μ_{20} by using the FP scheme and the CAT, respectively. Again we observe that changing the grid from rectangular into triangular does not improve the results for the higher moments using the FP method. However, the CAT gives better prediction for the higher moments using the along triangulation grid as compared to the other two grids. It should be mentioned that for this test problem we have also considered the case of the sum kernel and obtained similar observations for both the schemes.

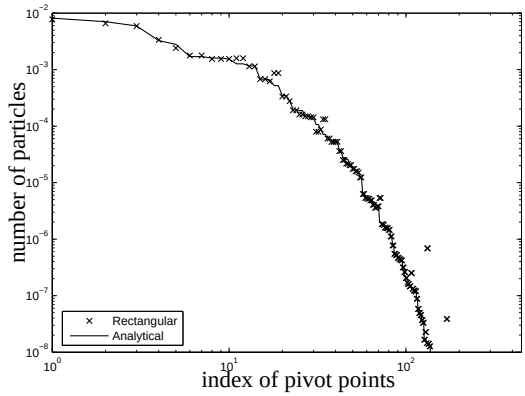

(a) Rectangular grid

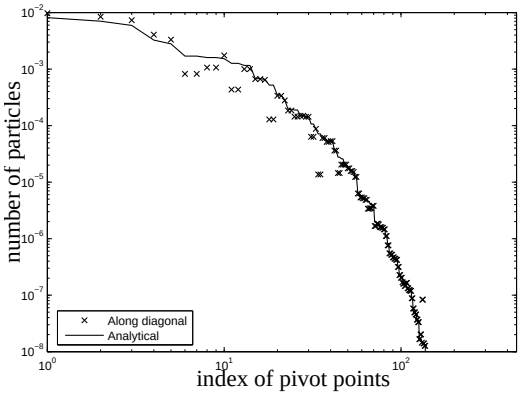

(b) Along diagonal

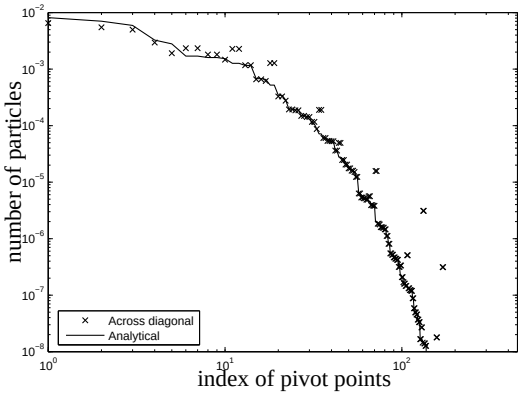

(c) Across diagonal

Figure 5.6: Test case 1: Number density for (a) rectangular grid (b) along diagonal and (c) across diagonal by using the CAT.

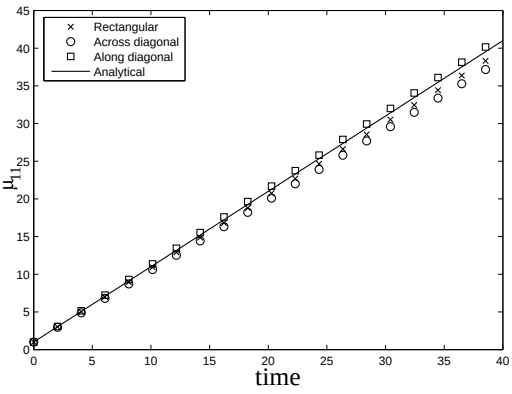

(a) 1-1 moment

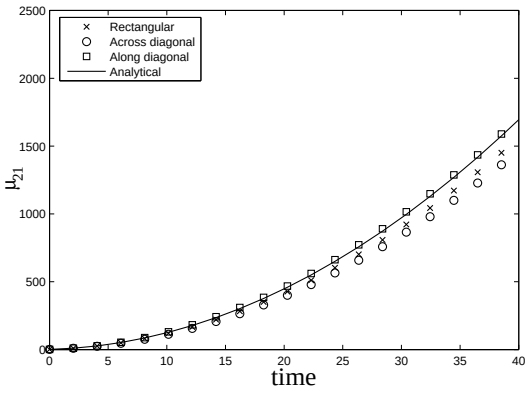

(b) 2-1 moment

Figure 5.7: Test case 1: Moment (a) 1-1 moment and (b) 2-1 moment by the CAT.

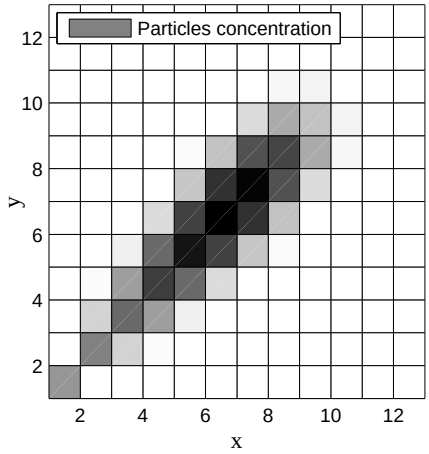

(a) Rectangular grid

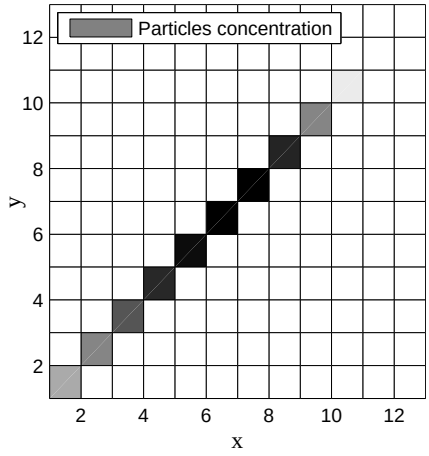

(b) Along diagonal

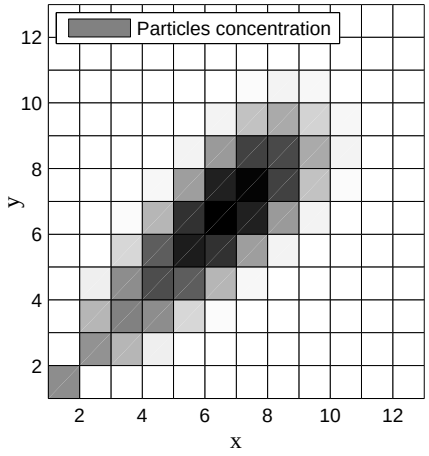

(c) Across diagonal

Figure 5.8: Test case 2: Comparison of the FP scheme showing numerical diffusion for three different grids.

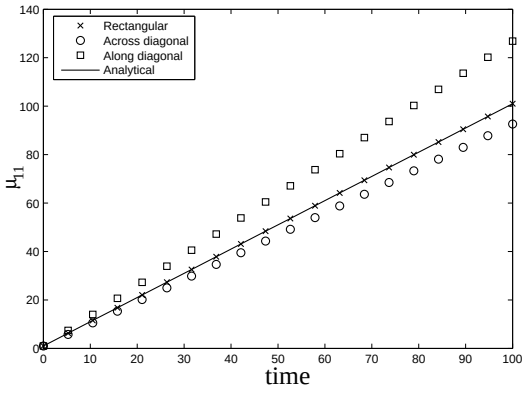

(a) 1-1 moment

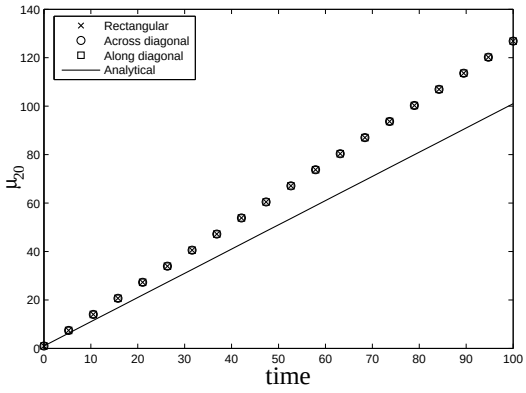

(b) 2-0 moment

Figure 5.9: Test case 2: Moment (a) 1-1 moment and (b) 2-0 moment by the FP technique.

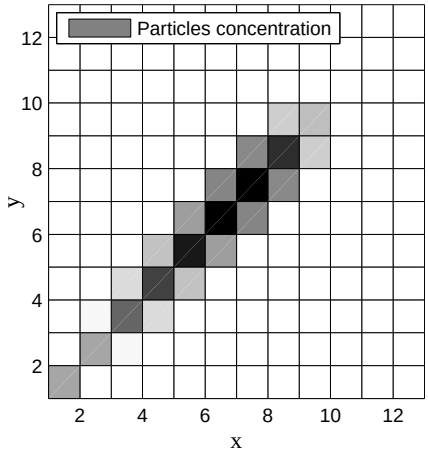

(a) Rectangular grid

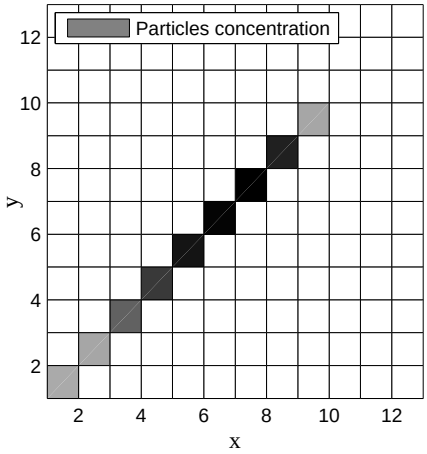

(b) Along diagonal

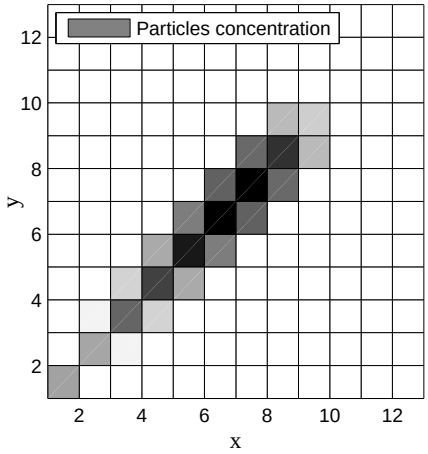

(c) Across diagonal

Figure 5.10: Test case 2: Comparison of the CAT showing numerical diffusion for three different grids.

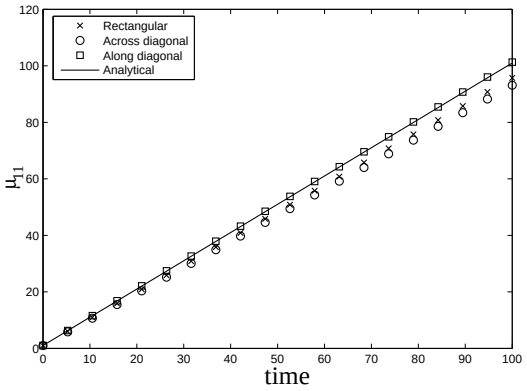

(a) 1-1 moment

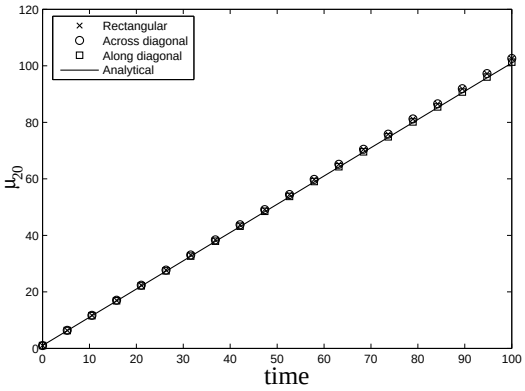

(b) 2-0 moment

Figure 5.11: Test case 2: Moment (a) 1-1 moment and (b) 2-0 moment by the CAT.

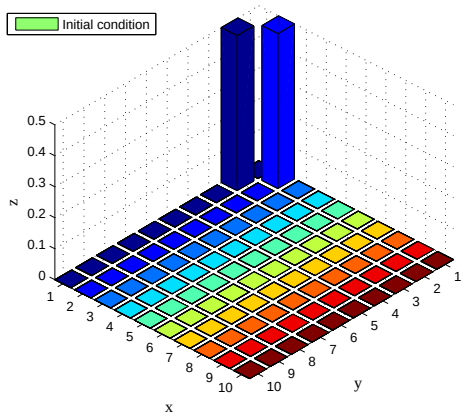

Figure 5.12: Test case 3: Initial condition.

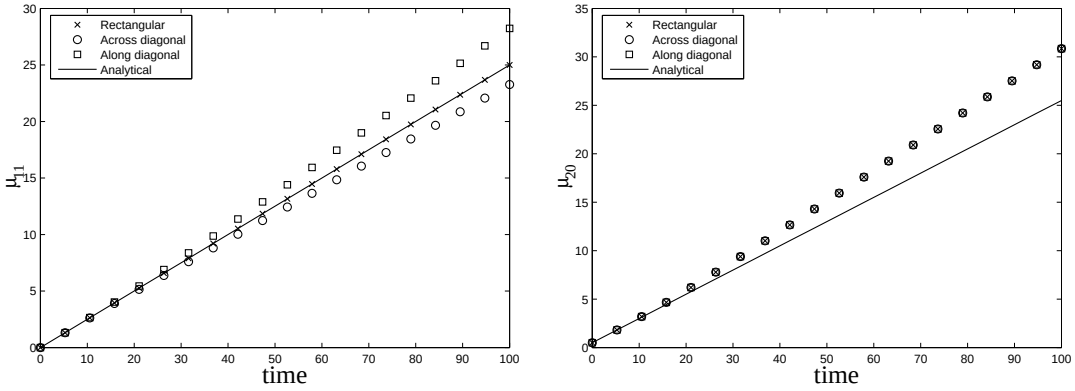

(a) 1-1 moment (b) 2-0 moment

Figure 5.13: Test case 3: Moment (a) 1-1 moment and (b) 2-0 moment by the FP method.

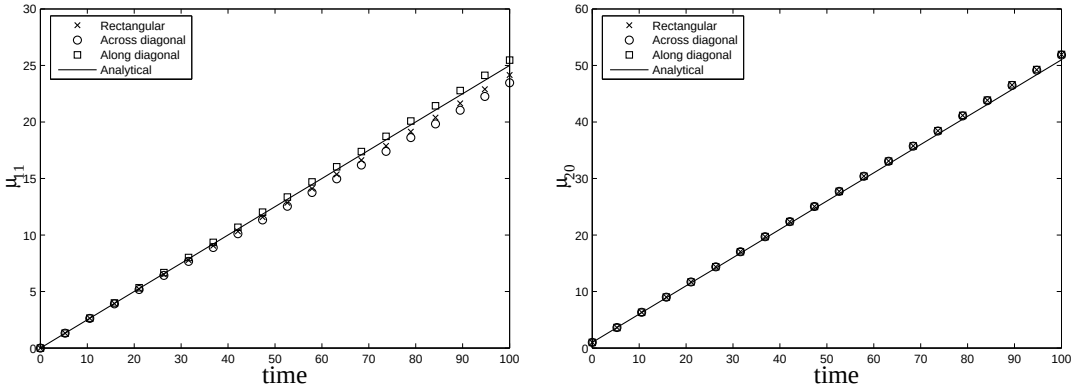

(a) 1-1 moment (b) 2-0 moment

Figure 5.14: Test case 3: Moment (a) 1-1 moment and (b) 2-0 moment by the CAT.

Chapter 6

Modeling in nano-technology

In this chapter we discuss the applications of aggregation and multiple breakage equations in nano-technology. The kinetics of the aggregation and breakage processes during titanium dioxide (TiO_2) nano-particle sol-gel synthesis is presented. Nano-particle precipitation in the batch reactor is discussed briefly and the particle size distributions (PSDs) are verified numerically by solving these equations. We use the cell average technique (CAT) to solve these equations by taking the shear flow aggregation kernel [89] together with two different breakage kernels given by Austin [1] and Diemer [12]. There is a good agreement between the experimental data for the PSDs and the simulation results.

The plan of the chapter is as follows. We start by giving a short introduction to the nano-particles, their applications and the process to make TiO_2 nano-particles in the experiment. This section was written with the help of a chemical engineering student, Yashodhan Gokhale, who did all the experimental work described below. Further in Section 6.2 we recall from Chapter 1 the aggregation-breakage equations, which are used to model the nano-particles. In this section the CAT is also reviewed briefly from Chapter 4 with the aggregation-breakage kernels. Finally in Section 6.3 we solve the model numerically and compare results with the experimental data.

6.1 Introduction

It is known that titanium dioxide has gained much attention in the last few years due to the prospects presented in applying it as a cheap, environmental friendly and nontoxic photocatalyst due to its high specific surface area and porosity. Due to these unique properties, the titanium dioxide particle coating is a very important material. This material has multifunctional applications such as in solar cells, photochromic and electrochromic devices, gas sensors, biosensors, corrosion protection, bactericides and optical devices, see [11, 96] and further citations. Therefore, it is important that nano-particles have to be produced in sufficient amounts before they can be applied on an industrial scale. For this application, the major problem encountered is how the aggregation and breakage of the particles can be controlled during the production process. Therefore, an active area of research in the particle technology is to study how the aggregation and breakage take place with TiO_2 nano-particles.

In the experiment, this control and the prediction of PSDs were based on the process conditions

and the nature of the chemicals. They investigated the synthesis of surface stabilized TiO_2 nano-particles with different surfactants. The steric stabilization of the polymer and various functional groups of dispersants were also considered. The influence of various precursor concentrations and different surfactants on the PSDs were observed. Narrow distributed spherical titania particles in the size range 10-100 nm were produced in a sol-gel synthesis from titanium tetra-isopropoxide.

Many efforts have been made to develope appropriate processes to prepare titania nano-particles experimentally. The most common procedures have been based on the hydrolysis of acidic solutions of titanium salts, gas-phase oxidation reactions of $TiCl_4$ and hydrolysis reactions of titanium alkoxides [74, 4]. Another approach for preparing micron size particles, e.g. particles with a very narrow size distribution was by dispersion polymerization [2]. Recently, chemical vapour deposition was also used to make such nano-particles by thermal decomposition [37].

The sol-gel process for the preparation of nano-particles was preferred among other methods mentioned above because it provided a possibility for deriving special shapes depending on the gel state. This process was rapid, had a low cost and gave better stability at the end of the reaction.

Below we briefly discuss the experimental methodology for synthesizing surfactant based titanium dioxide nano-particles. We also explain in characterization of TiO_2 nano-particles, how the PSDs were measured. For a detailed description readers are referred to Gokhale [27].

Experimental methodology

Titanium dioxide nano-particles have been prepared in the laboratory in a beaker. This beaker was kept inside a temperature bath and maintained at an optimum constant temperature of 50^0C for the redispersion reaction. They used the organic components titanium tetra isopropoxide (TTIP) $Ti(OC_3H_7)_4$ as a precursor, Nitric acid (HNO_3) as stabilizer and different surfactants such as Polyethylene Glycol (PEG) ($H(OCH_2CH_2)_nOH$), Ethylene Glycol (EG) ($HOCH_2CH_2OH$) as well as Sodium Chloride (NaCl). Further, to generate such nano-particles a specified amount of 0.1 M HNO_3 (90 ml) was placed into the batch reactor. Then they measured 50 ml of surfactant (PEG, EG and NaCl with concentration of 0.1 M each) in separate experiments and added this to the HNO_3 in the beaker. The organic precursor TTIP (9.7 ml) was also measured with the syringe and needle and then added to the heated solution under stirrer shear rate $\dot{\Upsilon} = 350s^{-1}$ (corresponding to a stirred rotational speed of 500 revolutions per minute). Precipitation reaction started instantaneously and the solutions or samples were taken periodically on an hourly basis.

Characterization of TiO_2 nano-particles

Particle sizes smaller than 1 μm have been measured via dynamic light scattering (Zetasizer, Malvern Instruments) using a He-Ne laser as light source ($\lambda = 633\ nm$). For particle size distributions in the micrometer size range, a laser diffraction method was used (Mastersizer 2000, Malvern Instruments, He-Ne laser as red light source ($\lambda = 633\ nm$), solid state laser as blue light source ($\lambda = 466\ nm$)) [82]. All size measurements have been performed at a scattering angle of 90 degree and 25 degree. The first samples were taken after 4 hours into the experiment as samples taken before this time were in the micro range.

6.2 Aggregation-breakage model

Aggregation-breakage PBEs are the most frequently used modeling tool to describe and control a wide range of particulate processes like comminution, crystallization, granulation, flocculation, protein precipitation, aerosol dynamics and polymerization. An extensive review of the applications of such equations to particulate systems in engineering is given by Ramkrishna [87]. In process modeling, mass and energy balances are essential tools to describe the changes that occur during the physico-chemical reactions. We know from (1.10), the dynamic behavior of the particle size distributions undergoing simultaneous aggregation and breakage processes is governed by

$$\begin{aligned}\frac{\partial f(t,x)}{\partial t} =& \frac{1}{2}\int_0^x \beta(x-y,y)f(t,x-y)f(t,y)dy - \int_0^\infty \beta(x,y)f(t,y)f(t,x)dy \\ &+ \int_x^\infty b(x,y)S(y)f(t,y)dy - S(x)f(t,x). \end{aligned} \tag{6.1}$$

To solve this equation numerically we first fix a computational domain $]0,R]$ with $R<\infty$ and the truncated equation is obtained from (6.1) replacing ∞ by R. There are many numerical methods to solve the problem. However, here we use the CAT.

The cell average technique

It was shown by Kumar and Warnecke [45] that the CAT is a very accurate and efficient numerical scheme. By using the CAT, reasonably good results are achieved for complete number density distributions on a very coarse grid as well. The mathematical formulation relies on approximating the number density using point masses concentrated at representative points in the cell. Since, we are already familiar with the mathematical formulation of the CAT for these equations from Subsection 4.3.2, we omit the details here.

For the numerical computations later, a shear aggregation kernel e.g.

$$\beta(x,y) = \sqrt{\frac{8\pi}{15\eta}}\dot{\Upsilon}(x^{1/3}+y^{1/3})^3 \tag{6.2}$$

is used, see Saffman and Turner [89]. Here, the parameter $\dot{\Upsilon}$ is known to be the shear rate and η is the viscosity of the suspending fluid. Furthermore, for the breakage process, we use the selection function

$$S(y) = S_0\,(y)^\mu \tag{6.3}$$

where S_0 and μ are positive constants. This selection function is used together with two different breakage functions proposed by Austin [1] and Diemer [12] which are defined in the following.

Diemer kernel

We recall from Chapter 4, equation (4.75) that the Diemer kernel is given as follows

$$b(x,y) = \frac{px^c(y-x)^{c+(c+1)(p-2)}\Gamma[c+(c+1)(p-1)+1]}{y^{pc+p-1}\Gamma(c+1)\Gamma[c+(c+1)(p-2)+1]},$$

where the exponent p describes the number of fragments per breakage event and c determines the shape of the daughter particle distributions.

Austin Kernel

The normalized cumulative breakage function for the formation of particles of size x when a particle of size y breaks has the form proposed by Austin as follows,

$$\mathcal{B}(x,y) = \begin{cases} \phi\left(\frac{x}{y}\right)^{\gamma} + (1-\phi)\left(\frac{x}{y}\right)^{\alpha}; & y > x \\ 1; & y = x, \end{cases} \tag{6.4}$$

where γ, ϕ and α are dimensionless material constants. The term ϕ is called the weight parameter to quantify the mass content of first breakage distributions. The exponents γ and α are width of the fragment distributions ϕ and $1-\phi$, respectively. For the simulation the breakage function $b(x,y)$ is used rather than cumulative function $\mathcal{B}(x,y)$. The calculation steps are provided below.

Since $\mathcal{B}(x,y)$ is the normalized cumulative breakage function, it can also be written as

$$\mathcal{B}(x,y) = \frac{1}{N(y)} \int_0^x b(z,y)dz$$

with $N(y)$ the total number of particles of volume y. Equivalently, we have

$$\frac{d\mathcal{B}}{dx} = \frac{1}{N(y)} b(x,y). \tag{6.5}$$

We can also use (6.4) to obtain

$$\frac{d\mathcal{B}}{dx} = \frac{\phi\gamma x^{\gamma-1}}{y^{\gamma}} + \frac{(1-\phi)\alpha x^{\alpha-1}}{y^{\alpha}}.$$

Multiplying the equation (6.5) by x and integrating with respect to x from 0 to y give

$$\int_0^y x\frac{d\mathcal{B}}{dx}dx = \int_0^y \frac{x}{N(y)} b(x,y)dx.$$

By using the mass conservation condition (1.9), i.e. $\int_0^y xb(x,y)dx = y$, this equation reduces to

$$\int_0^y \left(\phi\gamma\left(\frac{x}{y}\right)^{\gamma} + (1-\phi)\alpha\left(\frac{x}{y}\right)^{\alpha}\right)dx = \frac{1}{N(y)}y.$$

Thus we get

$$\frac{\phi\gamma}{\gamma+1}y + \frac{(1-\phi)\alpha}{\alpha+1}y = \frac{1}{N(y)}y$$

which implies that

$$\frac{1}{N(y)} = \frac{\phi\gamma}{\gamma+1} + \frac{(1-\phi)\alpha}{\alpha+1}.$$

Finally, this equation together with (6.5) imply that the breakage function b is given by

$$b(x,y) = N(y)\frac{d\mathcal{B}}{dx} = \frac{\left(\frac{\phi\gamma x^{\gamma-1}}{y^{\gamma}} + \frac{(1-\phi)\alpha x^{\alpha-1}}{y^{\alpha}}\right)}{\left(\frac{\phi\gamma}{\gamma+1} + \frac{(1-\phi)\alpha}{\alpha+1}\right)}.$$

6.3 Results and discussions

In this section, the simulation results are compared with experimental data by using a shear aggregation and two breakage kernels. Here, we just mention few results. For more details and findings, see [28, 29, 49].

The parameters used for our numerical computations with the Austin kernel are, $\gamma = 0.18$, $\phi = 0.08$, $\alpha = 10$ and for the Diemer kernel $p = 2$, $c = 10$. The constants $\mu = 0.33, 0.70$ are taken together with $S_0 = 1$ in the selection function (6.3) for the Austin and the Diemer kernel, respectively. The synthesis and the numerical results are given here for the shear rate $\dot{\Upsilon} = 370s^{-1}$. Results using shear rates $\dot{\Upsilon} = 623,960$ and $1342s^{-1}$ can be found in Gokhale [27] where the author has also summarized the calculations for these shear rates. It was observed in [27] that $\dot{\Upsilon} = 1342s^{-1}$ is the optimum for generating the TiO_2 nano-particles. A steady state is reached at this value which implies that particle sizes no longer change with time. The computational domain $[4, 1e{+}4]$ is taken for all the cases. We have used the 4 hours experimental result as our initial condition for the numerical computations. Then we compare the results at 6, 8 and 10 hours. The results with different surfactants; PEG, EG and NaCl are plotted. The comparisons are done for the cumulative particle size distributions for each PSD at different time intervals.

Figure 6.1 shows the comparisons for PEG-TiO_2 between the experimental and the simulation results by using the Austin and the Diemer kernels. We observe from Figure 6.1(a) that the numerical results, using the Austin kernel, are in excellent agreement with the experimental data for each time interval. From Figure 6.1(b), we find that the Diemer kernel gives also good-predictions for the experimental results. For both cases there is a general decreasing trend of the particle sizes with time from $t = 4$ hours to $t = 10$ hours.

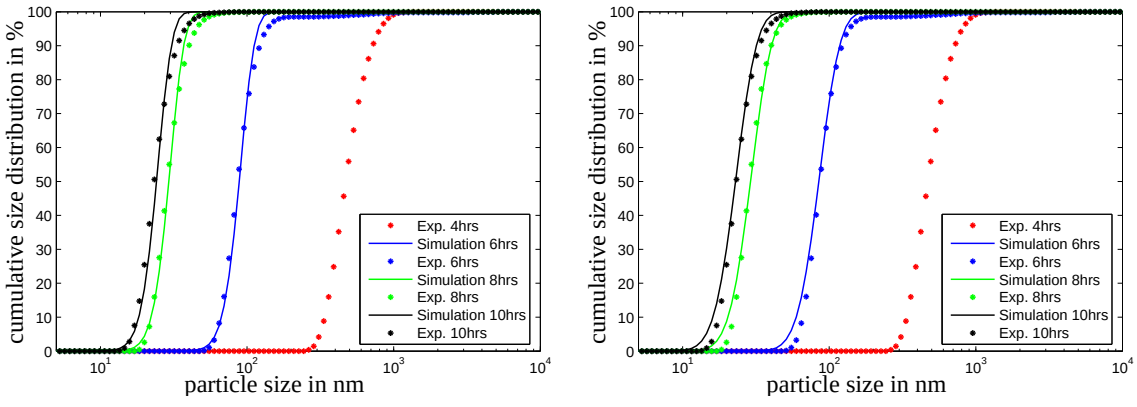

(a) Austin kernel (b) Diemer kernel

Figure 6.1: Experimental sol-gel TiO_2 nano-particles in the presence of 0.374 g/ml Polyethylene Glycol (PEG) and numerical results of PSD by (a) the Austin kernel and (b) the Diemer kernel.

It can be seen from Figure 6.2, during the initial stages at $t = 6$ and 8 hours, polydisperse particles are obtained with Ethylene Glycol. Moreover, after the reaction period of 10 hours

monodisperse particles are produced. We observe from these figures that the Austin and the Diemer kernels show good accuracy with the experimental data.

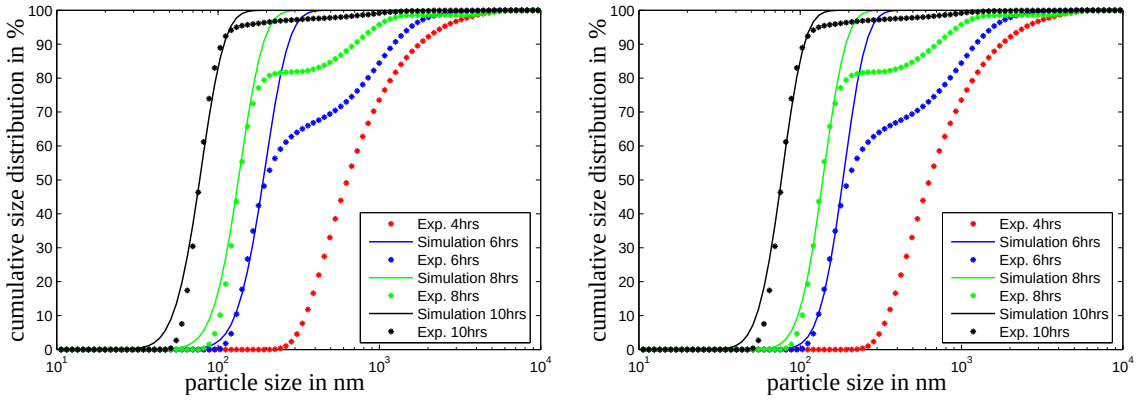

(a) Austin kernel (b) Diemer kernel

Figure 6.2: Experimental sol-gel TiO_2 nano-particles in the presence of 0.372 g/ml Ethylene Glycol and numerical simulations of PSD by (a) the Austin kernel and (b) the Diemer kernel.

Narrow size distributions are obtained after 8 hours with the NaCl. In general, polydisperse particles are achieved during the initial stages of the precipitation reaction as can be seen from Figure 6.3. However, we observe that after the reaction at $t = 8$ hours monodisperse particles are achieved. Similar to the case of Polyethylene Glycol and Ethylene Glycol, here again we find from Figures 6.3(a) and 6.3(b) that the Austin and Diemer kernels indicate the exact predictions with the experimental data.

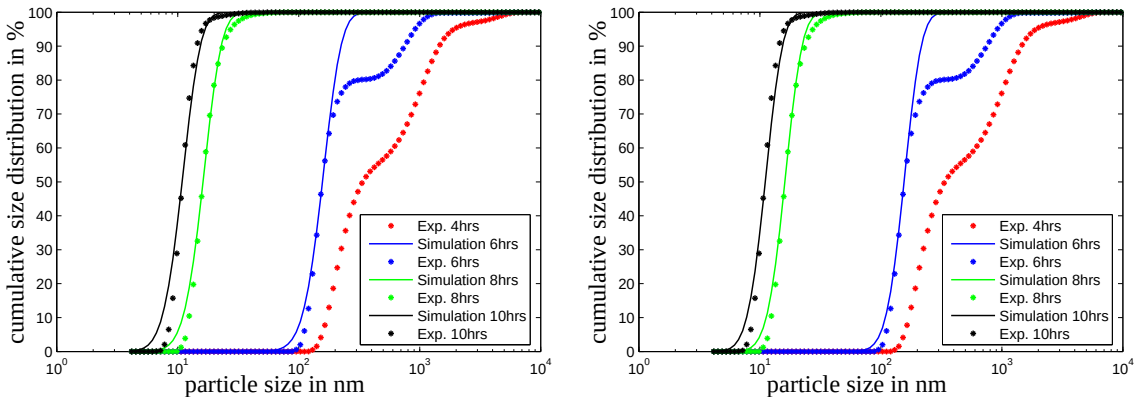

(a) Austin kernel (b) Diemer kernel

Figure 6.3: Experimental sol-gel TiO_2 nano-particles in the presence of 0.720 g/ml NaCl and numerical simulations of PSD by (a) the Austin kernel and (b) the Diemer kernel.

Chapter 7

Conclusions

In this thesis we have studied the numerical analysis and computations for population balance equations in particulate processes using finite volume schemes. Five different observations have been made for such equations. Here we give the conclusions to each of these observations. Finally some open problems are suggested.

Conclusions and future work

First we have discussed the convergence of the discretized finite volume solutions towards the weak solutions to the continuous multiple fragmentation equations. The convergence proof has been shown in $L^{\infty}(]0,T], L^{1}]0,R])$ space by using the weak L^{1} compactness method and the La Vallée Poussin theorem. For the analysis, a locally bounded multiplicative breakage kernel was considered.

In the second goal the stability and the convergence analysis of the finite volume technique were studied for the non-linear aggregation and multiple breakage equations. We have shown the consistency and then proved the Lipschitz continuity of the numerical fluxes to complete the convergence results. This investigation was based on the basic theorems and definitions from the book of Hundsdorfer and Verwer [33] and the paper of Linz [68]. It was noticed that the scheme was second order consistent and convergent for a family of meshes for the pure breakage problem. For the aggregation and combined aggregation-breakage processes, it was not straightforward to evaluate the consistency and the convergence error on general meshes. This depended upon the type of grids chosen for the computations. Moreover, in these cases the technique gave second order consistency and convergence only on uniform, non-uniform smooth and locally uniform meshes while on oscillatory and random grids it shown to be only of first order. The mathematical results of the convergence analysis were verified numerically by taking several examples of pure aggregation, pure breakage and the combined problems. These numerical verifications were made on five different types of uniform and non-uniform meshes.

In our third aim we examined in detail the moment preservation issue for the coupled problems. We introduced the definition of moment preservation as a new concept in this work. Based upon this concept, the zeroth and first moment preserving conditions were obtained for aggregation, breakage, growth and source terms separately. Later we have proposed one moment preserving numerical schemes composed of finite volume methods for the aggregation-breakage terms as

well as source terms and upwind scheme for the growth process. These schemes showed either zeroth moment or first moment preservation depending upon the process under consideration. In case of pure aggregation, pure breakage or both it was total mass preservation while for growth or source terms we found total number preservation. This preservation was obvious due to the well-known property of conservative schemes. Nevertheless, surprising numerical results were observed by considering coupled mass and number preserving processes. In this case no moment was preserved. To avoid the non-preservation for the coupled processes we took the cell average technique as a basis, Kumar and Warnecke [42, 45, 43]. However, for the aggregation, breakage and source terms we rewrote these formulations in a finite volume conservation law. For the aggregation-breakage terms, these formulations gave mass conservation. Further, we found out that the resulting formulations together with a modified upwind scheme for the growth term showed both number and mass preservation for the combined problems. The moment preservation or non-preservation were verified analytically. Finally it was demonstrated by means of numerical results for several coupled processes that the prediction of the moments using two moment preserving methods were very accurate while very poor for one moment preserving schemes.

Further in our next target we introduced the mathematical formulations of the CAT for the two-component aggregation PBEs for two different types of triangular grids, i.e. along and across diagonal arrangement of the triangles. For the numerical investigations we considered three test problems. The results obtained by the CAT and the FP technique for rectangular and triangular grids were compared with the exact solutions. For an along triangulation grids, the FP scheme showed a better prediction only for the number density but not for the higher moments compared to rectangular meshes. Moreover, the CAT improved the results both for the number density and for the higher moments. Therefore, the CAT is a quite stable scheme as compared to the FP method. It should be noted that both schemes were implemented in such a way that they reproduced exactly the analytical solutions for the zeroth and first moments irrespective of the meshes chosen. The formulation of the CAT can easily be extended to more than two-dimensional problems but it will be computationally very expensive.

Finally, we did numerical simulations with the CAT and compared our results with the experimental data of TiO_2 nano-particles by Gokhale et al. [28, 29]. These data were prepared in the lab by sol-gel method using three different surfactants PEG, EG and NaCl. The modeling of these nano-particles was based on the aggregation-breakage processes. We solved these equations numerically by taking a shear aggregation kernel and two different breakage kernels proposed by Austin and Diemer. It was observed that both the breakage kernels gave good agreement with the experimental particle size distributions. Moreover, the Austin kernel was found to be better in terms needed to the computational time.

Now, in the following we would like to mention some open problems related to our work for the future developments.

- It would be interesting to study the finite volume schemes for aggregation and multiple breakage equations which cover the case of singular kernels. Therefore, there is room for improvement in the results of Chapter 2.

- The complexity of the indices $\alpha_{i,k}$ in the numerical flux for aggregation makes the convergence analysis difficult for the case of locally uniform meshes using the finite volume schemes. However, numerically we have observed second order convergence on such meshes. Hence, it would be challenging to see how one can obtain the same order of convergence by mathematical analysis.

- The second moment of the particle size distributions is also very important in some applications. There are no numerical schemes which show second moment preservation for the coupled particulate processes. This is not even available for the individual process of aggregation and breakage problems with simple kernels. Hence, there is much to be done in this direction.

- So far we have discussed the case of bi-component aggregation problems. But the extension for multi-component is still missing using the CAT. One can also include the breakage process to solve the two or multi-dimensional combined equations by the CAT.

- A probable future work would be the implementation of the finite volume approaches to solve the combined aggregation-breakage equations in two or higher dimensions. The mathematical analysis has not been done for such problems as well.

Appendix A

Finite volume analysis

A.1 Conservative formulation

Here we give the calculation steps of determining the finite volume formulations (3.11) of the aggregation and breakage equations from the standard form of the population balance equations.

A.1.1 Finite volume scheme for aggregation

The mass balance population balance equation for aggregation is given by

$$\frac{\partial x n(x,t)}{\partial t} = \frac{x}{2}\int_0^x \beta(x-\epsilon,\epsilon)n(t,x-\epsilon)n(t,\epsilon)d\epsilon - x\int_0^{x_{\max}} \beta(x,\epsilon)n(t,x)n(t,\epsilon)d\epsilon. \tag{A.1}$$

The preceding equation can be rewritten as

$$\frac{\partial x n(x,t)}{\partial t} = \int_0^x \epsilon\beta(x-\epsilon,\epsilon)n(t,x-\epsilon)n(t,\epsilon)d\epsilon - x\int_0^{x_{\max}} \beta(x,\epsilon)n(t,x)n(t,\epsilon)d\epsilon.$$

Integration over a cell gives

$$\frac{\partial G_i(t)}{\partial t} = \int_{x_{i-1/2}}^{x_{i+1/2}} \left[\int_0^x \epsilon\beta(x-\epsilon,\epsilon)n(t,x-\epsilon)n(t,\epsilon)d\epsilon - x\int_0^{x_{\max}} \beta(x,\epsilon)n(t,x)n(t,\epsilon)d\epsilon\right] dx.$$

Changing the order of integration of the birth term we get

$$\begin{aligned}\frac{\partial G_i(t)}{\partial t} &= \int_0^{x_{i-1/2}}\int_{x_{i-1/2}}^{x_{i+1/2}} \epsilon\beta(x-\epsilon,\epsilon)n(t,x-\epsilon)n(t,\epsilon)dxd\epsilon \\ &+ \int_{x_{i-1/2}}^{x_{i+1/2}}\int_{\epsilon}^{x_{i+1/2}} \epsilon\beta(x-\epsilon,\epsilon)n(t,x-\epsilon)n(t,\epsilon)dxd\epsilon - \int_{x_{i-1/2}}^{x_{i+1/2}} x\int_0^{x_{\max}} \beta(x,\epsilon)n(t,x)n(t,\epsilon)d\epsilon dx.\end{aligned}$$

Simplifying first term and application of the mid point rule in the last two terms, we obtain

$$\begin{aligned}\frac{\partial G_i(t)}{\partial t} &= \sum_{k=1}^{i-1}\int_{x_{k-1/2}}^{x_{k+1/2}}\int_{x_{i-1/2}}^{x_{i+1/2}} \epsilon\beta(x-\epsilon,\epsilon)n(t,x-\epsilon)n(t,\epsilon)dxd\epsilon \\ &+ x_i n_i \Delta x_i \int_{x_i}^{x_{i+1/2}} \beta(x-x_i,x_i)n(t,x-x_i)dx - x_i n_i \Delta x_i \sum_{j=1}^{I}\int_{x_{j-1/2}}^{x_{j+1/2}} \beta(x_i,\epsilon)n(t,\epsilon)d\epsilon + \mathcal{O}(\Delta x^3).\end{aligned}$$

Further by applying the mid point rule in the first term entails that

$$\frac{\partial G_i(t)}{\partial t} = \sum_{k=1}^{i-1} x_k n_k \Delta x_k \int_{x_{i-1/2}}^{x_{i+1/2}} \beta(x - x_k, x_k) n(t, x - x_k) dx$$
$$+ x_i n_i \Delta x_i \int_{x_i}^{x_{i+1/2}} \beta(x - x_i, x_i) n(t, x - x_i) dx - x_i n_i \Delta x_i \sum_{j=1}^{I} \int_{x_{j-1/2}}^{x_{j+1/2}} \beta(x_i, \epsilon) n(t, \epsilon) d\epsilon + \mathcal{O}(\Delta x^3).$$

An appropriate substitution can be applied to get

$$\frac{\partial G_i(t)}{\partial t} = \sum_{k=1}^{i-1} x_k n_k \Delta x_k \int_{x_{i-1/2}-x_k}^{x_{i+1/2}-x_k} \beta(\epsilon, x_k) n(t, \epsilon) d\epsilon + x_i n_i \Delta x_i \int_{0}^{x_{i+1/2}-x_i} \beta(\epsilon, x_i) n(t, \epsilon) d\epsilon$$
$$- x_i n_i \Delta x_i \sum_{j=1}^{I} \int_{\Lambda_j} \beta(x_i, \epsilon) n(t, \epsilon) d\epsilon + \mathcal{O}(\Delta x^3).$$

Denoting the integer $\alpha_{i,k}$ by the index of a cell such that $x_{i+1/2} - x_k \in \Lambda_{\alpha_{i,k}-1}$, we can rewrite the above equation as

$$\frac{\partial G_i(t)}{\partial t} = \sum_{k=1}^{i-1} x_k n_k \Delta x_k \int_{x_{i-1/2}-x_k}^{x_{\alpha_{i-1,k}-1/2}} \beta(\epsilon, x_k) n(t, \epsilon) d\epsilon - \sum_{k=1}^{i-1} x_k n_k \Delta x_k \int_{x_{i+1/2}-x_k}^{x_{\alpha_{i,k}-1/2}} \beta(\epsilon, x_k) n(t, \epsilon) d\epsilon$$
$$+ \sum_{k=1}^{i-1} x_k n_k \Delta x_k \sum_{j=\alpha_{i-1,k}}^{\alpha_{i,k}-1} \int_{\Lambda_j} \beta(\epsilon, x_k) n(t, \epsilon) d\epsilon + x_i n_i \Delta x_i \sum_{j=1}^{\alpha_{i,i}-1} \int_{\Lambda_j} \beta(\epsilon, x_i) n(t, \epsilon) d\epsilon$$
$$- x_i n_i \Delta x_i \int_{x_{i+1/2}-x_i}^{x_{\alpha_{i,i}-1/2}} \beta(\epsilon, x_i) n(t, \epsilon) d\epsilon - x_i n_i \Delta x_i \sum_{j=1}^{I} \int_{\Lambda_j} \beta(x_i, \epsilon) n(t, \epsilon) d\epsilon + \mathcal{O}(\Delta x^3).$$

It can be further simplified as

$$\frac{\partial G_i(t)}{\partial t} = \sum_{k=1}^{i-1} x_k n_k \Delta x_k \left[(xn)_{\alpha_{i-1,k}-1} \int_{x_{i-1/2}-x_k}^{x_{\alpha_{i-1,k}-1/2}} \frac{\beta(\epsilon, x_k)}{\epsilon} d\epsilon - (xn)_{\alpha_{i,k}-1} \int_{x_{i+1/2}-x_k}^{x_{\alpha_{i,k}-1/2}} \frac{\beta(\epsilon, x_k)}{\epsilon} d\epsilon \right]$$
$$+ \sum_{k=1}^{i-1} x_k n_k \Delta x_k \sum_{j=\alpha_{i-1,k}}^{\alpha_{i,k}-1} x_j n_j \int_{\Lambda_j} \frac{\beta(\epsilon, x_k)}{\epsilon} d\epsilon + x_i n_i \Delta x_i \sum_{j=1}^{\alpha_{i,i}-1} x_j n_j \int_{\Lambda_j} \frac{\beta(\epsilon, x_i)}{\epsilon} d\epsilon$$
$$- x_i n_i \Delta x_i (xn)_{\alpha_{i,i}-1} \int_{x_{i+1/2}-x_i}^{x_{\alpha_{i,i}-1/2}} \frac{\beta(\epsilon, x_i)}{\epsilon} d\epsilon - x_i n_i \Delta x_i \sum_{j=1}^{I} x_j n_j \int_{\Lambda_j} \frac{\beta(x_i, \epsilon)}{\epsilon} d\epsilon + \mathcal{O}(\Delta x^3).$$

Note that here we use $(xn)_j = x_j n_j$. Combining the terms together we get

$$\frac{\partial G_i(t)}{\partial t} = \sum_{k=1}^{i-1} x_k n_k \Delta x_k \left[(xn)_{\alpha_{i-1,k}-1} \int_{x_{i-1/2}-x_k}^{x_{\alpha_{i-1,k}-1/2}} \frac{\beta(\epsilon, x_k)}{\epsilon} d\epsilon + \sum_{j=\alpha_{i-1,k}}^{\alpha_{i,k}-1} x_j n_j \int_{\Lambda_j} \frac{\beta(\epsilon, x_k)}{\epsilon} d\epsilon \right]$$
$$- \sum_{k=1}^{i} x_k n_k \Delta x_k (xn)_{\alpha_{i,k}-1} \int_{x_{i+1/2}-x_k}^{x_{\alpha_{i,k}-1/2}} \frac{\beta(\epsilon, x_k)}{\epsilon} d\epsilon - x_i n_i \Delta x_i \sum_{j=\alpha_{i,i}}^{I} x_j n_j \int_{\Lambda_j} \frac{\beta(x_i, \epsilon)}{\epsilon} d\epsilon + \mathcal{O}(\Delta x^3).$$

Again, some simplifications lead to

$$\Delta x_i \frac{\partial x_i n_i(t)}{\partial t} = -\Bigg[\sum_{k=1}^{i} x_k n_k \Delta x_k \Bigg(\sum_{j=\alpha_{i,k}}^{I} x_j n_j \int_{\Lambda_j} \frac{\beta(x_k,\epsilon)}{\epsilon} d\epsilon + (xn)_{\alpha_{i,k}-1} \int_{x_{i+1/2}-x_k}^{x_{\alpha_{i,k}-1/2}} \frac{\beta(\epsilon,x_k)}{\epsilon} d\epsilon \Bigg)$$
$$- \sum_{k=1}^{i-1} x_k n_k \Delta x_k \Bigg(\sum_{j=\alpha_{i-1,k}}^{I} x_j n_j \int_{\Lambda_j} \frac{\beta(x_k,\epsilon)}{\epsilon} d\epsilon + (xn)_{\alpha_{i-1,k}-1} \int_{x_{i-1/2}-x_k}^{x_{\alpha_{i-1,k}-1/2}} \frac{\beta(\epsilon,x_k)}{\epsilon} d\epsilon \Bigg) \Bigg] + \mathcal{O}(\Delta x^3)$$
$$= -[I_1 - I_2] + \mathcal{O}(\Delta x^3). \tag{A.2}$$

Here, it should be mentioned that the above formulation gives exactly the same aggregation numerical flux using a finite volume scheme as proposed by Filbet and Laurençot [23]. However, considering β is a two times smooth function in our work we can still apply the mid point approximation on I_1 to get

$$I_1 = \sum_{k=1}^{i} x_k n_k \Delta x_k \Bigg(\sum_{j=\alpha_{i,k}}^{I} x_j n_j \frac{\beta(x_k,x_j)}{x_j} \Delta x_j + (xn)_{\alpha_{i,k}-1} \int_{x_{i+1/2}-x_k}^{x_{\alpha_{i,k}-1/2}} \frac{\beta(\epsilon,x_k)}{\epsilon} d\epsilon \Bigg) + \mathcal{O}(\Delta x^2).$$

Taylor series expansion of the second term about the point $x_{\alpha_{i,k}-1}$ gives

$$I_1 = \sum_{k=1}^{i} x_k n_k \Delta x_k \Bigg(\sum_{j=\alpha_{i,k}}^{I} n_j \beta_{j,k} \Delta x_j + n_{\alpha_{i,k}-1} \beta_{\alpha_{i,k}-1,k} \left(x_{\alpha_{i,k}-1/2} - (x_{i+1/2} - x_k) \right) \Bigg) + \mathcal{O}(\Delta x^2)$$
$$= J^{\text{agg}}_{i+1/2} + \mathcal{O}(\Delta x^2).$$

The term I_2 is same as I_1 but we replace i by $i-1$. Hence, from (A.2) the finite volume formulation for aggregation can be written as

$$\Delta x_i \frac{\partial x_i n_i(t)}{\partial t} = -\left[J^{\text{agg}}_{i+1/2} - J^{\text{agg}}_{i-1/2} \right],$$

where the numerical flux

$$J^{\text{agg}}_{i+1/2} = \sum_{k=1}^{i} x_k n_k \Delta x_k \Bigg(\sum_{j=\alpha_{i,k}}^{I} n_j \beta_{jk} \Delta x_j + n_{\alpha_{i,k}-1} \beta_{\alpha_{i,k}-1,k} \left(x_{\alpha_{i,k}-1/2} - (x_{i+1/2} - x_k) \right) \Bigg). \tag{A.3}$$

This is exactly the same finite volume discretization (3.16) for the aggregation obtained by applying the finite volume schemes on modified form, i.e. mass conservation laws of the aggregation population balance equations.

A.1.2 Finite volume scheme for breakage

The mass balance population balance equation for breakage is given by

$$\frac{\partial x n(x,t)}{\partial t} = x \int_x^{x_{\max}} b(x,\epsilon) S(\epsilon) n(t,\epsilon)\, d\epsilon - x S(x) n(t,x).$$

Substituting $x = \int_0^x \epsilon b(\epsilon,x)\, d\epsilon$, the above equation can be rewritten as

$$\frac{\partial x n(x,t)}{\partial t} = x \int_x^{x_{\max}} b(x,\epsilon) S(\epsilon) n(t,\epsilon)\, d\epsilon - S(x) n(t,x) \int_0^x \epsilon b(\epsilon,x)\, d\epsilon.$$

Integration over a cell gives

$$\frac{\partial G_i(t)}{\partial t} = \int_{x_{i-1/2}}^{x_{i+1/2}} x \int_{x}^{x_{\max}} b(x,\epsilon) S(\epsilon) n(t,\epsilon)\, d\epsilon dx - \int_{x_{i-1/2}}^{x_{i+1/2}} S(x) n(t,x) \int_0^x \epsilon b(\epsilon, x)\, d\epsilon dx.$$

Changing the order of integration of the first term we get

$$\begin{aligned}\frac{\partial G_i(t)}{\partial t} = &\left(\int_{x_{i-1/2}}^{x_{i+1/2}} \int_{x_{i-1/2}}^{\epsilon} + \int_{x_{i+1/2}}^{x_{\max}} \int_{x_{i-1/2}}^{x_{i+1/2}} \right) x b(x,\epsilon) S(\epsilon) n(t,\epsilon) dx\, d\epsilon \\ &- \int_{x_{i-1/2}}^{x_{i+1/2}} S(x) n(t,x) \int_0^x \epsilon b(\epsilon, x)\, d\epsilon dx.\end{aligned}$$

Further simplification gives

$$\begin{aligned}\frac{\partial G_i(t)}{\partial t} = &- \int_{x_{i-1/2}}^{x_{i+1/2}} S(x) n(t,x) \int_0^{x_{i-1/2}} x b(x,\epsilon) dx\, d\epsilon \\ + \sum_{k=i+1}^{I} \int_{x_{k-1/2}}^{x_{k+1/2}} S(\epsilon) n(t,\epsilon) \int_0^{x_{i+1/2}} &x b(x,\epsilon)\, dx d\epsilon - \sum_{k=i+1}^{I} \int_{x_{k-1/2}}^{x_{k+1/2}} S(\epsilon) n(t,\epsilon) \int_0^{x_{i-1/2}} x b(x,\epsilon)\, dx d\epsilon.\end{aligned}$$

Applying mid point rule in all terms, we obtain finally

$$\begin{aligned}\frac{\partial G_i(t)}{\partial t} = &- S(x_i) n_i \Delta x_i \sum_{j=1}^{i-1} x_j b(x_j, x_i) \Delta x_j + \sum_{k=i+1}^{I} S(x_k) n_k \Delta x_k \sum_{j=1}^{i} x_j b(x_j, x_k) \Delta x_j \\ &- \sum_{k=i+1}^{I} S(x_k) n_k \Delta x_k \sum_{j=1}^{i-1} x_j b(x_j, x_k) \Delta x_j + \mathcal{O}(\Delta x^2) \\ = &J^{\text{brk}}_{i+1/2} - J^{\text{brk}}_{i-1/2} + \mathcal{O}(\Delta x^2).\end{aligned}$$

Thus finite volume discretization for breakage is given as

$$\Delta x_i \frac{\partial x_i n_i(t)}{\partial t} = - \left[J^{\text{brk}}_{i+1/2} - J^{\text{brk}}_{i-1/2} \right],$$

where

$$J^{\text{brk}}_{i+1/2} = - \sum_{k=i+1}^{I} S(x_k) n_k \Delta x_k \sum_{j=1}^{i} x_j b(x_j, x_k) \Delta x_j. \tag{A.4}$$

This is again the same formulation we obtained as in (3.13) using the finite volume schemes on the mass conserving form of the breakage population balance equations.

A.2 Bound on total number of particles

We give the proof of Lemmas 3.3.9 and 3.3.10 in Appendices A.2.1 and A.2.2, respectively.

A.2.1 Continuous aggregation and multiple breakage equation

Proof. [Lemma 3.3.9]
Integrating the equation (3.4) with respect to x from 0 to $x_{\max}$ gives

$$\frac{d}{dt}\int_0^{x_{\max}} n(t,x)dx = \int_0^{x_{\max}} -\frac{1}{x}\frac{\partial}{\partial x}(F^{\text{agg}} + F^{\text{brk}})dx. \tag{A.5}$$

We know from (3.5) that

$$\frac{\partial}{\partial x}(F^{\text{agg}}(t,x)) = \frac{\partial}{\partial x}\int_0^x \int_{x-u}^{x_{\max}} u\beta(u,v)n(t,u)n(t,v)dvdu.$$

Applying the Leibniz integration rule we obtain

$$\begin{aligned}\frac{\partial}{\partial x}(F^{\text{agg}}(t,x)) &= \int_0^x \frac{\partial}{\partial x}\int_{x-u}^{x_{\max}} u\beta(u,v)n(t,u)n(t,v)dvdu + \int_0^{x_{\max}} x\beta(x,v)n(t,x)n(t,v)dv \\ &= -\int_0^x u\beta(u,x-u)n(t,u)n(t,x-u)du + \int_0^{x_{\max}} x\beta(x,v)n(t,x)n(t,v)dv. \end{aligned}\tag{A.6}$$

From (3.6) we have

$$\frac{\partial}{\partial x}(F^{\text{brk}}(t,x)) = -\frac{\partial}{\partial x}\int_x^{x_{\max}} \int_0^x ub(u,v)S(v)n(t,v)dudv.$$

Again with the Leibniz integration rule we determine

$$\frac{\partial}{\partial x}(F^{\text{brk}}(t,x)) = -\int_x^{x_{\max}} xb(x,v)S(v)n(t,v)dv + \int_0^x ub(u,x)S(x)n(t,x)du \tag{A.7}$$

Inserting (A.6) and (A.7) into (A.5) to get

$$\begin{aligned}\frac{dN(t)}{dt} &= \int_0^{x_{\max}}\int_0^x \frac{u}{x}\beta(u,x-u)n(t,u)n(t,x-u)dudx - \int_0^{x_{\max}}\int_0^{x_{\max}} \beta(x,v)n(t,x)n(t,v)dvdx \\ &+ \int_0^{x_{\max}}\int_x^{x_{\max}} b(x,v)S(v)n(t,v)dvdx - \int_0^{x_{\max}}\int_0^x \frac{u}{x}b(u,x)S(x)n(t,x)dudx. \end{aligned}\tag{A.8}$$

Changing the order of integration for the first and third integrals on the right-hand side of (A.8), we obtain

$$\begin{aligned}\frac{dN(t)}{dt} &= \int_0^{x_{\max}}\int_u^{x_{\max}} \frac{u}{x}\beta(u,x-u)n(t,u)n(t,x-u)dxdu - \int_0^{x_{\max}}\int_0^{x_{\max}} \beta(x,v)n(t,x)n(t,v)dvdx \\ &+ \int_0^{x_{\max}}\int_0^v b(x,v)S(v)n(t,v)dxdv - \int_0^{x_{\max}}\int_0^x \frac{u}{x}b(u,x)S(x)n(t,x)dudx. \end{aligned}\tag{A.9}$$

Since $x \geq u$ for the first integral, this implies that $u/x \leq 1$. Substituting $x = z + u$ such that $dx = dz$, we estimate this equation as

$$\frac{dN(t)}{dt} \leq \int_0^{x_{\max}} \int_0^{x_{\max}-u} \beta(u,z)n(t,u)n(t,z)dzdu - \int_0^{x_{\max}} \int_0^{x_{\max}} \beta(x,v)n(t,x)n(t,v)dvdx + \int_0^{x_{\max}} S(v)n(t,v) \int_0^v b(x,v)dxdv - \int_0^{x_{\max}} \frac{S(x)n(t,x)}{x} \int_0^x ub(u,x)dudx.$$

We observe that the first two integrals combined give a negative value. Using the mass conserving property (1.9) of the breakage function in the last integral, we obtain the estimate

$$\begin{aligned}\frac{dN(t)}{dt} &\leq \int_0^{x_{\max}} S(v)n(t,v) \int_0^v b(x,v)dxdv - \int_0^{x_{\max}} S(x)n(t,x)dx \\ &\leq \int_0^{x_{\max}} n(t,v) \int_0^v S(v)b(x,v)dxdv.\end{aligned}$$

From the bounds (3.9) we know that $bS \leq Q_1$. It leads to

$$\frac{dN(t)}{dt} \leq Q_1 \int_0^{x_{\max}} v\, n(t,v)dv.$$

Finally, estimating $v \leq x_{\max}$, we get

$$\frac{dN(t)}{dt} \leq Q_1 x_{\max} N(t).$$

Therefore, the total number of particles is bounded and the bound is given as

$$N(t) \leq N(0)\exp(x_{\max}Q_1 t) \leq N(0)\exp(x_{\max}Q_1 T) = C_{T,x_{\max}}.$$

□

A.2.2 Discrete aggregation and multiple breakage equation

Proof. [Lemma 3.3.10]
Multiplying the equation (3.11) by $\Delta x_i/x_i$ and summing with respect to i gives

$$\frac{d(\sum_{i=1}^I \hat{n}_i(t)\Delta x_i)}{dt} = -\sum_{i=1}^I \frac{1}{x_i}\left[J^{\text{agg}}_{i+1/2} - J^{\text{agg}}_{i-1/2} + J^{\text{brk}}_{i+1/2} - J^{\text{brk}}_{i-1/2}\right]. \tag{A.10}$$

We write out the summation over i of the aggregation fluxes $J^{\text{agg}}_{i\pm1/2}$ to get

$$\begin{aligned}-\sum_{i=1}^I \frac{1}{x_i}\left[J^{\text{agg}}_{i+1/2} - J^{\text{agg}}_{i-1/2}\right] &= -\left[\frac{1}{x_1}(J^{\text{agg}}_{1+1/2} - J^{\text{agg}}_{1-1/2}) + \frac{1}{x_2}(J^{\text{agg}}_{2+1/2} - J^{\text{agg}}_{2-1/2}) + \cdots \right. \\ &\qquad \left. + \frac{1}{x_I}(J^{\text{agg}}_{I+1/2} - J^{\text{agg}}_{I-1/2})\right] \\ &= -\left[-\frac{1}{x_1}J^{\text{agg}}_{1/2} + J^{\text{agg}}_{1+1/2}\left(\frac{1}{x_1} - \frac{1}{x_2}\right) + \cdots + J^{\text{agg}}_{I-1/2}\left(\frac{1}{x_{I-1}} - \frac{1}{x_I}\right) + \frac{1}{x_I}J^{\text{agg}}_{I+1/2}\right].\end{aligned}$$

For the breakage fluxes $J^{\text{brk}}_{i\pm1/2}$ in (A.10) we substitute the definition (3.13). Introducing the notations $\hat{N}_i(t) = \hat{n}_i(t)\Delta x_i$ and $\hat{N}(t) = \sum_{i=1}^{I} \hat{N}_i(t)$, we obtain

$$\begin{aligned}\frac{d\hat{N}(t)}{dt} =& \frac{1}{x_1} J^{\text{agg}}_{1/2} - \sum_{i=1}^{I-1} J^{\text{agg}}_{i+1/2} \left(\frac{1}{x_i} - \frac{1}{x_{i+1}} \right) - \frac{1}{x_I} J^{\text{agg}}_{I+1/2} \\ &+ \sum_{i=1}^{I} \sum_{k=i+1}^{I} \hat{N}_k(t) S(x_k) b(x_i, x_k) \Delta x_i - \sum_{i=1}^{I} \hat{N}_i(t) S(x_i) \sum_{j=1}^{i-1} \frac{x_j}{x_i} b(x_j, x_i) \Delta x_j.\end{aligned}$$

Due to positivity of $J^{\text{agg}}_{i+1/2}$ for all i and $J^{\text{agg}}_{1/2} = 0$, we estimate

$$\frac{d\hat{N}(t)}{dt} \leq \sum_{i=1}^{I} \sum_{k=i+1}^{I} \hat{N}_k(t) S(x_k) b(x_i, x_k) \Delta x_i - \sum_{i=1}^{I} \hat{N}_i(t) S(x_i) \sum_{j=1}^{i-1} \frac{x_j}{x_i} b(x_j, x_i) \Delta x_j.$$

Changing the order of summation for the first term and the summation indices in the second term yield

$$\begin{aligned}\frac{d\hat{N}(t)}{dt} \leq& \sum_{k=1}^{I} \sum_{i=1}^{k-1} \hat{N}_k(t) S(x_k) b(x_i, x_k) \Delta x_i - \sum_{k=1}^{I} \hat{N}_k(t) S(x_k) \sum_{i=1}^{k-1} \frac{x_i}{x_k} b(x_i, x_k) \Delta x_i \\ =& \sum_{k=1}^{I} \hat{N}_k(t) S(x_k) \left[\sum_{i=1}^{k-1} b(x_i, x_k) \Delta x_i (1 - x_i/x_k) \right].\end{aligned}$$

Since $i < k$ implies that $x_i < x_k$ we have $1 - x_i/x_k < 1$. Similar to the previous lemma we have $bS \leq Q_1$. This implies that

$$\frac{d\hat{N}(t)}{dt} \leq x_{\max} Q_1 \hat{N}(t).$$

Therefore, we obtain the following bound on the total number of particles by using the finite volume scheme as

$$\hat{N}(t) \leq \hat{N}(0) \exp(x_{\max} Q_1 t) \leq \hat{N}(0) \exp(x_{\max} Q_1 T) = C_{T, x_{\max}},$$

which is the same bound as explained in the previous lemma, provided $\hat{N}(0) = N(0)$. □

Appendix B

Moment preservation

B.1 Analytical solutions of moments for coupled processes

In this section, we determine the exact solutions for the zeroth and the first moments for various coupled processes by solving the population balance equations (4.1).

Combined aggregation and breakage

Multiplying the aggregation, breakage ($G, B_{\text{src}} = 0$) equation (4.1) by x^r and integrating from 0 to ∞, we obtain the following differential equation for rth moment as

$$\begin{aligned}\frac{d\mu_r(t)}{dt} = &\int_0^\infty \int_0^\infty \left[\frac{1}{2}(x+y)^r - x^r\right] \beta(x,y) f(t,x) f(t,y) dx dy \\ &+ \int_0^\infty \left[\int_0^y x^r b(x,y) dx - y^r\right] S(y) f(t,y) dy.\end{aligned}$$

It is easy to show that $d\mu_1(t)/dt = 0$ provided

$$\int_0^\infty \int_0^\infty x\beta(x,y) f(t,x) f(t,y) dx dy < \infty \text{ and } \int_0^\infty y S(y) f(t,y) dy < \infty.$$

Now we derive ordinary differential equation for zeroth moment

$$\frac{d\mu_0(t)}{dt} = -\frac{1}{2}\int_0^\infty \int_0^\infty \beta(x,y) f(t,x) f(t,y) dx dy + \int_0^\infty \big[p(y) - 1\big] S(y) f(t,y) dy.$$

Here the function $p(y)$ denotes the number of fragmentation per breakage event. It is given by

$$p(y) = \int_0^y b(x,y) dx.$$

If we assume that $p(y)$ is constant, the preceding equation can be further simplified as

$$\frac{d\mu_0(t)}{dt} = -\frac{1}{2}\int_0^\infty \int_0^\infty \beta(x,y) f(t,x) f(t,y) dx dy + \big(p-1\big) \int_0^\infty S(y) f(t,y) dy.$$

Table B.1 summarizes the analytical results for the zeroth moment using several combinations of kernels with β_0 and S_0 are positive constants.

Table B.1: Analytical solutions for zeroth moment

Case	$\beta(x,y)$	$S(x)$	Analytical solution $\mu_0(t)$
1	β_0	S_0	$\frac{2C_1\mu_0(0)\exp(\beta_0 C_1 t)}{(2C_1-\mu_0(0))+\mu_0(0)\exp(\beta_0 C_1 t)}$
2	β_0	$S_0 x$	$\mu_1\sqrt{C_1}\frac{1+C_2\exp(-\beta_0\mu_1\sqrt{C_1}t)}{1-C_2\exp(-\beta_0\mu_1\sqrt{C_1}t)}$
3	$\beta_0 xy$	S_0	$\frac{\mu_1^2}{2C_1}+\left(\mu_0(0)-\frac{\mu_1^2}{2C_1}\right)\exp\left(\beta_0 C_1 t\right)$
4	$\beta_0 xy$	$S_0 x$	$\mu_0(0)+\left(-\frac{1}{2}\beta_0\mu_1^2+\beta_0 C_1\mu_1\right)t$
5	$\beta_0(x+y)$	S_0	$\mu_0(0)\exp\left(-\beta_0\mu_1 t+\beta_0 C_1 t\right)$
6	$\beta_0(x+y)$	$S_0 x$	$C_1+\left(\mu_0(0)-C_1\right)\exp(-\beta_0\mu_1 t)$

$C_1=((p-1)S_0)/\beta_0$, $C_2=\frac{\left(\mu_0(0)-\mu_1\sqrt{C_1}\right)}{\left(\mu_0(0)-\mu_1\sqrt{C_1}\right)}$

Simultaneous breakage and growth

Similar to the previous case, multiplying the breakage, growth ($\beta, B_{\text{src}}=0$) PBEs (4.1) by 1 and x, integrating from 0 to ∞ and by doing simple calculations, we obtain the following expressions in Table B.2 for the zeroth and the first moments, respectively. The same breakage function (4.75) has been used. The parameters S_0 and G_0 are positive constants.

Table B.2: Analytical solutions for zeroth and first moments

Case	$S(x)$	$G(x)$	Analytical solution $\mu_0(t)$	Analytical solution $\mu_1(t)$
1	S_0	$G_0 x$	$\mu_0(0)\exp(S_0(p-1)t)$	$\mu_1(0)\exp(G_0 t)$
2	$S_0 x$	$G_0 x$	$\mu_0(0)+\frac{(p-1)S_0\mu_1(0)}{G_0}(\exp(G_0 t-1))$	$\mu_1(0)\exp(G_0 t)$

$S_0>0$,$G_0>0$

Combined aggregation, breakage and growth

By multiplying the general aggregation, breakage and growth ($B_{\text{src}}=0$) PBEs (4.1) by 1 and x, integrating from 0 to ∞ and some mathematical computation leads to the analytical solutions in Table B.3 for the zeroth and the first moments, respectively. The breakage function (4.75) and the sum aggregation kernel, i.e., $\beta(x,y)=\beta_0(x+y)$ have been considered. As discussed above β_0, S_0 and G_0 are positive constants.

Table B.3: Analytical solutions for zeroth and first moments

$Case$	$S(x)$	$G(x)$	Analytical solution $\mu_0(t)$	Analytical solution $\mu_1(t)$
1	S_0	$G_0 x$	$\mu_0(0)\exp\left(\frac{\beta_0\mu_1(0)}{G_0}(1-\exp(G_0 t))\right)\exp(Ct)$	$\mu_1(0)\exp(G_0 t)$
2	$S_0 x$	$G_0 x$	$\frac{1}{\beta_0}\left(C-(C-\mu_0(0)\beta_0)\exp\left(\frac{\beta_0\mu_1(0)}{G_0}(1-\exp(G_0 t))\right)\right)$	$\mu_1(0)\exp(G_0 t)$

$C=(p-1)S_0$,$\beta_0>0, S_0>0, G_0>0$

Pure source

In case of an exponential source term, i.e., $B_{\text{src}}(t,x)=\exp(-mx)$ for m is given positive constant, we solve the following PBEs

$$\frac{\partial f(t,x)}{\partial t}=B_{\text{src}}(t,x)$$

for the first two moments and the number density. The analytical solutions are as follows.

$$\mu_0(t)=1/m,\quad \mu_1(t)=1/m^2,\quad f(t,x)=f(0,x)+\exp(-mx)t.$$

Simultaneous breakage, growth and source

Proceeding as before, the analytical solutions for the first two moments are provided in Table B.4 using the linear selection rate together with the breakage function (4.75) and for linear growth rate. The negative exponential function has been taken for the source terms.

Table B.4: Analytical solutions for zeroth and first moments

$Case$	$S(x)$	$G(x)$	Analytical solution $\mu_0(t)$	Analytical solution $\mu_1(t)$
1	$S_0 x$	$G_0 x$	$\mu_0(0)+t+(p-1)S_0(A\exp(G_0 t)-A-t/G_0)$	$AG_0\exp(G_0 t)-1/G_0$

$A=(1+\mu_1(0)G_0)/G_0^2, S_0>0, G_0>0$

Coupled aggregation, breakage, growth and source

Analogously to the previous case if we add the aggregation terms too and take $\beta(x,y)=\beta_0(xy)$, the analytical solutions for the zeroth and first moments considering all the four combined processes are given by, respectively

$$\mu_0(t)=\mu_0(0)+t+\frac{\beta_0 G_0^2 A^2}{4}(1-\exp(2G_0 t))-\beta_0\left(A-A\exp(G_0 t)+t/(2G_0^2)\right)$$
$$+(p-1)S_0 G_0\left(A\exp(G_0 t)-A-t/G_0^2\right)$$

and

$$\mu_1(t)=AG_0\exp(G_0 t)-1/G_0.$$

B.2 Reformulation of the CAT into conservative formulations

Substituting the number density $n(t,x) \approx \sum_{k=1}^{I} n_k(t)\Delta x_k \delta(x - x_k)$ we know from (4.46) that the cell average technique for aggregation, breakage and source is given by

$$\frac{dn_i\Delta x_i}{dt} = B_i^{\mathrm{CA}} - D_i^{\mathrm{CA}}, \qquad i = 1, 2, ..., I.$$

Replacing B_i^{CA} from (4.47) gives

$$\begin{aligned}\frac{dn_i\Delta x_i}{dt} =& B_{i-1}\lambda_i^-(\bar{v}_{i-1})H(\bar{v}_{i-1} - x_{i-1}) + B_i\lambda_i^+(\bar{v}_i)H(\bar{v}_i - x_i) \\ &+ B_i\lambda_i^-(\bar{v}_i)H(x_i - \bar{v}_i) + B_{i+1}\lambda_i^+(\bar{v}_{i+1})H(x_{i+1} - \bar{v}_{i+1}) - D_i^{\mathrm{CA}}, \end{aligned} \tag{B.1}$$

where $B_i, \bar{v}_i$ and D_i^{CA} are defined according to the problem under consideration. From (4.48), we know

$$x_i\lambda_i^+(\bar{v}_i) + x_{i+1}\lambda_{i+1}^-(\bar{v}_i) = \bar{v}_i, \qquad x_i\lambda_i^-(\bar{v}_i) + x_{i-1}\lambda_{i-1}^+(\bar{v}_i) = \bar{v}_i.$$

By using the notation $N_i = n_i\Delta x_i$ and multiplying the equation (B.1) by x_i we get

$$\begin{aligned}\frac{x_i dN_i}{dt} =& B_{i-1}x_i\lambda_i^-(\bar{v}_{i-1})H(\bar{v}_{i-1} - x_{i-1}) + B_i x_i\lambda_i^+(\bar{v}_i)H(\bar{v}_i - x_i) \\ &+ B_i x_i\lambda_i^-(\bar{v}_i)H(x_i - \bar{v}_i) + B_{i+1}x_i\lambda_i^+(\bar{v}_{i+1})H(x_{i+1} - \bar{v}_{i+1}) - x_i D_i^{\mathrm{CA}}. \end{aligned} \tag{B.2}$$

Replacing $x_i\lambda_i^{\pm}(\bar{v}_i)$ from the equation (B.2)

$$\begin{aligned}&\frac{x_i dN_i}{dt} = B_{i-1}x_i\lambda_i^-(\bar{v}_{i-1})H(\bar{v}_{i-1} - x_{i-1}) - B_i x_{i+1}\lambda_{i+1}^-(\bar{v}_i)H(\bar{v}_i - x_i) + \bar{v}_i B_i\big[H(\bar{v}_i - x_i) \\ &+ H(x_i - \bar{v}_i)\big] - B_i x_{i-1}\lambda_{i-1}^+(\bar{v}_i)H(x_i - \bar{v}_i) + B_{i+1}x_i\lambda_i^+(\bar{v}_{i+1})H(x_{i+1} - \bar{v}_{i+1}) - x_i D_i^{\mathrm{CA}}. \end{aligned} \tag{B.3}$$

By the definition of Heaviside function, i.e.

$$[H(\bar{v}_i - x_i) + H(x_i - \bar{v}_i)] = 1, \tag{B.4}$$

the equation (B.3) becomes

$$\begin{aligned}\frac{x_i dN_i}{dt} =& B_{i-1}x_i\lambda_i^-(\bar{v}_{i-1})H(\bar{v}_{i-1} - x_{i-1}) - B_i x_{i+1}\lambda_{i+1}^-(\bar{v}_i)H(\bar{v}_i - x_i) + \bar{v}_i B_i \\ &- B_i x_{i-1}\lambda_{i-1}^+(\bar{v}_i)H(x_i - \bar{v}_i) + B_{i+1}x_i\lambda_i^+(\bar{v}_{i+1})H(x_{i+1} - \bar{v}_{i+1}) - x_i D_i^{\mathrm{CA}}. \end{aligned} \tag{B.5}$$

B.2.1 Conservative formulation for breakage

Replacing B_i by $B_i^{\mathrm{brk}}, \bar{v}_i$ by $\bar{v}_i^{\mathrm{brk}}$ and substitutions of $\bar{v}_i^{\mathrm{brk}}B_i^{\mathrm{brk}}, D_i^{\mathrm{CA}}$ from (4.54) and (4.55), respectively in the equation (B.5) yield

$$\begin{aligned}\frac{x_i dN_i}{dt} =& B_{i+1}^{\mathrm{brk}}x_i\lambda_i^+(\bar{v}_{i+1}^{\mathrm{brk}})H(x_{i+1} - \bar{v}_{i+1}^{\mathrm{brk}}) - B_i^{\mathrm{brk}}x_{i+1}\lambda_{i+1}^-(\bar{v}_i^{\mathrm{brk}})H(\bar{v}_i^{\mathrm{brk}} - x_i) \\ &- B_i^{\mathrm{brk}}x_{i-1}\lambda_{i-1}^+(\bar{v}_i^{\mathrm{brk}})H(x_i - \bar{v}_i^{\mathrm{brk}}) + B_{i-1}^{\mathrm{brk}}x_i\lambda_i^-(\bar{v}_{i-1}^{\mathrm{brk}})H(\bar{v}_{i-1}^{\mathrm{brk}} - x_{i-1}) \\ &+ \sum_{k\geq i} N_k S_k \int_{x_{i-1/2}}^{p_k^i} xb(t,x,x_k)\,dx - S_i N_i \int_0^{x_i} xb(x,x_i)dx. \end{aligned}$$

Further simplifications give the following form

$$\begin{aligned}\frac{x_i dN_i}{dt} =& B_{i+1}^{\text{brk}} x_i \lambda_i^+(\bar{v}_{i+1}^{\text{brk}}) H(x_{i+1} - \bar{v}_{i+1}^{\text{brk}}) - B_i^{\text{brk}} x_{i+1} \lambda_{i+1}^-(\bar{v}_i^{\text{brk}}) H(\bar{v}_i^{\text{brk}} - x_i) \\ & - B_i^{\text{brk}} x_{i-1} \lambda_{i-1}^+(\bar{v}_i^{\text{brk}}) H(x_i - \bar{v}_i^{\text{brk}}) + B_{i-1}^{\text{brk}} x_i \lambda_i^-(\bar{v}_{i-1}^{\text{brk}}) H(\bar{v}_{i-1}^{\text{brk}} - x_{i-1}) \\ & + \sum_{k=i+1}^{I} S_k N_k \int_0^{x_{i+1/2}} x b(x, x_k) dx - \sum_{k=i}^{I} S_k N_k \int_0^{x_{i-1/2}} x b(x, x_k) dx.\end{aligned}$$

In the flux form we can now write the conservative formulation for breakage as

$$\frac{x_i dn_i}{dt} = -\frac{1}{\Delta x_i} \left(J_{i+1/2}^{\text{brk,CA}} - J_{i-1/2}^{\text{brk,CA}} \right),$$

where the flux is given as

$$\begin{aligned}J_{i+1/2}^{\text{brk,CA}} = -\Bigg(& \sum_{k=i+1}^{I} S_k n_k \Delta x_k \int_0^{x_{i+1/2}} x b(x, x_k) dx \\ & + B_{i+1}^{\text{brk}} x_i \lambda_i^+(\bar{v}_{i+1}^{\text{brk}}) H(x_{i+1} - \bar{v}_{i+1}^{\text{brk}}) - B_i^{\text{brk}} x_{i+1} \lambda_{i+1}^-(\bar{v}_i^{\text{brk}}) H(\bar{v}_i^{\text{brk}} - x_i) \Bigg).\end{aligned}$$

B.2.2 Conservative formulation for aggregation

Substituting D_i^{CA} from (4.53) and replacing B_i by B_i^{agg}, $\bar{v}_i$ by $\bar{v}_i^{\text{agg}}$ in the equation (B.5), we get the following form of the cell average technique for aggregation

$$\begin{aligned}\frac{x_i dN_i}{dt} =& B_{i-1}^{\text{agg}} x_i \lambda_i^-(\bar{v}_{i-1}^{\text{agg}}) H(\bar{v}_{i-1}^{\text{agg}} - x_{i-1}) - B_i^{\text{agg}} x_{i+1} \lambda_{i+1}^-(\bar{v}_i^{\text{agg}}) H(\bar{v}_i^{\text{agg}} - x_i) + \bar{v}_i^{\text{agg}} B_i^{\text{agg}} \\ & - B_i^{\text{agg}} x_{i-1} \lambda_{i-1}^+(\bar{v}_i^{\text{agg}}) H(x_i - \bar{v}_i^{\text{agg}}) + B_{i+1}^{\text{agg}} x_i \lambda_i^+(\bar{v}_{i+1}^{\text{agg}}) H(x_{i+1} - \bar{v}_{i+1}^{\text{agg}}) - N_i x_i \sum_{k=1}^{I} \beta(x_i, x_k) N_k.\end{aligned} \tag{B.6}$$

From the equation (4.52), the third term on the right-hand side becomes

$$\begin{aligned}\bar{v}_i^{\text{agg}} B_i^{\text{agg}} =& \sum_{\substack{j,k \\ x_{i-1/2} \le (x_j + x_k) < x_{i+1/2}}}^{j \ge k} \left(1 - \frac{1}{2}\delta_{j,k}\right) \beta(x_j, x_k) N_j N_k (x_j + x_k) \\ =& \sum_{\substack{j,k \\ x_{i-1/2} \le (x_j + x_k) < x_{i+1/2}}} \beta(x_j, x_k) N_j N_k x_j \\ =& \sum_{j=1}^{i-1} N_j x_j \sum_{x_{i-1/2} \le (x_j + x_k) < x_{i+1/2}} \beta(x_k, x_j) N_k + N_i x_i \sum_{(x_i + x_k) < x_{i+1/2}} \beta(x_k, x_i) N_k.\end{aligned}$$

By using the indices $\ell_{i,j}$ from (4.60), the above equation can be formulated as

$$\begin{aligned}\bar{v}_i^{\text{agg}} B_i^{\text{agg}} =& \sum_{j=1}^{i-1} N_j x_j \sum_{k=\ell_{i-1,j}+\frac{1}{2}(1+r_{i-1,j})}^{\ell_{i,j}+\frac{1}{2}(-1+r_{i,j})} \beta(x_k, x_j) N_k + N_i x_i \sum_{k=1}^{\ell_{i,i}+\frac{1}{2}(-1+r_{i,i})} \beta(x_k, x_i) N_k \\ =& \sum_{j=1}^{i-1} N_j x_j \sum_{k=\ell_{i-1,j}+\frac{1}{2}(1+r_{i-1,j})}^{I} \beta(x_k, x_j) N_k - \sum_{j=1}^{i-1} N_j x_j \sum_{k=\ell_{i,j}+\frac{1}{2}(1+r_{i,j})}^{I} \beta(x_k, x_j) N_k \\ &+ N_i x_i \sum_{k=1}^{\ell_{i,i}+\frac{1}{2}(-1+r_{i,i})} \beta(x_k, x_i) N_k.\end{aligned}$$

Substituting this in the equation (B.6) we get

$$\begin{aligned}&\frac{x_i dN_i}{dt} = B_{i-1}^{\text{agg}} x_i \lambda_i^-(\bar{v}_{i-1}^{\text{agg}}) H(\bar{v}_{i-1}^{\text{agg}} - x_{i-1}) - B_i^{\text{agg}} x_{i+1} \lambda_{i+1}^-(\bar{v}_i^{\text{agg}}) H(\bar{v}_i^{\text{agg}} - x_i) - B_i^{\text{agg}} x_{i-1} \cdot \\ &\lambda_{i-1}^+(\bar{v}_i^{\text{agg}}) H(x_i - \bar{v}_i^{\text{agg}}) + B_{i+1}^{\text{agg}} x_i \lambda_i^+(\bar{v}_{i+1}^{\text{agg}}) H(x_{i+1} - \bar{v}_{i+1}^{\text{agg}}) - N_i x_i \sum_{k=\ell_{i,i}+\frac{1}{2}(1+r_{i,i})}^{I} \beta(x_k, x_i) N_k \\ &+ \sum_{j=1}^{i-1} N_j x_j \sum_{k=\ell_{i-1,j}+\frac{1}{2}(1+r_{i-1,j})}^{I} \beta(x_k, x_j) N_k - \sum_{j=1}^{i-1} N_j x_j \sum_{k=\ell_{i,j}+\frac{1}{2}(1+r_{i,j})}^{I} \beta(x_k, x_j) N_k.\end{aligned}$$

Finally, we obtain

$$\begin{aligned}\frac{x_i dN_i}{dt} =& - \left(\sum_{j=1}^{i} \sum_{k=\ell_{i,j}+\frac{1}{2}(1+r_{i,j})}^{I} - \sum_{j=1}^{i-1} \sum_{k=\ell_{i-1,j}+\frac{1}{2}(1+r_{i-1,j})}^{I} \right) \beta(x_k, x_j) x_j N_j N_k \\ &- B_i^{\text{agg}} x_{i+1} \lambda_{i+1}^-(\bar{v}_i^{\text{agg}}) H(\bar{v}_i^{\text{agg}} - x_i) + B_{i+1}^{\text{agg}} x_i \lambda_i^+(\bar{v}_{i+1}^{\text{agg}}) H(x_{i+1} - \bar{v}_{i+1}^{\text{agg}}) \\ &+ B_{i-1}^{\text{agg}} x_i \lambda_i^-(\bar{v}_{i-1}^{\text{agg}}) H(\bar{v}_{i-1}^{\text{agg}} - x_{i-1}) - B_i^{\text{agg}} x_{i-1} \lambda_{i-1}^+(\bar{v}_i^{\text{agg}}) H(x_i - \bar{v}_i^{\text{agg}}).\end{aligned}$$

In the flux form we can write

$$\frac{x_i dn_i}{dt} = -\frac{1}{\Delta x_i} \left(J_{i+1/2}^{\text{agg,CA}} - J_{i-1/2}^{\text{agg,CA}} \right),$$

where

$$\begin{aligned}J_{i+1/2}^{\text{agg,CA}} =& \sum_{j=1}^{i} \sum_{k=\ell_{i,j}+\frac{1}{2}(1+r_{i,j})}^{I} \beta(x_k, x_j) x_j n_j n_k \Delta x_j \Delta x_k + B_i^{\text{agg}} x_{i+1} \lambda_{i+1}^-(\bar{v}_i^{\text{agg}}) H(\bar{v}_i^{\text{agg}} - x_i) \\ &- B_{i+1}^{\text{agg}} x_i \lambda_i^+(\bar{v}_{i+1}^{\text{agg}}) H(x_{i+1} - \bar{v}_{i+1}^{\text{agg}}).\end{aligned}$$

B.2.3 Conservative formulation for source terms

Since there is no death term for source, therefore replacing B_i by B_i^{src} and $\bar{v}_i$ by $\bar{v}_i^{\text{src}}$ in (B.5) leads to the following equation for source terms by using the CAT

$$\begin{aligned}\frac{x_i dN_i}{dt} =& B_{i-1}^{\text{src}} x_i \lambda_i^-(\bar{v}_{i-1}^{\text{src}}) H(\bar{v}_{i-1}^{\text{src}} - x_{i-1}) - B_i^{\text{src}} x_{i+1} \lambda_{i+1}^-(\bar{v}_i^{\text{src}}) H(\bar{v}_i^{\text{src}} - x_i) + \bar{v}_i^{\text{src}} B_i^{\text{src}} \\ &- B_i^{\text{src}} x_{i-1} \lambda_{i-1}^+(\bar{v}_i^{\text{src}}) H(x_i - \bar{v}_i^{\text{src}}) + B_{i+1}^{\text{src}} x_i \lambda_i^+(\bar{v}_{i+1}^{\text{src}}) H(x_{i+1} - \bar{v}_{i+1}^{\text{src}}). \qquad \text{(B.7)}\end{aligned}$$

In the case of sources $B_{\text{src}}(t,x) > 0$ means that we have a birth term and a negative source $B_{\text{src}}(t,x) < 0$ is a sink or death term. Substituting the value of $\bar{v}_i^{\text{src}} B_i^{\text{src}}$ from (4.57), we have

$$\begin{aligned}\frac{x_i dN_i}{dt} =& B_{i-1}^{\text{src}} x_i \lambda_i^-(\bar{v}_{i-1}^{\text{src}}) H(\bar{v}_{i-1}^{\text{src}} - x_{i-1}) - B_i^{\text{src}} x_{i+1} \lambda_{i+1}^-(\bar{v}_i^{\text{src}}) H(\bar{v}_i^{\text{src}} - x_i) + \int_{x_{i-1/2}}^{x_{i+1/2}} x B_{\text{src}}(t,x) dx \\ & - B_i^{\text{src}} x_{i-1} \lambda_{i-1}^+(\bar{v}_i^{\text{src}}) H(x_i - \bar{v}_i^{\text{src}}) + B_{i+1}^{\text{src}} x_i \lambda_i^+(\bar{v}_{i+1}^{\text{src}}) H(x_{i+1} - \bar{v}_{i+1}^{\text{src}}).\end{aligned}$$

Furthermore, we can now write the above equation in the flux form as

$$\frac{x_i dn_i}{dt} = -\frac{1}{\Delta x_i}\left(J_{i+1/2}^{\text{src,CA}} - J_{i-1/2}^{\text{src,CA}}\right),$$

for the numerical flux given as

$$J_{i+1/2}^{\text{src,CA}} = B_i^{\text{src}} x_{i+1} \lambda_{i+1}^-(\bar{v}_i^{\text{src}}) H(\bar{v}_i^{\text{src}} - x_i) - B_{i+1}^{\text{src}} x_i \lambda_i^+(\bar{v}_{i+1}^{\text{src}}) H(x_{i+1} - \bar{v}_{i+1}^{\text{src}}) - \int_0^{x_{i+1/2}} x B_{\text{src}}(t,x) dx.$$

B.3 Reformulation of the FP method into conservative formulations

In the following two subsections we rewrite the FP formulations, given by Kumar and Ramkrishna [53], for the aggregation and breakage equations into the mass conservation laws.

B.3.1 Conservative formulation for breakage

The fixed pivot technique for pure breakage is defined as

$$\frac{dN_i}{dt} = \sum_{k=i}^{I} S_k N_k \int_{x_i}^{x_{i+1}} \lambda_i^+(x) b(x,x_k) dx + \sum_{k=i}^{I} S_k N_k \int_{x_{i-1}}^{x_i} \lambda_i^-(x) b(x,x_k) dx - S_i N_i. \tag{B.8}$$

where the function $\lambda_i^{\pm}(x)$ are used for the redistribution of particles and is given as

$$\lambda_i^{\pm}(x) = \frac{x - x_{i\pm1}}{x_i - x_{i\pm1}}. \tag{B.9}$$

Multiplying the equation (B.8) by x_i gives

$$\frac{dx_i N_i}{dt} = \sum_{k=i}^{I} S_k N_k \int_{x_i}^{x_{i+1}} x_i \lambda_i^+(x) b(x,x_k) dx + \sum_{k=i}^{I} S_k N_k \int_{x_{i-1}}^{x_i} x_i \lambda_i^-(x) b(x,x_k) dx - S_i N_i x_i. \tag{B.10}$$

Note that the first term in the first summation on the right-hand side is zero since $b(x,x_i)$ is zero in $]x_i, x_{i+1}]$. Furthermore, it can be seen that

$$x_i \lambda_i^-(x) + x_{i-1} \lambda_{i-1}^+(x) = x. \tag{B.11}$$

Substituting the value of $\lambda_i^-(x)$ in the equation (B.10) we obtain

$$\frac{dx_iN_i}{dt} = \sum_{k=i+1}^{I} S_kN_k \int_{x_i}^{x_{i+1}} x_i\lambda_i^+(x)b(x,x_k)dx + \sum_{k=i}^{I} S_kN_k \int_{x_{i-1}}^{x_i} \left(x - x_{i-1}\lambda_{i-1}^+(x)\right) b(x,x_k)dx - S_iN_ix_i.$$

Using the property of the breakage function $\int_0^{x_i} xb(x,x_i)dx = x_i$, the above equation can be rewritten as

$$\frac{dx_iN_i}{dt} = \sum_{k=i+1}^{I} S_kN_k \int_{x_i}^{x_{i+1}} x_i\lambda_i^+(x)b(x,x_k)dx - \sum_{k=i}^{I} S_kN_k \int_{x_{i-1}}^{x_i} x_{i-1}\lambda_{i-1}^+(x)b(x,x_k)dx + \sum_{k=i}^{I} S_kN_k \int_{x_{i-1}}^{x_i} xb(x,x_k)dx - S_iN_i \int_0^{x_i} xb(x,x_i)dx.$$

Again after some rearrangements of the terms we get

$$\frac{dx_iN_i}{dt} = \sum_{k=i+1}^{I} S_kN_k \int_{x_i}^{x_{i+1}} x_i\lambda_i^+(x)b(x,x_k)dx - \sum_{k=i}^{I} S_kN_k \int_{x_{i-1}}^{x_i} x_{i-1}\lambda_{i-1}^+(x)b(x,x_k)dx + \sum_{k=i}^{I} S_kN_k \int_0^{x_i} xb(x,x_k)dx - \sum_{k=i}^{I} S_kN_k \int_0^{x_{i-1}} xb(x,x_k)dx - S_iN_i \int_0^{x_i} xb(x,x_i)dx.$$

The last term can be combined with the third term on the right-hand side to give

$$\frac{dx_iN_i}{dt} = \sum_{k=i+1}^{I} S_kN_k \int_{x_i}^{x_{i+1}} x_i\lambda_i^+(x)b(x,x_k)dx - \sum_{k=i}^{I} S_kN_k \int_{x_{i-1}}^{x_i} x_{i-1}\lambda_{i-1}^+(x)b(x,x_k)dx + \sum_{k=i+1}^{I} S_kN_k \int_0^{x_i} xb(x,x_k)dx - \sum_{k=i}^{I} S_kN_k \int_0^{x_{i-1}} xb(x,x_k)dx.$$

Finally by using $N_i = n_i\Delta x_i$, we have

$$\frac{dx_in_i}{dt} = \frac{1}{\Delta x_i}\left[\sum_{k=i+1}^{I} S_kn_k\Delta x_k \left(\int_{x_i}^{x_{i+1}} x_i\lambda_i^+(x)b(x,x_k)dx + \int_0^{x_i} xb(x,x_k)dx \right) - \sum_{k=i}^{I} S_kn_k\Delta x_k \left(\int_{x_{i-1}}^{x_i} x_{i-1}\lambda_{i-1}^+(x)b(x,x_k)dx + \int_0^{x_{i-1}} xb(x,x_k)dx \right) \right].$$

Hence, in the flux form we can write as

$$\frac{dx_in_i}{dt} = -\frac{1}{\Delta x_i}\left[J_{i+1/2}^{\text{brk,FP}} - J_{i-1/2}^{\text{brk,FP}} \right],$$

where the numerical flux

$$J_{i+1/2}^{\text{brk,FP}} = -\sum_{k=i+1}^{I} S_kn_k\Delta x_k \left(\int_{x_i}^{x_{i+1}} x_i\lambda_i^+(x)b(x,x_k)dx + \int_0^{x_i} xb(x,x_k)dx \right).$$

B.3.2 Conservative formulation for aggregation

Again from Kumar and Ramkrishna [53], the FP method for pure aggregation is defined as

$$\frac{dN_i}{dt} = \sum_{\substack{j,k \\ x_{i-1}\le(x_j+x_k)<x_i}}^{j\ge k} \left(1-\frac{1}{2}\delta_{j,k}\right)\lambda_i^-(x_j+x_k)\beta(x_j,x_k)N_jN_k + \sum_{\substack{j,k \\ x_i\le(x_j+x_k)<x_{i+1}}}^{j\ge k} \left(1-\frac{1}{2}\delta_{j,k}\right)\lambda_i^+(x_j+x_k)\beta(x_j,x_k)N_jN_k - N_i\sum_{k=1}^{I}\beta(x_i,x_k)N_k. \tag{B.12}$$

Similar to the case of breakage, multiplying the above equation by x_i and using the relation $x_{i+1}\lambda_{i+1}^-(x) + x_i\lambda_i^+(x) = x$, we determine

$$\begin{aligned}\frac{dx_iN_i}{dt} = &\sum_{\substack{j,k \\ x_{i-1}\le(x_j+x_k)<x_i}}^{j\ge k} \left(1-\frac{1}{2}\delta_{j,k}\right)x_i\lambda_i^-(x_j+x_k)\beta(x_j,x_k)N_jN_k - N_ix_i\sum_{k=1}^{I}\beta(x_i,x_k)N_k \\ &- \sum_{\substack{j,k \\ x_i\le(x_j+x_k)<x_{i+1}}}^{j\ge k} \left(1-\frac{1}{2}\delta_{j,k}\right)x_{i+1}\lambda_{i+1}^-(x_j+x_k)\beta(x_j,x_k)N_jN_k \\ &+ \underbrace{\sum_{\substack{j,k \\ x_i\le(x_j+x_k)<x_{i+1}}}^{j\ge k} \left(1-\frac{1}{2}\delta_{j,k}\right)(x_j+x_k)\beta(x_j,x_k)N_jN_k}_{\mathcal{S}_4}.\end{aligned} \tag{B.13}$$

The last term ($\mathcal{S}_4$) on the right-hand side of the equation (B.13) is formulated by using the index $\gamma_{i,j}$ from (4.63) and the function $\mathrm{r}_{i,j}$ from (4.64) as

$$\begin{aligned}\mathcal{S}_4 &= \sum_{j=1}^{i}\sum_{k=\gamma_{i-1,j}+\frac{1}{2}(1+\mathrm{r}_{i-1,j})}^{\gamma_{i,j}+\frac{1}{2}(-1+\mathrm{r}_{i,j})} x_j\beta(x_j,x_k)N_jN_k \\ &= \sum_{j=1}^{i-1}\sum_{k=\gamma_{i-1,j}+\frac{1}{2}(1+\mathrm{r}_{i-1,j})}^{\gamma_{i,j}+\frac{1}{2}(-1+\mathrm{r}_{i,j})} x_j\beta(x_j,x_k)N_jN_k + \sum_{k=\gamma_{i-1,i}+\frac{1}{2}(1+\mathrm{r}_{i-1,i})}^{\gamma_{i,i}+\frac{1}{2}(-1+\mathrm{r}_{i,i})} x_i\beta(x_i,x_k)N_iN_k.\end{aligned}$$

Further simplification gives

$$\begin{aligned}\mathcal{S}_4 = \sum_{j=1}^{i-1}&\left[\sum_{k=\gamma_{i-1,j}+\frac{1}{2}(1+\mathrm{r}_{i-1,j})}^{I} - \sum_{k=\gamma_{i,j}+\frac{1}{2}(1+\mathrm{r}_{i,j})}^{I}\right]x_j\beta(x_j,x_k)N_jN_k \\ &+\left[\sum_{k=\gamma_{i-1,i}+\frac{1}{2}(1+\mathrm{r}_{i-1,i})}^{I} - \sum_{k=\gamma_{i,i}+\frac{1}{2}(1+\mathrm{r}_{i,i})}^{I}\right]x_i\beta(x_i,x_k)N_iN_k.\end{aligned}$$

Hence, we obtain

$$\mathcal{S}_4 = \Bigg[-\sum_{j=1}^{i} \sum_{k=\gamma_{i,j}+\frac{1}{2}(1+\mathrm{r}_{i,j})}^{I} + \sum_{j=1}^{i-1} \sum_{k=\gamma_{i-1,j}+\frac{1}{2}(1+\mathrm{r}_{i-1,j})}^{I} \Bigg] x_j \beta(x_j, x_k) N_j N_k + \sum_{k=1}^{I} x_i \beta(x_i, x_k) N_i N_k.$$

Substituting the value of $\mathcal{S}_4$ into the equation (B.13), we evaluate

$$\begin{aligned}
\frac{dx_i N_i}{dt} = & \sum_{\substack{j,k \\ x_{i-1} \le (x_j + x_k) < x_i}}^{j \ge k} \left(1 - \frac{1}{2}\delta_{j,k}\right) x_i \lambda_i^-(x_j + x_k) \beta(x_j, x_k) N_j N_k \\
& - \sum_{\substack{j,k \\ x_i \le (x_j + x_k) < x_{i+1}}}^{j \ge k} \left(1 - \frac{1}{2}\delta_{j,k}\right) x_{i+1} \lambda_{i+1}^-(x_j + x_k) \beta(x_j, x_k) N_j N_k \\
& + \Bigg[\sum_{j=1}^{i-1} \sum_{k=\gamma_{i-1,j}+\frac{1}{2}(1+\mathrm{r}_{i-1,j})}^{I} - \sum_{j=1}^{i} \sum_{k=\gamma_{i,j}+\frac{1}{2}(1+\mathrm{r}_{i,j})}^{I} \Bigg] x_j \beta(x_j, x_k) N_j N_k.
\end{aligned}$$

Finally in the flux form we obtain

$$\frac{x_i dn_i}{dt} = -\frac{1}{\Delta x_i} \left[J_{i+1/2}^{\mathrm{agg,FP}} - J_{i-1/2}^{\mathrm{agg,FP}} \right],$$

where the flux is defined as

$$\begin{aligned}
J_{i+1/2}^{\mathrm{agg,FP}} = & \sum_{j=1}^{i} \sum_{k=\gamma_{i,j}+\frac{1}{2}(1+\mathrm{r}_{i,j})}^{I} x_j \beta(x_j, x_k) n_j n_k \Delta x_j \Delta x_k \\
& + \sum_{\substack{j,k \\ x_i \le (x_j + x_k) < x_{i+1}}}^{j \ge k} \left(1 - \frac{1}{2}\delta_{j,k}\right) x_{i+1} \lambda_{i+1}^-(x_j + x_k) \beta(x_j, x_k) n_j n_k \Delta x_j \Delta x_k.
\end{aligned}$$

B.4 Conditions for the moment preservation

In this section, we derive the conditions for the preservation of the zeroth and the first moment for aggregation and breakage processes separately. It should be mentioned that these conditions are obtained by using the truncated PBEs.

Aggregation

Multiplying the equation (4.1) by x^p and integrate over 0 to $x_{I+1/2}$ yields the following moment equation of the truncated aggregation equation ($G = S = B_{\text{src}} = 0$)

$$\begin{aligned}\int_0^{x_{I+1/2}} x^p \frac{dn(t,x)}{dt} dx =& \frac{1}{2}\int_0^{x_{I+1/2}} \int_0^{x} x^p \beta(x-u,u) n(t,x-u) n(t,u) du dx \\ &- \int_0^{x_{I+1/2}} \int_0^{x_{I+1/2}} x^p \beta(x,u) n(t,x) n(t,u) du dx. \end{aligned} \tag{B.14}$$

Changing the order of integration for the first term in the right-hand side, equation (B.14) can be further simplified as

$$\begin{aligned}\frac{d}{dt}\int_0^{x_{I+1/2}} x^p n(t,x) dx = & \frac{1}{2}\int_0^{x_{I+1/2}} \int_0^{x_{I+1/2}-u} (x+u)^p \beta(x,u) n(t,x) n(t,u) dx du \\ &- \int_0^{x_{I+1/2}} \int_0^{x_{I+1/2}} x^p \beta(x,u) n(t,x) n(t,u) dx du.\end{aligned}$$

Taking $p = 0$ and $p = 1$ in the above equation gives the following form for the zeroth and the first moment, respectively

$$\begin{aligned}\frac{d}{dt}\int_0^{x_{I+1/2}} n(t,x) dx = & -\frac{1}{2}\int_0^{x_{I+1/2}} \int_0^{x_{I+1/2}-u} \beta(x,u) n(t,x) n(t,u) dx du \\ &- \int_0^{x_{I+1/2}} \int_{x_{I+1/2}-u}^{x_{I+1/2}} \beta(x,u) n(t,x) n(t,u) dx du,\end{aligned} \tag{B.15}$$

and

$$\frac{d}{dt}\int_0^{x_{I+1/2}} x n(t,x) dx = -\int_0^{x_{I+1/2}} \int_{x_{I+1/2}-u}^{x_{I+1/2}} x \beta(x,u) n(t,x) n(t,u) dx du. \tag{B.16}$$

Substituting the number density as point masses, i.e. $n(t,x) \approx \sum_{j=1}^{I} n_j \Delta x_j \delta(x - x_j)$, in the right-hand side integrals of the equations (B.15) and (B.16), we get

$$\frac{d\hat{\mu}_0}{dt} = -\frac{1}{2} \sum_{\substack{j,k \\ (x_j+x_k)<x_{I+1/2}}} \beta(x_j,x_k) n_j n_k \Delta x_j \Delta x_k - \sum_{\substack{j,k \\ x_{I+1/2}\le(x_j+x_k)}} \beta(x_j,x_k) n_j n_k \Delta x_j \Delta x_k,$$

and

$$\frac{d\hat{\mu}_1}{dt} = -\sum_{\substack{j,k \\ x_{I+1/2}\le(x_j+x_k)}} x_j \beta(x_j,x_k) n_j n_k \Delta x_j \Delta x_k.$$

By using the compact support on the kernel β from (4.9) leads to the following conditions for the first two moments preservation

$$\frac{d\hat{\mu}_0}{dt} = - \sum_{\substack{j,k \\ (x_j+x_k)<x_{I+1/2}}}^{j\geq k} (1 - \frac{1}{2}\delta_{jk})\beta(x_j, x_k)n_j n_k \Delta x_j \Delta x_k, \tag{B.17}$$

whereas

$$\frac{d\hat{\mu}_1}{dt} = 0.$$

Breakage

Similarly, multiplying the equation (4.1) by x^p and integrating over 0 to $x_{I+1/2}$ for breakage ($\beta = G = B_{\text{src}} = 0$) we get the following moment equation

$$\int_0^{x_{I+1/2}} x^p \frac{dn(t,x)}{dt} dx = \int_0^{x_{I+1/2}} \int_x^{x_{I+1/2}} x^p b(x,u) S(u) n(t,u) du dx - \int_0^{x_{I+1/2}} x^p S(x) n(t,x) dx.$$

The preceding equation can be further simplified by changing the order of summation in the first term on the right-hand side as

$$\int_0^{x_{I+1/2}} x^p \frac{dn(t,x)}{dt} dx = \int_0^{x_{I+1/2}} S(u) n(t,u) \int_0^u x^p b(x,u) dx du - \int_0^{x_{I+1/2}} x^p S(x) n(t,x) dx.$$

Taking $p = 0, 1$ and substituting the number density same as taken in the previous case leads to

$$\frac{d\hat{\mu}_0}{dt} = \sum_i^I S(x_i) n_i \Delta x_i \left(\int_0^{x_i} b(x, x_i) dx - 1 \right),$$

and

$$\frac{d\hat{\mu}_1}{dt} = 0$$

for the preservation of the zeroth and the first moment, respectively.

Bibliography

[1] L.G. Austin. A treatment of impact breakage of particles. *Powder Technology*, 126(1):85–90, 2002.

[2] K.E.J. Barreit. *Dispersion polymerization in organic media*. Wiley, London,UK, 1975.

[3] J.C. Barrett and J.S. Jheeta. Improving the accuracy of the moments method for solving the aerosol general dynamic equation. *Journal of Aerosol Science*, 27:1135–1142, 1996.

[4] E.A. Barringer and H.K. Bowen. Effects of particle packing on the sintered microstructure. *Applied Physics A: Materials Science and Processing*, 45:271–275, 1982.

[5] R. Becker and W. Döring. Kinetische Behandlung der Keimbildung in Übersättigten Dämpfen. *Annalen der Physik (5 Folge)*, 24:719–752, 1935.

[6] M.K. Bennett and S. Rohani. Solution of population balance equations with a new combined Lax-Wendroff/Crank-Nicholson method. *Chemical Engineering Science*, 56:6623–6633, 2001.

[7] J.P. Bourgade and F. Filbet. Convergence of a finite volume scheme for coagulation-fragmentation equations. *Mathematics of Computation*, 77:851–882, 2007.

[8] J.J. Burton. *Nucleation theory. In: Berne, B.J. ed. Statistical Mechanics, Part A: equilibrium techniques*. plenum Press, New York, New York, USA, 1977.

[9] J. Chakraborty and S. Kumar. A new framework for solution of multidimensional population balance equations. *Chemical Engineering Science*, 62:4112–4125, 2007.

[10] S. S. Chauhan, J. Chakraborty, and S. Kumar. On the solution and applicability of bivariate population balance equations for mixing in particle phase. *Chemical Engineering Science*, 65:3914–3927, 2010.

[11] W.A. Daoud and J.H. Xin. Low temperature sol-gel processed photocatalytic titania coating. *Journal of Sol-Gel Science and Technology*, 29:25–29, 2004.

[12] J.H. Diemer. *Moment methods for coagulation, breakage and coalescence problems*. Phd thesis, University of Delaware, USA, 1999.

[13] R.B. Diemer and J.H. Olson. A moment methodology for coagulation and breakage problems: Part 1-Analytical solution of the steady-state population balance. *Chemical Engineering Science*, 57:2193–2209, 2002.

[14] R.L. Drake. A general mathematical survey of the coagulation equation, in: Topics in current aerosol research (Part2). *International reviews in Aerosol physics and chemistry, Pergamon Press, Oxford, UK*, pages 203–376, 1972.

[15] P.B. Dubovskiĭ, V.A. Galkin, and I.W. Stewart. Exact solutions for the coagulation-fragmentation equations. *Journal of Physics A: Mathematical and General*, 25:4737–4744, 1992.

[16] N. Dunford and J.T. Schwartz. *Linear operators Part 1: General theory.* Interscience publishers, Inc., New York, New York, USA, 7th edition, 1957.

[17] R.E. Edwards. *Functional Analysis: Theory and Applications.* Holt, Rinehart and Winston, New York, 1965.

[18] A. Eibeck and W. Wagner. An efficient stochastic algorithm for studying coagulation dynamics and gelation phenomena. *SIAM Journal on Scientific Computing*, 22:802–821, 2000.

[19] L.D. Erasmus, D. Eyre, and R.C. Everson. Numerical treatment of the population balance equation using a spline-Galerkin method. *Computers and Chemical Engineering*, 18:775–783, 1994.

[20] M. Escobedo, P. Laurençot, S. Mischler, and B. Perthame. Gelation and mass conservation in coagulation-fragmentation models. *Journal of Differential Equations*, 195:143–174, 2003.

[21] M. Escobedo, S. Mischler, and B. Perthame. Gelation in coagulation and fragmentation models. *Communications in Mathematical Physics*, 231:157–188, 2002.

[22] R. Eymard, T. Gallouët, and R. Herbin. *Finite volume methods, in hand book of numerical analysis, Vol. VII, 713-1020.* Handb. Numer. Anal., VII, North-Holland, Amsterdam, 2000.

[23] F. Filbet and P. Laurençot. Numerical simulation of the Smoluchowski coagulation equation. *SIAM Journal on Scientific Computing*, 25:2004–2028, 2004.

[24] N. Fournier and P. Laurençot. Well-posedness of Smoluchowski's coagulation equation for a class of homogeneous kernels. *Journal of Functional Analysis*, 233:351–379, 2006.

[25] S.K. Friedlander. On the particle size spectrum in a condensing vapour. *Phys. Fluid*, 3:693–696, 1960.

[26] F.M. Gelbard and J.H. Seinfeld. Coagulation and growth of a multicomponent aerosol. *Journal of Colloid and Interface Science*, 63:472–479, 1977.

[27] Y.P. Gokhale. *Synthesis and modeling of silver and titanium dioxide nanoparticles by population balance equations.* Phd thesis, Otto-von-Guericke-University Magdeburg, Germany, 2010.

[28] Y.P. Gokhale, R. Kumar, J. Kumar, G. Warnecke, J. Tomas, and W. Hintz. Disintegration process of surface stabilized sol-gel TiO_2 nanoparticles by population balances. *Chemical Engineering Science*, 64:5302–5307, 2009.

[29] Y.P. Gokhale, R. Kumar, J. Kumar, G. Warnecke, J. Tomas, and W. Hintz. Coupled aggregation and disintegration process of TiO_2 nanoparticles by population balance modeling. *Submitted*, 2010.

[30] F. Guias. A Monte Carlo approach to the Smoluchowski equations. *Monte Carlo Methods Appl.*, 3:313–326, 1997.

[31] L.C. Hoàn. *Etude de la classe des opérateurs m-accrétifs de* $L^1(\Omega)$ *et accrétifs dans* $L^\infty(\Omega)$. Thèse de $3^{ème}$ cycle, Université de Paris VI, 1977.

[32] M.J. Hounslow, J.M.K. Pearson, and T. Instone. Tracer studies of high shear granulation: II. Population balance modelling. *AIChE Journal*, 47:1984–1999, 2001.

[33] W. Hundsdorfer and J.G. Verwer. *Numerical solution of time-dependent advection-diffusion-reaction equations*. Springer-Verlag New York, USA, 1st edition, 2003.

[34] C.D. Immanuel and F.J. Doyle. Solution technique for a multi-dimensional population balance model describing granulation processes. *Powder Technology*, 156:213–225, 2005.

[35] S.M. Iveson. Limitations of one-dimensional population balance models of wet granulation processes. *Powder Technology*, 124:219–229, 2002.

[36] I. Jeon. Existence of gelling solution for coagulation-fragmentation equations. *Comm. math. Phys.*, 194:541–567, 1998.

[37] X. Jiang, T. Herricks, and Y. Xia. Monodispersed spherical colloids of titania: Synthesis, characterization and crystallization. *Advanced Materials*, 15:1205–1209, 2003.

[38] Y.P. Kim and J.H. Seinfeld. Simulation of multicomponent aerosol dynamics. *Journal of Colloid and Interface Science*, 149:425–449, 1992.

[39] M. Kostoglou. Extended cell average technique for the solution of coagulation equation. *Journal of Colloid and Interface Science*, 306:72–81, 2007.

[40] M. Kostoglou and A.J. Karabelas. On sectional techniques for the solution of the breakage equation. *Computers and Chemical Engineering*, 33:112–121, 2009.

[41] F.E. Kruis, A. Maisels, and H. Fissan. Direct simulation Monte Carlo method for particle coagulation and aggregation. *AIChE Journal*, 46:1735–1742, 2000.

[42] J. Kumar. *Numerical approximations of population balance equations in particulate systems*. Phd thesis, Otto-von-Guericke-University Magdeburg, Germany, 2006.

[43] J. Kumar, M. Peglow, G. Warnecke, and S. Heinrich. An efficient numerical technique for solving population balance equation involving aggregation, breakage, growth and nucleation. *Powder Technology*, 179:205–228, 2007.

[44] J. Kumar, M. Peglow, G. Warnecke, and S. Heinrich. The cell average technique for solving multi-dimensional aggregation population balance equations. *Computers and Chemical Engineering*, 32:1810–1830, 2008.

[45] J. Kumar, M. Peglow, G. Warnecke, S. Heinrich, and L. Mörl. Improved accuracy and convergence of discretized population balance for aggregation: The cell average technique. *Chemical Engineering Science*, 61:3327–3342, 2006.

[46] J. Kumar and G. Warnecke. Convergence analysis of sectional methods for solving breakage population balance equations-I: The fixed pivot technique. *Numerische Mathematik*, 21:1433–1440, 2008.

[47] J. Kumar and G. Warnecke. A note on moment preservation of finite volume schemes for solving growth and aggregation population balance equations. *SIAM J. Sci. Comput.*, 32:703–713, 2010.

[48] J. Kumar, G. Warnecke, M. Peglow, and S. Heinrich. Comparison of numerical methods for solving population balance equations incorporating aggregation and breakage. *Powder Technology*, 189:218–229, 2009.

[49] R. Kumar, O.I. Imole, Y.P. Gokhale, G. Warnecke, J. Tomas, and W. Hintz. Investigation of the process parameters during the sol-gel process of TiO_2 nanoparticles by population balances. *Submitted*, 2010.

[50] R. Kumar, J. Kumar, and G. Warnecke. Convergence analysis of a finite volume scheme for solving non-linear aggregation-breakage population balance equations. *Submitted*, 2010.

[51] R. Kumar, J. Kumar, and G. Warnecke. Moment preserving finite volume schemes for solving population balance equations incorporating aggregation, breakage, growth and source terms. *Under Revision in SIAM J. Sci. Comput.*, 2010.

[52] R. Kumar, J. Kumar, and G. Warnecke. Numerical methods for solving two-dimensional aggregation population balance equations. *Computers and Chemical Eng. Science, to appear*, doi:10.1016/j.compchemeng.2010.08.002, 2010.

[53] S. Kumar and D. Ramkrishna. On the solution of population balance equations by discretization - I. A fixed pivot technique. *Chemical Engineering Science*, 51:1311–1332, 1996.

[54] S. Kumar and D. Ramkrishna. On the solution of population balance equations by discretization - III. Nucleation, growth and aggregation of particles. *Chemical Engineering Science*, 52:4659–4679, 1997.

[55] P.L.C. Lage. Comments on the "An analytical solution to the population balance equation with coalescence and breakage-the special case with constant number of particles" by D.P. Patil and J.R.G. Andrews. *Chemical Engineering Science*, 57:4253–4254, 2002.

[56] W. Lamb. Existence and uniqueness results for the continuous coagulation and fragmentation equation. *Mathematical Methods in the Applied Sciences*, 27:703–721, 2004.

[57] P. Laurençot. On a class of continuous coagulation-fragmentation equations. *Journal of Differential Equations*, 167:245–274, 2000.

[58] P. Laurençot and S. Michler. The continuous coagulation-fragmentation equations with diffusion. *Archive for Rational Mechanics and Analysis*, 162:45–99, 2002.

[59] P. Laurençot and S. Mischler. From the discrete to the continuous coagulation-fragmentation equations. *Proceedings of the Royal Society of Edinburgh*, 132 A:1219–1248, 2002.

[60] I.J. Laurenzi, J.D. Bartels, and S.L. Diamond. A general algorithm for exact simulation of multicomponent aggregation processes. *Journal of Computational Physics*, 177:418–449, 2002.

[61] K. Lee and T. Matsoukas. Simultaneous coagulation and breakage using constant-N Monte Carlo. *Powder Technology*, 110:82–89, 2000.

[62] M.H. Lee. On the validity of the coagulation equation and the nature of runaway growth. *Icarus*, 143:74–86, 2000.

[63] R.J. LeVeque. *Numerical methods for conservation laws. Lectures in Mathematics.* Birkhauser-Verlag, Basel, ETH Zürich, Switzerland, 1st edition, 1990.

[64] R.J. LeVeque. *Finite Volume Methods for Hyperbolic Problems.* Cambridge University Press, Cambridge, U.K., 1st edition, 2002.

[65] F. Leyvraz. Existence and properties of post-gel solutions for the kinetic equations of coagulation. *J. Phys. A*, 16:2861–2873, 1983.

[66] F. Leyvraz and H.R. Tschudi. Singularities in the kinetics of coagulation processes. *J. Phys. A*, 14:3389–3405, 1981.

[67] Y. Lin, K. Lee, and T. Matsoukas. Solution of the population balance equation using constant-number Monte Carlo. *Chemical Engineering Science*, 57:2241–2252, 2002.

[68] P. Linz. Convergence of a discretization method for integro-differential equations. *Numer. Math.*, 25:103–107, 1975.

[69] A.A. Lushnikov. Evolution of coagulating systems. *Journal of Colloid and Interface Science*, 54:94–101, 1976.

[70] G. Madras and B.J. McCoy. Reversible crystal growth-dissolution and aggregation-breakage: Numerical and moment solutions for population balance equations. *Powder Technology*, 143-144:297–307, 2004.

[71] A.W. Mahoney and D. Ramkrishna. Efficient solution of population balance equations with discontinuities by finite elements. *Chemical Engineering Science*, 57:1107–1119, 2002.

[72] J. Makino, T. Fukushige, Y. Funato, and E. Kokubo. On the mass distribution of planetesimals in the early runaway stage. *New Astronomy*, 3:411–417, 1998.

[73] D.L. Marchisio and R.O. Fox. Solution of population balance equations using the direct quadrature method of moments. *Journal of Aerosol Science*, 36:43–73, 2005.

[74] E. Matijevic, M. Budnik, and L. Meites. Preparation and mechanism of formation of titanium dioxide hydrosols of narrow size distribution. *Journal of Colloid and Interface Science*, 61:302 – 311, 1977.

[75] D.J. McLaughlin, W. Lamb, and A.C. McBride. Existence and uniqueness results for the non-autonomous coagulation and multiple-fragmentation equation. *Mathematical Methods in the Applied Sciences*, 21:1067–1084, 1998.

[76] Z.A. Melzak. A scalar transport equation. *Transactions of the American Mathematical Society*, 85:547–560, 1957.

[77] G. Menon and R.L. Pego. Approach to self-similarity in Smoluchowski's coagulation equations. *Communications on Pure and Applied Mathematics*, LVII:1–36, 2003.

[78] S. Motz, A. Mitrovic, and E. D. Gilles. Comparison of numerical methods for the simulation of dispersed phase systems. *Chemical Engineering Science*, 2002:4329–4344, 2002.

[79] H. Mueller. Zur allgemeinen Theorie der raschen Koagulation. *Kolloidchemische Beihefte*, 27:223–250, 1928.

[80] M. N. Nandanwar and S. Kumar. A new discretization of space for the solution of multi-dimensional population balance equations. *Chemical Engineering Science*, 63:2198–2210, 2008.

[81] M. Nicmanis and M.J. Hounslow. A finite element analysis of the steady state population balance equation for particulate systems: Aggregation and growth. *Computers and Chemical Engineering*, 20:S261–S266, 1996.

[82] T. Nikolov, W. Hintz, V. Jordanova, and J. Tomas. Synthesis and Characterization of titanium dioxide nanoparticles. *Journal of the University of Chemical Technology and Metallurgy (Sofia)*, 38:725–734, 2003.

[83] M. Peglow, J. Kumar, S. Heinrich, G. Warnecke, E. Tsotsas, L. Mörl, and B. Wolf. A generic population balance model for simultaneous agglomeration and drying in fluidized beds. *Chemical Engineering Science*, 62:513–532, 2007.

[84] S. Qamar and G. Warnecke. Solving population balance equations for two-component aggregation by a finite volume scheme. *Chemical Engineering Science*, 62:679–693, 2007.

[85] S. Qamar, G. Warnecke, and M. Peter. On the solution of population balances for nucleation, growth, aggregation and breakage processes. *Chemical Engineering Science*, 64:2088–2095, 2009.

[86] T.E. Ramabhadran, T.W. Peterson, and J.H. Seinfeld. Dynamics of aerosol coagulation and condensation. *AIChE Journal*, 22:840–851, 1976.

[87] D. Ramkrishna. *Population balances. Theory and applications to particulate systems in engineering.* Academic Press, New York, USA, 1st edition, 2000.

[88] S. Rigopoulos and A.G. Jones. Finite-element scheme for solution of the dynamic population balance equation. *AIChE Journal*, 49:1127–1139, 2003.

[89] P.G. Saffman and J.S. Turner. On the collision of drops in turbulent clouds. *Journal of Fluid Mechanics*, 1:16–30, 1956.

[90] W.T. Scott. Analytic studies of cloud droplet coalescence. *Journal of the Atmospheric Sciences*, 25:54–65, 1968.

[91] A. Seifert and K.D. Beheng. A double-moment parameterization for simulating autoconversion, accretion and selfcollection. *Atmospheric Research*, 59-60:265–281, 2001.

[92] M. Smith and T. Matsoukas. Constant-number Monte Carlo simulation of population balance. *Chemical Engineering Science*, 53:1777–1786, 1998.

[93] M. Sommer, F. Stenger, W. Peukert, and N.J. Wagner. Agglomeration and breakage of nanoparticles in stirred media mills- a comparison of different methods and models. *Chemical Engineering Science*, 61:135–148, 2006.

[94] M. Strumendo and H. Arastoopour. Solution of bivariate population balance equations using the finite size domain complete set of trial functions method of moments (FCMOM). *Ind. Eng. Chem. Res.*, 48:262–273, 2009.

[95] H. Tanaka, S. Inaba, and K. Nakazawa. Steady-state size distribution for the self-similar collision cascade. *Icarus*, 12:450–455, 1996.

[96] F.L. Toma, G. Bertrand, S.O. Chwa, C. Meunier, D. Klein, and C. Coddet. Comparative study on the photocatalytic decomposition of nitrogen oxides using TiO2 coatings prepared by conventional plasma spraying and suspension plasma spraying. *Surface and Coatings Technology*, 200(20-21):5855 – 5862, 2006.

[97] H.M. Vale and T.F. McKenna. Solution of the population balance equation for two-component aggregation by an extended fixed pivot technique. *Industrial and Engineering Chemistry Research*, 44:7885–7891, 2005.

[98] M. Vanni. Approximate population balance equations for aggregation-breakage processes. *Journal of Collid and Interface Science*, 221:143–160, 2002.

[99] M. von Smoluchowski. Versuch einer mathematischen Theorie der Koagulationskinetik kolloider Lösungen. *Zeitschrift für Physikalische Chemie*, 92:129–168, 1917.

[100] D. L. Wright, R. McGraw, and D. E. Rosner. Bivariate extension of the quadrature method of moments for modeling simultaneous coagulation and sintering of particle populations. *Journal of Colloid and Interface Science*, 236:242–251, 2001.

[101] Y. Xiong and S.E. Pratsinis. Formation of agglomerate particles by coagulation and sintering-Part I. A two-dimensional solution of the population balance equation. *Journal Aerosol Science*, 24:283–300, 1993.

[102] R.M. Ziff. New solution to the fragmentation equation. *Journal of Physics A: Mathematical and General*, 24:2821–2828, 1991.

[103] R.M. Ziff and E.D. McGrady. The kinetics of cluster fragmentation and depolymerization. *Journal of Physics A: Mathematical and General*, 18:3027–3037, 1985.

[104] A. Zucca, D. Marchisio, M. Vanni, and A. Barresi. Validation of bivariate DQMOM for nanoparticle processes simulation. *AIChE Journal*, 53:918–931, 2007.

Curriculum Vitae

Personal Information

Name	**Rajesh Kumar**
Date of birth	08.07.1981
Place of birth	Jhajha, India

Education and Employment

1987 - 1999	Schooling, Jhajha, India
2000 - 2003	B.A. (Honours) in Mathematics, Delhi University, Delhi, India
2003 - 2005	Master of Science (M.Sc.) in Applied Mathematics, Indian Institute of Technology (IIT) Roorkee, India
2005 - 2006	Master of Science (M.Sc.) in Industrial Mathematics: Modelling and Scientific Computing, Technical University of Kaiserslautern, Germany
2006 - 2007	Master of Science (M.Sc.) in Industrial Mathematics, Johannes Kepler University Linz, Austria
2007 - 2010	PhD Graduation (DFG Scholarship) within the Graduiertenkolleg 828, Faculty of Mathematics, Otto-von-Guericke University, Magdeburg, Germany

Academic Honors

- Qualified CSIR-UGC National Eligibility Test (NET-2005)
- Erasmus Mundus fellowship from European Commission for (2005-2007)
- German Research Foundation (DFG) Graduiertenkolleg Scholarship (2007-2010)